Consiglio Nazionale
delle Ricerche

3RD ANNUAL CONFERENCE OF THE
COST ACTION MP1302

Optical Nanospectroscopy III

a cura di

Antonio Cricenti

PROCEEDINGS

P.le Aldo Moro, 7 - Roma
www.edizioni.cnr.it
bookshop@cnr.it
ISBN 978 88 8080 207 5
Giugno 2016

EUROPEAN COOPERATION IN SCIENCE AND TECHNOLOGY

3RD ANNUAL CONFERENCE OF THE COST ACTION MP1302
NANOSPECTROSCOPY

OPTICAL NANOSPECTROSCOPY III

Book of ABSTRACTS

EDITOR ANTONIO CRICENTI

NATIONAL RESEARCH COUNCIL
ROME – ITALY

March 22nd-25th 2016

Istituto Struttura della Materia

National Research Council of Italy

COST is supported by the EU Framework

ESF provides the COST Office through a European Commission

Sponsors


PI


OPTOPRIM


HORIBA
Scientific


Massimo
Bonfante
Rappresentanze
per l'elettro-ottica


LOT
QuantumDesign


NT-MDT

Preface

Over the last few decades tremendous progress has been seen in the efforts to observe, understand and control light-matter interactions at the nanoscale using nanofabrication and high temporal, spectral and spatial resolution techniques. With today's research and industry aiming for ever smaller objects and feature sizes, there is an increasing demand for spectroscopic methods to investigate *processes*, objects, and material properties with unprecedented resolution as well as chemical specificity. The new insights are important for issues such as understanding life at a (sub-) cellular level, light-matter-interaction, light-to-energy conversion, devices and materials engineering. The interdisciplinary approach of nanospectroscopy encompasses the fields of physics, (bio-)chemistry, biology, medicine, nanotechnology, and materials science.

This conference and the accompanying COST Action are dedicated to UV/vis/NIR/Raman nanospectroscopic techniques and their application to tailored materials and nanostructures (organic/inorganic, semiconducting, metallic, hybrid, bio) to gain deeper understanding of nanoscale processes. The conference brings together renowned experts and early stage researchers in the field. We are pleased that over 200 scientists from more than 25 countries participate in this conference. About 33 posters, 6 invited and 54 contributed talks cover a wide range of topics from methods development and nanofabrication to fundamental investigations and applications of nanospectroscopy. This week of knowledge exchange and in-depth discussion offers an excellent opportunity for defining the state-of-the- art and identifying future directions in the field.

We would like to express our gratitude to National Research Council of Italy for supporting and hosting this conference, to the European Cooperation in Science and Technology (COST), THE European Science Foundation and the EU RTD Framework Program for support through COST ACTION mp1302 Nanospectroscopy, to our sponsors for their contributions to the success of the conference, and to the local organizing team for their time and commitment. We would also like to take this opportunity to thank all the invited speakers for their ready agreement to take part in this conference and to thank all attendants for their interest and their contributions.

The Conference Chair

Antonio Cricenti

Rome, March 2016

About COST

COST – EUROPEAN COOPERATION IN SCIENCE AND TECHNOLOGY is an intergovernmental framework aimed at facilitating the collaboration and networking of scientists and researchers at European level. It was established in 1971 by 19 member countries and currently includes 35 member countries across Europe, and Israel as a cooperating state.

COST funds pan-European, bottom-up networks of scientists and researchers across all science and technology fields. These networks, called "COST Actions2, promote international coordination of nationally-funded research.

By fostering the networking of researchers at an international level, COST enables break-through scientific developments leading to new concepts and products, thereby contributing to strengthening Europe's research and innovation capacities.

COST's mission focuses in particular on:

- Building capacity by connecting high quality scientific communities throughout Europe and worldwide;
- Providing networking opportunities for early career investigators;
- Increasing the impact of research on policy makers, regulatory bodies and national decision makers as well as the private sector.

Through its inclusiveness, COST supports the integration of research communities, leverages national research investments and addresses issues of global relevance.

Every year thousands of European scientists benefit from being involved in COST Actions, allowing the pooling of national research funding to achieve common goals.

As a precursor of advanced multidisciplinary research, COST anticipates and complements the activities of EU Framework Program, constituting a "bridge" towards the scientific communities of emerging countries. In particular, COST Actions are also open to participation by non-European scientists coming from neighbor countries (for example Albania, Algeria, Armenia, Azerbaijan, Belarus, Egypt, Georgia, Jordan, Lebanon, Libya, Moldova, Montenegro, Morocco the Palestinian Authority, Russia, Syria, Tunisia and Ukraine) and from a number of international partner countries.

COST's budget for networking activities has traditionally been provided by successive EU RTD Framework Program. COST is currently executed by the European Science Foundation (ESF) THROUGH THE cost Office on a mandate by the European Commission, and the framework is governed by a Committee of Senior Officials (CSO) representing all its 35 member countries.

More information about COST is available at **www.cost.eu .**

Conference Chair

Dr. Antonio Cricenti

Istituto di Struttura della Materia
CNR – Area della Ricerca di Tor Vergata, Via del Fosso del Cavaliere, 100
00133 Roma, Italy
http://www.ism.cnr.it/scanning-probe-microscopy/

Local Organizing Team

Antonio Cricenti
Daniela De Fazio
Franca Rossi
Marco Luce
Marco Ortenzi
Massimiliano Rinaldi
Alessandro Ippoliti
Raffaella Rossi
Bruna Ponzi
Maria Rita Bruni

Scientific Committee

Antonio Cricenti (ISM-CNR)
Pietro G. Gucciardi (IPCF-CNR)
Margherita Zavelani Rossi (POLIMI)
Mario D'Acunto (ISTI-CNR)
Michele Celebrano (POLIMI)
Francesco Fuso (UNI-Pisa)
Michele Ortolani (UNI-Roma1)

Invited Speakers

Julietta Rau
CNR-ISM, Rome, Italy

Vesna Vasic Vinca
Institute of Nuclear Sciences, Serbia, Belgrade

Antonio Radoi
IMT-Bucharest, Bucharest, Romania,

Beata Kalska-Szostko
University of Bialystok, Bialystok, Poland

Augusto Marcelli
INFN, Rome, Italy

Mustafa Culha
Yeditepe University, Istanbul, Turkey

Towards a reliable Raman and SNOM spectroscopy for tissue imaging and cancer diagnostics

J.V. Rau[a], A. Crescenzi[b], M. Caricato[b], V. Graziani[a], M. Fosca[a], C. Taffon[b], V. Valentini[a], V. La Vaccara[b], M.R.F. Siggel-King[c], T. Craig[c], J. Ingham[c], D. Martin[c], P. Weightman[c], M. Ortenzi[a], M. Luce[a], A. Cricenti[a]**

[a]Istituto di Struttura della Materia (ISM-CNR), via del Fosso del Cavaliere 100, 00133 Rome, Italy
[b]Policlinico Universitario Campus Bio-medico, via Álvaro del Portillo 200, 00128 Rome, Italy
[c]Department of Physics, University of Liverpool, Liverpool L69 7ZE, United Kingdom

**e-mail: giulietta.rau@ism.cnr.it*
**e-mail: antonio.cricenti@ism.cnr.it*

Keywords: Raman spectroscopy, SNOM, imaging, cancer, tissues

Introduction

We present a fully implemented Raman and Scanning Near-field Optical Microscopy (SNOM) in their spectroscopic mode for tissue imaging and early cancer diagnostics. Raman spectroscopy (RS) is a non-invasive optical label-free tool increasingly used to get molecular fingerprints of biological tissues. It is able to provide bioanalytical information on any molecule with high specificity. Technological advances over the last decade have created a new and faster Raman imaging microscope instrument, providing morphological tissue investigation of large areas, coupled with point-by-point spectral analysis of biochemical composition. This option is important not only for discrimination between healthy and pathological tissues, but especially for pre-cancerous tissue state earlier detection and understanding. Our results of Raman mapping of Thyroid and Lung tissues have shown that the Raman imaging microscope can operate at a few micron resolution, in order to distinguish between healthy and malignant tissues.

For early diagnosis of cancer and the development of diagnostic imaging, a SNOM has been coupled with an infrared light source, based on Free Electron Laser at the ALICE facility in Daresbury. The potential of IR spectroscopy to characterise cancerous tissues has long been recognised. Studies of various cancers by many groups have established that regions of malignant tissue can be easily identified on the basis of its IR spectrum. The oesophageal adenocarcinoma, the cancer with the fastest rise in incidence in the Western world, requires an instrument providing specific chemical images at sub-cellular level of oesophagus tissue. This approach demonstrates the potential of the IR spectroscopy for yielding an accurate diagnostic test for oesophageal and other types of cancers.

Results and Discussion

Carcinomas are complex biochemical systems and in the past their diagnosis was based on morphological differences between malignant cells and their benign counterpart. Recently the paradigm has changed and great interest is focused now on the biochemical profile of tumours in view of the availability of new drugs that specifically target neoplastic cells. This new paradigm requires biochemical analysis of each tumour in order to establish the correct personalized oncological "target therapy". Understanding the mechanism of molecular alterations of a specific tumour is a critical issue to prognosticate its behaviour and to predict the response to personalized therapy.

There are many recent studies strongly suggesting that RS can be used as a clinical tool for cancer diagnosis, improving clinical accuracy in decision-making [1-3]. *In vivo* RS clinical applications are extremely challenging and nowadays remain limited mainly by the time-consuming spectral measurements. However, recent advances in optical technologies and instrumentation and rapidly growing clinical translational purpose RS investigations, has lead to several *in vivo* applications of RS in biomedicine [4-6]. With this regard, the aim of the present research is to demonstrate that Raman spectroscopy with the increased acquisition speed is able to reliably discriminate between healthy and carcinoma tissues, based on its biochemical profile. Several patients with the same diagnosis were enrolled for RS studies. The collected Raman data were processed applying the statistical multivariate map data analysis, used for complex systems with high internal variability: principal component analysis and linear discriminant analysis, both validated through the Hypothesis test. Particular attention has been dedicated to the biochemical profile study of the collected Raman spectra. For each tissue section several Raman maps containing up to 30 000 spectra per map were analysed. The average map spectra, according to the tissue type (healthy or pathological), have been analysed and compared as well.

In **Figure 1**, a Raman map of Thyroid tissue is shown, containing both healthy and papillary carcinoma zones. False colours evidence healthy tissues (blue) and carcinoma (red-yellow-green). Each colour corresponds to a certain kind of spectrum, and hence to a certain chemical composition. Papillary structures can be well observed.

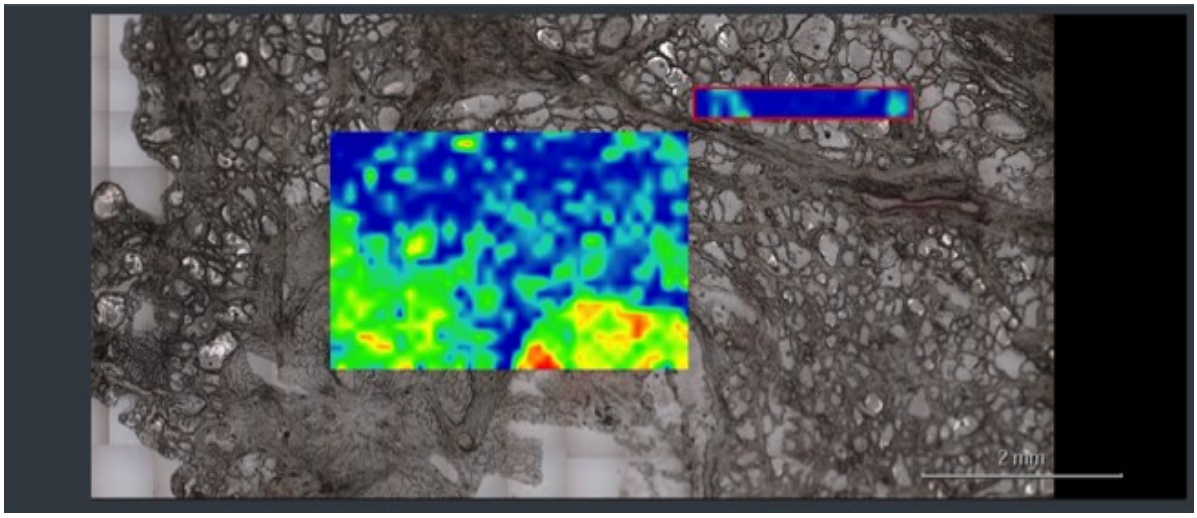

Figure 1: Raman map of Thyroid tissue, evidencing papillary structures of papillary carcinoma (green-yellow-red). Healthy tissue corresponds to blue zone.

In **Figure 2**, a Raman map of Lung tissue is presented. Carcinoma zone is evidenced with red-yellow-green colours, whereas healthy tissue is in blue. As one can see, the differences between the spectra corresponding to healthy and pathologic tissue zones are significant.

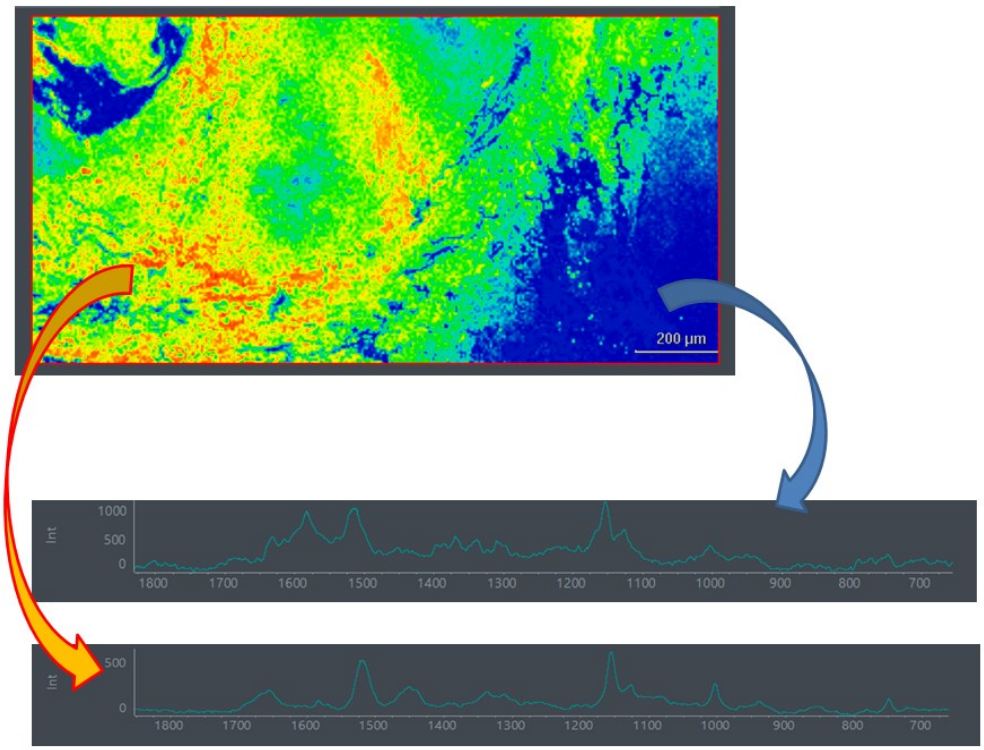

Figure 2: Raman map of Lung tissue. In red-yellow-green colour carcinoma zone is evidenced, while healthy tissue is in blue. The upper spectrum corresponds to healthy tissue zone, while the lower one – to the pathologic tissue.

The SNOM employed in this work was developed on the IR FEL at Vanderbilt and established on the IR FEL on the ALICE energy recovery linear accelerator at Daresbury [7]. Preliminary results of IR-SNOM on oesophageal adenocarcinoma have shown that the system can operate at nanometer resolution and has been able to distinguish between healthy and malignant tissues [8]. The optical fibre has been driven in particular areas of the oesophageal tissue and topographical and optical images have been collected simultaneously at different wavelengths. **Figure 3** shows a videocamera view of the oesophageal tissue (specimen) and of the optical fibre (tip) approaching the desired area.

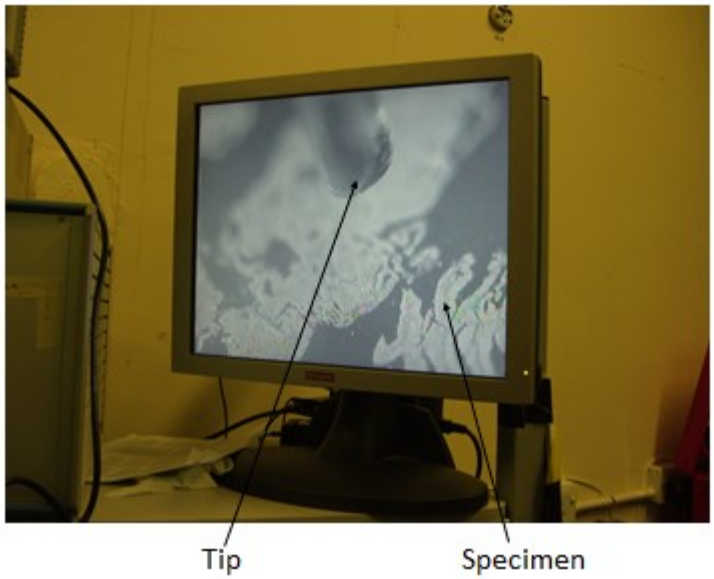

Figure 3: Videocamera view of the oesophageal tissue (specimen) and of the optical fiber (tip) approaching the desired area.

In particular, SNOM images were collected at wavelengths of 7.0 □m (no strong biomarker), 7.3 □m (protein/glycoprotein), and 8.05 □m (DNA).

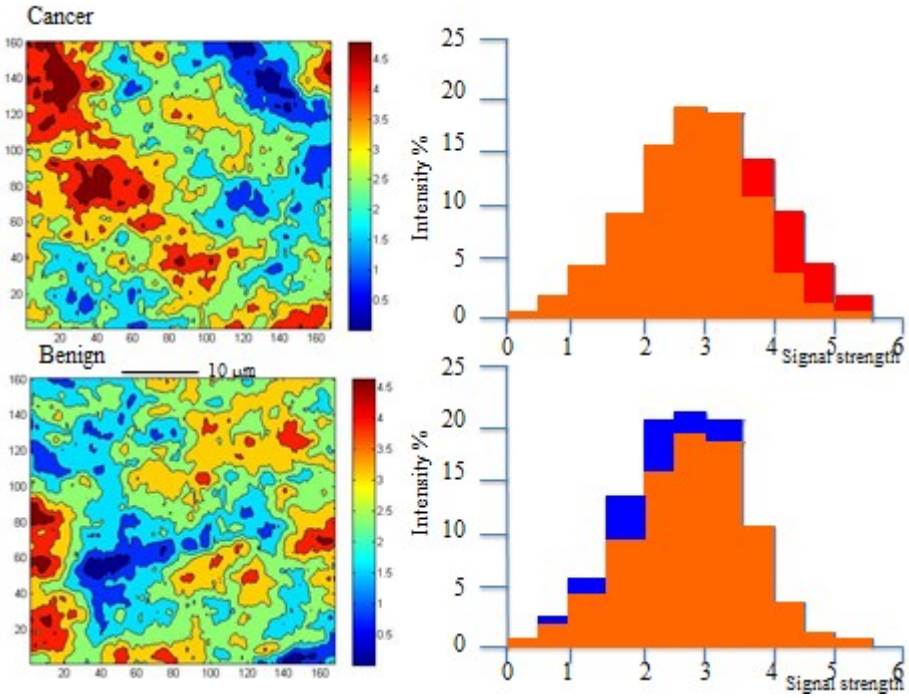

Figure 4: IR-SNOM image maps showing the location of intense DNA (red), intense protein/glycoprotein (blue) and of strong overlap of DNA and protein/glycoprotein (orange).

Figure 4 shows 40 □m x 40 □m optical SNOM images for two samples, labelled Cancer and Benign: the colour maps show the location of intense DNA (red), intense protein/glycoprotein (blue) and of strong overlap of DNA and protein/glycoprotein (orange). As clearly visible, Cancer sample shows a large spread of intense signal from DNA whereas Benign sample shows a lower overall density of DNA, which is more dispersed and exhibits more localised centres.

Conclusions and perspectives

The combination of Raman and Scanning Near-field Optical Microscopy (SNOM) approaches, in their spectroscopic mode, can be an important tool for tissue imaging and early cancer diagnostics. It is expected to produce a major advance in imaging of malignant tissues, leading to the development of portable diagnostic devices for hospital use for various types of cancer. It is also planned to utilise the powerful combination of high spatial resolution and chemical specificity of the mentioned methodologies to study the key components, responsible for cancer formation.

Acknowledgements

Authors of ISM-CNR and Biomedical Campus are grateful to Thermo Fisher Scientific Company for DXR Raman system supplied in the frames of the Raman DXR Seed Unit Program (2016). This work was also supported by the Cockcroft Institute via the STFC core grant ST/Goo8248/1 and STFC's Daresbury Laboratory via its ASTeC centre and ALICE operation team.

References:

[1] Mayerhoefer T, Krafft C, Neugebauer U, et al; Moving Raman spectroscopy into the clinic EuroPhotonics Summer 2014.www.Photonics.com

[2] Çulha M; Raman spectroscopy for cancer diagnosis: how far have we come? Bioanalysis; 7(21) (2015) 2813-2824;

[3] Kong K, Kendall C, Stone N, Notingher I; Raman spectroscopy for medical diagnostics — From in-vitro biofluid assays to in-vivo cancer detection; Advanced Drug Delivery Reviews; 89 (2015) 121–134;

[4] Bergholt MS, Zheng W, Ho KY, Teh M, Yeoh KG, Huang Z, et al.; Raman Endoscopy for Objective Diagnosis of Early Cancer in the Gastrointestinal System; J. Gastroint. Dig. Syst.; S:1 (2013);

[5] Bergholt MS, Zheng W, Lin K, Ho KY, Teh M, Yeoh KG, Bok Yan Sod J and Huang Z; Raman endoscopy for in vivo differentiation between benign and malignant ulcers in the stomach; Analyst; 135 (2010) 3162–3168;

[6] Lui H, Zhao J, Mclean D, et al.; Real-time Raman spectroscopy for in vivo skin cancer diagnosis; Cancer Res.; 72(10) (2012) 2491–2500;

[7] Cricenti A, Luce M, Tolk NH, Margaritondo G; Nanosci. Nanotechnol. Lett.; 3 (2011) 913;

[8] Smith AD, Siggel-King MRF, Holder GM, Cricenti A, Luce M, Harrison P, Martin DS, Surman M, Craig T, Barrett SD, Wolski A, Dunning DJ, Thompson NR, Saveliev Y, Pritchard DM, Varro A, Chattopadhyay S, Weightman P; Near-field optical microscopy with an infra-red free electron laser applied to cancer diagnosis; Applied Physics Letters; 102 (2013) 053701.

SERS-based diagnostics: selective targeting of different human cancer cells using functionalized gold nanoparticles.

C. Fasolato[a,b], *I. Silvestri*[c], *S. Giantulli*[c], *F. Ripanti*[a], *F. Mazzarda*[a], *F. Mura*[d], *F. Costantini*[d], *F. Bordi*[a], *P. Postorino*[a], *and F. Domenici**[a,e]

[a] Dipartimento di Fisica, Università Sapienza, Rome, Italy
[b] Center for Life Nanoscience@Sapienza, Istituto Italiano di Tecnologia, Rome, Italy
[c] Dipartimento di Medicina Molecolare, Università Sapienza, Rome, Italy
[d] Dipartimento di Chimica, Università Sapienza, Rome, Italy
[e] Dipartimento di Scienze e Tecnologie Chimiche, Università di Tor Vergata, Rome, Italy

**e-mail: fabiodomenici@gmail.com*

Keywords: SERS, nanovector, early cancer detection, diagnostics

Introduction

In the last few decades, the development of novel spectroscopic techniques, often combining a very high sensitivity with huge spatial resolution, allowed the possibility of investigating down-scaled phenomena, as for example biochemical and biophysical processes in living systems. Surface Enhanced Raman Spectroscopy (SERS) is one of the most established techniques in this framework [1]. SERS is based on the plasmonic resonance of metal nanostructures: the collective electronic excitation at the metal surface can indeed be excited by light and give rise to the localization of strong electromagnetic fields close to the nanoparticle surface, which can be used for spectroscopy.

In the past years, SERS has allowed to reach not only the threshold of single molecule vibrational spectroscopy [2], but also the implementation of devices in the field of biosensing, capable of detecting specific biomolecules at very low concentration by means of Raman spectroscopy [3]. Moreover, the implementation of SERS-labelled nanomaterials, such as functionalized metallic nanoparticles, paved the way for the application of these systems in the emerging field of nanomedicine [4].

Much interest has lately risen, indeed, around the concept of "theranostics", i.e. combining diagnostics with therapy, the latter to perform selectively on cancer cells without damaging the healthy tissue [4]. Plasmonics-based theranostics is often designed combining SERS and photothermal bleaching. One of the open problems in biomedicine is the early detection of cancer, i.e. the capability of reveal the presence of the disease when it is not yet advanced.

Addressing this problem, we designed a biocompatible system based on gold nanoparticles functionalized with the Raman active bifunctional linker 4-aminothiophenol and further conjugated with folic acid, a biomolecule with an essential role in cell reproduction. Our system can be considered a nanobiovector, as it is capable of targeting a specific kind of cell and locate on the folate receptors, on the cell membrane [5]. Folic acid receptors are generally overexpressed in many types of cancer cells, as these reproduce more frequently then ordinary ones [6]. The presence of folate receptors on the membrane strongly depends on the physiology of the cell line considered. In this presentation, we will show that the high specificity of our system allowed us not only to target cancer cells, but also to be able to distinguish different cell lines based on their level of expression of folate receptors [5].

Results and Discussion

After briefly presenting the system characterization, we will illustrate the interaction of our nanobiovector with different cell cultures.

SERS mapping, performed on different cells, allowed us to detect our nanovector bound to the cell membrane and, therefore, to map the presence of the folate receptors even at subcellular level.

We developed a SERS screening protocol, which allowed us to estimate the density of folate receptors on different cell types. For this experiment we chose three cell lines, showing a different expression of folic acid receptors [6,7]. As expected, the detected SERS signal was higher on cancer cells (HeLa, human cervical cancer, and Pc-3, human prostatic cancer) than on healthy ones (HaCaT, human keratinocytes). Moreover, the values of SERS intensity measured on the different cell lines were clearly distributed in three distinct statistical populations, that we were able to fit with lognormal statistical distributions, as shown in Figure 1. As previously explained, the different response of these cell lines to the treatment with the nanovector is related to the level of expression of folate binding proteins on the cell membrane. For this reason, HeLa cells (indicated as "cancer 2" in Figure 1) show a higher signal than Pc-3 cells ("cancer 1").

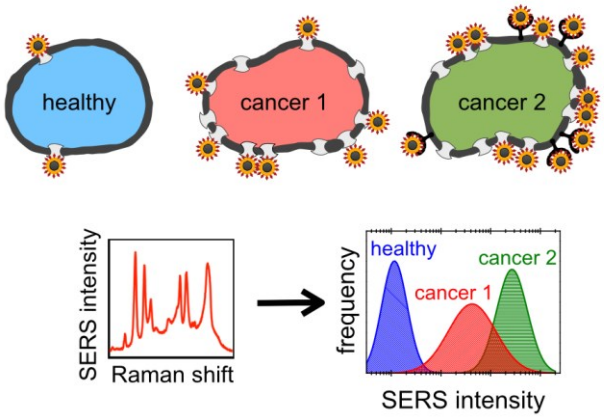

Figure 1: Sketch of the experiment, which consists in the treatment of three different cell lines (one healthy, two cancerous) with the folate-functionalized nanovector. By measuring the average SERS signal on the cells, it is possible to discriminate between healthy and cancer cells and to distinguish three different populations, namely HaCaT (healthy), Pc-3 (cancer 1) and HeLa (cancer 2) cells.

Conclusions and Outlook

Biofunctionalized gold nanoparticles covered with folic acid allowed the selective targeting of two types of cancer cell with different efficiency, giving information on the level of folate receptors on the cell membrane. The results suggest the possibility to combine the nanovector plasmonic properties with opportune functionalizations, with the aim of performing SERS-based biophysical investigations, as for example to map the molecular receptors on cell membranes.

References:

[1] Kiefer W, Schlücker S (ed.); Surface enhanced Raman spectroscopy: analytical, biophysical and life science applications; John Wiley & Sons, (2011).
[2] Kneipp K, Wang Y, Kneipp H, Perelman L T, Itzkan I, Dasari R R, Feld M S; Single molecule detection using surface-enhanced Raman scattering (SERS); Physical Review Letters; 78 (1997) 1667;
[3] Das G, *et al*.; Fabrication of large-area ordered and reproducible nanostructures for SERS biosensor application; Analyst; 137 (2012) 1785-1792;
[4] Janib, S M, e al; Imaging and drug delivery using theranostic nanoparticles; Advanced drug delivery reviews; 62 (2010) 1052-1063;
[5] Fasolato C, et al., to be submitted to Nanomedicine NBM;
[6] Paulos C M, et al.; Ligand Binding and Kinetics of Folate Receptor Recycling in Vivo: Impact on Receptor-Mediated Drug Delivery; Mol. Pharmacol.; 66 (2004) 1406.

Linear and non-linear optical properties of bi-metallic heterodimers

A.-L. Baudrion[a*], *J. Wang*[a,b], *A. Horrer*[c], *G. Lévêque*[d], *J. Butet*[e], *A. Horneber*[b], *M. Fleischer*[c], *D. Zhang*[b] *and P.-M. Adam*[a]

[a] Laboratoire de Nanotechnologie et d'Instrumentation Optique (LNIO)
Institut Charles Delaunay - UMR CNRS 6281, Université de technologie de Troyes, France
[b] Institute of Physical and Theoretical Chemistry, University of Tuebingen, Germany
[c] Institute for Applied Physics, University of Tuebingen, Germany
[e] Institut d'Electronique de Microelectronique et de Nanotechnologie (IEMN), Université de Lille, France
[f] Nanophotonics and Metrology Laboratory (NAM), Swiss Federal Institute of Technology, Lausanne, Switzerland

**e-mail: anne_laure.baudrion@utt.fr*

Keywords: Plasmonics, scattering, SHG, TPPL, heterodimers

Introduction

Metal nanoparticles have attracted great scientific and technological interest in many application fields, mainly due to their ability to sustain Localized Surface Plasmon Polaritons (LSPP). Linear optical properties and LSPP resonances of metallic nanoparticles or nano-antennas have been well described, since decades, in the literature by extinction and/or scattering spectroscopies and by radiation patterns in direct or in Fourier space. However, much less is known on their non-linear optical properties, and on the role of LSPP resonances in the enhancement of these effects. Two-photon photoluminescence (TPPL) and second harmonic generation (SHG) are both prominent examples of nonlinear effects observed on metallic nanoparticles. Compared to the TPPL process, a third-order process which intrinsically relies on a high local optical field, SHG additionally requires materials with a high second order susceptibility and an inversion symmetry breaking. Such selection rules have to be considered in addition to the 'plasmonic molecular hybridization' model, in order to understand the SHG and the TPPL efficiencies in metallic dimers.

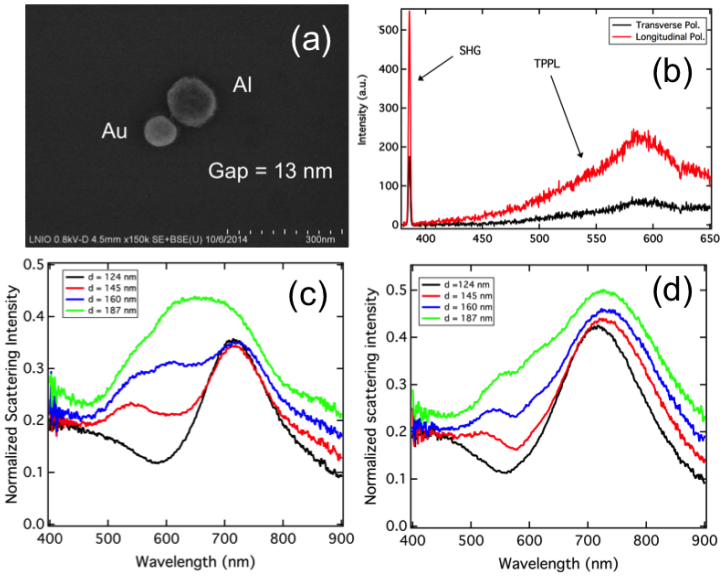

Figure 1: (a) SEM image of a Au-Al dimer. (b) Nonlinear spectra of a Au-Al hetero-dimer where both the gold and aluminum nanoparticle have a diameter of 160 nm. The gap distance is about 20 nm. The incident wavelength is 774 nm and the incident polarization is oriented along either the short axis (black curve) or the long axis (red curve) of the dimer. (c) and (d) Scattering spectra recorded on single Au-Al dimers with polarization oriented along the short (c) or the long (d) axis of the dimers. Each spectrum has been normalized by the lamp spectrum. The diameter of the gold nanoparticle is 160 nm and the diameter of the aluminum nanoparticle varies between 124 and 187 nm. The gap is fixed at 20 nm.

Results and Discussion

In this study, we focused on the linear and nonlinear optical characterization of Au-Al heterodimers (Fig1). These metallic dimers have been fabricated by a two-step electron-beam lithography process where the diameters of the Au and Al nanoparticles have been independently varied, as well as the gap distance. The linear optical properties (single dimer scattering spectra) and the non-linear optical properties (SHG and TPPL spectra) have been compared to understand the main physical phenomena involved.

Design of long-term solution-stable plasmonic dimers

I. Haidar,[a] *L. Boubekeur-Lecaque,**[a] *G. Lévi,*[a] *S. Lau-Truong,*[a] *J. Grand,*[a] *J. Aubard,*[a] *D.R. Neuville,*[b] *N. Félidj*[a]

[a] Uni Paris Diderot, Laboratoire ITODYS UMR7086, - 75205 Paris cedex 13, France
[b] IPGP, CNRS, Sorbonne Paris Cité, 1, rue Jussieu - 75238 Paris, cedex 05, France

**e-mail: leila.boubekeur@univ-paris-diderot.fr*

Keywords: Raman; Enhancement; Gold Nanorod; Coupling; Plasmonics

Introduction

The design of **coupled colloidal nanoparticles (NPs)** to achieve small-aggregates is a challenging task. In fact, colloids are inherently quasi-stable systems, and the **controlled assembly of nanoparticles** to build up small clusters of NPs aggregates with a well defined composition such as dimers relies on the delicate balance between repulsive forces ensuring colloidal stability and the attractive interactions required for NPs assembly leading *in fine* to aggregation. [1]

The considerable effort that has been devoted by the scientific community to devise robust assembly and quenching strategies in solution highlights the challenge of **mastering NPs aggregation to form stable dimers in solution.** Most of the reported optical studies of nanoparticles dimers are performed on dry samples obtained by drop-casting the colloidal solution during the assembly process and thus freezing the aggregation at the desired stage. This simple quenching approach allows the investigation of single and well defined assembled particles. Conversely, freezing the assembly process in solution remains the critical step to yield stable and controlled small NPs clusters in solution. [2-4]

Results and Discussion

In this work, we developped a facile and reproducible strategy to assemble gold nanorods (GNRs) into dimers by using bifunctional linker acting as the coupling agent and the Raman reporter (**Figure 1**). The progression of the assembly was monitored by UV−vis absorption spectroscopy revealing the gradual decrease over time of the longitudinal LSP mode of GNRs while a new red shifted peak rises concomitantly. The latter pointed to end to end assembled GNRs, and the amplitude of this red shift (ca. 150 nm) suggested that the particles were strongly coupled with a small gap distance (1 nm or less).

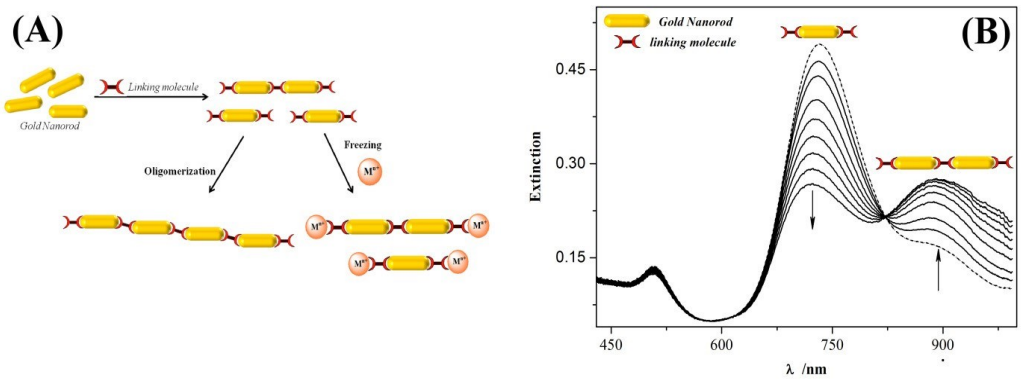

Figure 1: (A) GNRs dimerization strategy. **(B)** Extinction spectra of the gold nanorods dimers assembly in solution. The different spectra are recorded over time following the addition of the bifunctional molecular linker.

Taking advantage of the stability of GNRs dimers after addition of silver to freeze the assembly process, solution-based surface-enhanced Raman scattering (SERS) studies were performed to assess the enhancement for coupled GNRs in comparison to monomers. Besides, the selected molecular linker used to initiate the assembly, features an excellent Raman cross section that was exploited to probe the enhancement in the interparticle gap (**Figure2**).

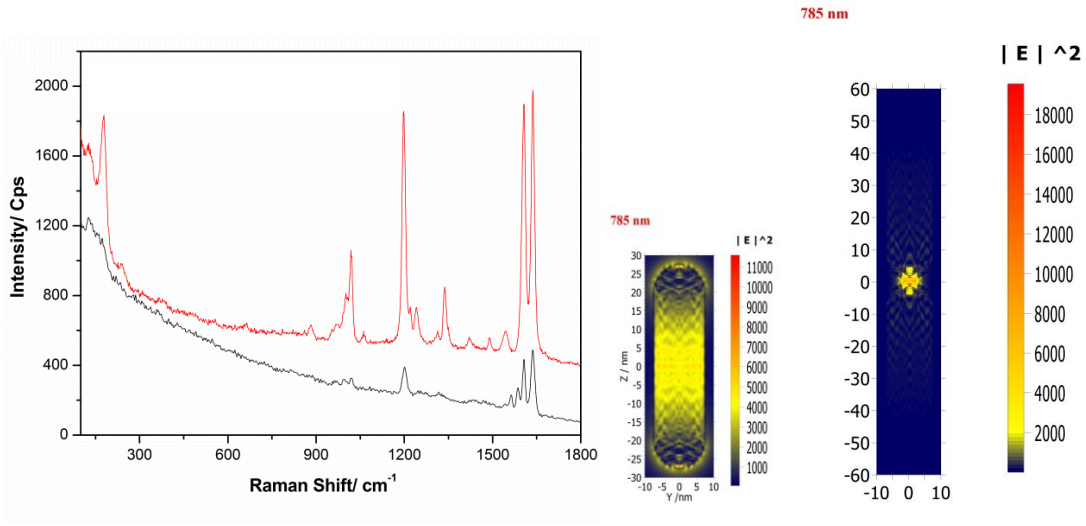

(A) **(B)** **(C)**

Figure 2: (A) Solution-based SERS spectra recorded with 785 nm laser excitation for GNRs for isolated GNRs (black line) and after GNRs dimerization (red line). Mapping of Electric field intensity for **(B)** isolated and **(C)** two coupled GNR monomer (excitation at 785 nm with polarization along the main axis of the rod)

The combination of SERS studies with electrodynamic calculations (Discrete Dipole Approximation method) revealed that the enhancement factor for dimers in comparison to monomers increased by two-orders of magnitude.

Conclusions

We demonstrate how **the control of kinetic and thermodynamic processes** is a fundamental prerequisite to master the assembly and form stable gold nanorods dimers in solution. When encapsulated in solution immediately after assembly termination, the coupled particles are stable for at least 5 months. The benefit of the resulting coupled gold nanorods in terms of stability and field enhancement was assessed by **surface enhanced Raman spectroscopy** and extinction spectroscopy opening new perspectives to this challenging field.

References:

[1] L. Guerrini and D. Graham, *Chem. Soc. Rev.*, 2012, **41**, 7085-7107.
[2] M. Grzelczak, A. Sanchez-Iglesias, H. H. Mezerji, S. Bals, J. Perez-Juste and L. M. Liz-Marzan, *Nano Lett.*, 2012, **12**, 4380-4384.
[3] A. F. Stewart, A. Lee, A. Ahmed, S. Ip, E. Kumacheva and G. C. Walker, *ACS Nano*, 2014, **8**, 5462-5467.
[4] Haidar, I.; Aubard, J.; Levi, G.; Lau Truong, S.; Mouton, L.; Neuville, D.; Felidj, N.; Boubekeur-Lecaque, L. *J. Phys. Chem. C* **2015**, 119, 23149-23158

Experimental studies and electromagnetic modeling of localized plasmon surface on a new SERS platform

M.Edely[1], *N.Delorme*[1], *G.Louarn*[2], *L.Douillard*[3], *J-F.Bardeau*[*1]

[1] Institut des Molécules et Matériaux du Mans - UMR CNRS 6283- PRES LUNAM - Université du Maine, Avenue Olivier Messiaen, F-72085 Le Mans Cedex 9, France
[2] Institut des Matériaux Jean Rouxel, Université de Nantes, BP 32229, F-44322 Nantes, France
[3] Nanophotonics Laboratory, Service de Physique de l'État Condensé, IRAMIS, CEA, UMR CNRS 3680 F-91191 Gif-sur-Yvette Cedex, France

**e-mail: Jean-Francois.Bardeau@univ-lemans.fr*

Keywords: SERS, gold, lithography, nanostructuration,

Introduction

Since the first observation of Surface Enhanced Raman Scattering (SERS) in 1974 [1], a variety of methods have been developed to control physically the arrangement of metallic nanostructures onto a surface in order to enhance Raman signals. It is now generally believed that the magnitude of the SERS enhancement factor is mainly driven by the enhanced local electromagnetic field in nanostructured metal surfaces [2]. Previous studies revealed that gaps between adjacent nanoparticles or roughness give rise to strong enhancement effects, often referred as 'hot spots'. Therefore, one way to produce highly efficient SERS substrates is to develop a reproducible system of interacting metal nanostructures capable of high field enhancement.

Results and Discussion

In 2014, we patented a force-assisted Atomic Force Microscopy lithographic method [3] allowing fabricating a metallic substrate locally decorated with various nanostructures of dots, lines, grids, concentric circle,.(**Figure 1)**

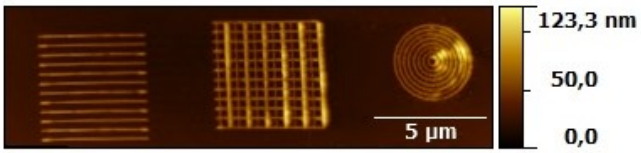

Figure 1: AFM image of a substrate decorated with different nanostructure geometries

It will be shown that this method provides a relatively simple approach to realize reproducible patterns with controlled geometry that can be used for the study of the influence of the pattern geometry on the SERS effect, (**Figure 2**).

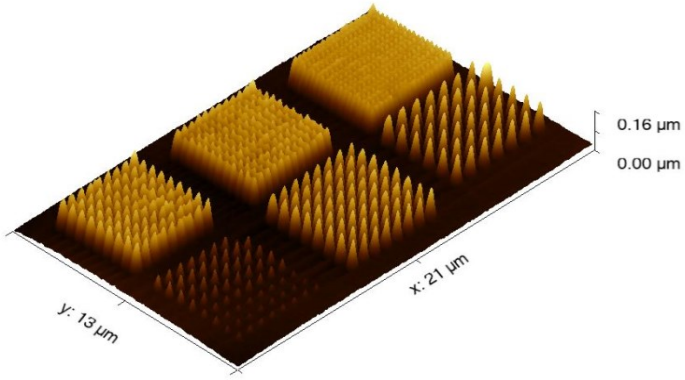

Figure 2 : Lithographically designed substrate with different periodic nanostructured gold surfaces

Whereas electric field enhancement regions (Hot spot) are characterized with PhotoEmission Electron Microscopy (PEEM) (**Figure 3**), SERS effect is demonstrated by performing Raman measurements using several standard molecules (Crystal Violet and Thiophenol) (**Figure 4**).

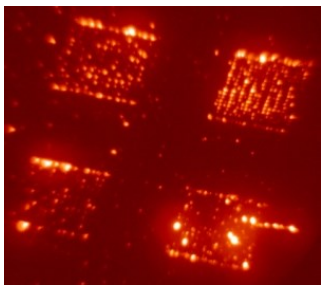

Figure 3 : PEEM picture of nanstructured gold surface (= 624 nm)

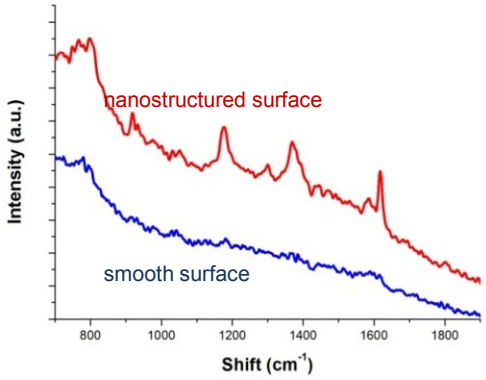

Figure 4 : Raman spectra of crystal violet molecules adsorbed on nanostructured substrate after incubation in a 10^{-6} M solution.

In order to investigate the relationship between optical properties and the pattern geometry localized surface plasmon resonance (LSPR) and surface-enhanced Raman scattering (SERS) gains are simulated using COMSOL Multiphysics®.

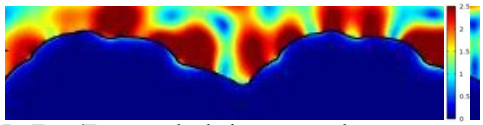

Figure 5 : $E_{local}/E_{incident}$ calculation on a real nanostructure profile

Conclusion

Correlations between PEEM measurements, Raman exaltation and local field calculations are presented in relation with the geometrical parameters of the nanostructures patterns.

References

[1] Fleischmann, M., P.J. Hendra, and A.J. McQuillan, *Raman spectra of pyridine adsorbed at a silver electrode.* Chemical Physics Letters, 1974. **26**(2): p. 163-166.
[2] Moskovits, M., *Surface-enhanced spectroscopy.* Reviews of Modern Physics, 1985. **57**(3): p. 783-826.
[3] FR Patent deposit n° 1461880, December 2014

Optical properties of 1-D plasmonic nanogratings and coupling effects in their hybrid systems with small-molecule organic semiconductors

D. A. Gollmer, C. Lorch, F. Schreiber, D. P. Kern, M. Fleischer***

Institute for Applied Physics and Center LISA$^+$, University of Tuebingen, Auf der Morgenstelle 10, 72076 Tuebingen, Germany

**e-mail: dominik.gollmer@uni-tuebingen.de*
***e-mail: monika.fleischer@uni-tuebingen.de*

Keywords: plasmonic gratings, lattice resonances, absorption enhancement, enhanced fluorescence

Introduction

Plasmonic nanostructures have been thoroughly investigated in recent years [1]. By preparing hybrid systems of such structures and organic molecules, the optical properties of the hybrid systems can be tuned [2, 3]. These include the enhancement of spontaneous emission and light absorption [2-4]. These properties are related to localized plasmon resonances (LSPR) [2-4]. Beside the plasmonic resonances of single structures also collective modes can occur when arranging these structures in chains or gratings with separations of the single structures in the range of optical wavelengths [5,6]. A special type of such collective resonances are parallel lattice resonances which occur when the electric field vector of the incident light is parallel to the wave vector which is added through diffraction by the grating [7]. These modes have been just recently investigated in 2-D gratings [7,8].

We fabricated 1-D plasmonic nanogratings with different geometries of the single structures, which show parallel grating modes. The optical properties of these systems were investigated by white light extinction spectroscopy with angle-resolved illumination. The plasmonic systems are combined with the small-molecule organic semiconductor diindenoperylene (DIP) for investigation of enhanced absorption and fluorescence emission in this hybrid system.

Results and Discussion

Two types of plasmonic systems were investigated, planar Au gratings with line widths in the range of 100 nm and heights of 20-30 nm and wedge-shaped gratings with a width at the base of ~100 nm and a height of ~120 nm (**Figure** 1b). For the investigation of the optical properties of these systems white light extinction spectroscopy was used with TM- and TE-polarized incident light for different illumination angles from 0-20°. The planar gratings were combined with the small-molecule organic semiconductor diindenoperylene. The DIP-film with a thickness of ~20 nm is evaporated under ultra-high vacuum conditions. For this system extinction and fluorescence measurements were performed. The results of the optical properties of the plasmonic systems and the hybrid systems are compared to simulations with the finite element method.

The results for the characterization of the bare plasmonic grating systems show LSPR and grating induced modes (**Figure** 1a). For nanogratings with wedge-shaped structures beside the in-plane localized plasmon resonance, also out-of-plane localized modes occur for oblique illumination (**Figure** 1a), similar to modes that have been observed for plasmonic nanocones [9]. The localized modes and the collective modes in this system show an avoided crossing behaviour, which also have been observed for in-plane LSPRs and orthogonal lattice resonances in 2-D plasmonic gratings [10].

The results of the optical characterization of the hybrid system consisting of the plasmonic system and the organic film indicate an enhanced absorption in the DIP-Film. Additionally the fluorescence properties of this hybrid system were investigated. These results show an enhanced and polarized emission which correlates with the optical properties of the plasmonic grating.

The data of the optical characterization of the planar and wedge-shaped plasmonic gratings by white light extinction geometry will be shown together with results of simulations of the plasmonic systems. Additionally data of the extinction measurements and of the fluorescence measurements for the hybrid systems will be presented.

Conclusions and Outlook

In this work, the optical properties of 1-D plasmonic nanogratings and hybrid systems of the nanogratings and an organic semiconductor were investigated. Planar nanogratings and wedge-shaped systems were fabricated and optically characterized by white light extinction spectroscopy. The planar plasmonic system was combined with a small-molecule organic semiconductor. The results of the optical characterization of this system indicate an enhanced absorption in the DIP. Additionally enhanced and polarized fluorescence of the organic semiconductor in the hybrid system was observed. The absorption and emission properties of the hybrid systems are related to LSPRs of the single structures or collective modes in the plasmonic nanogratings.

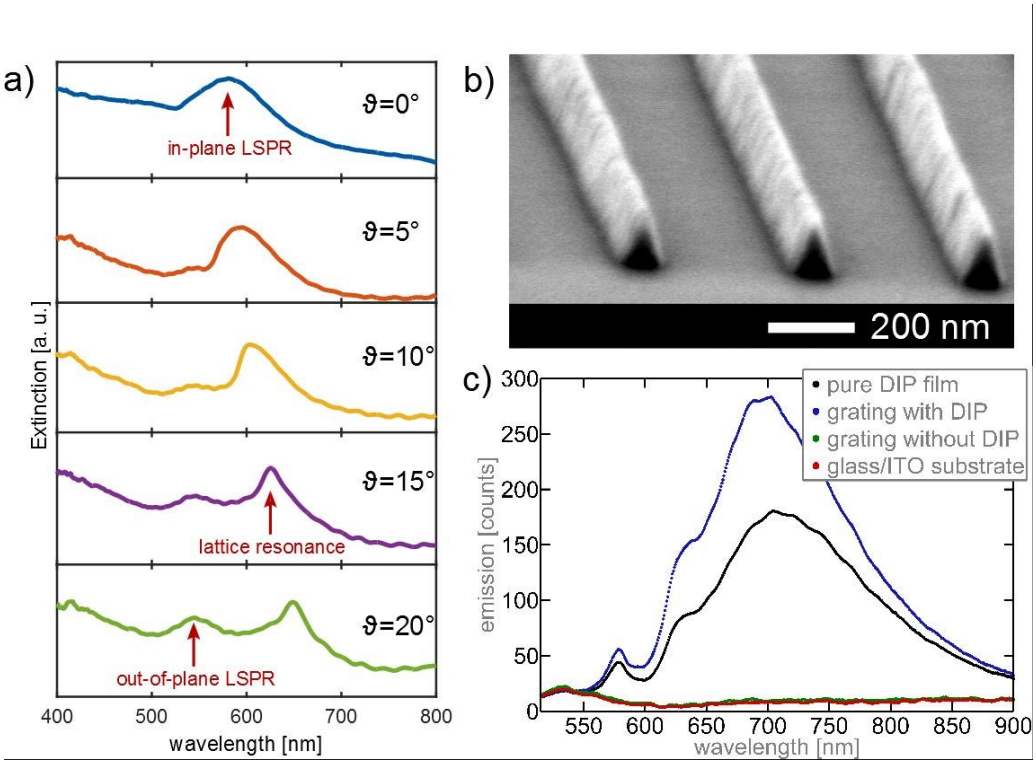

Figure 1: a) Extinction spectra of a wedge-shaped gold nanograting (period 350 nm) for different illumination angles. Several different modes can be observed. b) SEM image of a Au wedge-shaped nanograting (viewing angle 80°). c) Fluorescence spectra of a DIP-film on a planar nanograting (period 400 nm) and a pure DIP-film. Additionally the very low fluorescence signal of the substrate and the bare Au grating is shown. [11, 12]

In further experiments the enhancement mechanisms through localized plasmon modes or lattice resonances will be investigated. This way enhanced absorption or emission in hybrid systems for specific wavelengths in the visible may be achieved by using parallel lattice resonances. The optical properties of the 1-D plasmonic nanogratings in such a system can be spectrally tuned by the grating geometry without changing the geometry of the single structures.

References:

[1] Kreibig U, Vollmer M; Optical properties of metal clusters; Springer; Berlin Heidelberg; (1995)
[2] Anger P, Bharadwaj P, Novotny L; Enhancement and Quenching of Single-Molecule Fluorescence; Physical Review Letters; 96 (2006)
1130021-1130024
[3] Sugawara Y, Kelf T A, Baumberg J J, Abdelsalam M E, Bartlett P N; Strong Coupling between Localized Plasmons and Organic
Excitons in Metal Nanovoids; Physical Review Letters; 97 (2006) 2668081-2668084
[4] Kühn S, Håkanson U, Rogobete L, Sandoghdar V; Enhancement of Single-Molecule Fluorescence Using a Gold Nanoparticle as an
Optical Nanoantenna; Physical Review Letters; 97 (2006) 0174021-0174024
[5] Meier M, Wokaun A, Liao P F; Enhanced fields on rough surfaces: dipolar interactions among particles of sizes exceeding the Rayleigh limit; J. Opt. Soc. Am. B; 2 (1985) 931-949
[6] Zou S, Schatz G C; Narrow plasmonic/photonic extinction and scattering line shapes for one and two dimensional silver nanoparticle arrays; The Journal of Chemical Physics; 121 (2004) 12606-12612
[7] Vitrey A, Aigouy L, Prieto P, García-Martín J M, González M U; Parallel Collective Resonances in Arrays of Gold Nanorods; Nano
Letters; 14 (2014) 2079-2085
[8] Lin L, Yi Y; Orthogonal and parallel lattice plasmon resonance in core-shell SiO2/Au nanocylinder arrays; Optics Express; 23 (2015)
130-142
[9] Schäfer C, Gollmer D A, Horrer A, Fulmes J, Weber-Bargioni A, Cabrini S, Schuck P J, Kern D P, Fleischer M; A single particle plasmon resonance study of 3D conical nanoantennas; Nanoscale; 5 (2013) 7861-7866
[10] Väkeväinen A I, Moerland R J, Rekola H T, Eskelinen A P, Martikainen J P, Kim D H, Törmä P; Plasmonic Surface Lattice Resonances
at the Strong Coupling Regime; Nano Letters; 14 (2014) 1721-1727
[11] Gollmer D A, Kern D P, Fleischer M; Coupling of out-of-plane localized modes and collective modes in 1-D plasmonic wedge-shaped gratings; in preparation
[12] Gollmer D A, Lorch C, Schreiber F, Kern D P, Fleischer M; Polarized and enhanced fluorescence emission in a plasmonic nanograting/organic semiconductor hybrid system; in preparati

The influence of graphene on the optical properties of plasmonic bioconjugate

Izabela Kamińska[a,b], Magdalena Twardowska[a], Kamil Wiwatowski[a], Justyna Grzelak[a], Sebastian Maćkowski[a]

[a] Institute of Physics, Department of Physics, Astronomy and Informatics, Nicolaus Copernicus University, Toruń, Poland

[b] Institut für Physikalische & Theoretische Chemie – NanoBioSciences, TU Braunschweig, Germany

e-mail: ikaminska@fizyka.umk.pl

Keywords: graphene, fluorescence, photosynthetic complexes, silver nanowires, energy transfer

Graphene and related 2D carbon materials have become very important from the point of view of applications in sensing, optoelectronics, and alike.(1) Due to its two-dimensionality and consequent optical properties graphene is a very good energy acceptor.(2) The factors that strongly influence the efficiency of fluorescence resonance energy transfer are: a distance between a donor and an acceptor, and structural properties of graphene.(3) It is also well-known that optical properties of emitters can be strongly influenced in the presence of metallic nanostructures.

In this work we use confocal microscopy and time-resolved fluorescence spectroscopy to study energy transfer in three-component system containing natural photosynthetic complexes, silver nanowires and graphene. We found that the fluorescence of photosynthetic complexes, primarily enhanced by silver nanowires due to plasmonic interactions (4), can be efficiently quenched by graphene. We focus on determining factors influencing the efficiency of this process. The ability to describe excitation energy dependence of the energy transfer efficiency is provided by broad absorption of photosynthetic complexes, spanning over the whole visible range. Energy transfer was also studied for varied graphene morphologies and arrangement of all components.

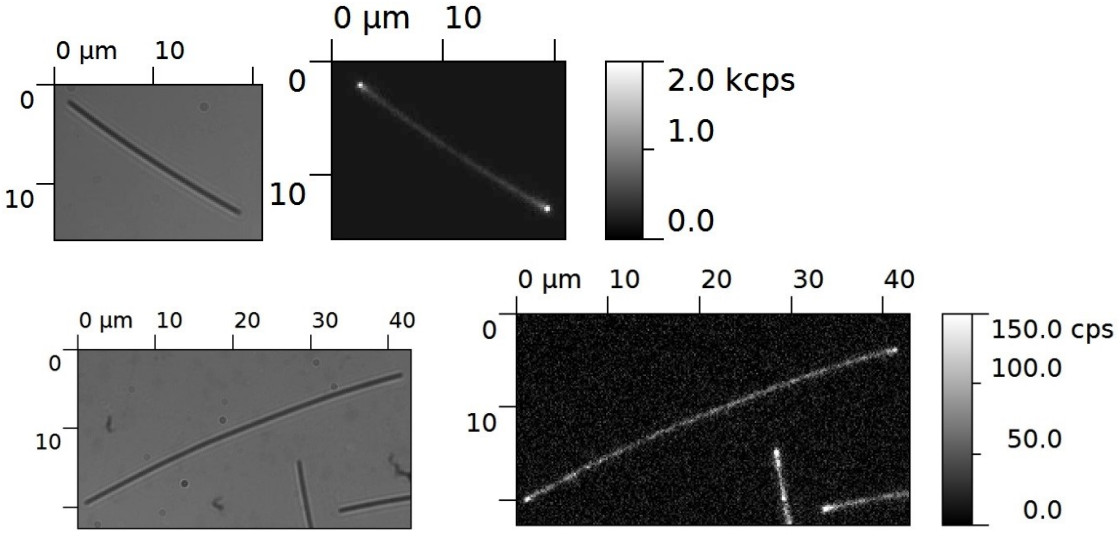

Figure 1: Transmission images and fluorescence of PCP-silver nanowires bioconjugates on a glass and graphene.

The results, which indicate pronounced energy transfer in our structures that strongly depends on the mutual orientation of donor and acceptor, as well as the number of graphene layers, show considerable potential for using graphene as a component of biologically functional hybrid nanostructures.

Research was supported by the DEC-2013/10/E/ST3/00034 project from the National Research Center of Poland and the grant ORGANOMET No: PBS2/A5/40/2014 from the National Research and Development Center (NCBiR). IK acknowledges support from the Foundation for Polish Science.

References:

[1] Novoselov K S, Fal'ko V I, Colombo L, Gellert P R, Schwab M G, Kim K; A roadmap for graphene; Nature; 490 (2012) 192-200;

[2] Nair R. R.; Blake P.; Grigorenko A. N.; Novoselov K. S.; Booth T. J.; Stauber T.; Peres N. M. R.; Geim A. K. Fine structure constant defines visual transparency of graphene *Science* **2008**, 320, 1308.

[3] Gaudreau, L.; Tielrooij, K.J.; Prawiroatmodjo, G.E.D.K.; Osmond, J.; García de Abajo, F.J.; Koppens, F.H.L. Universal Distance-Scaling of Nonradiative Energy Transfer to Graphene *Nano Lett.* **2013**, 13, 2030-2035.
[4] Kowalska, D.; Krajnik, B.; Olejnik, M.; Twardowska, M.; Czechowski, N.; Hofmann, E.; Maćkowski S. Metal-Enhanced Fluorescence of Chlorophylls in Light-Harvesting Complexes Coupled to Silver Nanowires *The Scientific World Journal* **2013,** 2013, 670412.

J-aggregation of cyanine dyes on the surface of noble metal nanoparticles

V.Vasić

Vinča Institute of Nuclear Sciences, University of Belgrade,P.O. Box 522, Belgrade, Serbia
e-mail: evasic@vinca.rs

Keywords: thiacyanine dyes, J – aggregation, Au, Ag nanoparticles

Introduction

The natural light harvesting complexes (LHCs) of plants and photosynthetic bacteria are one of the most fascinating functional molecular assemblies. Their main purpose is strong absorption of light followed by fast energy transfer to neighboring LHCs and the photochemical reaction centre where an electron transfer process leads to charge separation[1]. The effectiveness of these processes relies on two fundamental physicochemical principles. First *self-organization* of dye molecules, preferentially of chlorophyll derivatives mediated by proteins, into precisely ordered structures of large spatial size to obtain extraordinarily high cross-sections for light absorption. Second, extremely fast *energy migration* of the absorbed light within the LHC can ensure that the excitation energy is extremely fast available at any place where it is needed for photo-induced energy or electron transfer (PET) processes.

The self-association of dyes in solution or at the solid-liquid interface is a frequently encountered phenomenon in dye chemistry owing to strong intermolecular van der Waals-like attractive forces between the molecules. The aggregates in solution exhibit distinct changes in the absorption band as compared to the monomeric species. In order to achieve a high degree of molecular order, it was tried to build artificial light harvesting systems by adsorbing dye molecules on solid substrates. In such heterogeneous systems, the underlying crystal lattice of the solid substrate acts as a matrix for stable fixation and precise stacking of the dye molecules by epitaxial growth.

H- and J-aggregation of cyanine dyes

Cyanine dyes is the non-systematic name of a synthetic dye family belonging to polymethine group of compounds, synthesized to build up artificial light harvesting systems. They consist of two nitrogen centers, one of which is positively charged and is linked by a conjugated chain of an odd number of carbon atoms to the other nitrogen[2]. Two nitrogens are joined by a polymethine chain, each of them being the independent part of a heteroaromatic moiety, such as pyrrole, imidazole, thiazole, pyridine, quinoline, indole, benzothiazole. They have the wide application in many fields of science and practice. Firstly, they are used to increase the sensitivity range of photographic emulsions, and also to label proteins, antibodies, peptides, nucleic acid probes, and any kind of other biomolecules to be used in a variety of fluorescence detection techniques. The structural formula of the cationic thiacyanine dyes is presented in Fig.1.

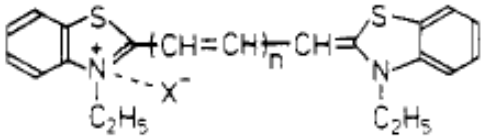

Figure 1 General structure formula of polymethine thiacyanine days: n- number of methyl groups, X^- = Br^-, Cl^-, ClO_4^-, and various anions

An outstanding feature of cyanine dyes is the very high ground state polarizability of the π-electrons along the polymethine group in the ground state, which gives rise to strong dispersion forces (van der Waals forces) between two cyanine molecules in solution [28, 29]. International Journal of Photoenergy Volume 2006, Article ID 20363, Pages 1–21). One of the main features of cyanine dyes is their ability for spontaneous self-organization into highly ordered aggregates of various structures and morphologies (International Journal of Photoenergy, Volume 2006, Article ID 20363).. They can be organized in a parallel way (plane-to plane stacking) to form a sandwich-type arrangement (H-dimmer) or in a head-to-tail arrangement (end-to end stacking) to form J-dimmer. This organization enables the high polarizability of the π-electrons along the polymethine group in the ground state and the efficient exciton coupling including the fast exciton energy migration. Extensive studies on J - and H - aggregates have resulted in the proposal that these aggregates exist as a one - dimensional assembly in solution that could be in brickwork, ladder, or staircase type of arrangement [3](Fig.2). They have the high polarizability of the π-electrons along the polymethine group in the ground state and are characterized by the efficient exciton coupling and fast exciton energy migration over thousands of molecules within a few picoseconds.

Figure 2. Schematic representation of the different arrangement of

The dye molecule is regarded as a point dipole and the excitonic state of the dye aggregate splits into two levels through the interaction of transition dipoles. An electron transition to the upper state in parallel aggregates having parallel transition moments and to a lower state in a head - to - tail arrangement with perpendicular transition moments leads to hypsochromic (red) and bathochromic (blue) shifts of the absorption spectra, respectively[3] (Fig.3).

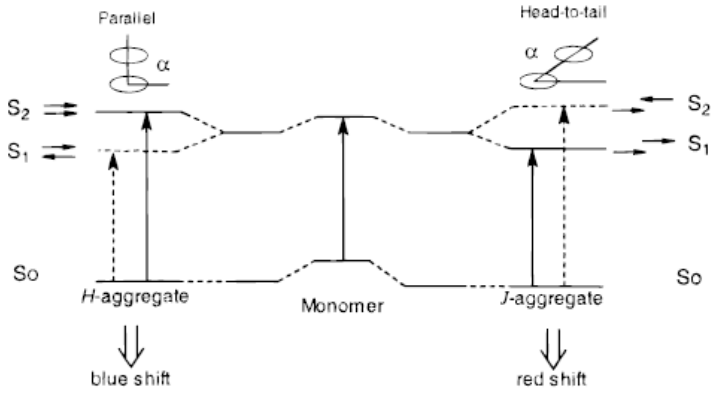

Figure 3. Schematic representation of the relationship between chromophore arrangement and spectral shift

H- and J-aggregation is strongly dependent on dye concentration, ionic strength, pH, dielectric constant, metal ions, nanoparticles, polymers, and also on solid surface. However, the molecules show novel properties, such as linear and nonlinear optical response, photoelectric, photorefractive, photochromism, superradiance, superfluorescence, electroluminescence, photoluminescence, attenuated total reflection which have the applications in major fields of science. As an example of concentration dependent self organization of cyanine dyes, Fig.4 shows the absorption spectra of thiacarbocyanine (TCC), the dye which forms both H- and J- aggregates which are dependent on its concentration in solution.

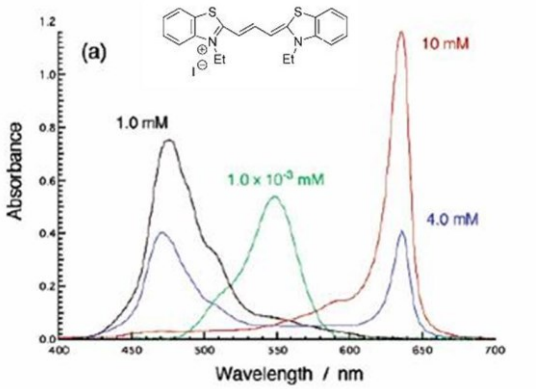

Figure 4. *Absorption spectra of thiacarbocyanine (TCC)*

J-aggregation of thiacyanine dyes on nanoparticles surface

Noble metal nanostructures consisting of Au or AgNPs have been studied extensively because of their unique optical properties arising from localized surface plasmon resonance in the visible region. Modification of their surface by thiacyanine dyes leads to changes in their electronic properties[4-7]. The modulation of the chromophore's optical characteristics is obtained due to the electronic coupling of the dye exciton to the polarization of the metal NPs. However, thiacyanine dyes form J-aggregates on the surface of silver and gold

nanoparticles (NPs) which strongly depend on particle size and surface capping, as well on the dyes structure. Self-organization of these molecules mediated by NPs is especially interesting because of the application of dye – NPs assemblies for nanoelectronics, medical diagnostics, drug delivery, chemical sensing and catalysis. The hybrid J-aggregate –NPs assemblies are usually characterized by UV-vis spectrophotometry, TEM, AFM, DLS, FTIR, Raman spectroscopy, fluorescence measurements and DFT calculations.

In our studies, we focused mainly on the J-aggregation of the anionic thyacyanine dye 3,3'-disulfopropyl-5,5'-dichlorothiacyanine sodium salt (TC) on the surface of citrate and borate capped Au and AgNPs which were obtained by the reduction of Au(III) or Ag(III) solution by Na-citrate or $NaBH_4$. TEM and AFM measurements confirmed that NPs were spherical in shape with the particle size diameter from 6 – 30 nm. Their negative surface charge was confirmed by zeta potential and particle mobility measurements, suggesting their surface covering by citrate or borate anions. The initial Au and Ag colloid dispersions exhibit an intense surface plasmon resonance (SPR) peak at ~520 nm and ~387 nm, respectively. Their positions are sensitive on the size and shape of the NPs as well as on the dielectric constant of the medium.

The formation of the TC dye J-aggregates on the surface of the NPs was followed by the appearing of a characteristic deep in the case of AuNPs or new peak in the case of AgNPs, both at 481 nm (Fig. 5) due to a coupling of J-aggregate excitons and polarizations in NPs. The position of the deep and the peak is very close to the position of J – band of the pure dye (464 nm)[4,8]. However, the stability and intensity of the absorbance is strongly dependent on TC, NPs and KCl concentrations, time as well as on NPs type. Moreover, the spectral deep appeared only by AuNPs with 6 nm particle diameter[4], which were obtained by borhydride reduction of Au(III) salt.

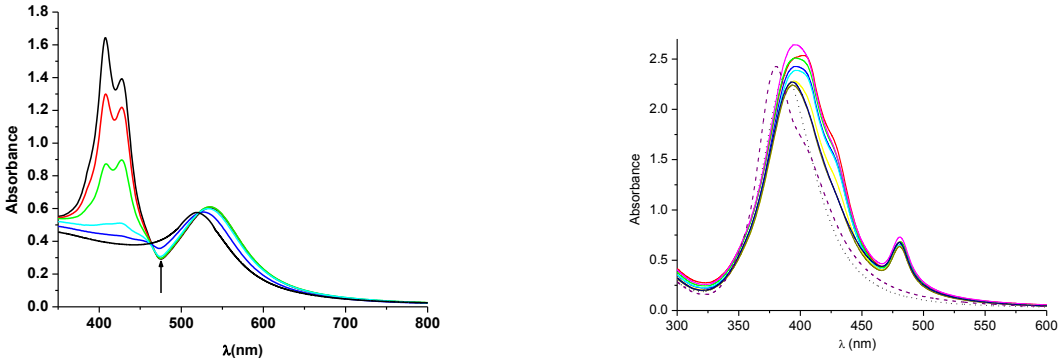

Fig. 5. Absorption spectra of Au (left) and Ag colloidal dispersion in the presence of TC; concentrations from 0 - 1.67×10^{-5} M[

The TEM study of NPs in the presence of TC dye confirmed aggregation tendency (Fig. 6), visible also in the slightly change of the plasmon position in the absorption spectra of dye – NPs assembly[4]. The reason for this behavior is attributed to TC molecules adsorbed on NPs surface in J-aggregate forms, which are involved in the interlinking of NPs. However, the question aroused how partially negative SO_3^- groups of TC dye will overcome the electrostatic barrier imposed by negatively charged citrate anions or borate anions which are tightly bound to the NPs surface.

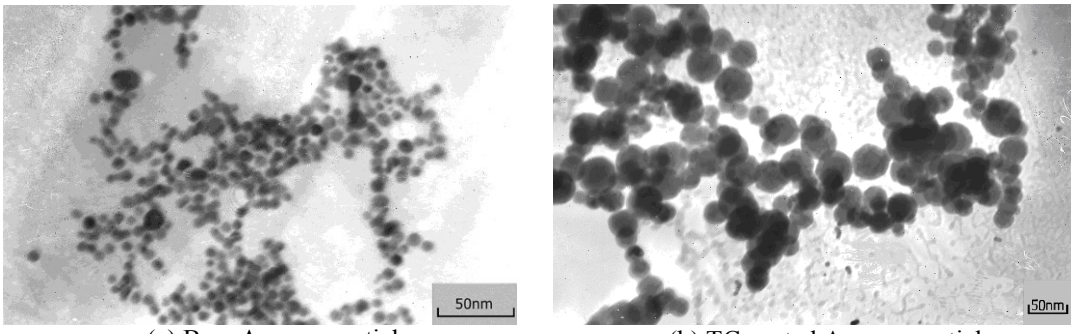

(a) Bare Au nanoparticles (b) TC coated Au nanoparticles

Figure 6. TEM analysis of (a) bare Au nanoparticles and (b) TC-coated Au nanoparticles.

Using the simple model which considered NPs surface as a single atom, interacting with different parts of the dye molecule anion, DFT calculations were performed to elucidate the mode of TC binding to the NPs surface. It must also be taken into account that TC J-aggregation on AgNPs occurs only in the presence of K^+ ions in significant excess. The precise surface model, consisting of 18-atom metal cluster was used for calculation. The conclusion was made that TC dye is, from the thermodynamical point of view, most likely to interact with Au and

AgNPs via oxygen atom from SO_3^- groups. The attractive interaction between adsorbed citrate or borate anions and K^+ ions provides a thermodynamical driving force to drive at least one K^+ ion per adsorbed anion out of its hydratation sphere and deposit it onto the AgNP surface. As the consequence, the interaction between K^+ ions and adsorbed citrate inevitably weakens citrate adsorption on the AgNPs surface, thus favoring replacement of anion by TC dye.

In the elucidation of dyes binding on the surface of NPs, they are usually considered as macromolecules with several binding sites and dye is considered as a ligand. The dye - NPs assemblies usually exert concentration-dependent fluorescence quenching properties[6,7,9], Fig.7. The analysis of the Stern–Volmer relation, accounting for both static and dynamic quenching, suggests that NPs quench the fluorescence with an extraordinarily high Stern–Volmer constant (K_{SV}) in the range of $10^8 M^{-1}$ in many cases. Additionally, the kinetics of J-aggregation of dyes in the presence of NPs was studied using a stopped–flow technique. Kinetic measurements performed as a function of the dye and NPs concentration, yielded sigmoid kinetic curves[5,8]. The concentration dependence of the parameters of the kinetic curves indicated that J-aggregate formation on the NPs surface occurred via a two-step process; the first was adsorption of the initial dye layer, followed by the growth of consecutive layers[4,8].

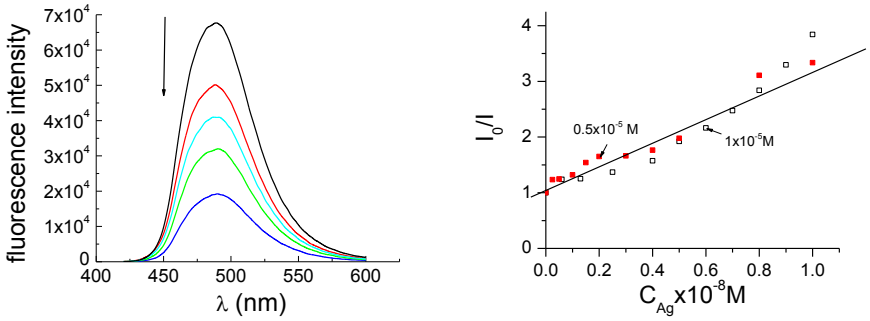

Figure 7. Concentration dependent fluorescence quenching of TC induced by increase of AgNPs concentration(right) and Stern Volmer graph for this process

Conclusions and/or Outlook

The interaction of Au and AgNPs with the thiacyanine dyes is very well characterized by application of various nanospecroscopic methods, such as UV Vis spectroscopy, fluorescence spectroscopy, TEM, AFM, DLS, FTIR, Raman spectroscopy and other techniques. However, the mechanism of interaction can be elucidated by application of the methods considering NPs as macromolecule and dye as ligand. DFT calculations usually clarify and the nature of dye binding to NPs surface. Moreover, NPs with different capping agents and with a wider range of diameters will be synthetized, for future use in medical diagnostics, catalysis, drug delivery, nanoelectronics and for chemical sensing.

References:

[1] X. Hu, T. Ritz, A. Damjanovi´c, and K. Schulten, Pigment organization and transfer of electronic excitation in the photosynthetic unit of purple bacteria, J. Physi. Chem.y: B, 101, no. 19, (1997) 3854–3871.

[2] T. B. Tang, H. Yamamoto, K. Imaeda, H. Inokuchi, Electronic Structure of Thiacyanine Dyes in the Solid State, J. Phys. Chem. 93 (1989) 3970-3973

[3] G. B Behera, P. K. Behera, B. K. Mishra, Cyanine dyes: self organization and behavior in surfactants, J.Surface Sci. Technol., 23(1-2) (2007) 1-31

[4]Ana Vujačić, Vesna Vasić, Miroslav Dramićanin, Sofija P. Sovilj, Nataša Bibić,Jasmina Hranisavljevic and Gary P. Wiederrecht Kinetics of J-Aggregate Formation on the Surface of Au Nanoparticle Colloids, J. Phys. Chem. C 116(7) (2012) 4655−4661

[5] Laban B, Vodnik V, Vasić V; Spectrophotometric observations of thiacyanine dye J-aggregation on citrate capped silver nanoparticles, Nanospectroscopy 1 (2015) 54–60

[6]Ana Vujačić, Vesna Vodnik, Sofija P. Sovilj, Miroslav Dramićanin, Nataša Bibić, Slobodan Milonjić and Vesna Vasić, Adsorption and Fluorescence Quenching of 5,5'-disulfopropyl-3,3'-dichlorothiacyanine Dye on Gold Nanoparticles, New Journal of Chemistry, New J. Chem., New J. Chem., 37 (2013) 743--751

[7] Vujačić, Ana; Vasić, Vesna; Dramićanin, Miroslav; Sovilj, Sofija; Bibić, Nataša; Milonjić, Slobodan; Vodnik, Vesna, Fluorescence Quenching of 5,5'-Disulfopropyl-3,3'- Dichlorothiacyanine Dye Adsorbed on Gold Nanoparticles, J. Phys. Chem. C, 117 (2013) 6567−6577….

[8]Laban B, Vodnik V, Dramićanin M , Novaković M, Bibić N, Sovilj S, Vasić V, Mechanism and kinetics of J-aggregation of thiacyanine dye in the presence of silver nanoparticles, *J. Phys. Chem. C*, 118 (40) (2014) 23393–23401.

[9] B. B. Laban, V. Vodnik, A. Vujačić, S. P. Sovilj, A. B. Jokić, V. Vasić, Spectroscopic and fluorescence properties of silver-dye composite nanoparticles, Russian Journal of Physical Chemistry A, 87(13) (2013) 2219–2224.

Coupled Metal-Nanoparticles near the Contact-Limit

Gernot Schaffernak, Markus K. Krug, Joachim R. Krenn, Andreas Hohenau*

Institute of Physics, University of Graz, Universitätsplatz 5, 8010 Graz, Austria

**e-mail: gernot.schaffernak@uni-graz.at*

Keywords: strong coupling, nanoparticles, plasmonics, contact-limit

Introduction

Metal nanoparticles interact with light through their free conduction electrons. At optical wavelengths, the electrons act as a plasma and the collective charge-density oscillations driven by the radiation are called plasmons. Surface plasmon resonances lead to a very strong optical near-field that can be further enhanced by electromagnetic coupling of two nanoparticles separated only by a fraction of the optical near-field range. Strong coupling affects the charge distribution at the resonance wavelengths and leads to plasmon hybridization [1].

Results and Discussion

We approach this strong coupling regime experimentally and present results from lithographically fabricated gold particle-pairs with controlled vertical gap widths in the range of 1-20 nm [2]. Measured extinction spectra of coupled particle pairs are compared to the results of simulations done with the boundary element method [3]. Special emphasis is put on the dispersion relations of the coupled system of two particles with respect to previous work for single particles [4].

An example for the measured extinction spectra for gold disks of diameter 100 nm and height 30 nm as well as for coupled gold disks separated by a 10 nm SiO_2 layer is given in **Figure 1**.

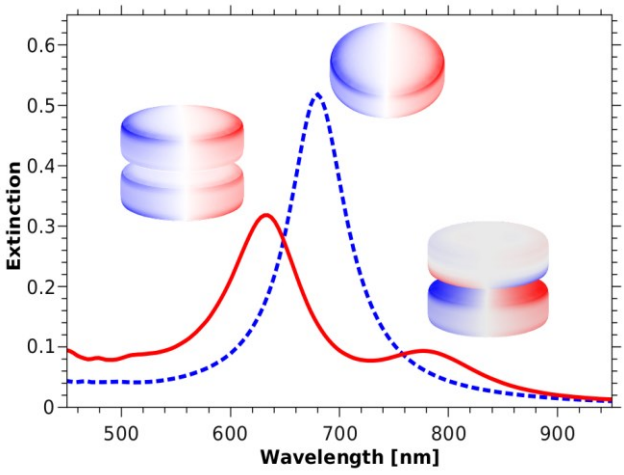

Figure 1: Optical extinction spectra of single gold disks and pairs of particles separated by a 10 nm dielectric layer. The insets show the simulated surface charge distribution at the peaks.

Conclusions and Outlook

As the inter-particle distance can be controlled very well for this structure, it is well-suited to study the enhanced interaction with fluorophores embedded in the spacer layer, and first results from dye molecules in the gap region are presented.

Acknowledgements

Funding by FWF (project P 25034) and NAWI Graz is gratefully acknowledged.

References:

[1] Dmitriev A, Pakizeh T, Käll M, Sutherland D S; Gold–Silica–Gold Nanosandwiches: Tunable Bimodal Plasmonic Resonators; small; 3 (2007) 294-299;

[2] Schaffernak G, Gruber C, Krenn J R, Krug M K, Gašparić M, Belitsch M, Hohenau A; Fluorescence coupling to plasmonic nanoparticles; Photonics, Devices, and Systems VI, Proc. SPIE; 9450 (2015) 94501S;

[3] Hohenester U, Trügler A; MNPBEM – A Matlab toolbox for the simulation of plasmonic nanoparticles; Comp. Phys. Commun.; 183 (2012) 370;

[4] Schmidt F, Ditlbacher H, Hohenester U, Hohenau A, Hofer F, Krenn J R; Universal dispersion of surface plasmons in flat nanostructures; Nature Communications; 5 (2014) 3604

Hydrogen Chemical Configuration and Stability in Hydrogen Plasma Exposed Tungsten Disulfide Nanoparticles

A. Laikhtman[a], *A. Zak*[a], *M. Sezen*[b], *J. Alonso*[c], *J. I. Martinez*[d], *and M. Enachescu*[e]

[a] Holon Institute of Technology (HIT), Holon, Israel
[b] Sabanci University Nanotechnology Research and Application Center (SUNUM), 34956 Istanbul, Turkey
[c] Department of Theoretical, Atomic and Optical Physics, University of Valladolid, Valladolid, Spain
[d] Institute of Material Science of Madrid (ICMM-CSIC), Madrid, Spain
[e] Center for Surface Science and Nanotechnology (CSSNT), University Politehnica of Bucharest, Romania

**e-mail: alexl@hit.ac.il*

Keywords: nanoparticles, Raman, hydrogen, DFT, tungsten disulfide

Introduction

inorganic nanotubes (INT) and inorganic fullerene-like (IF) nanoparticles (NP) of WS_2 are appealing as hydrogen storage media because of their extremely high surface area and layered structure, where potentially many sites can either chemi- or physisorb hydrogen. An attempt to test WS_2 INT and IF as possible candidates for hydrogen storage material can be of significant industrial potential. Plasma activated hydrogenation was proposed as a method to improve hydrogen absorption concentration. This enhancement in the hydrogen absorption concentration could be attributed to more effective interaction of activated vs. molecular hydrogen with NP substrate surface and due to higher energy and momentum of the H_2 in the plasma environment. In addition, plasma originated hydrogen ions and electrons may interact with the WS_2 NP producing new or modify existing defects and pores, and so contribute to hydrogen binding, diffusion and higher stability. The main goal of this work is to study chemical configuration of the absorbed hydrogen and to elaborate on its thermal stability inside the WS_2 NP. Micro-Raman spectroscopy was extensively used to evaluate chemical configuration of hydrogenated compounds due to its capability to detect chemical bonds involving hydrogen atoms.[1,2] It is highly sensitive and allows to discover molecular hydrogen inside amorphous and crystalline solids.[2] In addition, we used deuterium plasma instead of hydrogen in several experiments to unambiguously prove that the measured features are due to the hydrogenation by plasma and not due to residual water or hydrogen retained from the synthesis of WS_2 NP. Transmission electron microscopy (TEM) and electron diffraction (ED) analysis of NP after plasma treatment was used to accurately examine the pristine changes on the individual NPs' surface and in their interlayer distances.

Results and Discussion

To determine the chemical configuration of the absorbed hydrogen, micro-Raman measurements were performed. The laser induced heating accounted for a significant problem, as it could result in immediate desorption of hydrogen from the irradiated sample area and oxidation of WS_2. In order to prevent or diminish these disturbances, the lower laser power was used. The micro-Raman scattering for all samples was measured in the spectral range of 0-4400 cm^{-1}. A narrower region of 3400-4300 cm^{-1} for the hydrogenated and non- hydrogenated NP was measured. In **Figure 1** (lines 1,2) the spectra for INT-WS_2 are presented. A small peak centered at ~4150 cm^{-1} was observed for the hydrogenated samples only. This feature was previously attributed to the H–H stretching mode in H_2 molecules,[2-4] and, therefore, its appearance in our spectra reveals that indeed hydrogen absorption took place and is present in the molecular form. One should take into account a very small Raman cross section of this H-H. We may suppose that H_2 molecules were adsorbed on the surface of the NT, in the hollow core or being intercalated between the layers in the WS_2 NP. To finally prove that the Raman feature measured at 4150 cm^{-1} is indeed due to physisorbed H_2 molecules, the sample was heated in vacuum to 450 ºC for up to 2 h. The intensity of the H_2 mode peak gradually decreased until disappeared, as shown in **Figure 1** (line 3). To determine the presence of chemisorbed hydrogen (H-S bonding) the Raman scattering in the 1500-3000 cm^{-1} region was performed. However, the features which could be attributed to H-S bonds[5] never appeared so indicating that no chemisorbed hydrogen was present in the WS_2 NP. Nevertheless, to unambiguously prove that micro-Raman spectroscopy is indeed capable to reveal molecular hydrogen in WS_2, deuterium gas in the RF plasma was used instead. To determine the chemical configuration of so absorbed deuterium, micro-Raman measurements were performed in the spectral range of 2500-4000 cm^{-1}, as showed in **Figure 2**. Indeed, a small peak, now centered at ~2970 cm^{-1} was observed (**Figure 2**, line 1). This feature was previously attributed to the D–D stretching mode in D_2,[3] and, therefore, its appearance in our spectra proves that deuterium is present in the molecular

form as was in the case of hydrogen. No features related to D-S bonds were observed.[6] Furthermore, RF plasma deuterated WS_2 samples (IF and INT) were heated in vacuum to 450 ºC for up to 2 h. As seen from **Figure 2**, line (2), the intensity of the ~2970 cm^{-1} peak decreased to nearly zero. High resolution ED pattern measured by TEM on the individual NP shows that the interlayer distance of the RF plasma hydrogenated samples increased from 0.62 nm for the unexposed NP to 0.63-0.64 nm for the hydrogenated NP, as presented in **Figure 3**. The intercalation of hydrogen between the WS2 layers could be the native explanation for thisexpansion, however the DFT calculations, shown in the next paragraph, did not confirm this assumption but are rather indicative on adsorption of hydrogen on the surface and its effect on the distance between the inner lying WS_2 layers.

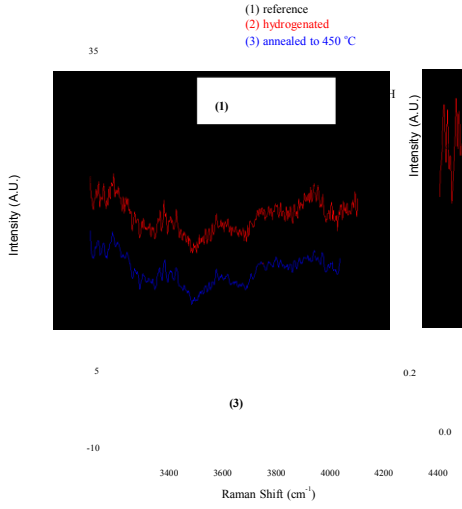

Figure 1. Micro-Raman spectra (1) of the RF-plasma hydrogenated and (2) non-hydrogenated WS_2 NP, (3) annealed.

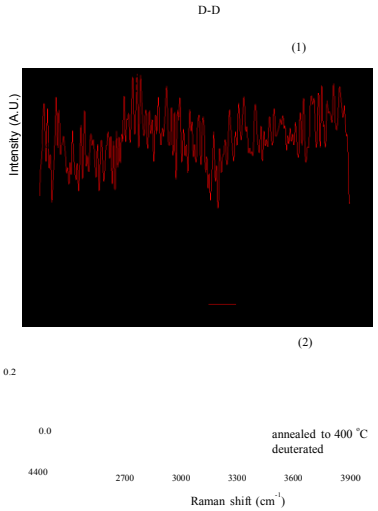

Figure 2. Micro-Raman spectra of (1) deuterated and (2) vacuum-annealed WS_2 NP.

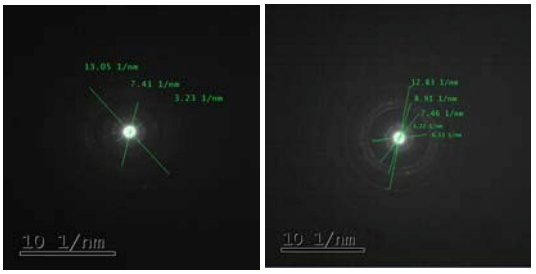

Figure 3. Electron diffraction pattern of the reference (left) and deuterated (right) WS_2 IF-NP.

DFT calculations have been performed to model the adsorption of hydrogen on planar and curved layered WS_2 nanostructures.[7] The H_2 adsorption energies and distances have been monitored as a function of H_2 coverage, ranging between 0.0625 monolayers (ML) coverage up to full 1 ML coverage. The adsorption energies are positive; that is, molecular adsorption is favourable. As the H_2 coverage increases, adsorption energies tend to decrease and adsorption distances tend to increase, although these changes are small. A relevant result is that the H_2 adsorption on the topmost layer of the WS_2 multilayers induces a small increase of the distance between the topmost and the second WS_2 layers, and this decoupling is enhanced by increasing the H_2 coverage: this agrees with the increase of the interlayer distance observed in the ED measurements shown above. The calculations indicate that H_2 can be adsorbed on the surface of the NP and on the outermost and innermost walls of the NT, but cannot be intercalated between layers. This conclusion has been obtained by simulating the intercalation of the trilayer with increasing amounts of molecular hydrogen; more specifically, H_2 molecules were placed in between the first and second layers of the trilayer (**Figure 4**). The energy of intercalation is negative in all cases; that is, intercalation is unfavourable due to the energy needed to largely expand the interlayer distances.

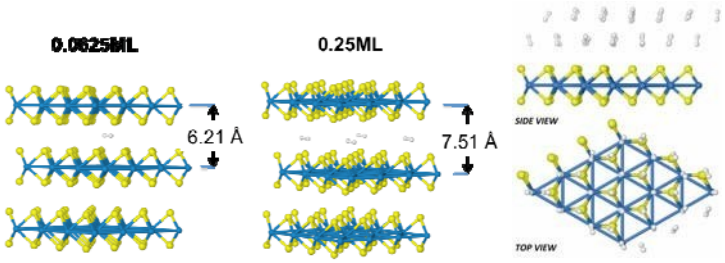

Figure 4. Optimal structures for intercalation of H_2 between the first and the second layers of the WS_2 trilayer: 0.0625 ML H_2 (left panel); 0.25 ML H_2 (central panel), two layers of H_2 adsorbed on top of a WS_2 layer.

Conclusions and Outlook

As revealed by the micro-Raman measurements, hydrogenation by the RF plasma results in physisorption only of hydrogen with yet no evidence of H-S bonds. The operational parameters of the micro-Raman spectroscopy were optimized to decrease local heating while maintain sufficient signal intensity to observe the low cross section features. As revealed by the DFT calculations, the physisorbed hydrogen molecules are not intercalated between the layers of the NP but adsorbed, probably as two or three layers, on the very surface of the NP. Additional study is required for better understanding of possible atomic intercalation. For this purpose, we suggest to use tip-enhanced Raman spectroscopy trying to measure hydrogen in the individual NP: the accuracy of the determination of hydrogen chemical configuration in WS_2 NP will be greatly improved.

References:

[1] D.J. Ross, M.D. Halls, A.G. Nazri and R.F. Aroca; Chem. Phys. Lett.; 388 (2004), 430.
[2] B. Panella and M. Hirscher; Phys. Chem. Chem. Phys.; 10 (2008), 2910.
[3] C.M. Hartwig and J. Vitko Jr.; Phys. Rev. B; 18 (1978), 3006.
[4] B.C. Schmidt, F.M. Holtz and J.-M. Bény; J. Non-Cryst. Solids; 240 (1998), 91.
[5] S.D. Thompson, D.G. Carroll, F. Watson, M. O'Donnell and S.P. McGlynn; J. Chem. Phys.; 45 (1966), 1367.
[6] A. Anderson, S. Binbrekt and H.C. Tang; J. Raman Spectrosc.; 6 (177), 213.
[7] S. Baroni, A.D. Corso, S. Gironcoli, P. Giannozzi; QUANTUM ESPRESSO Package 2005, in www.quantum-espresso.org.

Heat generation by plasmon absorption in Au and Al nanoparticles arrays

Gennaro Picardi[a], Florent Colas[b], Raymond Gillibert[a], Guillaume Baffou[c] and Marc Lamy de la Chapelle[a]*

[a] Université Paris 13, Laboratoire CSPBAT, UMR CNRS 7244, 74 rue Marcel Cachin, 93017 Bobigny
[b] IFREMER, RER-RDT-LDCM, Pointe du Diable, 29280 Plouzané, France
[c] Institut Fresnel, UMR 7249, CNRS, Aix MarseilleUniversité, Centrale Marseille, 13013 Marseille, France

**e-mail: genn.picardi@gmail.com*

Keywords: Surface plasmon resonances, gold, aluminium, thermoplasmonics, thermal imaging

Introduction

Enhanced light absorption by metal nanoparticles due to the excitation of localized surface plasmon resonances generates light triggerable nanosources of heat attractive for medical therapy and in nano-chemistry. Optical phase analysis,[1] based on the refractive index variation of a liquid medium surrounding the metal nanostructures, allows the accurate and local measurement of the temperature increase around the nanostructures upon laser illumination and the retrieval of the absorption cross section.

Results and Discussion

The plasmon resonance of (arrays of) gold nanodisks with diameters ranging from 100 nm to 200 nm fabricated by electron beam lithography can be clearly tracked by the temperature increase at the metal surface. However, maximal heating is obtained for exciting wavelengths slightly (~15 nm) red shifted with respect to the extinction maximum (Fig. 1). Numerical simulations using the discrete dipole approximation support these experimental findings. The observed shift is tentatively related to the actual near-field probing of the temperature as opposed to the far-field optical extinction and the energy shift between the electromagnetic field intensity associated with the plasmon excitation in the near and far field regimes.[2,3] Influence of the absolute absorption cross section at resonance for different particle sizes on the overall heating will also be discussed.

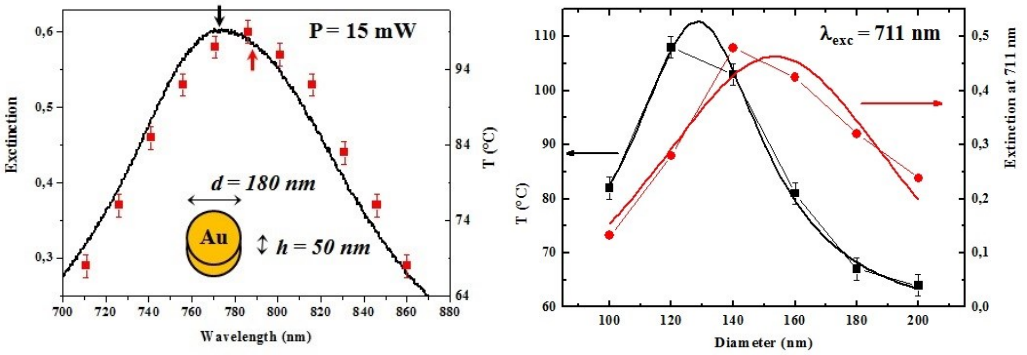

Figure 1: (left) The red dots report the temperature measured upon illumination of the same array of gold nano-cylinders (180 nm in diameter, 50 nm thickness) with laser wavelength varying from 711 nm to 860 nm under constant power (15 mW). The optical extinction spectrum relative to the same array is shown in black. **(Right)** Measured temperature (black squares) and optical extinction (red circles) as a function of disks diameter. The red and black curves are fit to experimental points. λ_{exc} = 711 nm, P = 14 mW.

Outlook

Preliminary results on aluminium nanodisks, displaying multipolar plasmon resonances in the wavelength range 500 nm to 900 nm are also presented. Gold and aluminium have very different bulk dielectric properties affecting plasmon lifetime and de-phasing mechanisms.[4] In particular, aluminium presents a sharp inter-band transition centred at 820 nm, which when overlapping to the surface plasmon absorption may provide an additional non-radiative decay channel.

References:

[1] Baffou G, Bon P, Savatier J, Polleux J, Zhu M, Merli M, Rigneault H and Monneret S, ACS Nano (2012) 2452-2548.
[2] Moreno F, Albella P., Nieto-Vesperinas, Langmuir (2013) 6715-6721.
[3] Zuloaga J, Nordlander P, Nano Lett (2011) 1280-1283.
[4] Zoric I, Zäch M, Kasemo B and Langhammer C, ACS Nano (2011) 2535-2546.

Mid-infrared molecular sensing with germanium antennas on silicon

L. Baldassarre[a,b*], *E. Sakat*[c], *A. Samarelli*[d], *K. Gallacher*[d], *J. Frigerio*[c,e], *G. Pellegrini*[c], *V. Giliberti*[a], *M.P. Fischer*[f], *D. Brida*[f], *G. Isella*[c,e], *D.J. Paul*[d], *M. Ortolani*[a] *and P. Biagioni*[c]

[a] Department of Physics, Sapienza University of Rome, Rome, 00185 Italy
[b] Center for Life Nanosciences, Istituto Italiano di Tecnologia, Rome, 00185 Italy
[c] Dipartimento di Fisica, Politecnico di Milano, Milano, 20133 Italy
[d]School of Engineering, University of Glasgow, Glasgow, G12 8LT, U.K.
[e]L-NESS, Dipartimento di Fisica del Politecnico di Milano, Como, 22100 Italy
[f]Department of Physics and Center for Applied Photonics, University of Konstanz, Konstanz, 78457 Germany

**e-mail: leonetta.baldassarre@roma1.infn.it*

Keywords:

Introduction

The quest for novel plasmonic materials has been a lively area of research over the last few years[1]. In the mid-infrared (mid-IR) spectral region, in particular, localized plasmon resonances in nanoparticles and nanoantennas hold promise for enhanced IR spectroscopies, with key applications in biology, medicine, and security. In this frame, the development of a CMOS-compatible plasmonic platform in the mid-IR could have disruptive effects for future technologies, allowing for integrated and cost-effective sensing devices [2].

Results and Discussion

We report on the growth, fabrication and optical characterization of heavily-doped Ge antennas integrated on a Si substrate and we exploit them for the sensing of solid-phase and liquid-phase analytes.

Epitaxial Ge is grown on Si by plasma-enhanced chemical vapour deposition, exploiting P as the dopant and achieving plasma frequencies above 1000 cm^{-1}, as demonstrated by infrared reflectance measurements. Antennas were fabricated by electron-beam lithography and reactive ion etching techniques, displaying localized plasmon resonances in the important 8 to 13 μm molecular fingerprint region.

We target the sensing of a thin polydimethylsiloxane (PDMS) layer (thickness of about 40 nm) and demonstrate an enhancement of two orders of magnitude in the collected signal on gap antennas, as derived from a comparison with the results of detailed numerical simulations. We also apply the developed antennas to the sensing of an explosives simulant, chloroethyl methyl sulfide (CEMS). Our results represent a first experimental benchmark for group-IV mid-IR plasmonics and confirm that future CMOS integration of cost-effective sensing platforms could largely benefit from plasmonic enhancement in heavily-doped Ge-based devices.

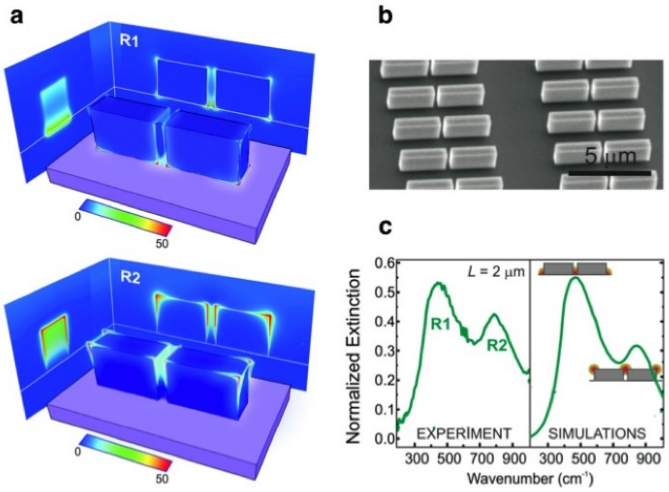

Figure 1: a) The simulated near-field intensity enhancement associated to the localized plasmon resonances (R1 and R2); b) A SEM image of the antennas; c) The measured experimental and simulated extinction spectra.

Conclusions and/or Outlook

We report on a novel all-group-IV semiconductor material platform for mid-IR plasmonics, based on heavily doped Ge epitaxially grown on standard Si wafers. We demonstrate localized plasmon resonances in Ge antennas and exploit the

fabricated devices for sensing experiments based on the resonant detection of molecular vibrational fingerprints of both condensed-phase and liquid-phase analytes.

The research leading to these results has received funding from the European Union's Seventh Framework Programme under grant agreement n°613055.

References:

[1] Boltasseva A., Atwater, H.A.; Low-Loss Plasmonic Metamaterials; Science; 331 (2011), 290.
[2] Baldassarre L., Sakat E., Frigerio J., Samarelli A., Gallacher K., Calandrini E., Isella G., Paul D.J., Ortolani M., Biagioni P.; Mid-Infrared Plasmon-enhanced with germanium antennas on silicon substrates; Nano Letters; 15 (2015) 7225

Optimising biosensors labels components and discrimination efficiency combining high-throughput screening and SEIRA technique

A. Hornemann[a], D. Eichert[b], S. Flemig[c], G. Ulm[a], B. Beckhoff[a]*

[a] Physikalisch-Technische Bundesanstalt, Abbestr. 2-12, 10587 Berlin, Germany
[b] Elettra-Sincrotrone Trieste, S. S. 14 Area Science Park, 34149 Basovizza, Trieste, Italy
[c] BAM Bundesanstalt für Materialforschung und –prüfung, Richard-Willstätter-Str. 10, 12489 Berlin, Germany
**e-mail: burkhard.beckhoff@ptb.de*

Keywords: biosensors labels, Surface-Enhanced Infrared Absorption Spectroscopy, Principal components analysis, antibody-fluorophore conjugates, gold nanoparticles

Introduction

The need for technological progress in bio-diagnostic assays of high complexity requires both fundamentalresearch and constructing efforts on nano-scaled assay recognition elements that can provide unique selectivity and design-enhanced sensitivity features for reliable high-performance analysis. Indeed, high-throughput capabilities require the simultaneous detection of various analytes combined with appropriate bioassay components. To design bioassays that function as molecular probes, a selective binding event has to be optimized considering the overall physicochemical properties which may influence the successful readout of signals. This constitutes the core of the first design steps to elaborate multi-purposes bioassay platforms. Nanoparticle induced sensitivity enhancement, and its related application to multiplexed capability Surface - Enhanced InfraRed Absorption (SEIRA) assay formats are fitting well these purposes. SEIRA constitutes an ideal platform to isolate vibrational spectroscopic signatures of bioassays' targeted and active molecules (as antibodies).

The potential of diverse targeted bio-labels, here fluorophore-labeled antibody conjugates, chemisorbed onto low-cost biocompatible gold and silver nano-aggregates SEIRA substrates has been explored for their use in assay platforms [1]. Extensive areas of dried sample films were analyzed by synchrotron radiation (SR) FTIR/SEIRA microspectroscopy and the resulting complex hyperspectral datasets, containing molecular SEIRA fingerprints, were submitted to automated statistical analysis, namely principal components analysis (PCA). Relationships and dependencies between chemical functional groups of the various antibody-fluorophore conjugation systems were determined for revealing their spectral discrimination capabilities.

These studies illustrate the potentiality of SEIRA methodology to select, optimize and qualify bio-label molecules, but what is more to evaluate, adjust and increase the efficiency of the substrates for ultimately screening in biological environment, too. We demonstrate that robust spectral encoding via SEIRA fingerprints opens up new opportunities for a fast, reliable, enhanced and multiplexed high-end screening not only in bio- diagnostics but also in in vitro biochemical imaging.

Results and Discussion

The spectral features of unlabeled and labeled Goat Anti-Mouse antibody (**Figure 1a**) were investigated by SR-FTIR with and without Au NP, i.e. within SEIRA and "conventional" technique, respectively. The signature of Goat Anti-Mouse IgG exhibits two strong IR bands at 1535 cm^{-1} and 1635 cm^{-1} that refer to the Amide II and Amide I bands [2] being characteristic for proteins. In the spectral region from 3300 to 3100 cm^{-1} stretching (str.) vibrations of –NH and –OH groups of amino acid residues are detected (e.g. 3278 cm^{-1}) that contribute to the secondary structure of the antibody. These IR bands are identifiable in other protein-Au bio-conjugates and are enhanced in the presence of Au NP. The metallic substrate also induces for some of the bands a modification of their spectral shapes as well as their intensities and positions, such as for the Amide I bands of the Goat IgG- FITC conjugate (see enhanced modes highlighted in bold). The FTIR spectrum of FITC exhibits bands referring to str. vibrations (1643 cm^{-1}) of the xanthene ring moiety and external group modes mainly related to C-O bonds, at 1200 – 1100 cm^{-1}. The SEIRA spectrum of FITC displays str. vibrations of the carbonyl groups of FITC (see asterisks *) and new bands originating from –C=N and –C=C str. modes. The enhancements observed, i.e. at 2098 – 2029 cm^{-1} (ν C–O), at 1597 cm^{-1} (arom. C–C) and at 1180 cm^{-1} (ν C–OH) for Au NP-FITC are due to the formation of large colloidal Au NA, presumably induced by the drop-coating process. In addition, the Au NA chemisorbed FITC molecules orient their dipole moments to be in line with the local electric field of the metal NA, resulting in much larger absorptions, which can be exploited for building up complex conjugates of sensitive multiplexed assays. Both the Goat Anti-Mouse IgG-FITC and SEIRA spectrum comprise bands (i.e. Amide I at 1643 cm^{-1} and

C–C str. at 1597 cm^{-1}) which can be assigned typically to FITC (see asterisks *), and bands at ~ 1527 cm^{-1} and a shifted band at 3286 cm^{-1} (ν NH) referring to the antibody specific signatures. This fact confirms that SEIRA is able to detect with high sensitivity fluorophore molecules in their conjugated states along with their molecular orientation. Chemical enhancement is another contribution which may explain the observed spectral differences. The FTIR/SEIRA signatures of Mouse Anti-Goat IgG were studied for evaluating its potential as targeting counterpart (i.e. antibody) in immunoassays. SEIRA signature of the Mouse IgG antibody shows enhanced modes in the spectral region between 1441 cm^{-1} (δ_{as} CH_3) and 1344 cm^{-1} (ν C=N), in addition to antigen specific bands.

Figure 1b shows the scores plots (PC1 – PC4) of diverse biolabels and fluorophore-antibody conjugates.

The datasets of the Goat Anti-Mouse IgG are well separated from the antigen data in PC1 vs PC2. The PCA results confirm that in average 85 % of the variance of the spectral datasets, i.e. the discrimination capability up to the third order could be explained by the fluorophore FITC. The scores (PC1 vs PC2) of Goat Anti -Mouse IgG are positive and lie in the second quadrant of the variance-weighted room. In PC1 vs PC3, the Goat Anti-Mouse IgG antibody data are well separated from the unenhanced spectra. The spectral differences observed in the SEIRA spectrum of FITC are also reflected by PC1 vs PC2. Likewise and also in PC1 vs PC2, FITC is separated from the FITC-labeled antibody.

Consequently, the simultaneous multivariate analysis of numerous spectral signatures is an efficient method to discriminate beforehand the best molecular configuration both for the biolabel and for the enhancing platform in order to achieve to establish a functionally specific bioassay.

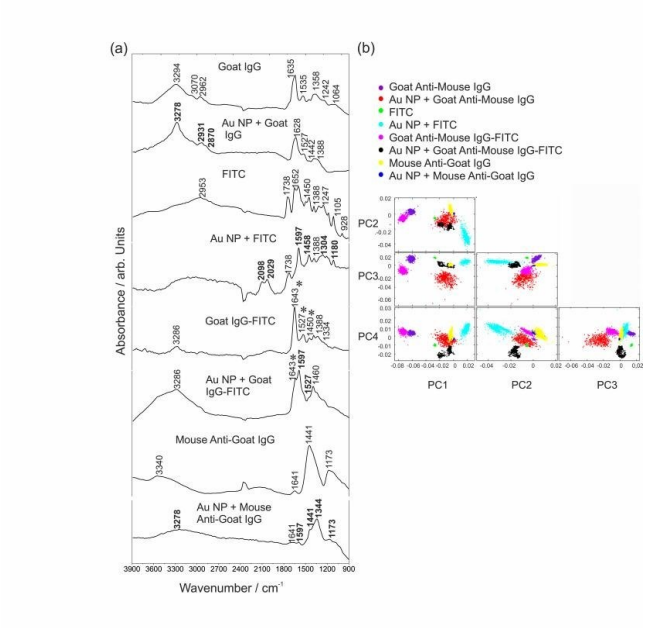

Figure 1: (a) MIR spectra on biolabel components. Vibrations of FITC are highlighted by asterisks *. Enhanced vibrations are labeled in bold. (b) PCA from PC1 to PC4. Adapted from [1] and reproduced by permission of the PCCP Owner Societies.

Conclusions and Outlook

The efficiency of the SEIRA technique to probe and unequivocally discriminate the molecular characteristics of biolabel components and antibody-fluorophore NP conjugation has been demonstrated. This study supports the qualification of SEIRA to the development and characterization of new complex SEIRA-based biolabels for multiplexed bioassay applications. It also provides a reliable background and tool for further investigations on tailored spectral responses of different antibody-fluorophore NP complexes, either by varying the molecular targeting elements or the substrate for triggering specific bio-molecular responses. Our results show that different and specific spectral FTIR/SEIRA signatures of both the native antibody Goat Anti-Mouse IgG and the conjugated FITC are preserved and enhanced in the proximity of Au NA. PCA enabled a clear discrimination of the functionalized systems, which ascertain their potential for multiplexed bioassay and biosensor applications of high efficiency with customized responses.

References:

[1] Hornemann A, Eichert D, Flemig S, Ulm G, Beckhoff B; Qualifying label components for effective biosensing using advanced high-throughput SEIRA methodology; Physical Chemistry Chemical Physics, 17 (2015) 9471-9479;

[2] Dukor RK; Handbook of Vibrational spectroscopy, ed. J. M. Chalmers, P. R. Griffiths, Wiley, New York, vol. 5 (2012) 3335-3361;

Mid-infrared near-field microscopy with scanning probe tips made of epitaxial semiconductor

V. Giliberti[a,b], *E. Sakat*[c], *L. Baldassarre*[a,b], *M. Bollani*[d,e], *M. V. P.Altoe*[f], *M. Melli*[f], *A. Weber-Bargioni*[f], *A. Notargiacomo*[d], *M. Pea*[d], *M.Celebrano*[c], *M. Finazzi*[c], *J. Frigerio*[c], *G. Isella*[c,e], *P.Biagioni*[c], *S. Cabrini*[f] *and M. Ortolani*[a]

[a] Dipartimento di Fisica, Sapienza University of Rome, Rome, Italy.
[b] Center for Life and Nano Sciences, Italian Institute of Technology, Rome, Italy.
[c] Dipartimento di Fisica, Politecnico di Milano, Milan, Italy.
[d] Istituto di Fotonica e Nanotecnologie, National Research Council of Italy.
[e] L-NESS, Dipartimento di Fisica del Politecnico di Milano, Como, Italy.
[f] Molecular Foundry, Lawrence Berkeley National Labs, Berkeley, United States.

**e-mail: valeria.giliberti@roma1.infn.it*

Keywords: epitaxial germanium, scanning probe tips, mid-infrared spectroscopy, near-field, ZnO nanowires

Introduction

The functionalization of scanning probe tips is a research area of great interest aiming to the tailoring of tip functionalities in order to probe specific material properties at the nanoscale. Whitin this field, a number of sophisticated probe tips with precise electromagnetic designs have been proposed for the development of scanning probe nanospectroscopy techniques based on a tip-sample interaction at the nanoscale, achieving unprecedented resolution and sensitivity both in the visible [1] and mid-infreard range [2].

In this work we present a new type of functionalized scanning probe tips fabricated out of electron-doped epitaxial germanium, transferring the electronic and optical functions of the as-grown epitaxial material to the nanometer tip. Heavily-doped germanium allows for the possibility to engineer the tip optical constants in a wide mid-infrared (mid-IR) frequency range through heterostructuring, doping, and alloying during the material growth process [3, 4]. Therefore, it is possible to fabricate scanning probe tips displaying a sharp crossover from a metallic regime, below the plasma frequency ω_p of germanium, to a lossy regime, above ω_p, where the permittivity of germanium becomes positive but the conductivity is still high. Such new mid-IR frequency- dependent behaviour cannot be achieved with metal-coated or dielectric tip typically used for aperture-less scanning near-field optical microscopy (SNOM) techniques. We have exploited the frequency-dependent behaviour of the n-Ge tips to demonstrate high-contrast mid-IR nanoimaging of conducting ZnO nanowires (NWs) embedded in a dielectric matrix (PDMS) by using a commercial scattering-type SNOM setup.

Results and Discussion

In **Figure 1** (a) and (b) the maps of the s-SNOM near-field signal (demodulated at the third-harmonic of the tapping frequency) are shown for two different frequencies of the external laser, respectively below (ω=884 cm-1, panel a) and above (ω=1250 cm^{-1}, panel b) the plasma frequency ω_p =1080 cm^{-1} of epitaxial germanium. When the epitaxial tip sits on the NW at ω=884 cm^{-1} a high near-field signal is detected, as expected from the coupled-dipole theory describing s-SNOM experiment for a metallic-like tip on a conducting sample. On the contrary, above the plasma frequency of germanium, almost no near-field signal is detected when the tip sits on the NW. We interpret this result as the quenching of the near-field scattering from the conducting NW due to the establishment of a lossy coupled tip-NW system. We also verified that the same mechanism allows for a higher contrast between highly- and poorly-conducting portions of single NWs, enabling a better visualization of spatial dishomogeneities of the carrier density.

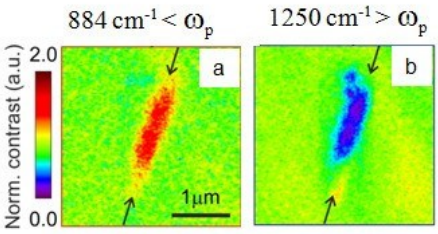

Figure 1: s-SNOM maps of a ZnO nanowire embedded in a dielectric matrix obtained with an epitaxial germanium tip at 884 cm^{-1} (a) and at 1250 cm^{-1} (b).

Conclusions and Outlook

In conclusion, we presented a novel functionalization of scanning probe tips using epitaxial germanium as the raw material for the tip fabrication. The mid-infrared frequency-dependent properties of the bulk epitaxial n-doped germanium have been exploited to perform high-contrast mid-infrared near-field microscopy of ZnO nanowires embedded in a conformal dielectric matrix. The nanotechnology process presented here opens new paths for the functionalization of scanning probe tips with any type of epitaxial semiconductors. Such novel generation of probes would benefit of the wide properties of the epitaxial bulk materials allowing to fabricate optical- and electrical-active scanning probe tips whose functionalities can be tailored in order to address specific nanoscale material properties.

References:

[1] Bao W. et al., Science 13 (2013) 1065.
[2] Huth F. et al., Nano Lett. 13 (2013) 1065.
[3] Biagioni P. et al, Journal of Nanophotonics 9 (2015) 093789. [4]
Giliberti V. et al., Microel. Engineering 141 (2015) 168.

Graphene quantum dots: properties and applications

A. Radoi[*a], *I. Mihalache*[a], *M. Kusko*[a], *S.A.V. Eremia*[b],

[a] National Institute for Research and Development in Microtechnologies (IMT-Bucharest), 126A Erou Iancu Nicolae, 077190, Bucharest, Romania
[b] Centre of Bioanalysis, National Institute of Research and Development for Biological Sciences - Bucharest, 296 Splaiul Independentei, 060031, Bucharest, Romania

e-mail: antonio.radoi@imt.ro

Keywords: graphene quantum dots, molybdenum disulfide

Introduction

Quasi spherical particles of graphitic or amorphous nature with size less than 10 nm have been produced by several approaches more or less complex depending on reaction time, cost or number of steps required [1]. Recent research on graphene quantum dots (GQDs) properties aimed to emphasize their emerging potential as active layer in optoelectronic devices and in electrochemical sensors or biosensors.

Compared to other carbonaceous nanomaterials, GQDs gave distinctive advantages including charge carriers quantum confinement, tunable band gap, strong luminescence and enhanced electronic conductivity. Structural properties together with appropriate surface functional groups enables the control of optical properties like optical bandgap, static and lifetime features of photoluminescence and quantum yield.

Results and Discussion

Few nanometers in size aqueous solution-processable GQDs with different surface groups were synthesized through a bottom-up approach starting from glucosamine and tris(hydroxymethyl)aminomethane or poly(ethyleneimine) as precursors. The performance of GQDs attached on nanoporous titanium oxide in a typical Gratzel solar cell was investigated and electrochemical impedance spectra (EIS) were acquired for GQDs and GQDs and MoS_2 nanoassembly ascertaining the enhanced electronic conductivity.

Conclusions

For a typical Gratzel solar cell it was demonstrated that carbonaceous material performs a significant role in charge separation and collection due to the cascaded alignment of energy levels. Energy transfer from GQD to ruthenium based dye also occurred due to the emission and absorption spectra overlap of the dye and the GQDs.

Previous reported EIS analyses concerning GQDs obtained via graphene oxide revealed their insulating nature. On the contrary our results confirmed that the network of GQDs obtained by microwave assisted hydrothermal route supplies excellent electronic conductivity. A further decrease in resistance to charge transfer (Rct) was achieved when MoS_2 and GQDs were mixed, the Rct change being more than two orders of magnitude, illustrating the synergistic interaction between GQDs and MoS_2 sheets.

Acknowledgements

This work was supported by a grant of the Romanian National Authority for Scientific Research and Innovation, CNCS – UEFISCDI, project number PN-II-RU-TE-2014-4-1095"

References:

[1] Li H, Kang Z, Liu Y and Lee S T; Carbon nanodots: synthesis, properties and applications; Journal of Materials Chemistry; 22 (2012) 24230 - 24253

First-principles nonequilibrium Green's function approach to time-resolved photoabsorption in nanoscale systems

*E. Perfetto**[a,b], *A.-M. Uimonen*[c], *R. van Leeuwen*[c], *G. Stefanucci*[a,b]

[a] Dipartimento di Fisica, Universita' di Roma Tor Vergata, Via della Ricerca Scientifica 1, 00133 Rome, Italy
[b] INFN, Laboratori Nazionali di Frascati, Via E. Fermi 40, 00044 Frascati, Italy
[c] Department of Physics, Nanoscience Center, University of Jyväskylä, FIN 40014 Jyväskylä, Finland

**e-mail: enrico.perfetto@roma2.infn.it*

Keywords: Ultrafast spectroscopy, Transient photoabsorption

We propose a first-principles nonequilibrium Green's function (NEGF) approach to calculate the time-resolved photoabsorption spectrum of nanoscale systems [1]. We can deal with arbitrary shape, intensity, duration and relative delay of the pump and probe fields. We present numerical simulations of atomic systems using different approximate self-energies and, whenever possible or available, find good agreement with Configuration Interaction (CI) calculations and experiments [2]. The NEGF approach offers a first-principle methodology to study systems are out of reach with CI and, at the same time, to include dynamical correlation effects that are difficult to describe with other methods [3]. If time permits we will also discuss future challenges and reachable goals..

References:

[1] Perfetto E., Stefanucci, G.; Some Exact Properties of the Nonequilibrium Response Function for Transient Photoabsorption; Physical Review A; 91 (2015) 033416.
[2] Perfetto E., Uimonen, A.-M., Van Leeuwen R., Stefanucci, G.; First-Principles Nonequilibrium Green's Function Approach to Transient Photoabsorption: Application to Atoms; Physical Review A; 92 (2015) 033419.
[3] Perfetto E., Sangalli D., Marini A., Stefanucci, G.; Nonequilibrium Bethe-Salpeter equation for Transient Photoabsorption Spectroscopy; Physical Review B; 92 (2015) 205304.

Modematching for metal nano antennas

Th. Feichtner [a,*], *S. Christiansen* [a,b], *B. Hecht* [c]

[a] Helmholtz Zentrum Berlin für Materialien und Energie GmbH, Institut Nanoarchitekturen für die Energieumwandlung, Hahn-Meitner-Platz 1, 14109 Berlin, Germany
[b] Max Planck Institute for the Science of Light – Christiansen Research Group, Günther-Scharowsky-Straße 1, 91058 Erlangen, Germany
[c] Nano-Optics & Biophotonics Group, Department of Experimental Physics 5, Röntgen Research Center for Complex Material Research (RCCM), Physics Institute, University of Würzburg, Am Hubland, D-97074 Würzburg, Germany

**e-mail: thorsten.feichtner@helmholtz-berlin.de*

Keywords: plasmonics, nano antennas, mode-matching, LDOS

Introduction

The efficient coupling of photons from propagating far-fields to nanoscale volumes is a fundamental problem in quantum optics and at the heart of light-matter interaction. A common model system is the coupling between a point-like two-level quantum emitter (QE) and the continuum of radiative modes, which can be expressed in terms of the frequency-dependent partial local density of states (LDOS) at the QE position. Resonant plasmonic nanoantennas can be designed to strongly localize fields into a small volume leading to an LDOS enhanced by a factor of 10^5 and possibly beyond.

Results and Discussion

Inspired by antenna geometries retrieved from an evolutionary algorithm [1] a description of power transfer between a QE and an optical antenna resembling a three-dimensional mode matching formalism is developed. After introducing a second dipole in the far-field, another mode-matching step leads to a set of novel optical antenna design guidelines for QE emission enhancement. Accordingly a plasmonic cavity antenna (PCA) geometries is devised and compared to an established dipolar two-wire antenna geometry (see Figure 1).

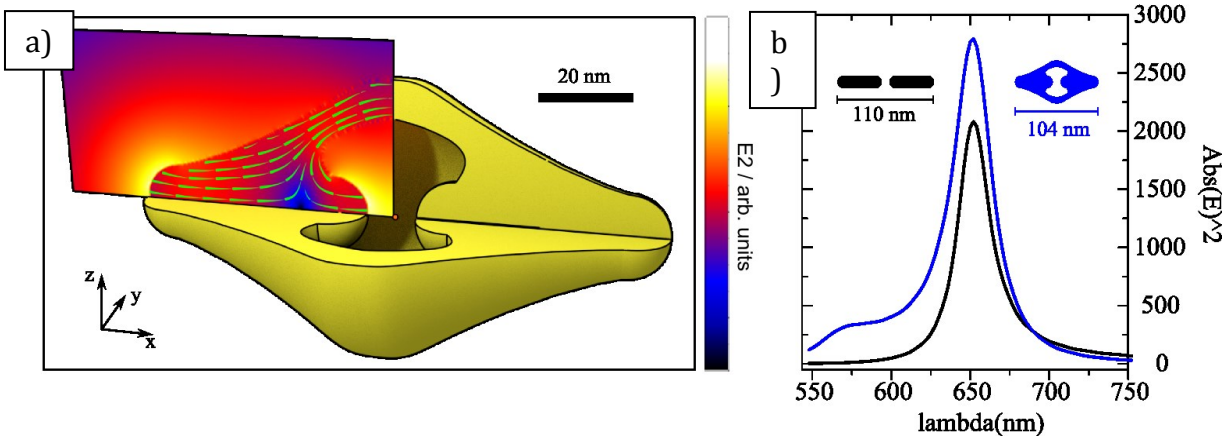

Figure 1: (a) Plasmonic cavity antenna (PCA) design supporting a mode that optimizes mode-matching. The rotational symmetric geometry is shown with a 90° cutaway for visualization. The near-field intensity (colour) as well as the current direction (green arrows) are overlaid to the quarter cross section. The small orange dot in the centre of the structure marks the focal point, where a QE is to be placed. (d) Near-field intensity enhancement spectra at the focal point (blue) as well as at the centre of a two wire dipole reference antenna (black), with identical spherical end cap radius. The small insets show a x-y-plane cross section of both geometries.

Conclusions and Outlook

Double mode-matching can explain the enhanced performance of complex shaped optical antenna geometries, e.g. structures resulting from evolutionary optimization and will in the future open a way to understand and tailor the coupling of single emitters to complex structured metal substrates in surface enhanced spectroscopies such as SERS.

References:

[1] T. Feichtner, O. Selig, and B. Hecht, Plasmonic nanoantenna design and fabrication based on evolutionary optimization; *arXiv1511.05438v1* .

Mode-matching in multiresonant plasmonic nanoantennas for enhanced second harmonic generation

M. Celebrano[1], X. Wu[2,3], M. Baselli[1], S. Großmann[2], P. Biagioni[1], A. Locatelli[4], C. De Angelis[4], G. Cerullo[1,5], R. Osellame[5], B. Hecht[2], L. Duò[1], F. Ciccacci[1], & M. Finazzi1[1]

[1]Physics Department, Politecnico Milano, P.zza Leonardo Da Vinci 32, 20133 Milano, Italy.
[2]Nano-Optics & Biophotonics Group - Department of Physics - Experimental Physics 5, University of Würzburg, Am Hubland, 97074 Würzburg, Germany.
[3]Present Address: Ultrafast Nanooptics Group – Department of Physics – Experimental Physics III, University of Bayreuth, Universitätsstraße 30, 95447 Bayreuth, Germany.
[4]Department of Information Engineering, University of Brescia, Via Branze 38, 25123 Brescia, Italy.
[5]IFN-CNR - Physics Department, Politecnico Milano, P.zza Leonardo Da Vinci 32, 20133 Milano, Italy.

e-mail: michele.celebrano@polimi.it

Keywords: Nonlinear Optics, Plasmonics, Nanostructures, Nonlinear properties of matter, Nano-optics

Introduction

Second Harmonic Generation (SHG) is well known to be a powerful imaging tool for background-free and non-damaging live tissues investigation. Field enhancements in plasmonic nanostructures are often exploited to effectively compensate for the lack of phase-matching in confined volumes with the aim of obtaining brighter nanoscale nonlinear probes. Recently, a nanoantenna design featuring a double resonance at both the excitation and the emission wavelengths has been realized to improve SHG [1]. However, the high degree of symmetry in plasmonic materials at the atomic scale and in nanoantenna designs have so far limited SHG efficiency [2].

Results and Discussion

Here we report on especially engineered gold single-crystalline nanoantennas (see Figure inset) working in
at both the excitation and SH wavelength, (ii) a significant spatial overlap of the localized fields at the wavelengths of interest and (iii) a broken-symmetry geometry to achieve dipole-allowed SHG. The effective combination of these key features in a single plasmonic antenna, characterized by the absence of local defects, allows optimizing SHG efficiency in a well-controlled fashion.

Once the antenna geometry is properly tuned to display a double resonance matching simultaneously the laser excitation (1560 nm) and the SHG wavelength (see dashed line in Figure), it demonstrates a SHG nonlinear coefficient

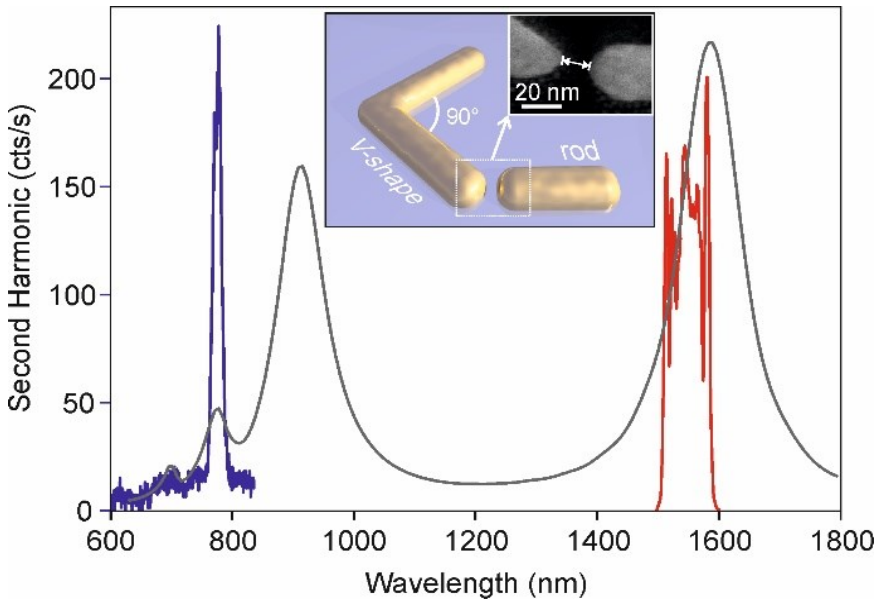

Figure 1: Superposition of the main nanoantenna modes with the excitation and emission lines. The measured SHG emission spectrum (blue line) and the excitation laser band (red line) show excellent overlap with the doubly-resonant antenna calculated spectrum (light-grey line). Inset: sketch of the devised nanostructure. Sub-inset: SEM image of the gap-region revealing a gap-size of about 17 nm.

$\gamma_{SHG} = \hat{P}_{SH}/\hat{P}_{FW}^2 \approx 5 \times 10^{-10}$, where $\hat{P}_{SH}$ and $\hat{P}_{FW}$ are the SH and excitation peak powers, respectively. This figure of merit is well above the ones retrieved by other SHG studies on broken-symmetry plasmonic structures [3, 4], achieving an extremely high conversion efficiency $\eta_{SHG} \sim 6.4 \times 10^{-9}$ [5].

Conclusions and/or Outlook

We evaluated the sensing performances of our devices by theoretically estimating the figure of merit FOM* = (□*I*/*I*)/□*n* of our nonlinear plasmonic devices. The nanostructure showing the best conversion efficiency features a FOM* = 40, which is about 4 times higher than the one of other individual plasmonic structures already applied to sensing. These results shed light on the optimization of nanoscale SHG via metal nanoantennas, paving the way to a new class of tunable molecular sensing devices and nanoscale coherent light sources based on nonlinear plasmonic platforms.

References:

[1] K. Thyagarajan et al., Opt. Express **20**, 12860 (2012).
[2] M. Finazzi et al., Phys. Rev. B **76**, 125414 (2007).
[3] H. Aouani et al., Nano Lett. **12**, 4997 (2012).
[4] Y. Zhang et al., Nano Lett. **11**, 5519–5523 (2011).
[5] M. Celebrano et al., Nature Nanotechnology **10**, 412-417 (2015)
[6] I. Ament et al. Nanolett. **12**, 1092–1095 (2012).

A highly directional room-temperature single photon device

Nitzan Livneh[1], Moshe G. Harats[2], Daniel Istrati[2], Hagai Eisenberg[2], and Ronen Rapaport[1,2]

[1]The Hebrew University of Jerusalem, Applied Physics Department, Jerusalem, 91904, Israel
[2]The Hebrew University of Jerusalem, Racah Institute for Physics, Jerusalem, 91904, Israel

e-mail: ronenr@phys.huji.ac.il

Keywords: single photon source, nano-antenna, semiconductor nanocrystal,

One of the most important challenges in modern quantum optical applications is the demonstration of efficient, scalable, on-chip single photon sources, which can operate at room temperature. In this talk I will present how we demonstrate a room-temperature single-photon source [1] based on a single colloidal nanocrystal quantum dot positioned inside a circular bulls-eye shaped [2] hybrid metal-dielectric nanoantenna [3]. Experimental results show that 20% of the photons are emitted into a very low numerical aperture (NA < 0.25), a 20-fold improvement over a free standing quantum dot, and with a probability of more than 70% for a single photon emission. With an NA = 0.65 more than 35% of the single photon emission is collected. The single photon purity is limited only by emission from the metal, an obstacle that can be bypassed with careful design and fabrication. The concept presented here can be extended to many other types of quantum emitters. Such a device paves a promising route for a high purity, high efficiency, on-chip single photon source operating at room temperature.

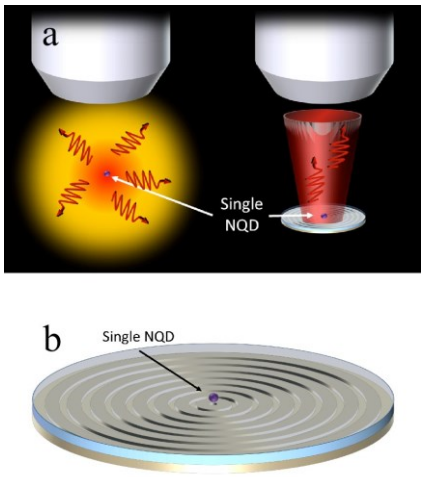

References:

[1] Nitzan Livneh, Moshe G. Harats, Daniel Istrati, Hagai Eisenberg, and Ronen Rapaport. A highly directional room temperature single photon device. Submitted (2015)

[2] Moshe G. Harats, Nitzan Livneh, Gary Zaiats, Shira Yochelis, Yossi Paltiel, Efrat Lifshitz, and Ronen Rapaport. Full Spectral and Angular Characterization of Highly Directional Emission from Nanocrystal Quantum Dots Positioned on Circular Plasmonic Lenses. Nano Letters, 14(10):5766-5771, October 2014, doi:10.1021/nl502652k

[3] Nitzan Livneh, Moshe G. Harats, Shira Yochelis, Yossi Paltiel, and Ronen Rapaport. Efficient Collection of Light from Colloidal Quantum Dots with a Hybrid Metal-Dielectric Nanoantenna. ACS Photonics, December 2015, doi:10.1021/acsphotonics.5b00433

Optical properties of single quantum dots placed on the tips of gold-nanocones

R. Jäger[*a], S. Jäger [ab], A. Bräuer[c], K. Scherzinger[a], J. Fulmes[c], S. zur Oven Krockhaus[a], D. A. Gollmer[c], D. P. Kern[c], M. Fleischer[c] and A. J. Meixner[a]*

[a] Institute of Physical and Theoretical Chemistry, Center for Light-Matter Interaction, Sensors & Analytics (LISA+), University of Tübingen, Auf der Morgenstelle 18, 72076 Tübingen, Germany

[b] now at: Bavarian Center for Applied Energy Research, Haberstraße 2a, 91058 Erlangen, Germany

[c] Institute for Applied Physics, Center for Light-Matter Interaction, Sensors & Analytics (LISA+), University of Tübingen, Auf der Morgenstelle 10, 72076 Tübingen, Germany

**e-mail: regina.jaeger@uni-tuebingen.de*

Keywords: quantum dots, single molecule spectroscopy, plasmonic coupling, nanocones

Introduction

Placing emitters in the vicinity of metallic nanostructures, results in coupling mechanisms. By means of single molecule spectroscopy the influence by e.g. scanning near field tips [1-2], single gold nanoparticles [3-4], discs [5] or bowtie antennas [6] has been studied. However, the interaction is still not fully understood to the extent that the optical properties of the hybrid structures can be controlled and tuned. We have chosen spherical CdSe/ZnS quantum dots (QDs) since they can be equally well excited in all three dimensions [7] in contrast to single-molecules with a fixed transition dipole moment axis. Besides the orientation of the emitter, the most crucial point is to reproduce and successively repeat experiments to achieve reasonable statistics. Therefore, we have developed a self-aligning technique to place QDs within the hot spot of a gold-nanocone for a whole nanocone-array at once [8]. In this way, we are able to show in this work how a gold-nanocone can alter the optical properties of a single QD. Prior to the investigations of the coupled system, we also characterized the optical properties of the gold-nanocones and single QDs separately.

Results and Discussion

Comparing the results obtained from single QDs on glass and QDs placed on gold-nanocones, we observe a change in the fluorescence intermittency behaviour, a shift of the emission wavelength, fluorescence enhancement and decreased fluorescence life time. [9] **Figure 1** shows a typical confocal image and the corresponding spectra obtained by raster scanning a hybrid sample through a focused radially polarized laser mode (RPM). (A detailed description of the setup and laser modes can be found in reference [9].) It can clearly be seen, that cone 1 has no QD attached, as in the confocal image no blinking is indicated, and in the spectrum only a background of residual resist appears. The hybrid structures 2-4 show blinking behaviour in the confocal image along with a higher intensity, while hybrid 3 exhibits less blinking. Looking at the spectra, cone 3 obviously has more than one QD attached, resulting in a broader non uniform spectrum. Hybrids 2 and 4 show narrow spectral bands with a full width at half maximum (FWHM) similar to spectra of single QDs on glass. However, the signal of hybrid 4 is weaker compared to hybrid 2. This difference can be explained by the efficiency of the coupling between QD and cone. The hybrid structure has been designed in such a way, that the out-of-plane resonance of the gold-nanocones corresponds to the nominal emission wavelength of the QDs at 650 nm in solution. Hence, QDs emitting at different wavelengths couple less efficiently to the gold-nanocone, resulting in a lower signal.

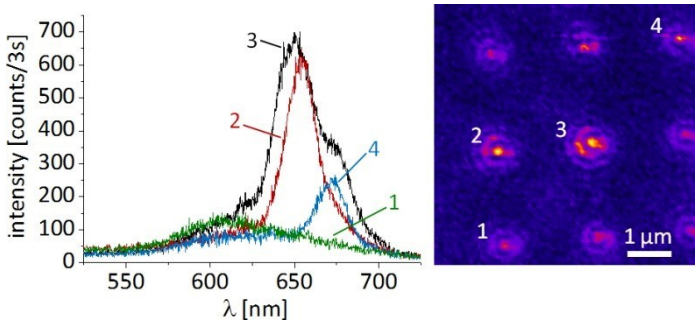

Figure 1: Spectra from different hybrid structures (left) and the corresponding confocal image (right) excited with a focused488 nm RPM. The individual cones are labelled 1-4, where the differences between cones with and without QDs, as well as cones with more than one QD can clearly be recognized.

These findings have been confirmed by acquiring data sets from 78 single QDs on glass and 51 single QDs on gold-nanocones. To determine whether indeed only one single QD is observed, spectral analysis and intensity trajectories were used. The spectrally integrated intensities of the hybrids are in average about one order of magnitude higher

than those of QDs on glass. Also the distribution of the spectral maxima exhibits a shift towards the plasmonic mode of the gold nanocones. The largest signal intensities are found at 650 nm, while the QDs on glass show maxima distributed around 640 nm.

Additionally, the measured life times differ dramatically. For QDs on glass we observed life times between 8 and 12 ns, while the hybrids show decay times as short as 120 ps to 230 ps. Shortening of the life times is usually observed for quenching processes, but as the fluorescence signal is clearly enhanced, it is obvious that the coupling within the hybrid structure contributes also to the shortening of the life-time, indicating that the emission rate of the QD is enhanced by the presence of the gold-nanocone tip.

Conclusion and outlook

In summary, efficient coupling between QDs and gold-nanocones has been achieved, altering the optical properties according to the characteristics of the cones. The hybrid structures show different fluorescence intermittency behaviour, fluorescence intensity and lifetimes compared to QDs on glass. Further experiments including more statistics, gold-nanocones with different plasmon resonances compared to the QD emission and polarization dependent measurements are planned to get a deeper insight into the coupling mechanism.

References:

[1] Gerton J M, Wade L A, Lessard G A, Ma Z, Quake S R; Tip-Enhanced Fluorescence Microscopy at 10 Nanometer Resolution; Physical Review Letters; 93 (2004) 180801-1 – 180801-4;

[2] Shafran E, Mangum B D, Gerton J M; Using the Near-Field Coupling of a Sharp Tip to Tune Fluorescence-Emission Fluctuations during Quantum-Dot Blinking; Physical Review Letters; 107 (2011) 037403-1 – 037403-4;

[3] Anger P, Bharadwaj P, Novotny L; Enhancement and Quenching of Single-Molecule Fluorescence; Physical Review Letters; 96 (2006) 113002-1 – 113002-4;

[4] Kühn S, Håkanson U, Rogobete L, Sandoghdar V; Enhancement of Single-Molecule Fluorescence Using a Gold Nanoparticle as an Optical Nanoantenna; Physical Review Letters; 97 (2006) 017402-1 – 017402-4;

[5] Ureña E B, Kreuzer M P, Itzhakov S, Rigneault H, Quidant R, Oron D, Wenger J; Excitation Enhancement of a Quantum Dot Coupled to a Plasmonic Antenna; Advanced Optical Meterials; 24 (2012) OP314 – OP320; [6] Kinkhabwala A, Yu Z, Fan S, Avlasevich Y, Müllen K, Moerner W E; Large single-molecule fluorescence enhancements produced by a bowtie nanoantenna; Nature Photonics; 3 (2009) 654 – 657;

[7] Chizhik A I, Chizhik A M, Khoptyar D, Bär S, Meixner A J; Excitation isotropy of Single CdSe/ZnS Nanocrystals; Nano Letters; 11 (2011) 1131 – 1135;

[8] Fulmes J, Jäger R, Bräuer A, Schäfer C, Jäger S, Gollmer D A, Horrer A, Nadler E, Chassé T, Zhang D, Meixner A J, Kern D P, Fleischer M; Self-aligned placement and detection of quantum dots on the tips of individual conical plasmonic nanostructures; Nanoscale; 7 (2015) 14691 – 14696;

[9] Meixner A J, Jäger R, Jäger S, Bräuer A, Scherzinger K, Fulmes J, zur Oven Krockhaus S, Gollmer D A, Kern D P, Fleischer M; Coupling single quantum dots to plasmonic nanocones: optical properties; Faraday Discussions; (2015) DOI: 10.1039/C5FD00074B;

Fabrication and characterization of $Ag@TiO_2$ and $Au@TiO_2$ core-shell nanostructures

*B. Bartosewicz, M. Gajda-Rączka,M. Michalska-Domańska, B.J. Jankiewicz**

Institute of Optoelectronics, Military University of Technology, Warsaw, Poland

**e-mail: bartlomiej.jankiewicz@wat.edu.pl*

Keywords: TiO_2, noble metals, core-shell, nanostructures, fabrication

Introduction

Nanoscale titanium dioxide (TiO_2) is one of the most widely investigated oxide semiconductor materials in many fields, such as environmental cleanup, catalysis, hydrogen production and photovoltaics, due to its excellent performances. However, applications of TiO_2 related to its optical properties are limited by the fact that its band gap energy corresponds to electromagnetic radiation in the UV region. Thus, one of the goals for improvement of the performance of TiO_2 nanomaterials is to increase their optical activity by shifting the onset of the response from the UV to the visible region [1].

One way to achieve this goal is to synthesize hybrid functional core-shell nanostructures based on the TiO_2 and noble metals. It has been already shown that Au or Ag nanoparticles (AuNPs or AgNPs), which exhibit strong optical responses resulting from the surface plasmon resonance, deposited on the surface of TiO_2 particles enhance the photocatalytic efficiency under visible light. The AuNPs or AgNPs act as an electron traps, promoting interfacial charge transfer and therefore delaying recombination of the electron–hole pair [2]. Similar effect can be achieved, when AuNPs or AgNPs will be covered by TiO_2 shell.

In this work we present results of studies on fabrication of metal-dielectric hybrid nanostructures, composed of gold and silver cores coated with a titania shell. The fabricated hybrid nanostructures were characterized using scanning electron microscopy (SEM), UV-Vis spectroscopy and tunable resistive pulse sensing (TRPS) method.

Results and Discussion

Metal colloids, which served as cores, were synthesized by reduction of $AgNO_3$ or $HAuCl_4$ with hydroxylamine hydrochloride or sodium citrate, respectively. The conditions of these well-known methods were adjusted in order to achieve mean diameters of Au and Ag particles in the range of 100 nm. $Ag@TiO_2$ and $Au@TiO_2$ core-shell structures were synthesized via sol-gel method using tetrabutyl titanate (TBT) as a precursor for TiO_2 shell [3]. This step of the fabrication of the final core-shell structures has been the most difficult to achieve due to the fact that organic titanates undergo much faster hydrolysis compared to organic silanes commonly used for the coating of Au and Ag particles. Thus, in order to carry out controlled coating of metal particles with titania shell and prevent formation of free titania particles special methodology for this synthesis was developed. The thickness of TiO_2 shell can be adjusted by changing concentration of TBT solution.

The morphology of fabricated Ag, Au, $Ag@TiO_2$ and $Au@TiO_2$ particles were characterized by SEM microscopy (**Figure 1**). Analysis of SEM images provides information about shape and size of investigated nanostructures. However, such obtained information about the size and size distribution of analysed nanostructures is rather limited due to the fact that usually small number of particles is included in statistical analysis. In order to provide higher quality statistical data regarding size and size distribution of fabricated nanostructures we additionally have analysed them using TRPS method. The TRPS method is based on Coulter principle, which states that particles passing through an aperture of defined size, concurrent with an electric current, produce a change in impedance that is proportional to the volume of the particle passing through an aperture [4]. The great advantage of TRPS method is that it monitors particles one-by-one and provides population statistics based on thousands of individual measurements. TRPS gives results closely resembling these obtained by using transmission electron microscopy, however time of analysis is much shorter and greater number of particles is analysed.

The optical properties of fabricated structures were characterized using UV-Vis spectroscopy. The UV-Vis spectra clearly indicate presence of the plasmon absorption bands corresponding to gold and silver particles. In both cases, in comparison to their spectra in aqueous solutions red shifts of the maxima of absorption are observed. This behaviour results from the change in the surrounding environment of the noble metal particles and associate with it increase of the host matrix dielectric constant being direct consequence of the increase in refractive index [5]. The observed red shift is smaller for Au particles (20 nm) than for Ag nanoparticles (40 nm).

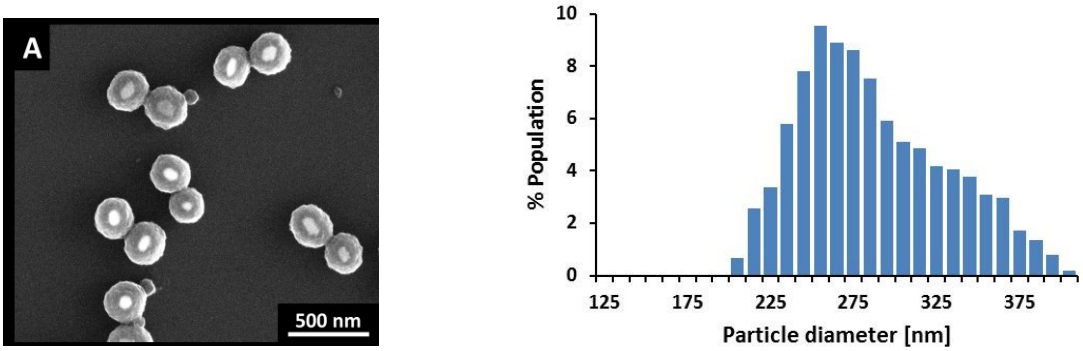

Figure 1: SEM image and TRPS histogram of Au@TiO_2 structures with 73 nm thick titania shell (mode value).

Outlook

The simple route to fabrication of Au@TiO_2 and Ag@TiO_2 core-shell nanostructures has been developed. This method allows for fabrication of titania shells in the range of 30-70 nm (mode values) for AuNPs and AgNPs. In addition, applicability of the Tunable Resistive Pulse Sensing for investigation of size and size distributions of core-shell nanostructures was demonstrated.

Acknowledgment

This work is funded by the National Science Centre under grant No. 2011/03/D/ST5/06038.

References:

[1] Chen X., Mao S.S.; Titanium Dioxide Nanomaterials: Synthesis, Properties, Modifications, and Applications; Chem. Rev. 107 (2007) 2891-2959.

[2] Pelaez M., Nolan N.T., Pillai S.C., Seery M.K., Falaras P., Kontos A.G., Dunlop P.S.M., Hamilton J.W.J., Byrne J.A., O'Shea K., Entezari M.H., Dionysiou D.D.; A review on the visible light active titanium dioxide photocatalysts for environmental applications; Appl. Catal. B 125 (2012) 331– 349.

[3] Mine E., Hirose M., Nagao D., Kobayashi Y., Konno M.; Synthesis of submicrometer-sized titania spherical particles with a sol–gel method and their application to colloidal photonic crystals; J. Colloid Interface Sci.- 291 (2005) 162–168.

[4] Pal A. K., Aalaei I., Gadde S., Gaines P., Schmidt D., Demokritou P., Bello D.; High Resolution Characterization of Engineered Nanomaterial Dispersions in Complex Media Using Tunable Resistive Pulse Sensing Technology; ACS Nano 8 (2014) 9003-9015.

[5] Kelly K.L., Coronado E., Zhao L. L., Schatz, G. C.; The Optical Properties of Metal Nanoparticles: The Influence of Size, Shape, and Dielectric Environment J. Phys. Chem. B 107 (2003) 668-677.

Ultrafast carrier dynamics and amplified spontaneous emission in dual-color emitting dot-in-bulk nanocrystals

*A. Camellini[a], G. Sirigu[a], V. Pinchetti[b], F. Meinardi[b], S. Christodoulou[c], W. K. Bae[d], F. De Donato[c], L. Manna[c], I. Moreels[c], V. I. Klimov[d], S. Brovelli[b], M. Zavelani-Rossi[a]**

[a] Dipartimento di Fisica, IFN-CNR, Politecnico di Milano, P.zza L. da Vinci 32, 20133 Milano, Italy
[b] Dipartimento di Scienza dei Materiali, Università degli Studi di Milano-Bicocca, via Cozzi 55, 20125 Milano, Italy
[c] Istituto Italiano di Tecnologia, via Morego 30, 16163 Genova, Italy
[d] Chemistry Division, Los Alamos National Laboratory, Los Alamos, New Mexico 87545, United States
**e-mail: margherita.zavelani@polimi.it*

Keywords: colloidal semiconductor nanorystals, ultrafast spectroscopy, optical gain, CdSe/CdS NCs

Introduction

Colloidal semiconductor nanocrystals (NCs) are solution-processable functional materials with growing applicative potential in several technologies such as light emitting diodes, lasers, luminescent solar concentrators, photovoltaics, sensing and bioimaging. A particular interest in NCs arises from their tunable optical properties achieved through composition, size control, doping, strain effects, and wave-function-engineering. In this context heterostructured NCs present valuable advantages, among which the possibility of dual-color light emission as a result of radiative recombination of excitons localized in different compositional domains, such as the core and the shell regions [1-3]. This has been recently demonstrated in CdSe/CdS NCs, featuring a quantum confined CdSe core embedded into an ultra-thick CdS shell, so-called dot-in-bulk (DiB) NCs, emitting red and green light [2]. Despite various indications that the properties of DiB-NCs and the ability to emit two-color light are linked to the core/shell structure interface, its role is still not fully unraveled.

In this work we performed ultrafast pump-probe measurements, with 100-fs time resolution and gain experiments on two different dual emitting CdSe/CdS DiB-NCs, synthesized following similar synthetic routes [2,4] and differing from each other exclusively for their crystal structure: the firsts have a zincblende (ZB) CdSe core overcoated with a *polytypic* ZB/wurtzite (WZ) CdS shell (ZW-NCs), the seconds have a WZ CdSe core embedded in a *homogeneous* WZ CdS shell (WW-NCs). Data indicate that a Coulomb blockade effect is active only in the first structure. This mechanism leads to suppressed Auger recombination in the core and to a longshell exciton lifetime at high excitation fluence. Furthermore, in turns, it enables amplified spontaneous emissionfrom shell states using nanosecond pulsed excitation sources, which is instead not realizable with systems with homogeneous shell structure.

Results and Discussion

Dual emission in DiB NCs has been originally ascribed to the combination of an electrostatic repulsion effect (*dynamic Coulomb blockade*) that prevents the simultaneous localization of multiple holes in the core region, and by the presence of a thin interfacial potential barrier between the core and the shell regions that slows down the capture rate of photogenerated shell holes in the core [2]. In **Figure 1 a,b** we show the scheme of the DiB- NCs with and without the barrier. The NCs was produced using two variations of the 'fast' synthesis route [2,4].

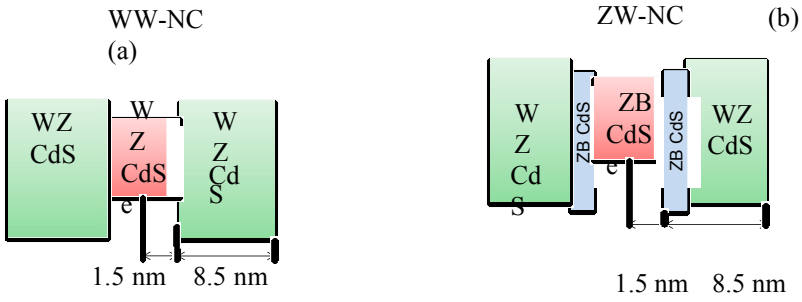

Figure 1: (a,b) Band alignment diagrams for WW-NCs and ZW-NCs respectively.

We performed ultrafast pump-probe measurements with the pump at high photon energies (3.1 eV, higher than the CdS bandgap), with different pump fluences (Φ_{exc}), and the probe over all the visible spectrum . We collected the probe differential transmission ($\Delta T/T$) at different pump-probe time delays. Measurements provide insight into the dynamics of excitons in the two material systems. $\Delta T/T$ spectra are dominated by an intense photobleaching (PB) band at ~2.4 eV, associated to shell states. The PB decay (**Figure 2 a,b**) in the single exciton regime is dominated, in both systems, by the slow (>100 ns) radiative recombination of core-bound excitons that, in quasi type II heterostructures, share the electron with the CdS shell. Upon increasing the Φ_{exc} the PB dynamics of the two systems have different behaviours. In ZW-NCs for <N> greater than 1 the PB show a faster decay as a result of the increasing fraction of the NCs that, in addition to a core exciton, also contain a shell exciton, but remains essentially unchanged for different Φ_{exc} (for <N> lower than about 10), with a long time constant (>1ns). This is consistent with the activation of the Coulomb blockade mechanism which hinders further holes relaxation in the core, hampers Auger recombination in the core, and gives rise to a PB signal related only to recombination of shell states. In contrast in WW-NCs the PB decay becomes faster monotonically with increasing Φ_{exc} , with time constants <1ns. In this case the Coulomb blockade mechanism is not active and therefore the occupancy of core states grows with increasing Φ_{exc}, leading to progressively increasing recombination of core excitons and in case to more efficient Auger recombination for core multiexcitons, that rapidly depletes the conduction band of photoexcited electrons. The initial faster PB decay appearing at very high pump fluencies (<N>>10) in ZW-NCs is finally most likely associated to activated Auger recombination for partial population of shell excitons, probably favored by coupling to surface states.
The difference in hole relaxation dynamics also affects optical gain properties of the two DiB-NC systems which we evaluate by comparing their behaviors in amplified spontaneous emission (ASE) measurements using close-packed NC films fabricated by dip-casting, collecting the emission after different pulsed excitations. Under 150 fs pumping (at 3.1eV) in both DiB samples, the emission spectra show two peaks corresponding to photoluminescence (PL) of core and shell states, with intensity increasing linearly with Φ_{exc} for low Φ_{exc}; at high Φ_{exc} the green band associated to shell PL show a clear line narrowing (ASE) and the output emission grows superlinearly as a result of amplified spontaneous emission. Shell-based excitons quickly recombine via amplified emission before holes relax into the core. A profound difference in optical gain properties of WW- and ZW-DiB NCs is observed under *nanosecond* pulsed excitation (5 ns at 3.5 eV): actually we could not achieve the ASE regime with WW-NCs, while it could be readily realized with ZW-NCs (**Figure 2c**). This different behavior is directly linked to the difference in the lifetimes of shell localized holes which in WW-NCs is much shorter than the ns pulse duration hindering the population inversion and the avalanche process, while in ZW-NCs is longer due to the Coulomb blockade effect enabling thus ASE also with ns pulse excitation.

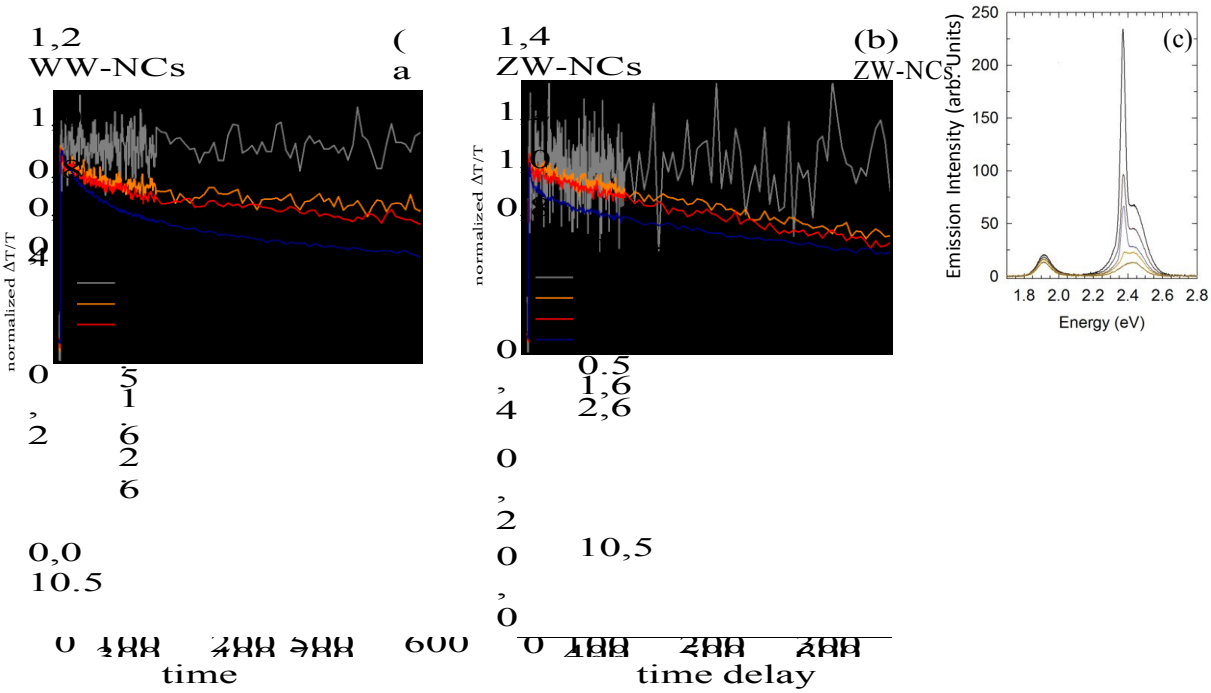

Figure 2: (a,b) (□T/T) PB dynamics at 2.4 probe energy for different excitation fluences, for WW-NCs and ZW-NCs respectively; (c) emission spectra of ZW-NC film under ns pulsed excitation, for different excitation fluences.

Conclusions

In conclusion, we compared CdSe/CdS DiB NCs differing exclusively for their crystal structure (ZW- and WW-NCs) in order to unveil the effect of the interfacial core/shell barrier in the dual-color emission properties. Our results demonstrate that dual emission can be obtained in both polytipic and homogeneous shell DiB-NCs. Data also indicate that the Coulomb blockade mechanisms for photogenerated shell holes is only active in structures with polytipic WZ-NCs and that it hinders the formation of multi-excitons in the NC core and core exciton Auger recombination. Moreover it allows for achieving ASE from shell states using simple nanosecond pulsed excitation sources, while ASE is obtained only with fs pulsed sources in homogenous WW-NCs.

References:

[1] Deutsch Z, Schwartz O, Tenne R, Popovitz-Biro R, Oron D; Two-Color Antibunching from Band-Gap Engineered Colloidal Semiconductor Nanocrystals; Nano Letters; 12 (2012) 2948–2952;

[2] Galland C, Brovelli S, Bae W K, Padilha L A, Meinardi F, Klimov V I; Dynamic Hole Blockade Yields Two-Color Quantum and Classical Light from Dot-in-Bulk Nanocrystals; Nano Letters; 13 (2013) 321-328;

[3] Zhao H G. Liang H Y, Gonfa B A, Chaker M, Ozaki T, Tijssen P, Vidal F, Ma D; Investigating photoinduced charge transfer in double- and single-emission PbS@CdS core@shell quantum dots; Nanoscale; 6 (2014) 215–225;

[4] Christodoulou S, Vaccaro G, Pinchetti V, De Donato F, Grim J Q, Casu A, Genovese A, Vicidomini G, Diaspro A, Brovelli S, Manna L, Moreels I; Synthesis of highly luminescent wurtzite CdSe/CdS giant-shell nanocrystals using a fast continuous injection route; Journal of Materials Chemistry C; 2 (2014) 3439-3447;

Nonlinear Optical Properties of Metallic Nanoantennas Investigated by Angle Resolved Confocal Microscopy with Femtosecond Laser Pulses

Jiyong Wang[a,b], *Jérémy Butet*[c], *Anne-Laure Baudrion*[b], *Gaëtan Lévêque*[d], *Andreas Horrer*[e], *Olivier J. F. Martin*[c], *Alfred J. Meixner*[a], *Monika Fleischer*[e], *Pierre-Michel Adam*[b], *Anke Horneber*[a] *and Dai Zhang**[a]

[a] Institute of Physical and Theoretical Chemistry, Eberhard Karls University of Tübingen, Auf der Morgenstelle 15, 72076, Tübingen, Germany
[b] Laboratoire de Nanotechnologie et d'Instrumentation Optique, ICD, CNRS UMR 6281, Université de Technologie de Troyes, 12 rue Marie Curie, CS 42060, 10004 Troyes Cedex, France
[c] Nanophotonics and Metrology Laboratory (NAM), Swiss Federal Institute of Technology, Lausanne (EPFL), 1015, Lausanne, Switzerland
[d] Institute of Electronics, Microelectronics and Nanotechnology (IEMN), UMR-CNRS 8520, UFR of Physics, University of Lille 1, 59655 Villeneuve d'Ascq, France
[e] Institute of Applied Physics, Eberhard Karls University of Tübingen, Auf der Morgenstelle 10, 72076 Tübingen, Germany

**e-mail: dai.zhang@uni-tuebingen.de*

Keywords: Plasmon, Nonlinear optics, Nanodimer, Second harmonic generation, Two-photon photoluminescence

Introduction

Metallic nanostructures exhibit fascinating linear and nonlinear optical properties once they are excited by appropriate incident light. Localized Surface Plasmons (LSPs) generated by a collective oscillation of electrons in the conduction band offer the possibility of enhancing and concentrating the electrical field in a subwavelength volume enabling the nanostructures to act similarly to antennas in the microwave or radiowave regime [1-2]. The influences of LSP resonances on the linear optical properties of plasmonic nanoantennas, such as the scattering, the absorption, and the one-photon photoluminescence have been rigorously and systematically investigated [3-4]. However, nonlinear optical processes in plasmonic nanoantennas, such as two-photon photoluminescence (TPL) and second harmonic generation (SHG), are still not fully understood.

Results and Discussion

A comprehensive study of TPL and SHG from separated and connected gold nanodimers fabricated using an electron-beam-lithographic technique was conducted here. In particular, the influence of the gap size and nanodisc diameter on their nonlinear optical response is addressed in detail. Analyzing the nonlinear optical spectra and performing polarization resolved measurements by rotating the excitation field, using an experimental setup combining a femtosecond laser source with a parabolic mirror, we show that SHG and TPL exhibit a different behavior despite the fact that these two nonlinear optical processes have the same fundamental intensity dependence, as shown in Fig. 1(a). The underlying physical mechanisms explaining the differences are revealed using a surface integral equation method for nonlinear computations [5-6], as shown in Fig. 1(b). The different evolutions of SHG and TPL with the nanodimer geometry are due to their distinct physical natures, resulting in different coherence properties and specific rules for plasmon enhancement [7-8].

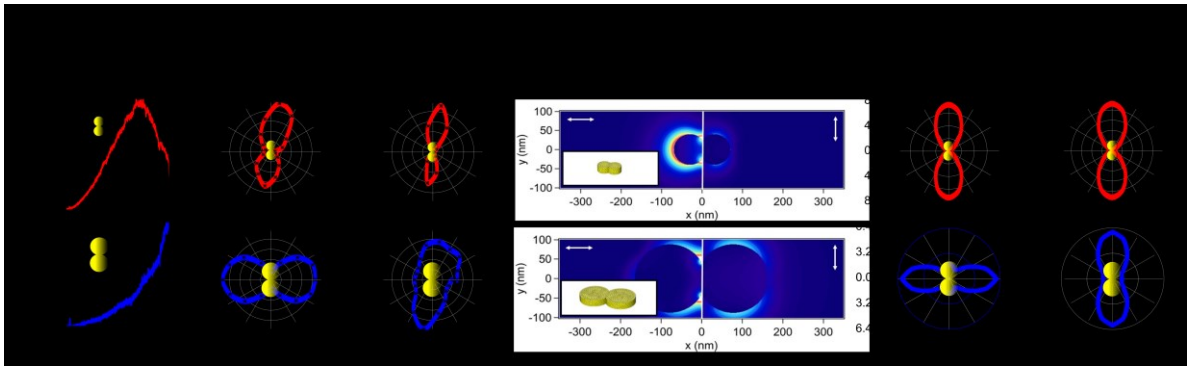

Figure 1:(a) Nonlinear spectra under longitudinal excitations and polarization resolved intensities of SHG and TPL for Au-Au connected dimers with diameters of 80 nm (red) and 160 nm (blue); (b) corresponding simulations combining near-field distributions.

Conclusions and Outlook

Our results clearly point out that the measurement of electromagnetic hot spots using nonlinear optical processes is not direct and that a competition between different enhancement mechanisms in the nonlinear response often occurs. Furthermore, these results emphasize that nonlinear light-matter interaction processes probe the internal field distribution and provide no direct information about the external fundamental near-field distributions and intensities around plasmonic nanostructures, despite the fact that these two distributions are closely related to each other. These results provide a new insight into the nonlinear optical properties of coupled plasmonic systems.

References:

[1] Barnes W L, Dereux A, Ebbesen T W; Surface plasmon subwavelength optics; Nature; 424(2003) 824-830;

[2] Horneber A, Baudrion A L, Adam P M, Meixner A J, Zhang D; Compositional-asymmetry influenced non-linear optical processes of plasmonic nanoparticle dimers; Physical Chemistry Chemical Physics; 15(2013) 8031-8034;

[3] Crut A, Maioli P, Del Fatti N, Vallée F; Optical Absorption and Scattering Spectroscopies of Single Nano-Objects; Chemical Society Reviews ; 43(2014) 3921-3956;

[4] Gaiduk A, Yorulmaz M, Orrit M; Correlated Absorption and Photoluminescence of Single Gold Nanoparticles. Chem PhysChem.; 12(2011) 1536-1541;

[5] Butet J, Duboisset J, Bachelier G, Russier-Antoine I, Benichou E, Jonin C, Brevet P F; Optical second harmonic generation of single metallic nanoparticles embedded in a homogeneous medium; Nano Letters; 10(2010) 1717-1721;

[6] Butet J, Thyagarajan K, Martin O J; Ultrasensitive optical shape characterization of gold nanoantennas using second harmonic generation; Nano Letters; 13(2013) 1787-1792;

[7] Horneber A, Braun K, Rogalski J, Leiderer P, Meixner A J, Zhang D; Nonlinear optical imaging of single plasmonic nanoparticles with 30 nm resolution; Physical Chemistry Chemical Physics; 2015 21288-21293;

[8] Dulkeith E, Niedereichholz T, Klar T, Feldmann J, Von Plessen G, Gittins D, Mayya K, Caruso F; Plasmon emission in photoexcited gold nanoparticles; Physical Review B; 70(2004) 205424;

Second harmonic generation in plasmonic nanostructures: multiresonant nanoantennas and eigenmodes

J. Butet, K.-Y. Yang, G. Bernasconi, O. J. F. Martin

Nanophotonics and Metrology Laboratory (NAM), Swiss Federal Institute of Technology Lausanne (EPFL), 1015, Lausanne, Switzerland

**e-mail: jeremy.butet@epfl.ch*

Keywords: Nonlinear optics, Nonlinear plasmonics, Mode matching, Nanostructure design

Introduction

It is well known that metallic nanoantennas are able to enhance and control light-matter interactions down to the nanoscale. Indeed, optical antennas have the ability to concentrate the electric field inside their nanogap beating the diffraction limit. The enhancement of the electric field enables the observation of nonlinear optical processes. For instance, second harmonic generation (SHG) from metallic nanoantennas [1], the process thereby two photons at the fundamental frequency are converted into one photon at the second harmonic (SH), has been experimentally reported recently [2]. Recently, multiresonant nanostructures (structures supporting one resonance at the fundamental wavelength and one resonance at the SH wavelength) have been proposed for increasing the nonlinear conversion down to the nanoscale [3, 4].

Results and Discussion

During this presentation, we provide a full understanding of the mechanisms that lead to SHG in multiresonant plasmonic structures. By combining experiments on aluminum plasmonic nanostructures with surface integral equation simulations, we have investigated the SHG from double resonant nanoantennas (DRAs) with a various geometries. Indeed, the long bar L_2 of the DRA has been first optimized and fixed at 160 nm, while the short bar L_1 is incrementally increased from 20 to 200 nm (see Figure 1). We clearly observe that the SH intensity is maximum when the short bar exhibits a maximum of scattering in the linear regime at 400 nm. The corresponding SH near-field distribution confirms that the near-field of the quadrupolar SH sources supported by the long bar L_2 excite the dipolar mode of the short bar L_1, resonant at the same wavelength, Figure 1(b). If the length oft he short bar L_1 is further increased, it becomes out of resonance and the SH intensity decreases dramatically, emphasizing the role of energy transfer between both bars in the nonlinear conversion, Figure 1(c). SHG increases again when the short bar L_1 is such that the structure becomes symmetric, L_1=160 nm in Figure 1(c), and strongly resonant at the fundamental wavelength. The agreement between calculations (red line) and experiments (blue line) is excellent, Figure 1(c).

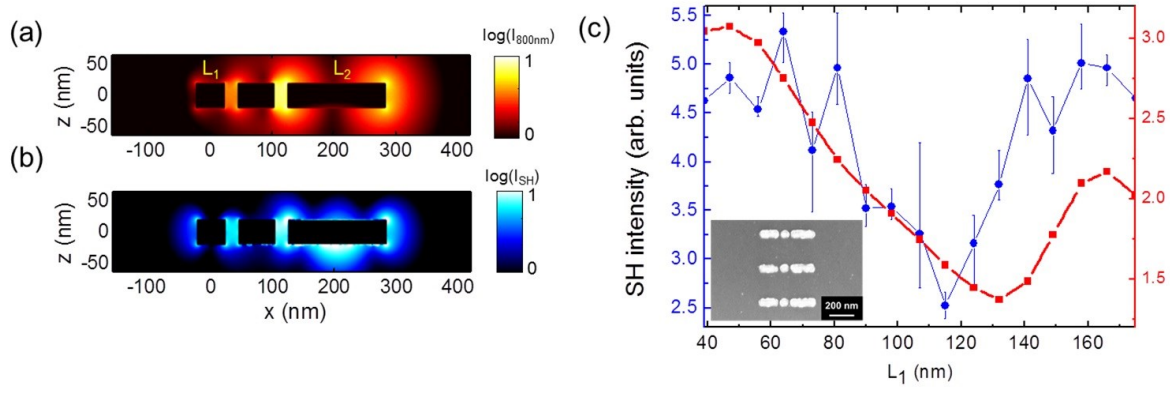

Figure 1: Near-field distributions of the DRA with L_1=47nm: (a) Fundamental intensity and (b) SH intensity. (c) Far-field SH intensity as a function of the length L_1.

In a second part, we will show that SHG can also provide information on the underlying modes supported by a given plasmonic nanostructure. Indeed, a combination of modes at the fundamental frequency can generate SH waves supported by modes that cannot be excited at the fundamental frequency, the so called dark modes [5]. SHG can then be used to measure the radiation pattern of those dark modes. If the fundamental frequency matches a resonance of the structure, the high field enhancement will yield a high SHG. Additionally, if the SH frequency matches another higher frequency mode, the SH emission will be stronger and thus more easily measurable as in the case of the DRAS. Being able to optimize the structure, *i. e.* that

both SHG and fundamental frequencies match resonant modes, is then very important for practical applications, as nonlinear plasmonic sensing [6, 7], and the proposed numerical approach is very convenient for this purpose.

Conclusions and/or Outlook

During this presentation, we have reviewed our recent work on the optimization of SHG from plasmonic nanostructures, mainly the ones supporting double resonances. This work paves the way to the design of efficient nonlinear plasmonic metasurfaces, combining the optimization of the fundamental and SH electromagnetic properties, with new nonlinear capabilities [8].

References:

[1] Butet J, Brevet P-F, Martin O J F; Optical Second Harmonic Generation in Plasmonic Nanostructures: From Fundamental Principles to Advanced Applications; ACS Nano 9 (2015), 10545–10562.

[2] Butet J, Duboisset J, Bachelier G, Russier-Antoine I, Benichou E, Jonin C, Brevet P-F; Optical Second Harmonic Generation of Single Metallic Nanoparticles Embedded in a Homogeneous Medium; Nano Lett. 10 (2010), 1717-1721.

[3] Thyagarajan K, Rivier S, Lovera A, Martin O J F; Enhanced second-harmonic generation from double resonant plasmonic antennae; Opt. Express 20 (2012), 12860-12865.

[4] Thyagarajan K, Butet J, Martin O J F; Augmenting Second Harmonic Generation Using Fano Resonances in Plasmonic Systems; Nano Lett. 13 (2013), 1847-1851.

[5] Butet J, Dutta-Gupta S, Martin O J F; Surface Second-Harmonic Generation from Coupled Spherical Plasmonic Nanoparticles: Eigenmode Analysis and Symmetry Properties; Phys. Rev. B 89 (2014), 245449.

[6] Butet J, Russier-Antoine I, Jonin C, Lascoux N, Benichou E, Brevet P-F; Sensing with Multipolar Second Harmonic Generation from Spherical Metallic Nanoparticles; Nano Lett. 12 (2012), 1697-1701.

[7] Butet J, Martin O J F; Refractive index sensing with Fano resonant plasmonic nanostructures: a symmetry based nonlinear approach; Nanoscale 6 (2014), 15262-15270.

[8] Butet J, Martin O J F; valuation of the nonlinear response of plasmonic metasurfaces: Miller's rule, nonlinear effective susceptibility method, and full-wave computation; J. Opt. Soc. Am. B 33 (2016), A8-A15.

Femtosecond time-resolved optical studies of functionalized metal nanoparticle systems.

D. Catone,[1] P. O'Keeffe,[2] A. Paladini,[2] F. Toschi,[2] S. Turchini,[1] G. Testa,[3] A. Cartoni,[2,3] I. Fratoddi,[3] I. Venditti,[3] L. Avaldi[2]

[1]CNR-ISM, Area della Ricerca di Roma Tor Vergata, 100 Via del Fosso del Cavaliere, Rome, Italy
[2]CNR-ISM, Area della Ricerca di Roma 1, Monterotondo Scalo, Italy
[3]Department of Chemistry, University of Rome La Sapienza, P.le A.Moro 5, 00185 Rome, Italy

Keywords: nanoparticles, femtosecond laser, time-resolved spectroscopy, surface plasmon resonance

The interaction of visible light with gold nanoparticles (AuNPs) has been the subject of intensive study in recent decades [1, 2]. Much of this interest has been stimulated by the presence of the surface plasmon resonance (SPR) of AuNPs in the visible range arising due to a resonance between the oscillating dipole created by displaced electrons in the NPs and the light field impinging on the NPs. In isolated gold NPs this leads to absorption of green light (max. 520 nm) and to the photon confinement induced by the SPR that strongly enhances all radiative and non-radiative processes in the vicinity of the surface of the particles. These properties have led to the widespread applicative use of NPs in many fields such as surface enhanced Raman spectroscopy [3], biosensors [4], biomedicine [5], and biodiagnostics to name but a few. An interesting up-start of the SPR is that it can be used to monitor shape and morphology of AuNPs during synthesis/modification processes. The situation is somewhat more complicated in the case of dye-stabilized AuNPs due to the inter-particle coupling effects which lead to a distortion of the SPR. Indeed the SPR splits into two with one resonance remaining in the vicinity of that of the isolated AuNPs and is generally called the transverse SPR while a second resonance due to an extended excitation spanning across multiple particles appears to the lower energies. The precise spectral energy and shape of the extended plasmon resonance depends on the inter-particle distance, the particle disposition and the number of particles involved.
The first experimental activities of the new EUROFel Support Laboratory (EFSL) are concentrated on the time resolved studies of these plasmonic effects in dye-stabilized AuNPs. The femtosecond EFSL laser system is used to optically pump the NP systems and a white light probe is used to record the transient absorption spectrum. The femtosecond resolution of these experiments gives us access to the electron-phonon and phonon-phonon coupling time scales in these systems.

References:
[1] M. C. Daniel, D. Astruc, Chemical Reviews 104, 293 (2004).
[2] P. K. Jain, W. Huang, M. A. El-Sayed, Nano Letters, 7, 2080 (2007).
[3] S. Nie and S. R. Emory, Science, 275, 1102 (1997).
[4] K. Saha, S. S. Agasti, C. Kim, X. Li and V. M. Rotello, Chemical Reviews, 112, 2739 (2012).
[5] E. C. Dreaden, A. M. Alkilany, X. Huang, C. J. Murphy, M. A. El-Sayed, Chem. Soc. Rev. 41, 2740 (2012).

From ripples to spikes: a hydro-dynamical physical mechanism to interpret femtosecond laser induced self-assembled structures

*G. D. Tsibidis1**

1Institute of Electronic Structure and Laser (IESL), Foundation for Research and Technology (FORTH), N. Plastira 100, Vassilika Vouton, 70013, Heraklion, Crete, Greece

*E-mail: * tsibidis@iesl.forth.gr*

Materials irradiated with multiple femtosecond laser pulses in sub-ablation conditions are observed to develop various types of self-assembled morphologies that range from nano-ripples to periodic micro-grooves and quasi-periodic micro-spikes. We present a physical scenario that comprises: [1] (i) an electromagnetics component that describes the surface plasmon wave (SPW) excitation and interference with the incident beam that leads to a periodic modulation of the laser field energy density [2-3], (ii) a heat transfer component that accounts for carrier-lattice thermalisation through particle dynamics and heat conduction and carrier-phonon coupling, and (iii) a hydrodynamics component that describes the molten material dynamics and re-solidification process assuming an incompressible Newtonian fluid flow that includes recoil pressure and surface tension contributions as well as Marangoni effects [4]. We demonstrate the significant role of the hydrodynamical effects in the description of the formation of the grooves and spikes which is a process that is not yet understood. The proposed physical mechanism could be generally applicable to practically any conductive material structured by ultrashort laser pulses, therefore it can be useful for the interpretation of further critical aspects of light matter interaction.

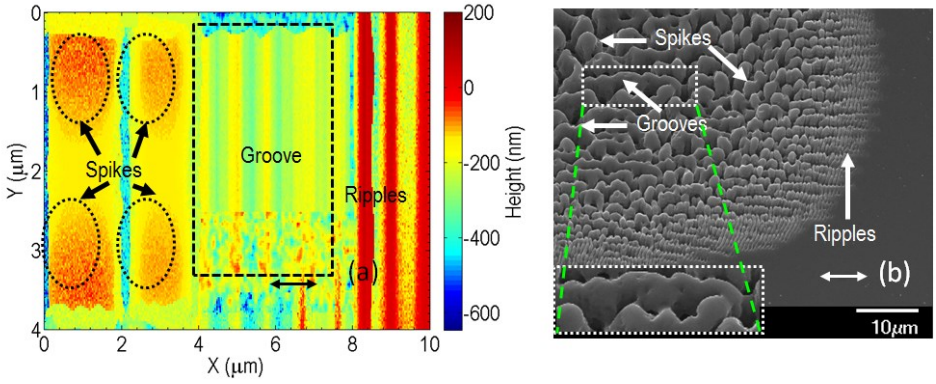

Fig. 1. Ripples, Grooves, Spikes: (a) Theoretical and (b) Experimental results.

Acknowledgement: The authors G.D.T and E.S. acknowledge financial support from the project *LINABIOFLUID*.

References

[1] G. D. Tsibidis, C. Fotakis, and E.Stratakis. **Physical Review B** 92, 041405(R) (2015)
[2] G. D. Tsibidis, E. Stratakis, P. A. Loukakos, and C. Fotakis, **Applied Physics A**, **114**:57–68 (2014).
[3] M. Barberoglou, G. D. Tsibidis, D. Grey, M. Magoulakis, C. Fotakis, E. Stratakis, and P. A. Loukakos P.A., **Applied Physics A**, **113**, 273-283 (2013).
[4] G. D. Tsibidis, M. Barberoglou, P. A. Loukakos, E. Stratakis, and C.Fotakis, **Physical Review B**, **86**, 115316 (2012).

Optical and magnetic properties of various bimetallic nanoparticles obtained by Laser Ablation Synthesis in Solution

Beata Kalska-Szostko[a], Stefano Scaramuzza[b], Vincenzo Amendola[b], Dariusz Satuła[c]*

[a]Institute of Chemistry, University of Bialystok, Bialystok, Poland
[b]University of Padova, Department of Chemical Sciences, Padova, Italy
[c]Department of Physics, University of Bialystok, Bialystok, Poland

*e-mail: kalska@uwb.edu.pl

Keywords: bimetallic nanoparticles, Laser Ablation Synthesis in Solution

Introduction

There are many fabrication methods of the nanograin systems where different quality nanostructures can be fabricated [1]. It is still challenging to obtain well defined nanoparticles with narrow size distribution, and with good stability in the solution. Many efforts have been made to achieve multifunctional materials with a simple synthetic procedure and easy processing for subsequent application. Nanoscale spices allows to improve quality and efficiency, for example, nanosensors with a sensing possibility going down to a single molecule. Application of the laser ablation method in modulation or stimulation of chemical reactions causes simplification of the fabrication processes and obtaining of a new class of nanomaterials [2]. Because many sophisticated fabrication procedures need to employ very expensive devices like ultrahigh vacuum chambers (MBE, or sputtering, etc.) or other techniques like lithograply, it is useful to develop new approaches which are less expensive. Wet chemistry combined with laser ablation is one of them. It opens new synthetic capability and access to larger variety of materials. It allows to perform synthesis of compounds from bulk source, which in principle can have many different compositions, which were not accessible by traditional synthesis. Laser ablation is a method which allow to obtain nanoparticles with controlled size distribution and composition, but still many effects (type of solution, laser wavelength, pulse parameters, etc.) can influence on the size of nanoparticles and its properties due to surface termination and not homogenous core composition.

Results and discussion

In presented studies bimetallic nanoparticles where obtained via LASiS technique. During preparation, bulk bimetallic alloys with presence of following elements: Ag, Au, Cu, Fe were used. Molar ratio of Fe:Me alloys was always kept 80:20. After synthesis nanoparticles were analyzed with UV-Vis spectrometry, X-ray diffraction and transmission electron microscopy. Obtained characterization allows to observe changes in optical response of nanoparticles, their size, shape and crystalline structure.

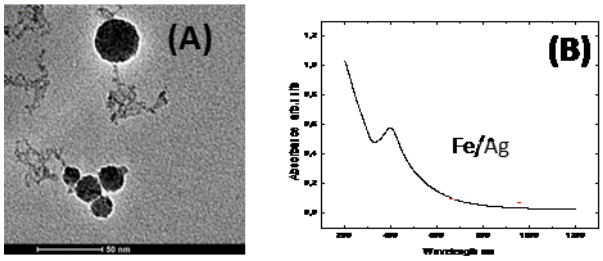

Figure. 1: (A) TEM image of Fe-Cu nanoparticles, (B) UV-Vis spectrum of Fe/Ag nanoparticles.

Conclusions and/or Outlook

Laser Ablation Synthesis in Solution (LASiS) is one of the option for easy and environment friendly nanostructures fabrication technology.

Acknowledgement: The work was partially financed by EU founds via projects with contract number POPW.01.03.00-20-034/09-00 and 3/N/ST5/00568 and COST-STSM-ECOST-STSM-MP1302-221115-068387

References:

[1] V. Cabral, R. Silva, Nanomaterials: Properties, Preparation, Processes, Nanotechnology Science and Technology, Nova Science Publishers 2011
[2] V. Amendola, S. Scaramuzza et. Al. Nano Research 11 (2015) 1-20

Size and gap distance dependences of non-linear optical polarization properties of gold dimers

A. Horneber[a,], J. Y. Wang[a,b], A.-L. Baudrion[b], P.-M. Adam[b], A. J. Meixner[a] and D. Zhang[a,*]*

[a]Institute of Physical and Theoretical Chemistry, Eberhard Karls University of Tübingen, Germany
[b]Laboratoire de Nanotechnologie et d'Instrumentation Optique (LNIO)
Institut Charles Delaunay - UMR CNRS 6281, Université de technologie de Troyes, France

**e-mail: anke.horneber@uni-tuebingen.de , dai.zhang@uni-tuebingen.de*

Keywords: nonlinear optical effect, 2PPL, SHG, fs-SNOM

Metallic nanoantennas with sub-wavelength dimensions exhibit usually strong plasmon resonances, which influence their optical properties dominantly. We have investigated the linear and non-linear optical effects from various plasmonic systems like nanoparticles, sharp tips and nanotriangles [1-3] with either confocal optical microscopy or scanning near-field optical microscopy (SNOM). The linear optical properties of dimer antennas consisting of two Au nanospheres with a small gap in between are very commonly investigated. They are known to exhibit strong near field inside a small gap between the two plasmonically coupled single nanoobjects. Based on the gap-field generated by the plasmonic coupling, nonlinear effects like second harmonic generation (SHG) and two photon photoluminescence (2PPL) can be investigated. We choose arrays of Au homo- and hetero-dimers to study the influences of particle size and gap distance on the non-linear polarisation properties of these dimer structures. Especially the angle resolved 2PPL and the SHG signals were measured and their different dependences on the electromagnetic near-field were discussed.

In our recent study, we reported to use SNOM tips studying the plasmonic coupling between a sharp tip apex and the different positions of one single Au nanotriangle. We presented SHG and 2PPL spectroscopy and microscopy in this Au-Au gap mode with sub 30 nm optical resolution [3]. To achieve a more precise and flexible control of the gap distance in the Au-Au dimer antenna especially at small distances of less than 5 nm, we will adopt a similar SNOM configuration where a sharp Au tip is positioned in the close proximity of a Au surface via sensitive shear-force feedback. By switching between the radial and azimuthal polarized doughnut modes, we will compare the dependence of the SHG and 2PPL intensity on the local near-field in the Au tip – Au substrate that is less than 5 nm wide.

References

[1] P. Reichenbach, A. Horneber, D. A. Gollmer, A. Hille, J. Mihaljevic, C. Schäfer, D. P. Kern, A. J. Meixner, D. Zhang, M. Fleischer, L. M. Eng, Opt. Express, 22 (2014)15484.
[2] A. Horneber, A. L. Baudrion, P. M Adam, A. J. Meixner, D. Zhang, Phys. Chem. Chem. Phys., 15 (2013) 8031.
[3] A. Horneber, K. Braun, P. Leiderer, A. J. Meixner, D. Zhang, Phys. Chem. Chem. Phys., 17 (2015) 21288.

THz and IR plasmonic absorption of 3D nanoporous graphene

S. Lupi[a], F. D'Apuzzo[b], F. Giorgianni[b], R.A. Piacenti[b], M. Autore[b], M. Cestelli Guidi[c], Y. Ito[d], M. Chen[d], A. Marcelli[c,e]*

[a]Dipartimento di Fisica and INFN, Università di Roma *Sapienza*, P.le Aldo Moro 2, 00185 Roma, Italy
[b]Center for Life Nano Science@Sapienza, IIT, V.le Regina Elena 291, 00186, Roma, Italy
[c]INFN and University of Rome *Sapienza*, Department of Physics, P.le A. Moro 2, 00185, Rome, Italy [d]WPI Advanced Institute for Materials Research, Tohoku University, Sendai 980-8577, Japan

[e]RICMASS, Rome International Center for Materials Science Superstripes, via dei Sabelli 119A, 00185 Rome, Italy.

**e-mail:marcelli@lnf.infn.it*

Keywords: 3D-Graphene; grapheme plasmons; Dirac carriers; nanoporous materials

Introduction

Graphene Plasmons hold promise of wide applications due to low-losses, tenability and extreme confinement at the nanoscale, and have been investigate in all sorts of 2D nanostructures and hybrid systems [1]. 3D Nanoporous Graphene (NPG) has recently been obtained with a new Chemical Vapor Deposition based fabrication process [2], obtaining graphene samples within a 3D conformation (see Fig.1a) while retaining the unique characteristics of massless Dirac fermions with a high electron mobility.

Results and Discussion

While NPG is the object of ongoing studies to demonstrate its application such as energy harvesting electrode [3], little is known about its optical properties. In this contribution we will show THz and IR optical conductivity measurements. The optical conductivity spectra (see Fig.1b) exhibit, beside the typical interband absorption of graphene above the threshold of $2E_F$ (chemical potential of the system), i.e. in the near-IR and visible part of the spectrum, a strong plasmonic absorption at THz (for low-doped samples) and Mid-IR (for E_F=250 meV) frequency. We will demonstrate that these plasmonic excitations strongly depend on the chemical doping and pore-size of the NPG 3D structure, following the behavior of 2D Dirac-plasmons like in 2D graphene [4].

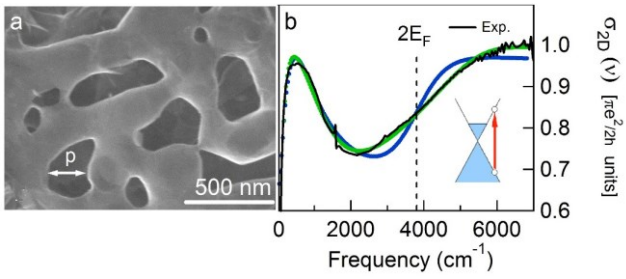

Figure 1: a) SEM image of nanoporous graphene with an average pore size of 200 nm; b) IR absorption spectrum for a doped sample showing interband transitions and a plasmonic peak, at high and low frequency,respectively.

Conclusions

In conclusion, this research represents a systematic optical investigation of 3D nanoporous structures made of monolayer graphene. The optical conductivity of such non-periodic array of graphene nano- and micro-pores exhibits both single-carrier interband transitions and collective plasmonic modes resonating at THz and Mid-IR frequencies.

The plasmonic excitation depends on the nanostructure geometry and by doping. In fact, the plasmon frequency in these 3D structures follows the behavior of the 2D-plasmon dispersion as a function of the pore-size. Furthermore, by tuning the Fermi Energy by nitrogen-doping, plasmon-modes can be shifted from 200 to 800 cm^{-1}, with a Fermi Energy dependence typical of Dirac-plasmons. The localized nature of plasmon excitations, probably around nanopores, combined with the extremely large surface area of NPG and N-NPG, holds promise for plasmonic sensing applications of these exotic 3D-like graphene structures.

References:

[1] T. Low and P. Avouris, ACS Nano 8, 1086 (2014)
[2] Y. Ito, M. Chen et al., Angewandte Chemie 126, 1 (2014)
[3] Y. Ito, M. Chen et al., Angewandte Chemie 54, 2131 (2015)
[4] F. D'Apuzzo et al., to be submitted (2016)

DNA-assisted generation of nanoparticle dimers on a glass surface

K. Goeken[a], *R. Gill*[*a]

[a] Nanobiophysics Group, Faculty of Science and Technology, University of Twente, Enschede, The Netherlands

**e-mail: r.gill@utwente.nl*

Keywords: Gold, Nanoparticles, Plasmonics, DNA

Introduction

Noble metal nanoparticles are a major class of nanostructures that have unique optical properties related to the fact that they support plasmon resonances. When two such particles are brought into close proximity from each other, interaction between the plasmons of the two particles give rise to a new spectral signature and to the generation of an enhanced electromagnetic field in between the two particles. This enhanced field can lead to enhancement of light matter interaction and give rise to high signals based on spectroscopies such as surface enhanced Raman spectroscopy (SERS) or surface enhanced fluorescence (SEF). While single nanoparticles can be generated by diverse chemical synthesis methods, the generation of dimer structures is much more challenging. Several methods based on DNA as the template for the preparation of nanoparticle dimers have been suggested in the last decade[1,2], however they usually require relative complex procedures.

Here we show a novel method for the creation of surface bound nanoparticle dimers based on DNA hybridization[3]. This method is relatively straight forward and allow the creation of not only homodimers, but also heterodimers in material or size.

Results and Discussion

In the last few years we have been working on the detection of DNA based on the difference in scattering spectra between single nanoparticles and particle dimers (or multimers)[4]. The basic scheme in depicted in **Figure** 1. We attach gold nanoparticles to a glass surface using the electrostatic attraction between amino-silane coated glass slides and gold (or silver) nanoparticles. We then add thiolated DNA capture probes that attach to the gold nanoparticles. Upon introduction of a target sequence, specific hybridization can occur between the target and the capture probe, leaving the other side of the target exposed to the solution. We then introduce a gold nanoparticles in the solution that are modified with thiolated DNA label sequences that can specifically hybridize to this second exposed part of the target. When target concentration is very large, we get many target DNA strands hybridizing on a single nanoparticles, which leads to the creation of nanoparticle multimers upon introduction of the DNA-modified gold nanoparticles in the solution. This causes the scattering colour of the particles to shift from green to orange, as can be captured by a CCD camera on a dark field microscope (see **Figure** 1, rightmost image). However, when the concentration of the target DNA is low, not all surface-bound nanoparticles will have a target strand hybridized on them, and those that do have will probably have only a single target strand. Therefore, upon addition of the solution of DNA-coated gold nanoparticles, nanoparticle dimers will be generated. This same scheme can be used to generate dimers by introduction of a specific concentration of target sequence, From our experimental results we found that the hybridization of target sequence at 0.1pM concentration for 2 hours will cause about 10% of the surface bound nanoparticles to be hybridized with a single target strand. This makes the change of any single surface-bound particles to have 2 or more DNA strands very low, and therefore the change for multimer generation very small.

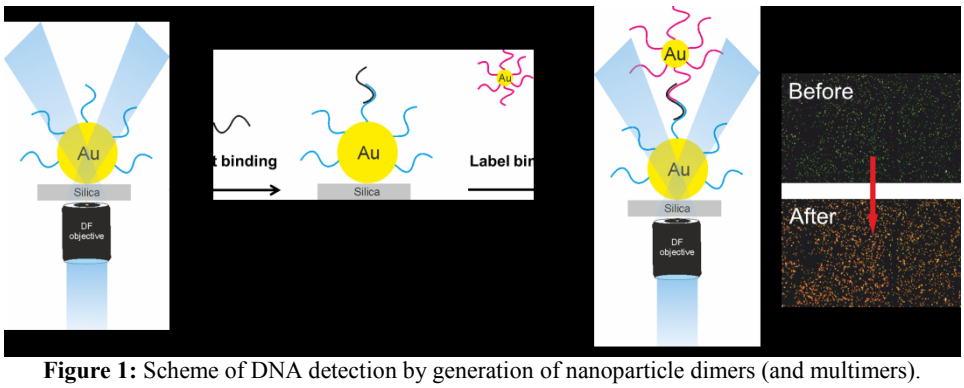

Figure 1: Scheme of DNA detection by generation of nanoparticle dimers (and multimers).

We have used this method to generate nanoparticle dimers of different sizes and materials. **Figure** 2 depicts the scattering spectra of single 80nm silver nanoparticles, and dimers of 80nm silver nanoparticles and 40nm gold nanoparticles. Although the length of DNA between the two nanoparticles should be the same in all cases, we

observe different spectra as there is some polydispersity in the size of the larger surface bound nanoparticles, and the exact angle between the two nanoparticles can be different in different dimers.

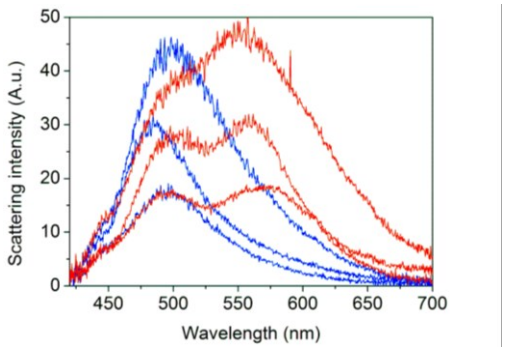

Figure 2: Nanoparticle scattering spectra for single 80nm Ag NPs (Blue lines) and 80Ag-40Au dimers (Red lines)

Conclusions

We have adapted a method we originally developed to detect and quantify an unknown concentration of a target DNA into a method for the generation of surface bound nanoparticle dimers. This method can be used for nanoparticles of different materials and different sizes, as long as there is an efficient chemical method to modify the nanoparticles with DNA. Although this method allows a relatively good control on the distance between the particles, since short double-stranded DNA is relatively stiff, the fact that the exact angle between the nanoparticles is not controlled and that there is some polydispersity in nanoparticle size can lead to different spectra from different nanoparticle dimers.

Acknowledgements

The authors acknowledge support from the Dutch Technology Foundation STW, project number 11818.

References:

[1] Acuna G P, Möller F M, Holzmeister P, Beater S, Lalkens B, Tinnefeld P; Fluorescence enhancement at docking sites of DNA-directed self-assembled nanoantennas; Science; 338 (2012) 506-10;

[2] Busson M P, Rolly B, Stout B, Bonod N, Larquet E, Polman A, Bidault S; Optical and topological characterization of gold nanoparticle dimers linked by a single DNA double strand; Nano Letters; 11 (2011) 5060-5;

[3] Goeken K L, Subramaniam V, Gill; Enhancing spectral shifts of plasmon-coupled noble metal nanoparticles for sensing applications; Physical Chemistry Chemical Physics 17 (2015) 422 – 427;

[4] Verdoold R, Gill R, Ungureanu F, Molenaar R, Kooyman R P H; Femtomolar DNA detection by parallel colorimetric darkfield microscopy of functionalized gold nanoparticles; Biosensors and Bioelectronics; 27 (2011) 77-81;

Formation and electrical control of flying dipolar exciton polaritons

I. Rosenberg[a]*, *Y. Harpaz*[a], *K. West*[b], *L. N. Pfeiffer*[b], *R. Rapaport*[a]

[a]The Racah Institute of Physics, The Hebrew University of Jerusalem, Jerusalem 91904, Israel.
[b]School of Engineering and Applied Science, Princeton University, Princeton, NJ 08540.

[*]*e-mail: Itamar.Rosenberg@mail.huji.ac.il*

Keywords: Dipolaritons,Waveguides

Exciton polaritons (henceforth, polaritons) are the dressed states of a strongly coupled quantum well (QW) exciton and a confined photon. Polaritons are realized mainly in planar semiconductor microcavities, however the strong coupling between QW excitons and photons confined in an optical waveguide (WG) mode was recently demonstrated [1](**Figure 1(a)**). WG-polaritons propagate over hundreds of microns from their excitation spot with high group velocities. Since these WG-polaritons consist of simple excitons, the ability to control their motion comes from manipulating their photonic part in the WG. This constraint also limits the strength of the polariton-polariton interactions.
When an electric field (EF) is applied across the growth direction of a QW, a charge separation is induced, the excitons become dipolar and their energy undergoes a quadratic Stark redshift with respect to the magnitude of the electric field (EFM)[2] (illustration in **Figure 1(b)**). Thus, electrical gating should add additional functionality to a polaritonic system. By controlling the EFM one can tune the energy of the now dipolar exciton and with it the energy of the dipolariton . In addition, due to the additional dipolar interactions, the inter-particle interaction should be much stronger.

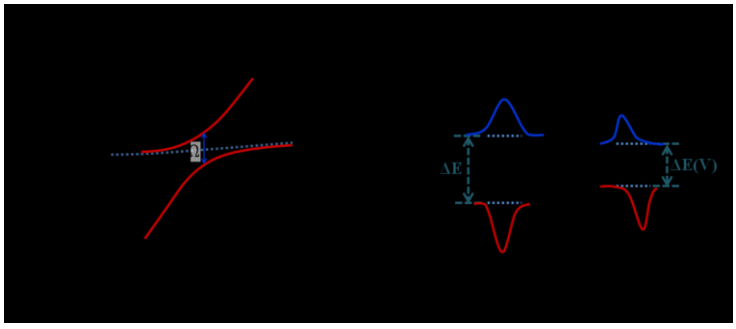

Figure 1: a) An illustration of the strong interaction between an exciton (dashed X) and a WG mode (dashed WG), the resulted modes are the lower and upper polaritons (solid LP,UP respectively). b) An illustration of the formation of dipolar excitons inside a gated QW. The energy of the dipolar exciton is lower due to its interaction with the EF.

Here we demonstrate for the first time the formation of WG-dipolaritons which result from the strong coupling between propagating WG-modes and dipolar-excitons in electrically gated (20nm wide) QWs (System schematics in **FIGURE 2**).

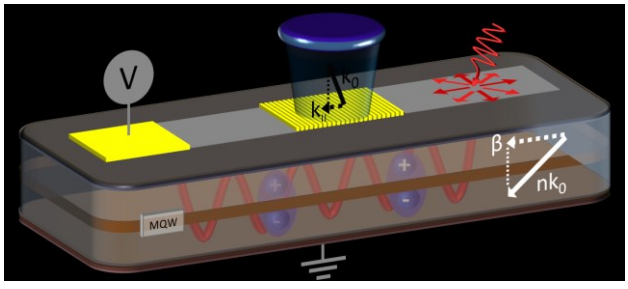

Figure 2: Schematics of our system of interest. Multiple QW are embedded inside a WG which is gated by a thin Ti electrode through which we can excite non resonantly. Emitted photons are coupled out via the metallic grating.

We show that this scheme allows for a flexible and spatially selective electrical tuning of the WG-dipolariton energy landscape using spatially patterned electrical gates and voltage tuning. We also present a scheme for selective excitation and control of WG-dipolaritons using metallic sub-wavelength gratings fabricated on top of the sample. The grating allow for both excitation and measurement of the propagating WG-dipolariton eigenmodes as well as a convenient interface for electrical gating, and extremely long propagation distances of hundreds of microns are easily achieved. Finally we show that by increasing the excitation power, we can achieve a blue shift of the polariton mode energies up to about 2meV, which we attribute to the dipole-dipole interaction between the WG-dipolaritons (**Figure 3**).

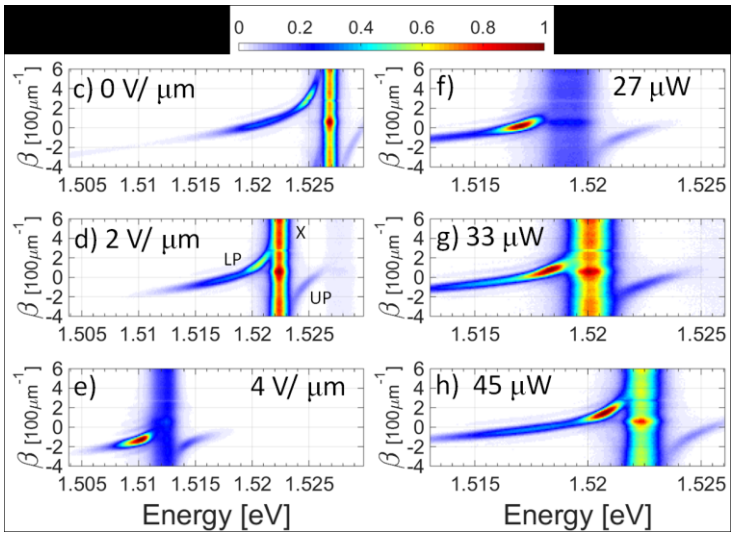

Figure 3: Various dispersion mearurements . (c-e) Polariton dispersions measured for three different EFM. The entire dispersion is red-shifted by ~14meV . (f-h) Polariton dispersions measured for different excitation powers while maintaining constant EFM of 2.4V/um. The experimental results were taken from a sample consisting of an AlGaAs waveguide in which twelve 20nm wide GaAs QWs were embedded.

References:

[1] Walker et al. Applied Physics Letters, 102, 012109 (2013)

[2] G. Bastard et al. Phys. Rev. B 28, 3241 (1983)

Angular Behaviour of 2D sub-wavelength Arrays of Au Nano-cylinders

R. Caputo[a,b], *J. Marae-Djouda*[b], *G. Lévêque*[c], *P.-M. Adam*[b] *and T. Maurer*[b]

[a] Department of Physics and CNR-NANOTEC, 87036 Arcavacata di Rende (CS), Italy
[b] Laboratoire de Nanotechnologie et d'Instrumentation Optique, ICD CNRS UMR n°6281, Université de Technologie de Troyes, CS 42060, 10004 Troyes, France
[c] Institut d'Electronique, de Microélectronique et de Nanotechnologie (IEMN, CNRS-8520), Cité Scientifique, Avenue Poincaré, 59652 Villeneuve d'Ascq, France

e-mail: roberto.caputo@fis.unical.it

Keywords: Sub-wavelength gratings, Au nano-cylinders, localized surface plasmons, vertical plasmon modes.

Introduction

The behaviour of a diffraction grating is governed by the so-called grating equation that is a simple relationship between incidence θ_{inc} and diffracted θ_{diff} angles, wavelength of the impinging light λ and grating pitch Λ.

Under certain conditions, typically when λ>>Λ, no radiative diffracted orders exist but only evanescent ones, and the system is defined as a sub-wavelength grating (SWG) [1]. In case a SWG is made of metallic stripes or nanoparticles, a peculiar behaviour emerges where the presence of the grating influences spectral position and shape of the excited plasmon modes.

In this work, we have designed and fabricated an array of Au nano-cylinders to operate in SWG configuration.

The grating has been characterized by performing angular resolved extinction measurements. Several plasmon modes have been excited that are usually not observed at normal incidence. A complete analysis of these excited plasmon modes and their origin has been possible by comparing obtained experimental results with theory. The appearance and behaviour of these modes by changing the incidence angle are interpreted by using a semi- quantitative approach. Numerical simulations have been performed on both isolated particles and arrays and confirm both the observed behaviour and proposed interpretation.

Results and Discussion

A 2D array of gold monomers was deposited by electron beam lithography on an ITO (Indium Tin Oxide, 30nm thick) coated glass. The array consists of Au nano-cylinders (200nm diameter, 50nm height) with a (center-to- center) pitch Λ_x=Λ_y=300nm. **Figure 1a** shows a SEM picture of the fabricated sample. A confocal transmission set-up, with angle resolved measurement possibility, was used for the optical characterization of the sample. An illumination part, a sample holder and a collection part compose the set-up. All the parts are mounted on a rotating stage to allow the maximum flexibility during measurements (**Figure 1b**).

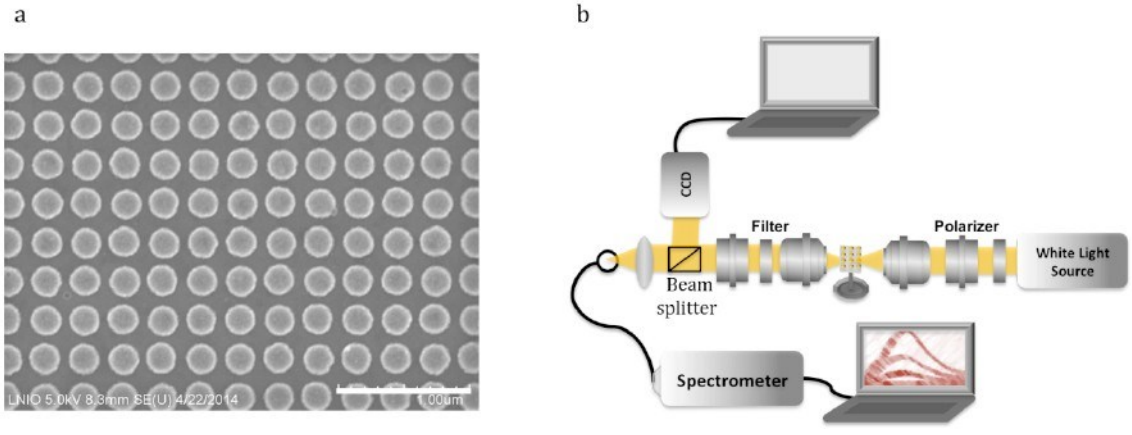

Figure 1: (a) SEM image of the grating of Au NPs, the scale bar is 1μm. The experimental set up is presented in (b).

For performing angle resolved extinction measurements, the sample holder was progressively turned along one of the array main axis, thus modifying the direction of the wave-vector impinging on the nano-

cylinders array. For each measurement, the incidence angle was equal to the collection one and, for all angles, both longitudinal (TE) and transverse (TM) polarizations were considered. The experimental extinction spectra measured at different angles (0°, 15°, 25°, 35°, 52° and 60°), in TE and TM polarizations, are reported in **Figure 2**. At normal incidence, the TE polarized light excites only the dipolar mode (λ=740nm). This mode is due to the coupling between the incident light and the in-plane plasmon oscillation induced along the diameter of the nano- cylinder [2,3] and corresponds to the localized surface plasmon mode at the interface between the Au NPs and the surface of the substrate. By increasing the incidence angle, this dipolar peak undergoes a red shift for both TE and TM polarizations (Fig. 4a,b).

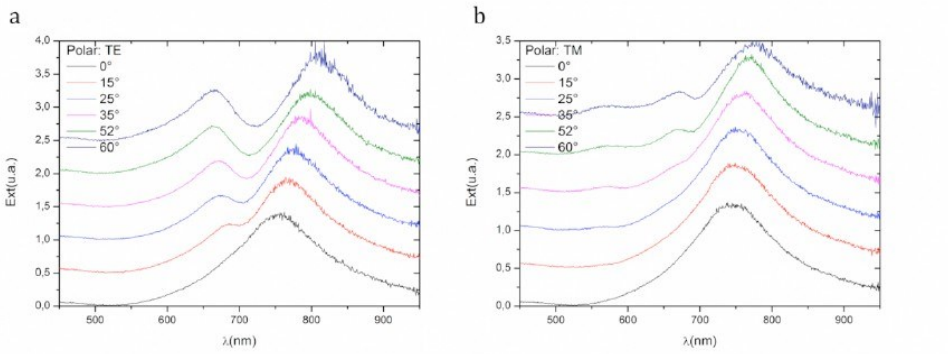

Figure 2: Extinction measurements resolved in angle in TE polarization (a). At normal incidence, only the dipolar mode is excited while by increasing the incidence angle, the quadrupolar mode is excited as well. In the TM polarization (b) only the dipolar mode is also excited. When the incidence angle increases the quadrupolar mode and the vertical mode are excited.

In **Figure 2a**, we can also observe another plasmon peak at lower wavelengths (λ~680nm) that appears at off- normal incidence. This mode can be identified as a quadrupolar charge distribution [3]; it grows in amplitude and is slightly blue-shifted by increasing the incidence angle. **Figure 2b** shows the spectra obtained for the same incidence angle values and for a TM polarization of the exciting light. Also this time the dipolar mode only is obtained at normal incidence and it has closely the same spectral position of that obtained with the TE polarization; this is because the grating is a square and the pitch is the same in both directions.

More interestingly, a new mode, different than both dipolar and quadrupolar ones, can be noticed in the spectra at λ~570nm (**Figure 2b**). This peak is already visible at θ_{inc}=25° and can be attributed to a vertical out-of-plane mode corresponding to the excitation of a plasmon oscillation in the direction along the height of the nano- cylinders. Indeed, it is reliable to consider that, in the TM mode only, the exciting field has a $sin\theta_{inc}$ component that is exactly parallel to this direction. Moreover, from the graphs it is visible that the amplitude of this mode is directly proportional to the incidence angle that matches well with the monotonously increasing behaviour of $sin\theta_{inc}$ in this angular interval. Both these arguments suggest that the observed mode is exactly the vertical one. In our knowledge, this is the first time that this mode has been observed while performing this kind of measurement.

Conclusions and/or Outlook

In this work, angular resolved extinction measurements have been performed on a 2D sub-wavelength grating made of an array of Au nano-cylinders. Exploiting this experimental approach, several plasmon modes have been excited that are usually not observed at normal incidence. The appearance and behaviour of these modes is strongly related to the incidence angle. In particular, by increasing the angle, a red-shift of the dipolar peak is observed that has been interpreted by using a semi-quantitative approach. Numerical simulations have been performed on both isolated particles and arrays and confirm both the observed behaviour and proposed interpretation.

References:

[1] Chartier, G. "Introduction to Optics" Springer (2005) p. 329.

[2] Salerno, M., J.R. Krenn, A. Hohenau, H. Ditlbacher, G. Schider, A. Leitner, and F.R. Aussenegg. 2005. "The Optical near-Field of Gold Nanoparticle Chains." Optics Communications (2005) 248 (4-6): 543–49.

[3] Li, Hongjian, Qiong Liu, Suxia Xie, Xin Zhou, Hui Xia, and Renlong Zhou. "Particle Plasmons Resonant Characteristics in Arrays of Strongly Coupled Gold Nanoparticles." Solid State Communications (2009) 149 (5-6).

Luminescence of organo-metal-halide perovskite nanostructures probed by super-resolution optical microscopy

*Aboma Merdasa, Monojit Bag, Yuxi Tian, Alexander Dobrovolsky, Daniela Täuber, Ivan G. Scheblykin**

[a] Chemical Physics, Lund University, Box 124, SE-22100, Lund, Sweden

**e-mail: ivan.scheblykin@chemphys.lu.se*

Keywords: super-resolution imaging, localization microscopy, perovkite, traps, semiconductor, luminescence, trap photo-curing

Introduction

Organo-metal halide (OMH) perovskites are probably the most studied materials for solar-cell applications during last couple of years. These solution processable semiconductors can give solar cells with 20% efficiency and even lasing. Despite of the great progress in devices, fundamental questions including the nature of photoluminescence and mechanisms of charge recombination and far from been understood. Although at the first approximation OMH perovkites can be seen as direct semiconductors, presence of defects, mechanical softness of the material, ion migration, unusual dielectric properties due to the organic molecule in the crystal structure, formation of crystals of different sizes and topology makes their optical and electrical properties quite peculiar. Here several phenomena we discovered by observation of luminescence of micro- and nanocrystals of $CH_3NH_3PbI_3$ are presented.

Results and Discussion

We employed luminescence microscopy and spectroscopy, super-resolution optical imaging based on localization of emitting sites (SUPERLUMS - super-resolution luminescence spectroscopy[1]), and electron microscopy for the very same sample in order to correlate the sample morphology and properties. We found a huge spatial inhomogeneity of the PL intensity and lifetime at the scales from nanometers and above and assigned it to a vast distribution of the PL quenching trap concentration.[2,3] The trap concentration can be changed by light irradiation which can lead to several orders of magnitude increase of the PL yield.[4] For crystals of less than one micrometer in size we observed PL blinking which shows that a single photoconvertible trap can control PL of the whole crystal.[3] Super-resolution PL microscopy demonstrated so-called emitting sites – small areas (ca 100 nm) having orders of magnitude higher PL yield than the rest of the material.

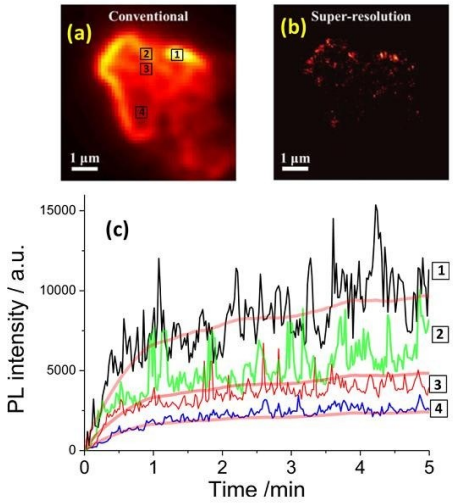

Figure 1: Differential super-resolution luminescence optical imaging. (a) The accumulated image (sum of all 500 frameswith exposure time of 0.1 s per frame taken every 1.32 s) of a large perovskite polycrystal under continuous excitation of 0.2W/cm^2. (b) The super-resolution image shows localized clusters less than 100 nm in size responsible for light emission (emitting sites). (c) Photoluminescence (PL) intensity transient measured locally from the squares marked in (a). The thick red lines are scaled PL intensity of the whole crystal, this data was additionally smoothed. Adapted from Ref.2.

We found that luminescence of ~100-nm crystals enhances much faster than that of larger, micrometer-sized ones. This crystal-size dependence of the photochemical light-passivation of charge traps responsible for PL quenching allowed us to conclude that traps are present in the entire crystal volume, rather than at the surface only. Due to this effect, "dark" micrometer sized perovskite crystals can be converted into highly luminescent smaller ones just by mechanical grinding.[2]

Conclusions and Outlook

SUPERLUMS – as a very simple realization of super-resolution imaging combined with luminescence spectroscopy shown its great potential for application to inhomogeneous semiconducting materials. Besides the possibility to create super-resolved images, luminescence blinking effect allowed us to address properties of traps in the OMH perosvkite semiconductor and directly monitor their formation. We are looking forward for more discoveries in material science by SUPERLUMS and other methods using combination of spectroscopy and super-resolution in optical imaging.

References:

[1] A. Merdasa, Á.J. Jiménez, R. Camacho, M. Meyer, F. Würthner, I.G. Scheblykin, Single Lévy States–Disorder Induced Energy Funnels in Molecular Aggregates, Nano Lett. 14 (2014) 6774–6781. doi:10.1021/nl5021188

[2] Y. Tian, A. Merdasa, E. Unger, M. Abdellah, K. Zheng, S. McKibbin, et al., Enhanced Organo-Metal Halide Perovskite Photoluminescence from Nanosized Defect-Free Crystallites and Emitting Sites, J. Phys. Chem. Lett. 6 (2015) 4171–4177

[3] Y. Tian, A. Merdasa, M. Peter, M. Abdellah, K. Zheng, C.S. Ponseca, et al., Giant Photoluminescence Blinking of Perovskite Nanocrystals Reveals Single-Trap Control of Luminescence, Nano Lett. 15 (2015) 1603–1608

[4] Y. Tian, M. Peter, E. Unger, M. Abdellah, K. Zheng, T. Pullerits, et al., Mechanistic insights into perovskite photoluminescence enhancement: light curing with oxygen can boost yield thousandfold, Phys. Chem. Chem. Phys. 17 (2015) 24978–24987

Optical spectroscopy of individual nano-objects in correlation with electron microscopy imaging: the plasmon response of strongly coupled systems

E. Cottancin[*,a], *C. Bonnet* [a], *M. Broyer* [a], *J. Lermé* [a], *A. Mosset* [a], *J. Ramade* [a], *J-M. Rye* [a] *and M. Pellarin*[a]

[a] Institute of Light and Matter, Université Claude Bernard Lyon 1, CNRS UMR 5306, University of Lyon, Villeurbanne, France

**e-mail: emmanuel.cottancin@univ-lyon1.fr*

Keywords: LSPR, SMS, silver and gold nanocubes, plasmonic coupling

Introduction

Metallic nanoparticles (NPs) have long been known for their particular optical response exhibiting a strong resonance, corresponding to an electromagnetic (EM) field enhancement and called Localized Surface Plasmon Resonance (LSPR). A greater enhancement of the EM field can be obtained when two NPs are in close proximity to each other, which then act as nanoantennas. The most striking effect for pairs of NPs in interaction is a red-shift of the LSPR (for a longitudinal excitation) when the interparticle distance is reduced. Moreover, in the very strong coupling regime and for subnanometric spacing, unexpected distortions of the LSPR may appear due to high order interactions between individual plasmon modes.

In order to understand the relation between the optical response and the morphology of the NPs in interaction, we have developed a highly sensitive spectrophotometer based on the spatial modulation spectroscopy (SMS) technique. This allows the measurement of the absolute extinction of light by a single nano-object over a broad spectral range (300 nm-1650 nm). Moreover, the nano-objects can *a posteriori* be observed by electron microscopy (classical or 3D TEM, SEM), thus allowing a direct correlation between their optical response and their exact morphology [1].

Results and Discussion

Thanks to the combination of optical measurements and electron microscopy, very small interparticle distances (< 1 nm) and morphological effects have been explored for pairs of spherical and cubic NPs made of gold or silver. In the case of spherical pairs, the electrostatic coupling between close but non-touching particles induces a red-shift of the dipolar surface plasmon resonance and the emergence of higher-order plasmon modes. These effects are understood on the basis of the generalized Mie theory and a correlation has been established between the main spectral features of the optical spectra and the interparticle distance *d* independently measured by TEM. Nevertheless, the morphology of the interparticle region is found to play a key role in the optical response for ultra-small interparticle distance.

Regarding nanocubes (NCs), in addition to the redshift of the resonance with decreasing interparticle distance, we observe a clear splitting (or anti-resonance dip) in the main dipolar LSPR. The analysis of the TEM images coupled with numerical simulations lead us to conclude that this dip can emerge when the cubes are sufficiently rounded and when the interparticle distance is small enough [2]. This phenomenon can be interpreted as a Fano resonance due to the coupling between the broad dipolar resonance of the dimer with gap plasmon modes confined to the interplanar zone of both cubes in regard (see Figure 1).

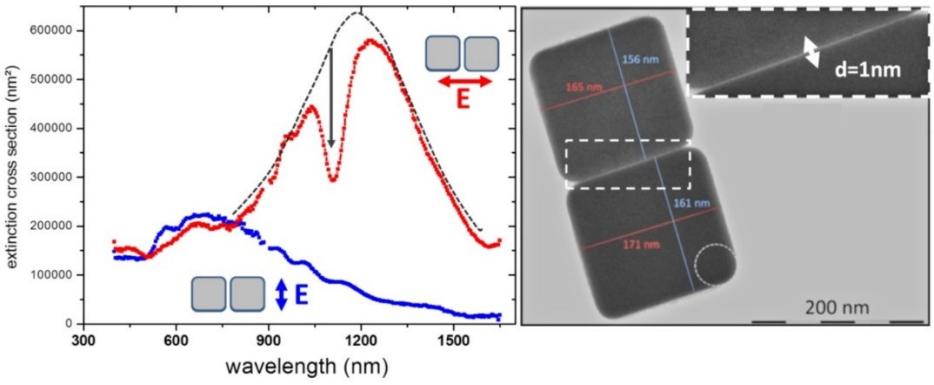

Figure 1: transmission electron microscopy image and extinction cross-sections for a longitudinal (red) and a transversal excitation (blue) of a dimer made of gold nanocubes

Conclusions and/or Outlook

We have shown that Fano resonances can develop in highly symmetric systems such as NC dimers of gold or silver. The high quality factor of the anti-resonance dip to the local environment could make them very efficient nano-sensors.

1. Billaud, P.; Marhaba, S.; Grillet, N.; Cottancin, E.; C. Bonnet; Lermé, J.; Vialle, J.-L.; Broyer, M.; Pellarin, M., Absolute optical extinction measurements of single nano-objects by spatial modulation spectroscopy using a white lamp. *Review of Scientific Instruments* **2010,** *81*, 043101.

2. Grillet, N.; Manchon, D.; Bertorelle, F.; Bonnet, C.; Broyer, M.; Cottancin, E.; Lermé, J.; Hillenkamp, M.; Pellarin, M., Plasmon Coupling in Silver Nanocube Dimers: Resonance Splitting Induced by Edge Rounding. *ACSNano* **2011,** *5* (12), 9450-9462.

Fluorescence microscopy of single organo-metal halide perovskite nanowires: temperature-dependent properties and effect of crystal-phase transition.

A. Dobrovolsky[*], *E. Unger, A. Yartsev, I. G. Scheblykin*

Department of Chemical Physics, Lund University, SE 22100 Lund, Sweden

**e-mail: alexander.dobrovolsky@chemphys.lu.se*

Keywords: organic-inorganic perovskites, nanowires, fluorescence microscopy

Introduction

Organic-inorganic lead halide perovskites $CH_3NH_3PbI_3$ have attracted much attention in last several years as very promising materials for solar cells, light-emitting diodes and laser devices. Organo-metal halide perovskites possess properties of traditional inorganic semiconductors, combined with the great advantage of low-cost solution processing. Their exceptional solar energy conversion and emission performance are driven by long carrier lifetimes, high carrier mobility, strong broadband optical absorption and high fluorescence quantum yield with possibility to tune the emission wavelength. Recent structural and photophysical studies concluded that $CH_3NH_3PbI_3$ has two accessible crystal forms below room temperature: a tetragonal phase from 160 K to room temperature and an orthorhombic phase for temperatures *T* below 160 K. The purpose of this work is to investigate effect of crystal-phase transition on luminescence properties of $CH_3NH_3PbI_3$ perovskites using optical microscopy techniques.

Results and Discussion

We studied $CH_3NH_3PbI_3$ nanowires (NWs) grown by a surface-initiated solution fabrication method. Scanning electron microscopy has shown that resulting NWs had length up to 4 □m and diameter varying from 100 to 500 nm with flat rectangular end facets indicating high-quality single crystal structure. Temperature-depended steady-state and time-dependent micro-photoluminescence measurements on the individual NWs were performed in temperature range of 77 – 295 K. Photoluminescence microscopy combined with spectroscopy allows us to study the local variations of photophysical properties in a single NW with high spatial resolution.

Fluorescence microscopy of single $CH_3NH_3PbI_3$ NWs at different temperatures reveals the coexistence of the tetragonal and orthorhombic phases in 120 K < T < 160 K. For the first time, temperature-dependent luminescence intensity variation along NW axis induced by crystal phase transition was observed. Emersion of bright areas characterized by the red-shifted luminescencespectra at the temperature region of the phase transition may be attributed to small inclusions of domains of the room-temperature phase with the narrower band gap, in which a large fraction of photoexcited carriers agglomerate. Processes of carrier migration between domains of different phases and spatial carrier localization are discussed.

Outlook

This effect can be potentially beneficial for optoelectronic device applications for emission enhancement in LEDs and decrease of the gain threshold in lasers.

Surface-enhanced Raman spectroscopy can assess cytotoxicty of nanomaterials

G. Kuku[a], M. Saricam[a], M. Culha[a]*

[a] Department of Genetics and Bioengineering, Faulty of Engineering, Yeditepe University, Atasehir, Istanbul, 34755, Turkey

**e-mail: mculha@yeditepe.edu.tr*

Keywords: Single cell, SERS, Nanotoxicity

Introduction

With the advance of nanomaterial (NM) science and its growing application areas the toxic effects of nanomaterials (NMs) on environment and human health has also become a major concern [1, 2]. On the other hand, the conventional cytotoxicity assays have been shown to be unreliable with most of the NPs including titanium dioxide (TiO_2), zinc oxide (ZnO) and quantum dots [3]. Therefore, reliable, faster yet cheaper approaches are investigated. At this point, surface-enhanced Raman spectroscopy (SERS) can be used as a powerful tool.

SERS requires almost no sample preparation, bypassing expensive reagents and labor intensive preparation steps. Also, by the help of a high-speed encoded stage a mammalian cell of approximately 30×30 μm2 area can be scanned with 2 μm steps in 3-4 minutes which makes live single cell imaging possible.

In the current study, we used two cell lines; a human dermal fibroblast (HDF) and a lung carcinoma (A549) to test three model nanoparticles (NPs) for their toxicity; ZnO NPs, TiO_2 NPs and single-walled carbon nanotubes (SWCNTs). As a SERS substrate 60 nm diameter sized AuNPs were used and the results from the SERS experiments were compared to WST-1 assay results. Moreover, the obtained SERS data were analysed with principal component analysis (PCA) to see whether it is possible to visualize any spectral differences by using multivariate statistical tools.

Results and Discussion

Exemplary results for ZnO NPs were shown in **Figure 1**. SERS results indicate a clear difference between the non-incubated control cells and the increasing concentrations of ZnO NP incubation. The most prominent changes were highlighted with grey circles in **Figure 1a** and these changes can be attributed to protein structural deformations (magenta and yellow highlighted bands) as well as to membrane related changes (blue highlighted bands).

It is also possible to see cell type dependent differences. In A549 cell line, the cells lose their integrity at higher doses compared to HDF cells. This conclusion can also be drawn out by the WST-1 results in **Figure 1b**. At 5 and 10 μg/ml concentrations the cell viability is not significantly lower than the control cells.

SERS data were also analysed by PCA to visualize spectral differences between each concentration. In **Figure 1c**, the results for A549 cells were plotted. A better separation from the control samples could be seen starting from 15 μg/ml concentration which was in agreement with the spectral results and WST-1 assay results.

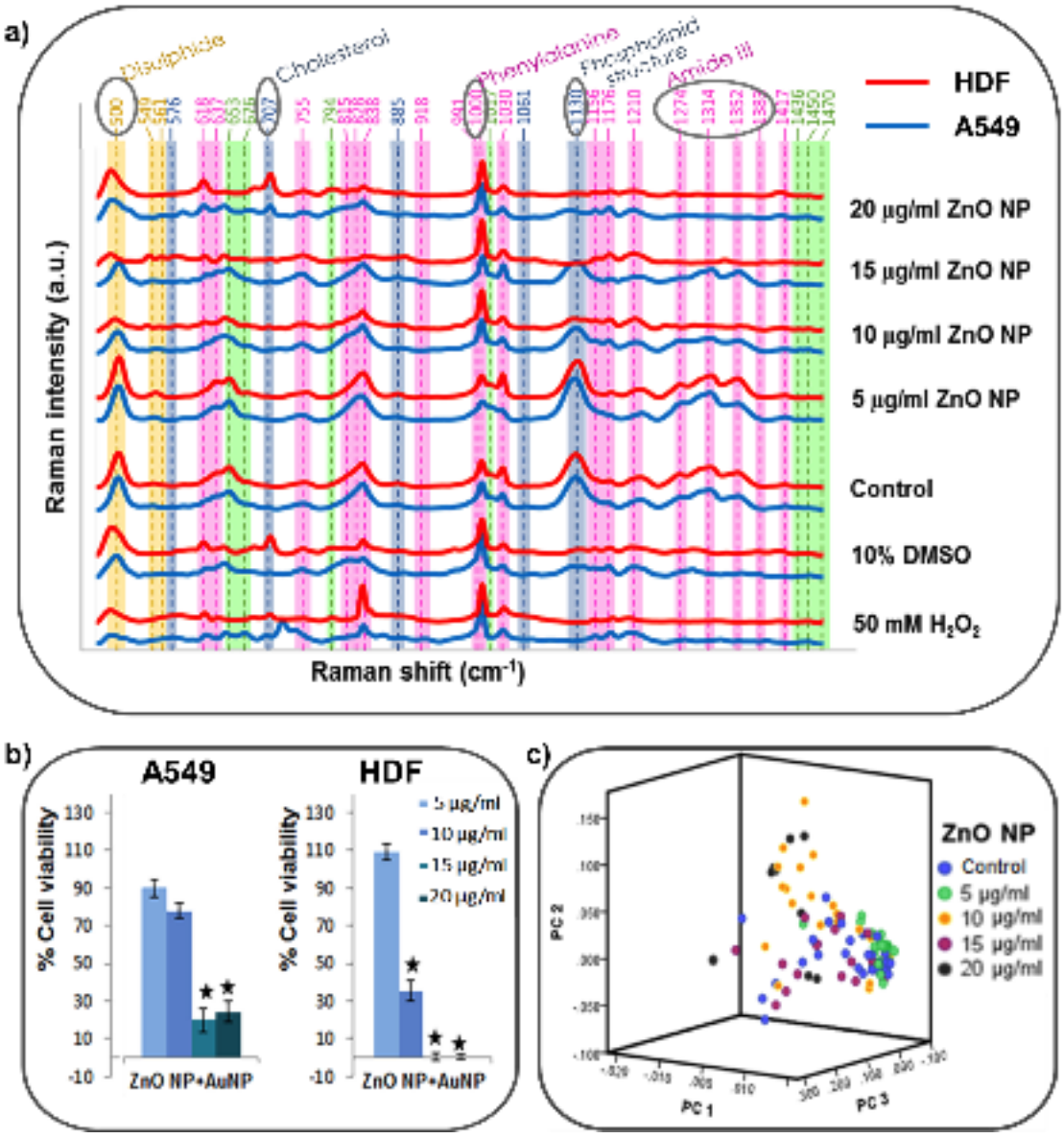

Figure 1: Assessment of ZnO NP toxicity at increasing concentrations by using SERS, WST-1 assay and PCA. **a)** SERS results of HDF (red specra) and A549 (blue spectra) cell lines incubated with increasing concentrations of ZnO NPs. 10% DMSO and 50 mM H_2O_2 were used as positive controls. **b)** WST-1 assay with A549 and HDF cell lines incubated with increasing concentrations of ZnO NPs. Control cells that were not incubated with ZnO NPs were set as 100% viable. **c)** PCA loading plot of A549 cell line incubated with increasing concentrations of ZnO NPs.

Conclusions and Outlook

In our study, we have shown that SERS can be used as a tool to investigate NP cytotoxicity. It is possible to extract more cellular information by analysing a SERS spectrum compared to the conventional cytotoxicity assays such as WST-1 assay or Annexin V-FITC/PI assay where only one aspect of the cellular conditions can be observed. As an improvement to this study, more detailed statistical analyses with better distinction algorithms such as partial least squares (PLS) analysis can be used to model NP cytotoxicity and our ongoing efforts are focused on this task with a larger set of cell lines and NPs.

References:

[1] Warheit D B, Borm, P J A, Hennes C, and Lademann, J; Testing Strategies to Establish the Safety of Nanomaterials: Conclusions of an ECETOC Workshop; Inhal. Toxicol.; 19 (2007) 631–643.

[2] Simkó M, Nosske D, and Kreyling W G; Metrics, Dose, and Dose Concept: The Need for a Proper Dose Concept in the Risk Assessment of Nanoparticles; Int. J. Environ. Res. Public. Health 11 (2014) 4026–4048.

[3] Tournebize J, Sapin-Minet A, Bartosz G, Leroy P and Boudier A; Pitfalls of assays devoted to evaluation of oxidative stress induced by inorganic nanoparticles; Talanta; 116 (2013) 753–763.

On the transfer of photon spin to electron orbital angular momentum in a retroreflecting partially metal coated dielectric tetrahedral tip

U.C.Fischer[a*], *F. Fontein*[a], *H. Fuchs*[a], *T. Grosjean*[b]

[a] Interface physics group, WWU, Muenster, Germany
[b]CNRS, FEMTO-ST Institute, Besançon, France

**e-mail: fischeu@wwu.de*

Keywords: photon spin; spin orbit coupling; Inverse Faraday effect, optical Spin Hall effect; retroreflection

Introduction

Mansuripur et al considered theoretically the transfer of the spin of a circularly polarized beam of light to orbital angular momentum in retroreflecting structures such as a hollow conical metal structure or a metal wedge [1]. We investigated the transfer of photon spin to electron orbital angular momentum in a retroreflecting partially gold coated tetrahedral glass tip which we previously used as a SNOM – probe [2]. A schematic view of the tip and the experimental configuration is shown in **Figure 1**. Two faces of the tip are coated with a 20 nm thick film of gold in a way that the edge between the metal coated faces is coated with a considerably thinner metal film and the metal coating of the edge extends only to a distance of about 30 µm from the tip. The 2 gold coated faces of the tip are connected to electrodes for photoelectrical measurements. The intensity of 0,5 mW of a 655 nm diode laser beam was modulated with a 1 kHz signal from a function generator. The polarization of the light beam was adjusted by a LC crystal plate phase modulator and the light beam was focused into the tip at an angle of 45° with respect to the metal coated edge. A photoinduced electromotive force between the 2 metal coated faces can be measured by recording the photovoltage between the electrodes. The voltage between the electrodes of the sample was fed into a lock in amplifier and the 1 kHz in phase AC signal was recorded as a function of the polarization of the incident beam.

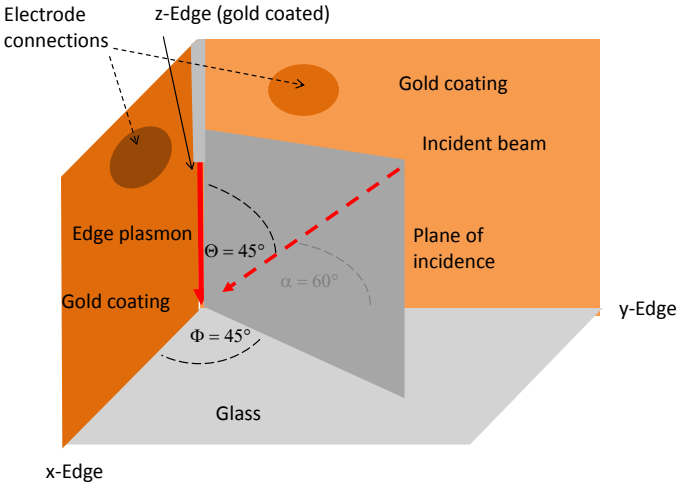

Figure 1 Schematic view of experimental configuration of the partially gold coated tetrahedral tip here with a p –polarized incident Gaussian focused beam exciting edge plasmon modes on the z-edge.

Results and Discussion

Table 1 shows the experimental results of a photoelectric measurement in comparison to a calculated relative values for different polarizations of the incident beam. Different voltages in the range of 0,1 to 0,2 µV were measured for different polarizations. We interpret the results obtained on our specific metal nanostructures on the basis of the coupling of photon spin to electron angular momentum. In this context we use the concept of the spin of a circularly polarized beam of light in terms of the classical Maxwell theory of electromagnetic radiation,

polarization	rcp	lcp	p	s
experimental value /μV	0,195 +/- 0,01	0,107 +/- 0,01	0,157 +/- 0,01	0,147 +/- 0,01
normalized experimental value	1	0,55	0,805	0,754
normalized calculated value	1	0,57	0,81	0,81
Calculated spin transfer/ $\frac{h}{2\pi}$	$\sqrt{\cos^2(60°)+\cos^2(45°)}$	$\cos(60°)$	$\cos(45°)$	$\cos(45°)$

Table 1 experimental results for different polarizations of the incident beam, right- left handed circular polarized (r-l cp), p- and s- polarized. Comparison to calculated values

where the model of a propagating right (left) handed circularly polarized photon is a wave packet of spin 1 with an angular momentum +(-)h/2 with the spin oriented in the direction of propagation [3]. As a boson, also a single linearly polarized photon carries a spin 1 with an associated angular momentum of h/2 which is oriented in the direction of its polarization [3]. For an estimation of the order of magnitude of an electromotive force which can be generated by a transfer of spin to electron orbital momentum we consider the case of normal incidence of a circular polarized photon into a retroreflecting nanostructure. Unlike in a normal reflection process, in the retroreflection process, the handedness of a circular polarized beam is conserved and consequently, its spin is inverted. Due to the conservation of angular momentum, angular momentum is transferred to the retroreflecting mirror. If the retroreflection process is entirely due to interaction of light with conduction electrons, the photon spin angular momentum will be transferred to the electrons. Assuming a tightly focused optical beam, the interaction area corresponds to a disk of a diameter of the wavelength. Assuming a transfer of the spin 1 of a photon of energy h to electrons circling on an orbit of diameter we obtain for the electromotive force giving rise to the spin a value of

$$V_{emf} = \frac{2h^2}{\pi^2 e m_e \lambda^2} = \frac{2h^2\nu^2}{\pi^2 e m_e c^2} = 1{,}422\,\mu\mathrm{V}\ (\text{for } \lambda = 655\mathrm{nm})$$

We obtain in our measurement a maximum voltage which is by about a factor of 7 smaller than this value. One reason is, that in the formula, has to be replaced by the real diameter d of the focused beam which has a numerical aperture smaller than 1. In order to evaluate the influence of polarization on the electromotive force in our specific configuration, we make the assumption that in the retroreflection process, the interaction of the incident beam with the conduction electrons can be described by the excitation of edge plasmon modes on the x- y- and z- edges of our structure (see **Figure 1**) [4]. Propagating edge plasmons are mixed longitudinal and transversal waves and carry a spin which has an oblique orientation with respect to their propagation direction. The photon spin movement in the process of retroreflection of an incident beam in our configuration can be traced by considering how the plasmons excited at the x- y- and z- edges by the incident beam converge at the tip and are there transmitted from one edge to another [4]. This transmission leads to a change in the photon spin direction leading to a transfer of spin to electron orbital angular momentum in the z direction giving rise to the electromotive force. The calculated spin to orbital angular momentum transfer is shown in**Table 1**

Conclusions and Outlook

The transfer of photon spin of linear and circular polarized light to electron angular momentum can be regarded as a current generator, which in our case was recorded by detecting the electromotive force giving rise to the currents. The associated current density is especially high at the concave edges and corners of our conical metal tip with a radius of curvature of only a few nm thus leading to high and strongly localised magnetic fields. Whereas the electromotive force can be regarded as a voltage arising from an optical spin Hall effect, the magnetic fields could be regarded as a manifestation of the inverse Faraday effect which can be considered as a nonlinear optical magnetization of a diamagnetic material [5].

References:

[1] Mansuripur M, Zakharian AM, Wright EM ; Spin and Orbital Angular Momenta of Light Reflected from a Cone; Physical Review A 84 (2011), 033813

[2] Fischer U C, Koglin J, Fuchs H; The Tetrahedral Tip as a Probe for Scanning Near- Field Optical Microscopy at 30 nm resolution; J. Microscopy 176 (1994), 231 - 237.

[3] Raman C V , Bhagavantam S; Experimental proof of the spin of the photon; Indian J. Phys**.** 6 (1931) 353-366.

[4] Tanaka K , Burr G W, Grosjean T, Maletzky T, Fischer U C; Superfocussing in a metal coated tetrahedral tip by dimensional reduction of surface- to edge- plasmon modes; Appl Phys B 93 (2008) 257–266.

[5] Landau L D, Lifshitz E M; Course of Theoretical Physics Vol 8; Electrodynamics of Continuos Media, 2nd edition, Pergamon Press (1984)

Super-resolution optical microscopy and spectroscopy for nano-scale characterization of organo-metal halide perovskites

*A. Merdasa**[a], *M. Bag*[a], *Y. Tian*[a], *I. Scheblykin*[a]

[a]Chemical Physics, Lund University, PO Box 124, 22100 Lund, Sweden

**e-mail: aboma.merdasa@chemphys.lu.se*

Keywords: Perovskite degradation, super-resolution microscopy, ion migration, nano-scale spectroscopy

Introduction

Over the past few years there has been a growing interest in organo-metal halide perovskites as good candidate materials for light-emitters and photovoltaics . These materials are very promising due to their broad absorption combined with extremely high power conversion efficiency over ~20 % [1].

With respect to the role organo-metal halide perovskites play in photovoltaics, there is still the major hurdle of stability under the exposure to sunlight to overcome. To date, most studies on photo-induced degradation of methylammonium lead iodide in particular ($MAPbI_3$) focus on the degradation of free-standing perovskite films or solar cell devices based on absorption spectroscopy and X-ray diffraction analysis. However, these bulk measurements do not reveal the nano-scale mechanistic process involved in the photo-induced degradation.

To understand the mechanistic processes of photo-induced degradation, we employ wide-field fluorescence microscopy where we simultaneously probe photoluminescence (PL) intensity, spectral and spatial features of individual nano-scale objects. We call the method Super-resolution Luminescence Micro-Spectroscopy (SuperLuMS) and have previously applied it to characterize photophysical and photochemical processes in 1D J-aggregates [2] and similar $MAPbI_3$ crystals studied here with a nano-scale precision [3].

Results and Discussion

Individual $MAPbI_3$ nanocrystals (~400×400×100 nm^3) were immobilized on a glass substrate and excited with 514 nm CW laser light having excitation power densities ranging from 0.1-100 W/cm^2. Movies were recorded with 100 ms exposure per frame. At excitation powers > 10 W/cm^2, a steady decrease of the PL intensity of diffraction limited $MAPbI_3$ crystals occurred at the time-scale of seconds. In conjunction with this, a PL spectral blue-shift was also observed (see **Figure 1a-b**). We attribute this to an accelerated degradation of the material.

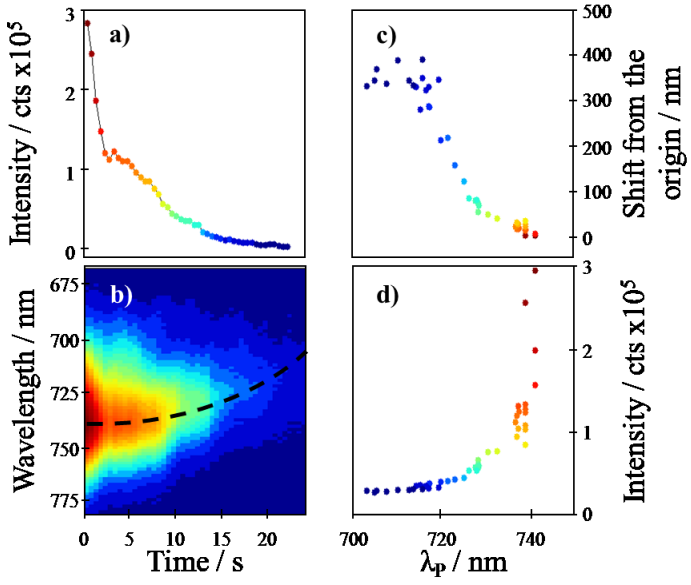

Figure 1: SuperLuMs applied to a nanocrystal of $MAPbI_3$. (a) Intensity decline correlated with (b) the spectral evolution over 25 s. (c) shows the shift of the emission profile from the origin. (d) shows the peak wavelength correlated with intensity. The color-coding in a,c,d are the same and represent intensity so that a comparison between the different domains can be made easily

Further, we studied the spatial fluctuation of emission with nanometer precision by fitting the diffraction limited emission profile with a 2D Gaussian surface in every frame to see how the mean position fluctuated in time. In **Figure 1c** we can see the spatial correlation of the emission to intensity, however, it appears non-linear. As intensity initially drops significantly, the spectrum remains rather stable and localization shifts are minimal. Only when the intensity is low, the majority of spectral (~ 40 nm) and spatial (~ 400 nm) shifts occur. Comparing the peak wavelength, λ_p, and intensity (**Figure 1d**) we note that the curve is characteristics for other studied crystals.

In addition, we observed that the PL emission from an object blinked 'off' and then 'on' again after 50 seconds (see **Figure 2**). Comparing λ_p and I_p for only those frames when emission was 'on', we see the same characteristic curve as see in **Figure 1d** (see inset in **Figure 2**). Thus, we conclude that degradation is 'paused' when emission is quenched which leads us to understand that free charges are important for the degradation process to occur.

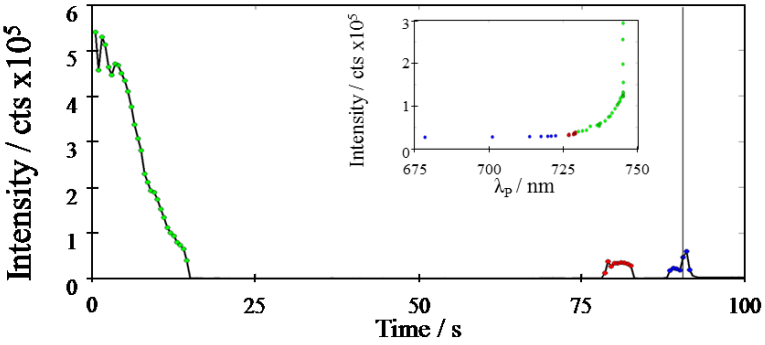

Figure 2: Blinking of an object suspends degradation. Intensity initially declines and blinks off after ~20 s. After an additional 50 s, emission blinks on again twice for about 5 seconds each time. Inset shows the same type of plot as **Figure 1d** where the peak wavelength is correlated to the peak intensity and a similar trend is observed despite of blinking.

From these observations we prose a model of the mechanistic process of how photo-induced degradation occurs in $MAPbI_3$. It is known that the methylammonium ion migrates under the exposure to light in $MAPbI_3$. As vacancies form, the lattice structure becomes locally unstable. When enough ions vacate a local region, the ionic void causes the bending of the I-Pb-I bond angle. A recent report shows that this bending causes an increased band gap [4]. Thus, we attribute the degradation to the perpetual collapse of 3-D $MAPbI_3$ structure to 2-D PbI_2 structure. It is not a new discovery that $MAPbI_3$ degrades into PbI_2, however, no study has been able to observe this in real time and describe the process at which it occurs since only initial and final conditions have been studied thus far. SuperLuMS provides a possibility to understand this process due to the fact that the spectroscopic characteristics can be studied at a nano-scale rather than in an ensemble.

Conclusion

We have directly observed photo-induced degradation of $MAPbI_3$ nanocrystals occurring over a time span of seconds rather than days or weeks. We observed that the PL intensity gradually decreases accompanied by a spectral blue-shift and localization shift of the emission. The gradual spectral change points to the bending of the I-Pb-I bond angle due to increasing ion vacancies caused by the photo-induced ion migration until the crystal structure collapses into non-emissive PbI_2. This collapse may initiate in a specific location and propagates throughout the crystal which appears as a spatial shift of the emission localization.

References:

[1] Liu M, Johnston, M.B, Snaith H; Efficient Planar Heterojunction Perovskite Solar Cells by Vapour Deposition; Nature; 501 (2013) 395-398

[2] Merdasa A, Jimenez A, Camacho R, Meyer M, Würthner F, Scheblykin I; 'Single Lévy States – Disorder Induced Energy Funnels in Molecular J-aggregates; Nano Letters; 14 (2014) 6774-6781

[3] Tian Y, Merdasa A, Peter M, Abdellah M, Zheng K, Ponseca C, Pullerits T, Yartsev A, Sundström V, Scheblykin I; Giant Photoluminescence Blinking of Perovskite Nanocrystals Reveals Single-Trap Control of Luminescence; Nano Letters 15 (2015) 1603-1608

[4] Filip M, Eperon G, Snaith H, Giustino F; Steric Engineering of Metal-Halide Perovskites with Tunable Optical Band Gaps; Nature Communications; 5 (2014) 5757

Theoretical investigation of SERS nanosensors based on hybrid waveguides of metallic slots and dielectric strips

F. Tang[a], *P.M. Adam**[a], *S. Boutami*[b]

[a] Laboratoire de Nanotechnologie et d'Instrumentation Optique, ICD, CNRS UMR 6281, Université de Technologie de Troyes, 12 rue Marie Curie, CS 42060, 10004 Troyes Cedex, France
[b] CEA, LETI, MINATEC, DOPT 17 rue des martyrs 38054 Grenoble cedex 9, France

**e-mail: pierre_michel.adam@utt.fr*

Keywords: Sensor, Surface-enhanced Raman scattering, Integrated optics.

Introduction

Surface-enhanced Raman spectroscopies (SERS) are widely used to sensitively detect molecules or markers in pharmacology, biology, etc[1]. In many applications, the SERS detections are implemented in a free space configuration, leading to quite bulky and costly systems. We study numerically the possibility to realize SERS detection directly on a photonic chip. In **Figure** 1 it is presented that a SERS sensor, which is created by combining a gold slot waveguide and a Si_3N_4 strip waveguide, can be designed to excite enhanced Raman effects and extract scattering signals on a chip[2,3]. In this frame, analytes are dripped into the gold slot where enhanced Raman scatterings occur, and only the *TE* mode ($E_x >> E_y, E_z$) of the Si_3N_4 strip can couple into the metallic slot due to the perpendicularity of E_x to the slot walls. SERS includes two main electromagnetic mechanisms: local field enhancement EF_{Loc} in the excitation process of surface plasmon, and radiation enhancement EF_{Rad} in the radiation process of induced Raman dipoles. In detections, the laser light propagating in the Si_3N_4 strip will couple into the Au slot and excite the intense plasmonic local fields, and then Raman dipoles are induced in molecules there. Meanwhile, the radiation of Raman dipoles could excite some plasmon guided modes of the slot and then couple into the Si_3N_4 strip.

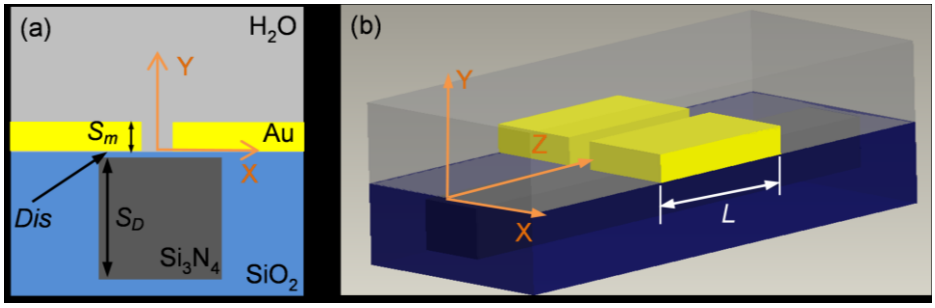

Figure 1: Layout of the SERS sensor structure: (a) Cross profile of the hybrid waveguide, where one square Si_3N_4 strip of side S_D is located at a distance *Dis* under one square gold slot of side S_m deposited on the silica substrate. (b) Sensor frame, where a *L*-length gold slot is located above a Si_3N_4 strip.

Results and Discussion

Using 3D finite-difference time-domain simulations, the processes, excitation of surface plasmon in the slot and radiation of induced Raman dipoles, are analysed to simulate SERS detections in reality. It also demonstrates the influence of the geometrical parameters on the electromagnetic fields in the slot and therefore the enhancements. Then some methods are proposed to magnify further the enhanced-Raman signals in the sensor.

Figure 2 shows the two simulations of the excitation of surface plasmon and the radiation of induced Raman dipoles. In the excitation process, an impulse of the fundamental *TE* mode is imported from the left end of the Si_3N_4 strip. The distribution of $|E_{Loc}|$ in the excitation is presented in **Figure 2** (b) with λ = 778 nm. It is seen that the plasmonic electric field is excited in the slot, particularly near the four corners. If analyte is located in the slot, the intense field could induce Raman dipoles in molecules with an enhancement factor EF_{Loc}. The EF_{Loc} of the point (23 nm, 22 nm, 0.805 µm) in the excitation is plotted with a blue curve in **Figure 2** (d). In the radiation simulation, one induced Raman dipole is located in the slot and its orientation is perpendicular to the slot walls. Similarly, the simulation can give the $|E_{Rad}|$ distribution on the x-y output plane with z = 1.3 µm, as shown in **Figure 2** (c). On this plane, only the component of the fundamental *TE* mode can couple into the strip. The EF_{Rad} of the radiation is plotted with a black curve in **Figure 2** (d), and the global enhancement factor $EF = EF_{Loc}EF_{Rad}$ is with a red curve. Although the biggest enhancement factor is just 29 in **Figure 2** (d), some points with intense E_{Loc} in **Figure 2** (b) could have more than 10^4 *EF* based on the $|E_{Loc}|^4$-approximation $EF \approx |E_{Loc}|^4$, where E_{Loc} has been normalized to the source.

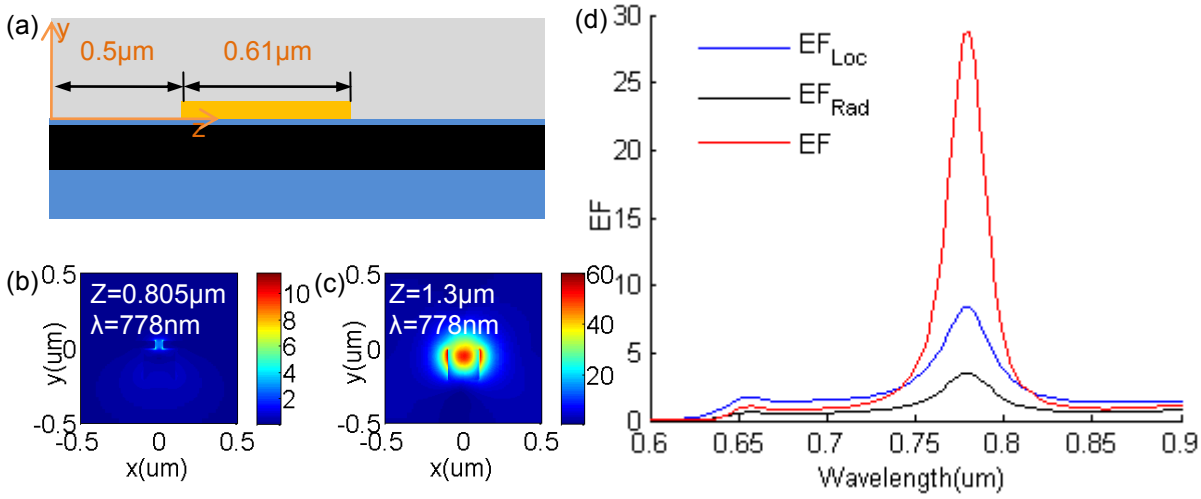

Figure 2: Simulations of the excitation and radiation processes with S_m = 48 nm, *Dis* = 10 nm, S_D = 200 nm and L = 0.61 μm: (a) Side view of the sensor. (b) $|\boldsymbol{E}_{Loc}|$ (normalized to the source) distribution on one x-y cross section with z = 0.805 μm in the excitation simulation. (c) $|\boldsymbol{E}_{Rad}|$ (normalized to the source) distribution on one x-y cross section with z = 1.3 μm in the radiation simulation, in which one x-direction induced Raman dipole is located at (23 nm, 22 nm, 0.805 μm). (d) Enhancement factors of the position where the induced Raman dipole is located.

The sensor is based on the coupling between the slot waveguide and the strip waveguide. Thus, the influence of the geometry on the sensor performance could be inferred via the guided modes and the interaction between waveguides. Simulations show that a bigger S_m or a smaller *Dis* strengthens the coupling between the slot and the strip while S_D only weakly influences the coupling efficiency. Although a big S_m is beneficial to couple more energy into the slot, it makes the electromagnetic confinement worse. On the whole, decreasing the structure parameters (S_m, *Dis*, S_D) could make the in-slot enhancement stronger.

To improve the sensor performance, some gold nanospheres can be laid in the sensor slot to create some tiny gaps between the sphere and the slot walls. These 1-2 nm gaps can brings the hotspot effect into the sensor and obtain very huge enhancement factors. Simulations show that the enhancement factor of the point in **Figure 2** (d) increases to 10^6 if one 44nm-diameter gold particle is laid at (0 nm, 22 nm, 0.805 μm) and the point becomes the centre of one 2 nm wide gap. The improvement is more than 4 orders of magnitude and the area in the sphere-slotwall gaps can be seen as the hotspot area or the probe area of the sensor.

Conclusions and/or Outlook

It is presented that one SERS nanosensor based on slot-strip hybrid waveguides could enhance Raman signals on a photonic chip in principal. It is demonstrated that the hybrid waveguide can transform energy effectively between light modes and plasmonic modes, solving the main challenge of extracting scattering signals from micro-sensors. The SERS processes, excitation of surface plasmon and radiation of induced Raman dipoles, are analyzed to show the corresponding working procedure of the sensor. The geometrical influence on the coupling between waveguides is investigated to show the strategy to optimize the electromagnetic field intensity in the metallic slot and the enhancements there. Some approaches like in-slot gold spheres are proposed to bring the hotspot effect into the sensor and make single molecule detections possible. The integration of this sensor with a micro-laser and a micro-demultiplexer, will be developed to achieve an on-a-chip and fully integrated SERS detection.

References:

[1] G. McNay, D. Eustace, W. E. Smith, K. Faulds, and D. Graham; Surface-enhanced Raman scattering (SERS) and surface-enhanced resonance Raman scattering (SERRS): a review of applications; Applied spectroscopy; 65 (2011) 825-837;

[2] C. Delacour, S. Blaize, P. Grosse, J. M. Fedeli, A. Bruyant, R. Salas-Montiel, G. Lerondel, and A. Chelnokov; Efficient directional coupling between silicon and copper plasmonic nanoslot waveguides: toward metal−oxide−silicon nanophotonics; Nano letters; 10 (2010) 2922-2926;

[3] Y. Jun, R. Kekatpure, J. White, and M. Brongersma; Nonresonant enhancement of spontaneous emission in metal-dielectric-metal plasmon waveguide structures; Physical Review B; 78 (2008) 153111.

Two Dimensional Nitrides: an ab-initio study

M.S. Prete*[a], A.Mosca Conte[b], Paola Gori[c], F. Bechstedt[d], O.Pulci[e]

[a] Dipartimento di Fisica, Università di Roma `Tor Vergata', Italy
[b] ETSF, CNR-ISC, MIFP, Dipartimento di Fisica, Università di Roma `Tor Vergata', Italy
[c] ETSF, MIFP, Dipartimento di Ingegneria, Università di Roma 'Roma 3' Italy
[d] IFTO, Friedrich-Schiller-Universit• at and ETSF, Max-Wien-Platz 1, 07743 Jena, Germany
[e] ETSF, MIFP, Dipartimento di Fisica, Università di Roma `Tor Vergata', Italy

*e-mail: stella.prete@gmail.com

Keywords: Nitrides, ab-initio calculation, excitons, tunable gap, 2D systems

Introduction

Group-III nitrides such as InN, GaN and AlN have received considerable attention for high-power, high-frequency and high-temperature electronic devices and for optoelectronic applications such as light-emitting and laser diodes. In particular in 2014 Akasaki, Amano e Nakamura were awarded for bright and highly efficient blue LEDs based on GaN heterostructures with the Nobel Prize in Physics [1].
In addition in recent years theoretical and experimental studies of graphene provided a wide range of knowledge for a new class of 2D materials and they opened up possibilities for the synthesis of many similar structures [2 -3-4-5-6].
Motivated by this recent developments we present here a sistematic ab-initio study of the electronic and optical properties of two-dimensional group III Nitrides (BN, AlN, GaN, InN, TlN). We show that, with increasing group-III atomic number, a decrease of the gap from 4.7 eV to a few meV takes place. The electron-hole confinement combined with the reduced screening, enhance excitonic effects, which remain sizeable also for the small gaps III-V compounds. By exploiting the reduced dimensionality and the chemical trend, we demonstrate that it is possible to engineer their electronic and optical response, and suggest that the possible emission range of optoelectronic devices based on 2D group-III Nitrides vary from UV to infra-red.

Results and Discussion

Our results on the geometry and on electronic properties are obtained within Density Functional Theory (DFT-LDA). For BN also GW and BSE calculations were performed. In these compounds gap opening occours, due to the different electronegativity of group III elements and Nitrogen, and the electronic gap is often indirect. In Fig 1 we demonstrate that with the increasing of the group-III atomic number Z, that is with the increasing of the covalent radii, the 2D lattice constants increase up to 50%, the gaps decrease up to almost 100%, and the 2D dielectric constant increases. As a consequence, the excitonic binding energy also decreases, with an increase of the exciton radius, due to the more efficient screening of the electron-hole interaction.

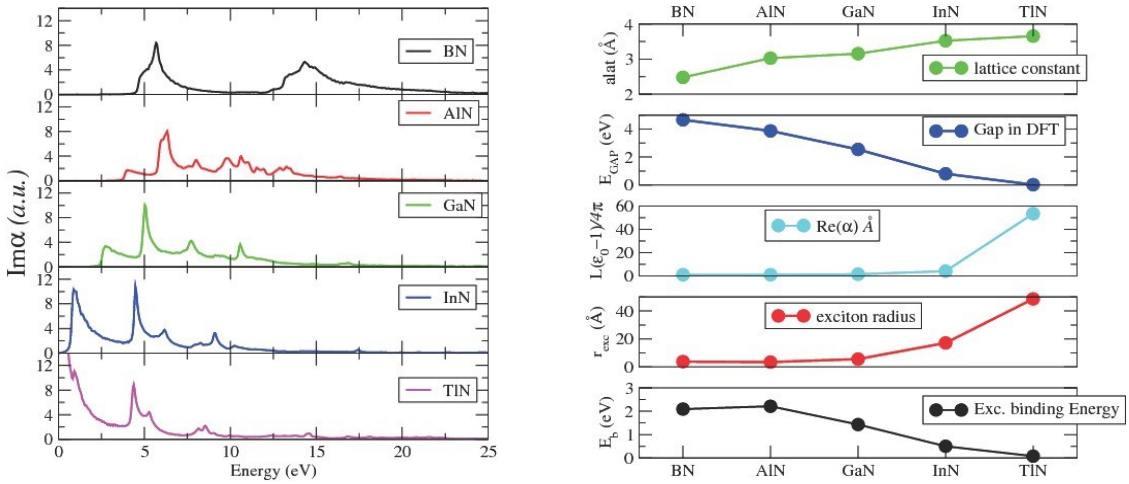

Figure 1: On the right: imaginary part of the 2D polarizability $\alpha_{2D}=(\varepsilon-1)L/4\pi$ for the III-N sheets compounds studied, calculated using DFT-LDA. On the left: lattice constant, energy gap (direct), and excitonic results for the III-N sheets compounds studied.

As regards the optical properties we have estimated binding energies E_b and the radii r_{exc} of the excitons of this class of materials with a simple analitical model for excitons in two dimensions[7],[8]. The violet circles in Fig 2 denote the points where $x = r_b/2\pi\alpha_{2D}$ for the materials under study. It is clear that neither the hydrogenoid nor the logarithmic-potential limit are fulfilled in this class of materials and we can note that the 2D sheets have an intermediate character between the two extreme behaviours. For BN we

verified via a full BSE calculation that our model provides a good estimate in terms of order of magnitude of the binding energies E_b and excitonic radii r_{exc} .

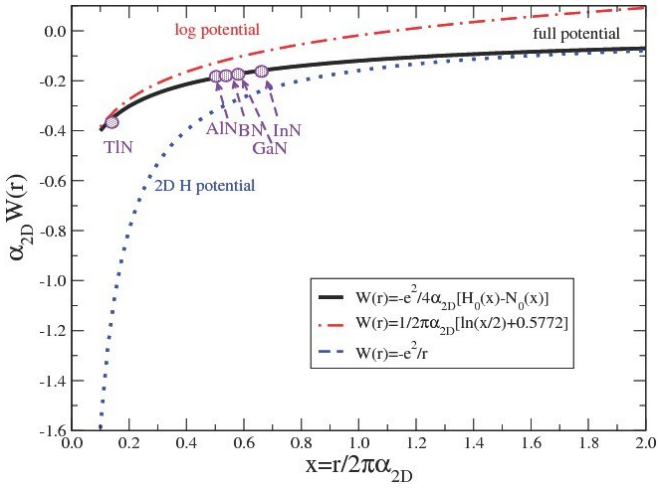

Figure 2 Effective electron-hole interaction potential used in the model (black line); logarithmic electron-hole attraction in the large polarizability (small exciton radius) limit (red dashed line); 2D hydrogenoid atomic potential in the vanishing polarizability (large excitonic radii) limit (blue dashed line).

Conclusions and/or Outlook

Using a combination of an ab-initio density functional theory for the ground-state properties and the prediction of an analytical model for excitons in two dimensions we have calculated the electron and optical properties of 2D Nitrides. These materials are predicted to have a honeycomb flat structure with gaps ranging from UV to IR. The results demonstrate that 2D sheets possess strongly bond excitons due to the interplay of low dimensionality, depressed screening and the presence of a gap. The only exceptions seems to be TlN that has zero gap. Confinement effect and reduced 2D screening strongly enhance excitonic effects, creating electron-hole pairs with large (~eV) binding energy and tunable optical gap, making these materials good candidates for novel optoelectronic devices.

Furthermore our model for exciton parameters calculations of 2D systems seems to be a reliable alternative to the computationally more demanding methods based on the solution of the BSE.

References:

[1] Amano H, Sawaki N, Akasaki I. and Toyoda Y; Metalorganic vapor phase epitaxial growth of a high quality GaN film using an AlN buffer layer; Appl. Phys. Lett. 48 (1986) 353;

[2] Novoselov K.S., Geim A.K , Morozov S. V, Jiang D, Zhang Y, Dubonos S. V, Grigorieva I .V, Firsov A. A; Electric Field Effect in Atomically Thin Carbon Films; Science 306,(2004) 666;

[3] Nagashima A, Tejima N, Gamou Y, Kawai T, Oshima C; Electronic dispersion relation of monolayer hexagonal boron nitride formed on the Ni (111) surface; Phys. Rev. B 51, (1995) 4606;

[4] Sahin H, Cahangirov S, Topsakal M, Bekaroglu E, Akturk E, Senger RT, Ciraci S; Monolayer honeycomb structures of group-IV elements and III-V binary compounds: First-principles calculations; Phys. Rev. B 80, (2009)155453;

[5] Bacaksiz C, Sahin H, Ozaydin H D, Horzum S, Senger R T, and Peeters F M; Hexagonal AlN: Dimensional-crossover- driven band-gap transition; Phys. Rev. B, 91,(2015) 085430;

[6] Tsipas P, Kassavetis S, Tsoutsou D, Xenogiannopoulou E, Golias E, Giamini S.A, Grazianetti C, Chiappe D, Molle A, Fanciulli M, Dimoulas A; Evidence of graphite-like hexagonal AlN nonosheets epitaxially grown on single crystal Ag (111); Appl. Phys. Lett. 103 (2013) 251605

[7] Cudazzo P, Ilya V, Tokatly I V and Rubio A; Dielectric screening in two-dimensional insulators: Implications for excitonic and impurity states in graphane Phys. Rev. B 84 (2011) 085406;

[8] Pulci O, Marsili M, Garbuio V, Gori P, Kupchak I, Bechstedt F; Excitons in two-dimensional sheets with honeycomb symmetry; Phys. Status Solidi b; 252 (2015) 72-77;

Tip-enhanced Raman spectroscopy: From plasmonic nanogap to single molecule detection and thin film imaging

*D. Zhang**, K. Swider, J. Rogalski, X. Wang, K. Braun, A. Horneber, A. J. Meixner*
[a] Institute of Physical and Theoretical Chemistry, Eberhard Karls University of Tübingen, Germany

**e-mail: dai.zhang@uni-tuebingen.de*

Keywords: Tip-enhanced Raman spectroscopy, plasmonics, semiconductor

Introduction
Tip-enhanced Raman spectroscopy (TERS) witnesses its active development since more than 15 years. Based on the lightning-rod and plasmonic resonance effects, the generation of strongly confined electromagnetic field within a nanogap between a sharp tip apex and a sample surface under laser illumination even makes the visualization of single molecules possible [1-3]. Our group has actively contributed to the development of TERS in a variety of aspects [4-7], such as low temperature TERS of dye molecules at 10 K [8], and TERS combined with fs- or ps-laser excitation [9, 10].

Results and Discussions
We have investigated a variety of radiation scenarios from plasmonic nanogaps. To realize a precise control over the nanogap distance down to 1 nm, we combined shear-force and tunneling current feedbacks with confocal optical microscopes. Both electrical and optical excitation can be applied to the plasmonic nanogap. This allows one to study either separately or simultaneously the plasmonic resonance effect and electric DC field on the optical radiation [9, 11]. In this talk, we will report our latest progresses of using TERS 1) to determine the nanometer-sized morphology in organic semiconductor crystalline film and 2) to identify molecular orientation changes within monolayer adsorbates on Au (111) crystals, as seen in figure 1.

Conclusions
With this work, we content that TERS has past the prove-of-the-concept phase and has grown into an effective technique finding wide applications.

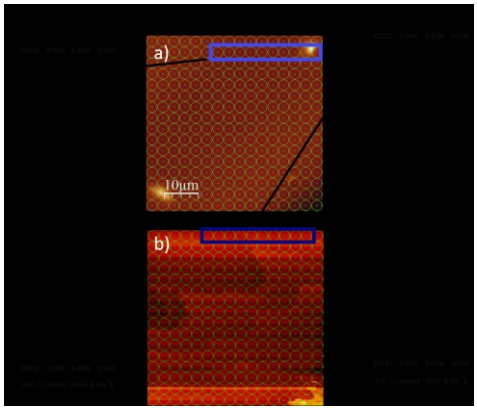

Figure 1 a) confocal Raman spectroscopic mapping of a pentacene monolayer evaporated on Au (111) crystal. Scan range: 50x50 um. The spectra on the left were taken from the blue frame marked area in a), revealing no obvious spectral profile differences due to the lack of optical resolution. Integration time: 30 s per spectrum. b) STM image of the sample surface. Scan range: 1x1 um. The TERS spectra on the right were taken from the blue frame marked area in b). New peaks and varying peak intensities due to the different molecular reorientation are visible in the TER spectra thanks to the high optical resolution and sensitivity. Integration time: 1 s per spectrum. The green circles indicate the positions where the spectra were taken.

References:
[1] Z. C. Dong, et al., Nature Photonics 4 (2010) 50.
[2] J. Steidtner, B. Pettinger, Phys. Rev. Lett., 100 (2008) 236101.
[3] A. Kern, D. Zhang, M. Brecht, A. J. Meixner, et al., Chem. Soc. Rev., 42 (2014)965.
[4] X. Wang, K. Braun, D. Zhang, A. J. Meixner et. al., Adv. Func. Mater., 20 (2010) 492.
[5] D. Zhang, U. Heinemeyer, C. Stanciu, A. J. Meinxer et al., Phys. Rev. Lett., 104 (2010) 056601.
[6] X. Wang, H. Azimi, A. J. Meixner, D. Zhang et al., Small, 7 (2011) 2793.
[7] S. Jäger, A. Kern, D. Zhang, A. J. Meixner et al., Nano Lett., 13 (2013) 3566.
[8] P. Anger, A. Feltz, T. Berghaus, A. J. Meixner, J. Microscoscopy, 209 (2003) 162.
[9] K. Braun, X. Wang, D. Zhang, A. J. Meixner et al., Beilstein J. Nanotech., 6 (2015) 1100.
[10] A. Horneber, K. Braun, A. J. Meixner, D. Zhang et al., Phys. Chem. Chem. Phys., 17 (2015) 21288.
[11] X. Wang, K. Braun, D. Zhang, A. J. Meixner et al., ACS Nano, 9 (2015) 8176.

Electrochemical tip-enhanced Raman spectroscopy (EC-TERS)

N. Martín Sabanés[a]*,*L. Driessen*[a], *K.F. Domke*[a]

[a] Max Planck Institute for Polymer Research, Mainz (Germany)
*e-mail: *martin@mpip-mainz.mpg.de*

Keywords: enhanced Raman spectroscopy, electrochemical interfaces

Introduction

The characterization of electrochemical interfaces with high sensitivity and resolution is crucial to understand and optimize, for example, energy conversion and storage schemes like sensitized solar cells or fuel cells. Understanding of the interplay between adsorbate and substrate in the presence of an electrolyte can be gained by vibrational spectroscopy in combination with conventional electrochemical methods, where the chemical fingerprint of the species in the interface is monitored when triggering redox reactions [1]. Electrochemical scanning probe techniques (SPM) are used to investigate topographical changes during oxidation and reduction with atomic resolution [2]. In tip-enhanced Raman spectroscopy (TERS), the combination of an SPM with a Raman system results in a powerful tool that simultaneously provides an in situ chemical fingerprint with sub-monolayer sensitivity and high-resolution topography information [3]. Very recently, the implementation of electrochemical conditions in TERS setups was demonstrated for the first time [4],[5]. Nonetheless, the operation of TERS under electrochemical conditions remains a huge challenge. In order to convert EC-TERS into a reliable tool for the investigation of electrified solid/liquid interfaces, further improvement of experimental conditions, like SPM sample cell design, tip coating choice of operating potential, as well as of data analysis is urgently required.

Results and Discussion

We have developed a backscattering EC-TERS setup with side illumination geometry (angle between tip and laser of 55 degrees) based on a scanning tunnelling microscope (STM), **Figure 1**. The side illumination configuration allows great substrate versatility because it overcomes the requirement for transparent and thin samples of the AFM-based bottom illumination geometry [5]. Classical electrochemical monolayer/metal single-crystal interfaces can thus be investigated. As a major drawback, the side illumination entails focus distortion due to aberrations originating from the laser beam traveling through media of different refractive indices (air, glass window, aqueous electrolyte). Such aberrations can be minimized by custom-designing an STM to reduce the distance the beam travels from the objective to the tip/sample gap, however, at the cost of STM stability and sample scanning flexibility [4]. In our setup, a specially designed liquid cell in combination with a low-cost commercially available electrochemical STM (EC-STM) permits us to work with a conventional long-working-distance air objective and detect the near-field Raman signal from (electrified) solid/liquid interfaces of electronically resonant as well as non-resonant species in spite of the far-field focus distortion.

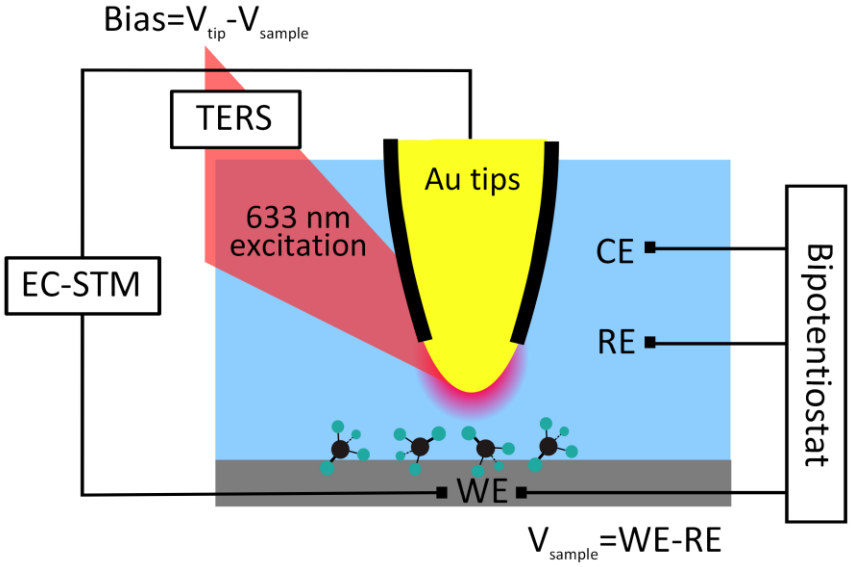

Figure 1: Schematics of the EC-TERS setup and electrode configuration. WE: working electrode; CE: counter electrode; RE: reference electrode; V_{tip}: tip potential; V_{sample}: working electrode potential

The development of an EC-TERS setup demands a step-by-step approach. Initially, we converted a conventional air-TERS setup into a liquid-TERS setup to explore the near-field generation for various reference molecules at solid/liquid interfaces and compare to in-air results. As a first standard, malachite-green isothiocyanate (MGITC), which chemisorbs to gold substrates, was chosen as a probe molecule, **Figure 2b**. In **Figure 2a**, STM images of the sample are presented in air (top) and water (bottom). The coupling with the Raman setup and the liquid cell requires a compromise between STM resolution and Raman performance. Since the STM cannot be isolated in a specific chamber to avoid vibrations, and the TERS experiment requires the use of long and soft Au tips (1 cm length, 0.25 mm diameter), the spatial and axial resolution of the (EC-)STM images is limited. While monoatomic Au steps and large terraces are seen, individual molecules are not distinguishable.

MGITC shows a maximum in the absorption spectrum at the excitation wavelength of 633 nm. This additional resonance enhancement renders possible resonant-TER (TERR) detection, even at very low adsorbate concentrations. In **Figure 2c**, TERRS data in air (green) and water (blue) of a monolayer of MGITC are shown. When the tip is approached to the sample in tunnelling conditions, the molecules on the substrate are located in the plasmonic near-field, and enhanced TERR bands are observed (spectra i and iii in **Figure 2c**). When the tip is retracted 20 nm from the surface, the near-field signal is lost and the spectra measured correspond to a conventional far-field Raman experiment (spectra ii and iv in **Figure 2c**). While the intensity in the far-field spectrum of liquid is slightly reduced with respect to the signal obtained in air (likely due to the distortion of the focus point), the TERR spectra recorded in air and water are of comparable intensity. The enhancement factors for the TERR band at 1375 cm^{-1} are $5.7 \cdot 10^3$ for both air and water, based on $EF=(I_{near\text{-}field} \cdot A_{far\text{-}field})/(I_{far\text{-}field} \cdot A_{near\text{-}field})$, and geometrical considerations as outlined in [7] and [8]. The position and relative intensities of the Raman bands both in air and water show excellent agreement with literature results. These results suggest that for the case of resonant species, the TERRS experiments show comparable enhancements in air and water.

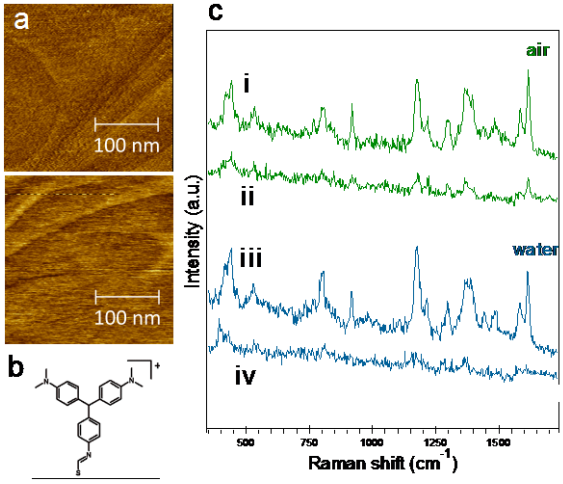

Figure 2: (a) STM images of a monolayer of MGITC on a Au(111) substrate in air (top) and water (bottom; (b) chemical structure of MGITC; (c) TERR spectra of MGITC in air (i) and water (iii), conventional Raman spectra corresponding to a tip retraction of 20 nm in air (ii) and water (iv)

To explore the possibilities of the setup for more generic adsorbate cases, we measured TERS in air and water of a monolayer of chemisorbed non-resonant thiophenol (PhS), **Figure 3**. The main bands of the molecule were detected in the TERS configuration in liquid, **Figure 3**(iii), showing good agreement with the results in air, **Figure 3**(i), and reports in literature [8]. The triplet of peaks at 998, 1022 and 1074 cm^{-1} and the mode at 1473 cm^{-1} are clearly detected in air and water, and allow unambiguous identification of PhS. However, the relative intensities of the triplet bands are not kept in water, particularly in the case of the ring vibration at 1074 cm^{-1} ($\nu_{CC}+\delta_{CH}$). The mode at 417 cm^{-1}($\nu_{CS}+\nu_{AuS}$) appears very intense in air, but is almost gone in the liquid case where the signal-to-noise ratio is too low to distinguish the band. The performance in liquid in this case cannot be evaluated in terms of enhancement factors since bands are not accessible in the far-field due the low Raman scattering cross sections of non-resonant PhS. The intensity of the TER bands in liquid is one order of magnitude lower than the ones detected in air (using the same power at the exit of the objective), unlike the results obtained for MGITC. As for non-resonant species, signal enhancement is largely generated through near-field enhancement (without electronic resonance contribution), focus distortion and the resulting deteriorated light-gap coupling are expected to have a more significant effect on the overall Raman enhancement than in the electronically resonant case of MGITC. The number of molecules in the near-field region generating the TERS peaks can be estimated (assuming a flat gold terrace, a tip diameter of 40 nm and a defect-free PhS monolayer), based on [9], to be less than 1200.

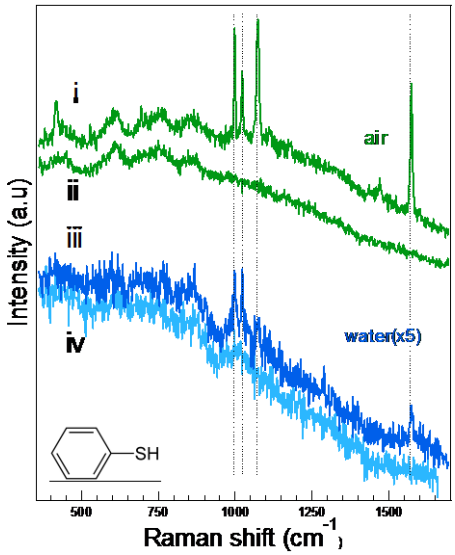

Figure 3: TERS of thiophenol in air (i) and water (iii), and the spectra resulting of a 20 nm retraction of the tip in air (ii) and water (iv).

After demonstrating that TERS in water is possible in both the resonant and non-resonant case, the next step is to substitute the water for an electrolyte and establish potential control of the sample. The probe molecule chosen for this experiment was adenine, a non-resonant DNA base that physisorbs on gold. Due to its importance in biology, adenine adsorption in Au electrodes has been extensively studied by TERS in air [10], electrochemical surface enhanced Raman [11] and EC-STM [12]. The results reported under electrochemical conditions vary with experimental conditions such as pH, electrolyte composition or configuration of the substrate, rendering complicated the correlation of the result obtained from different techniques. With our EC-TERS setup we can acquire vibrational and topographic information simultaneously, thus providing a concise tool to answer prevailing questions about adenine oxidation and its relation with molecular orientation, adsorption and desorption on Au electrodes. A bi-potentiostat with four electrodes (tip and sample as working electrodes, Pt wire as a counter electrode and a pseudo reference Pt wire) was used as sketched in Figure 1. We worked in constant bias mode ($Bias=V_{sample}-V_{tip}$) and ramped the potential of the sample with respect to the reference electrode; the STM adjusts accordingly the potential of the tip, which in this case was always 0.4 V lower than the sample potential. In Figure 4, the TER and corresponding far-field spectra are presented. The main band of the adenine fingerprint, the ring-breathing mode at 735 cm^{-1}, is detected with high intensity at low sample potentials, reaching a maximum at -0.3 V. The intensity decreases with increasing potential until 0.4 V, when the band completely disappears. A peak centred at 1315 cm^{-1}($\nu_{CN}+\delta_{NH}$), is also visible at negative potentials up to 0V. The changes in the spectra with increasing potential are reversible, i.e. the higher intensities are recovered when reducing the potential again after reaching 0.4 V. This result may suggest that at 0.4 V, when the adenine bands are no longer visible, a desorption of the monolayer happened, followed by a re-adsorption when the potential of the substrate were reduced again. The origin of the intense Raman bands around 1500 cm^{-1} in the TER spectrum at 0.4V is still under debate and requires further experiments; however, their presence demonstrate an effective near-field generation and supports the idea of desorption of the monolayer at high potentials. Some studies [11] suggest that the changes in intensity with increasing potential have their origin in orientational changes of adenine with respect to the substrate, starting with a parallel orientation of the rings with respect to the substrate at low potentials followed by a tilting when increasing potentials in different oxidation steps. Simulations of orientational changes and the effect on the Raman band intensities are currently under way in our laboratory.

Conclusions and/or Outlook

The different steps in the development of an EC-TERS setup, technical challenges and experimental solutions have been discussed. We have presented liquid-TERS results of monolayers of resonant (MGITC) and non-resonant (PhS) species. The calculated enhancement factors of about $5.7 \cdot 10^3$ demonstrate a good performance of the TERS setup in liquid for resonant adsorbates, with values very similar to the ones in air. . For non-resonant species, despite a loss of intensity by a factor of 10 in water with respect to air, near-field detection is possible from a monolayer of PhS and the detection of the main bands allows a clear identification of the adsorbate. Finally, the electrochemical behaviour of a monolayer of adenine on Au(111) was investigated. The results suggest re-orientation of the monolayer followed by desorption with increasing sample potential.

Our EC-TERS development paves the way for powerful in situ chemical nano-characterization of a wide range of electrified interfaces.

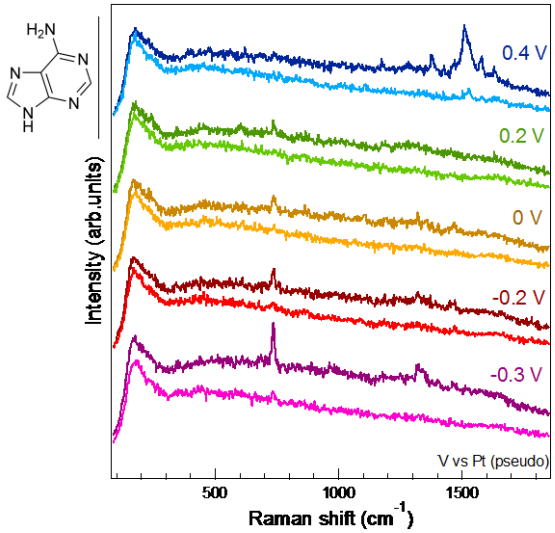

Figure 4: TER spectra of a monolayer of adenine adsorbed at Au(111) in a 0.01M of H_2SO_4 electrolyte at different sample potentials versus Pt pseudo reference electrode. The STM was operating at a constant bias mode (Bias=0.4 V), and therefore adjusting the potential of the tip to match the desired sample potential according to the expression Bias=V_{sample}-V_{tip}. For each pair of spectra in the same colors, the top one corresponds to TERS and the bottom to a retraction of the tip of 20 nm.

References:

[1] Wu DY, Li JF, Ren B, Tian ZQ; Electrochemical surface-enhanced Raman spectroscopy of nanostructures; Chem. Soc. Rev.; 37 (2008) 1025-1041

[2] Magnunssen OM; Ordered Anion Adlayers on Metal Electrode Surfaces; Chem. Rev.; 102 (2002) 679-726

[3] Domke KF, Pettinger B; Studying Surface Chemistry beyond the diffraction limit: 10 years of TERS; ChemPhysChem; 11 (2010) 1365-1373

[4] Zeng ZC, Huang SC, Wu DY, Meng LY, Li MH, Huang TX, Zhong JH, Wang X, Yang ZL, Ren B ; Electrochemical Tip-Enhanced Raman Spectroscopy; J. Am. Chem. Soc.; 137 (2015) 11928-11931

[5] Kurouski D, Mattei M, Van Duyne R; Probing redox reactions at the nanoscale with electrochemical tip-enhanced Raman spectroscopy; Nano Letters; 15 (2015) 7956-7962

[6] Domke KF, Zhang D, Pettinger B; Toward Raman fingerprints of single dye molecules at atomically smooth Au(111); J. Am. Chem. Soc.; 128 (2006) 14721-14727

[7] Kumar N, Rae A, Roy D; Accurate measurement of enhancement factor in tip-enhanced Raman spectroscopy through elimination of far-field artefacts; Appl. Phys. Lett.; 104 (2014) 123106-1-5

[8] Blum C, et al; Tip-enhanced Raman spectroscopy – an interlaboratory reproducibilty and comparison study; Journal of Raman spectroscopy; 45 (2014) 22-31

[9] Kang H, Lee H, Kang Y, Hara M, Noh J; Two-dimensional ordering of benzenethiol self-assembled monolayers guided by displacement of cyclohexanethiols on Au(111); Chem. Commun.; 41 (2008) 5197-5199

[10] Domke KF, Zhang D, Pettinger B; Tip-enhanced raman spectra of picomole quantities of DNA nucleobases at Au(111); J. Am. Chem. Soc.; 129 (2007) 6708-6709

[11] Ibanez D, Santidrian A, Heras A, Kalbac M, Colina A; Study of Adenine and Guanine Oxidation Mechanism by Surface-Enhanced Raman Spectroelectrochemistry; J. Phys. Chem. C; 119 (2015) 8191−819

[12] Vaz Dominguez C, Escudero-Escribano M, Cuesta A, Prieto-Dapena F, Cerrillos C, Rueda M; Electrochemistry communications, 35 (2013) 61-64

Interference-Enhanced Tip-Enhanced Raman Spectroscopy

E. Sheremet[a], R.D. Rodriguez**[b], A. Mukherjee[a], M. Hietschold[a], D.R.T. Zahn[b]*

[a] Solid Surfaces Analysis group and [b] Semiconductor Physics group
Technische Universität Chemnitz, Germany

*e-mail: evgeniya.sheremet@physik.tu-chemnitz.de
**e-mail: raul.rodriguez@physik.tu-chemnitz.de

Keywords: tip-enhanced Raman spectroscopy, interference, frustrated evanescent wave

Introduction

In tip-enhanced Raman spectroscopy (TERS) and related techniques the super-resolution is achieved due to concentrated electric field at the apex of plasmon-active tips [1]. In response to the high electric field, the Raman signal from the material directly in contact with the field is enhanced. However, in a presence of a SiO_2 film on a Si substrate supporting destructive interference we observe a different result. Destructive interference leads to trapping of the incident light in the SiO_2 film and its multiple rescattering, what is exploited in interference-enhanced Raman spectroscopy [2]. By introducing a TERS tip on the SiO2 surface, we induce efficient radiation of Raman photons from the underlying Si substrate, which is not in direct contact with the tip. It also provides improved spatial resolution characteristic for TERS. Simultaneously, the field at the surface of the SiO_2 film excites the tip apex locally thus enhancing the photoluminescence (PL) emission from the tip apex. The PL emission in plasmonic nanostructures was shown to provide information on the energy of localized surface plasmon resonance (LSPR), in our case, the PL and LSPR from the tip [3].

Results and Discussion

TERS imaging of an atomic force microscopy (AFM) calibration sample made of 119 nm thick SiO_2 stripes on a Si substrate as performed with a side illumination/collection TERS setup from AIST-NT/Horiba and with a custom built TERS system using an Agilent AFM and Horiba LabRam HR800 spectrometer. The resulting image (**Figure 1**) shows sub-diffraction resolution comparable to the resolution obtained in AFM. Contrary to expectations, we observe that in the presence of a TERS tip:

1) the Si Raman signal increases,
2) some bands in the PL background are selectively enhanced

above SiO_2 stripes as compared to Si substrate.

These observations cannot be explained by pure near-field signal enhancement characteristic of TERS. An important point here is that the 119 nm thickness, which supports destructive interference of the excitation wavelengths used (514.7, 532). We attribute the Raman signal enhancement to the antenna effect of the tip, which promotes radiation of the electromagnetic field on the SiO_2 surface created by destructive interference. The enhancement of photoluminescene band around 690 nm is attributed to local excitation of the tip apex by the evanescent wave on the surface of SiO_2 similar to the case of total internal reflection configuration [4].

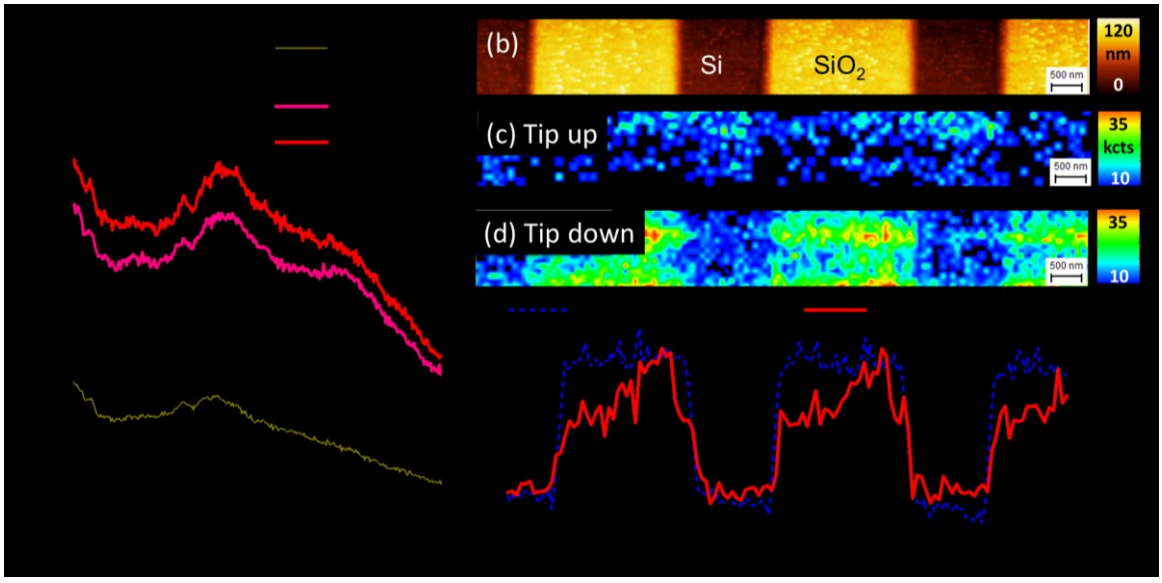

Figure 1: Left: Photoluminescence background for a gold tip above Si, SiO_2, and without substrate (far field). Right: AFM topography, respectively with Raman images of the Si intensity (at 520.5 cm^{-1}) for tip up and tip down, and respective cross-section profiles shown at the bottom.

Conclusions and/or Outlook

The scanning of the structured SiO_2 film appears to give information on radiation efficiency of TERS tips and, most importantly, its LSPR energy position that is directly correlated to the plasmonic photoluminescence emission. Additionally, being a well-tested AFM reference sample, periodic SiO_2 stripes on silicon offer robust performance over years of use and the chance to determine the tip radius due to sharp edges of the SiO_2 stripes. This work provides a long-sought solution for all-in-one TERS reference sample for the electromagnetic and geometrical characterization of the most critical component in TERS and other tip-enhanced nano-optics: the tip.

References:

[1] A. Hartschuh, Tip-enhanced optical spectroscopy, Phil. Trans. R. Soc. Lond. A 362 (2004), 807-819.
[2] R.J. Nemanich, C.C. Tsai, G.A.N. Connell, Interference-Enhanced Raman Scattering of Very Thin Titanium and Titanium Oxide Films, Phys. Rev. Lett. 44(4) (1980), 274-276.
[3] H. Hu, H. Duan, J.K.W. Yang, Z.X. Shen, Plasmon-Modulated Photoluminescence of Individual Gold Nanostructures, ACS Nano 6(11) (2012), 10147–10155.
[4] D. Mehtani, N. Lee, R.D. Hartschuh, A.P. Sokolov, A. Kisliuk, M.D. Foster, F. Cajko, I. Tsukerman, Optical properties and enhancement factors of the tips for apertureless near-field optics, J. Opt. A: Pure Appl. Opt. 8 (2006), 183–190.

Acknowledgments:

This work was supported by the DFG Cluster of Excellence “Center for Advancing Electronics Dresden” (cfaed), with financial support from the DFG Research Unit FOR1713 SMINT.

Seeing or feeling?
Tip-sample interaction in plasmon-enhanced nano-optics

Raul D. Rodriguez*[a,b], Evgeniya Sheremet[c], Hassan Banayee[a], Michael Hietschold[c], Dietrich R.T. Zahn[a,b]

[a] Semiconductor Physics, Technische Universität Chemnitz, 09107 Chemnitz, Germany
[b] Center for Advancing Electronics Dresden (cfaed), Technische Universität Chemnitz, 09107, Chemnitz, Germany
[c] Solid Surfaces Analysis Group, Technische Universität Chemnitz, 09107 Chemnitz, Germany

*e-mail: raul.rodriguez@physik.tu-chemnitz.de

Keywords: tip-enhanced Raman spectroscopy, TERS, atomic force microscopy, plasmonics

Introduction

The capability to visualize and correlate composition, sample properties, and morphology with a resolution at the nanoscale makes tip-enhanced Raman spectroscopy (TERS) one of the hottest topics in nanoscale characterization since first reported in 2000 [1-3]. Numerical models and previous experimental results showed that the electric field enhancement in TERS is a direct consequence of tip-sample geometry, composition, and laser excitation [4]. In this work, we demonstrate that the tip-sample interaction makes also a significant contribution to the electric field enhancement in TERS with atomic force microscopy (AFM) operated in dynamic mode. The phase shift between the cantilever excitation and its oscillation response is sensitive to tip-sample interactions and to variations in material properties such as stiffness and adhesion. Careful investigation of the phase contrast and its numerical modeling allow us to determine that the tip-sample interaction influences the degree of electric field enhancement in TERS.

Results and Discussion

Au nanoparticles prepared by electron beam lithography on a Si substrate were covered with an ultra-thin layer of cobalt phthalocyanine (2 nm) as the Raman probe. TERS imaging in the dynamic AFM mode was performed on this sample using a commercial all-metal tip using 638 nm laser excitation. We found a one-to-one correlation between phase and TERS images as illustrated in **Figure 1**, showing the impact of tip-sample interaction. The phase contrast above 90º shows that the tip-sample interaction dominated by attractive forces overlaps with the same region on the Au nanoparticles with the highest electric field enhancement. Numerical simulation results of the cantilever dynamics demonstrate that the electric field of the exciting light also influences the tip-sample interaction increasing the phase image contrast in agreement with experimental results.

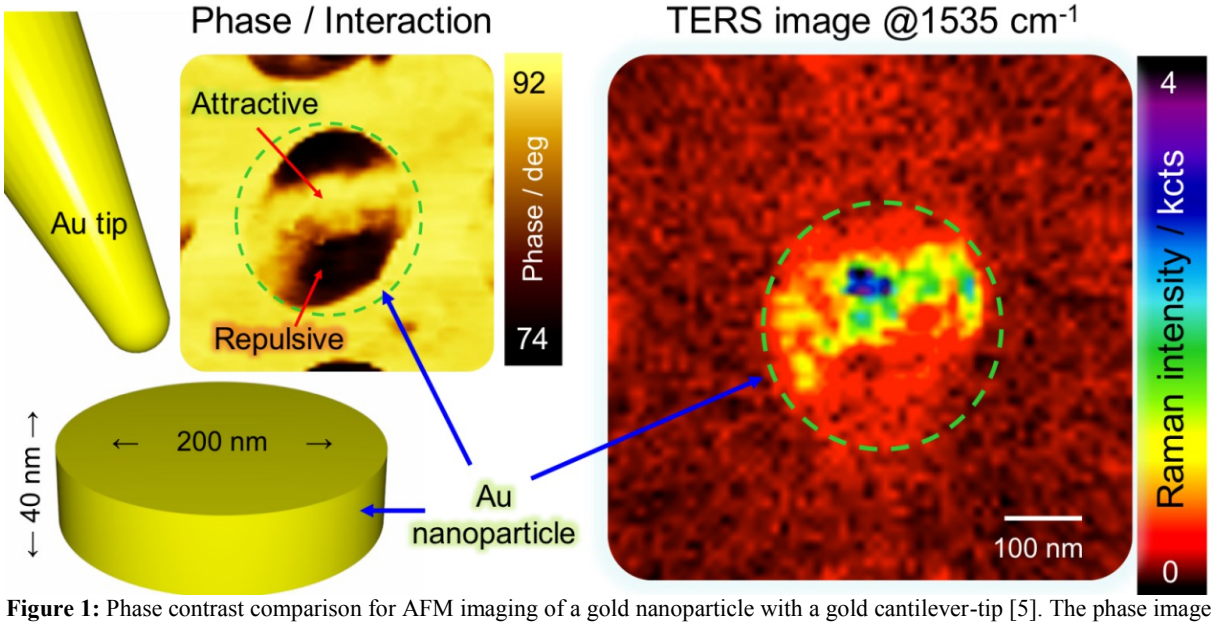

Figure 1: Phase contrast comparison for AFM imaging of a gold nanoparticle with a gold cantilever-tip [5]. The phase image correlation with TERS image contrast obtained under 638 nm excitation, the Raman probe was a 2 nm film of CoPc. The TERS image shows the spatial distribution of the B_{1g} mode intensity of CoPc at 1535 cm^{-1}. Both images were obtained simultaneously.

Conclusions and/or Outlook

This contribution demonstrates that tip-sample interaction must be considered in the interpretation of TERS imaging results obtained with dynamic mode AFM. The attractive tip-sample interaction makes a larger increase of electric field enhancement. The physical mechanism behind this result, associated with the longer and closer tip-sample interaction will be discussed.

This effect has implications in other scanning probe based nano-optics methods such as scanning near-field optics with a tuning fork. By tracking the friction force, the investigation of the tip-sample interaction for AFM in contact mode is underway.

References:
[1] R.M. Stockle, Y.D. Suh, V. Deckert, R. Zenobi, Nanoscale chemical analysis by tip-enhanced Raman spectroscopy, Chemical Physics Letters, 318 (2000) 131-136.
[2] N. Hayazawa, Y. Inouye, Z. Sekkat, S. Kawata, Metallized tip amplification of near-field Raman scattering, Optical Communications, 183 (2000) 333-336.
[3] M.S. Anderson, Locally enhanced Raman spectroscopy with an atomic force microscope, Applied Physics Letters, 76 (2000) 3130-3132.
[4] Z.L. Yang, J. Aizpurua, H.X. Xu, Electromagnetic field enhancement in TERS configurations, Journal of Raman Spectroscopy, 40 (2009) 1343-1348.
[5] E. Sheremet, R. D. Rodriguez, A. L. Agapov, A. P. Sokolov, M. Hietschold, and D. R. T. Zahn, Nanoscale imaging and identification of a four-component carbon sample, Carbon, 96, (2016), 588-593.

Acknowledgments:
We thank Alexander Milekhin and Ekaterina Rodykina from the Institute of Semiconductor Physics Novosibirsk for the Au nanostructures, and Andrey Krayev from AIST-NT for initial assistance with TERS experiments. This work was supported by the DFG Cluster of Excellence "Center for Advancing Electronics Dresden", cfaed, with financial support from the DFG Research Unit FOR1713 SMINT.

Reliable tip enhanced Raman cantilevers for nanometer scale imaging spectroscopy.

Dr. Sergey Lemeshko, Artem Shelaev, NT-MDT Co.

Stewart House, National Technological Park, Castletroy, Limerick, Ireland

Development of new instruments for material properties structural and chemical analysis studies like integrated scanning confocal Raman microscopes and scanning probe microscopes where metallised tip could play a role of plasmonic antenna dictate a development of a reproducible and reliable probes for reaching high enhancement factor and special resolution below optical diffraction limit .

Tip enhanced Raman scattering (TERS) has introduced more than decade ago as a promising technique that offers both chemical information and nanometre spatial resolution. The main idea of this approach is to probe samples using the surface enhanced Raman effects at the tip end of a sharp scanning metal probe. By matching a laser wavelength and tip material a nanometre spatial resolution can be achieved by the extreme localized enhancement effect. There were several approaches introduced by scientists in the realization of that plasmonic antennas on the as scanning probe using scanning tunnelling microscopy effect as feedback mechanism and electrochemically etched golden or silver wires; using tuning fork sensor and fix an small piece of electrochemical etched wire to the resonator and use share force feedback; or using micro fabricated silicon cantilevers and localizing metallic nanoparticle ; there were reports with simple gold or silver sputtering over silicon cantilevers where AFM laser deflectometer feedback could be used. All mentioned above types of probes have some advantages and disadvantages for TERS imaging on different samples, but until now there were no commercial available cantilevers utilising laser deflectometer as feedback [1-4].

In this report we like to introduce our achievements in fabrication reproducible and reliable TERS probes based on soft silicon cantilevers with coating of noble metals alloy of Silver and Gold film over “concord ” shape silicon cantilever which produced by traditional batch production process.

New type of TERS active cantilevers shows high enhancement factor more than 100 times on molecular layer of Briliant Crystic blue molecules deposited on atomically flat gold substrate in order to exclude possible surface plasmon resonances. Statistically more than 90% of tips from the batch. The enhancement factor when tip –in tip-out for spectra measurements is one criteria and what about spatial resolution, The alloy of two metals had demonstrated high reliability and that leading to extension life time. The high enhancement factor remain for the tips aged over 30 days. We would like to emphasise that one of the main advantage of using soft cantilevers for TERS mapping is the ability to operate in contact, noncontact modes with phase lock loop (PLL) feedback of Hybrid Mode. These modes allows to keep constant amplitude or distance between tip and sample for good Plasmon coupling which could not be the case for traditional tapping mode.

[1]. K L Andrew Chan and Sergei G Kazarian, Nanotechnology 21 (2010) 445704 (6pp)
[2]. S S Kharintsev, G G Hoffmann, P S Dorozhkin, G de With and J Loos, Nanotechnology 18 (2007) 315502 (9pp)
[3]. Valentinas Snitka , Raul D. Rodrigues, Vitas Lendraitis, Microelectronic Engineering
Volume 88, Issue 8, August 2011, Pages 2759–2762
[4]. Yuhua Lia, Changhui Xu and Min Han, Advanced Materials Research Vol. 643 (2013) pp 195-198

Molecular exciton-plasmon cupling in the strong copling limit for organic semicondutors on Au nanorod arrays

S. Fedele[1], M. Hakami[1], A. Murphy[2], R. Pollard[2], J.H. Rice[1]

[1] School of Physics, University College Dublin, Belfield, Dublin 4, Ireland.
[2] Centre for Nanostructured Media, Queen's University of Belfast, Belfast BT7 1NN, UK

**e-mail: james.rice@ucd.ie*

Keywords: Strong coupling, nanorod, array, exciton, semiconductor

Introduction

Active plasmonics nanomaterials such as nanorod array can be coupled with excitonic systems to give rise to hybrid plasmon–exciton modes (Plexcitons) when in the strong coupling regime. Such systems when within the strong coupling limit effect changes in the optical processes of an emitter or absorber excitonic system. This offers potential to enhance or control exciton processes in excitonic systems such as organic semiconductors which offers opportunities for enhanced photonic device designs such as in light harvesting, optical sensing or artificial light sources.

A number of studies have demonstrated plasmon-exciton in the strong coupling limit between an organic exciton semiconductor and localized surface plasmons geometries [1-2]. Studies have demonstrated that colloidal Au nanoshell-J-aggregate particles exhibit strong coupling between the localized plasmons of a nanoshell and the excitons of molecular J-aggregates adsorbed on its surface [1]. Dynamic tuning of plasmon–exciton coupling as been reported for strongly coupled exciton–plasmon states in Au nanodisk arrays coated with J-aggregate molecules achieved by changing the incident angle of incoming light, rather than changing the geometry of the plasmonic nanomaterial. Using such an angle resolved approach plasmon–exciton coupling of variable strengths was achieved [2].

Here we demonstrate dynamic strong coupling in self-standing nanorod arrays achieved though angular tuning. We report a Fano line shape in the differential reflection spectra associated with the formation of new hybrid states, leading to anti-crossing of the upper and lower cavity-polaritons with a Rabi frequency of 125 meV. The recreation of a fano like line shape was also found in photoluminescence demonstrating changes in the emission spectral profile under dynamic strong coupling in a J-aggragate/Au nanorod hybrid system.

Results and Discussion

Differential reflectance (ΔR/R) from the J-aggregate nanorod sample for TM polarized light at three different indecent angles were recorded (see **Figure 1**). Concentrating on the wavelength range nm 600-750 nm which corresponds to a spectral region where the J-aggregate S_1 exciton state absorbs and also where the nanorods longitudinal surface plasmon (SP) mode is present. The contour plot shows that there is a dip coinciding with the exciton energy replicating a fano resonance line-shape which indicates the presence of strong coupling. In the strong coupling regime plexcitons are formed from interaction of the $|S_1\rangle$ state of the exciton molecular J-aggregate with the longitudinal ($|SP_L\rangle$) surface plasmon modes of the gold nanorod array. The hybrid plexcitons possessing two branches (e.g. $|S_1\text{-}SP_L\rangle^+$ and $|S_1\text{-}SP_L\rangle^-$). The reflection spectrum shows two dips marked $\Box S_1\text{-}SP_L\rangle^+$ at 645 nm and $\Box S_1\text{-}SP_L\rangle$ at 700 nm respectively (which corresponds to Rabi splitting ($\Box$) energy of 150 meV). The S_1 Q band from the J-aggregates absorption spectrum is c.a midway between the $\Box S_1\text{-}SP_L\rangle^+$ and $\Box S_1\text{-}SP_L\rangle$ hybrid states. To confirm the presence of strong coupling a dispersion plot was made as a function of the

single longitudinal SP mode of pristine nanorod with the Plexciton hybrid modes of the J-aggregate/nanorod complex with incident angle. The dispersion plot shows a characteristic anti-crossing of the two hybrid peaks (□S_1-SP_L>$^+$ and□□S_1-SP_L>$^-$). This is associated with Rabi splitting of the SP peak, where the molecular resonance of the J-aggregate and the longitude mode of the nanorod array overlap characteristic of the strong coupling. `

Photoluminescence (PL) spectra were recorded as a function of incident angle. As angle increases the main peak in the PL spectra shifts progressively to the blue. Following substration of the J-aggregate emission (□=0) on glass from that of J-aggregate/nanorod at each angle as clear progression can be seen in line with similar spectral profiles have been reported for PL from systems in the strong-coupling limit. Such studies reported that the modification in the fluorescence profile is associated with the spectral dependence of the radiative and non-radiative decay rate of the molecular exciton complex closely follows the plasmon scattering spectrum. This indicates that the PL arises from the polaritonic emission, resulting from the Plexciton SP/exciton mixed states.

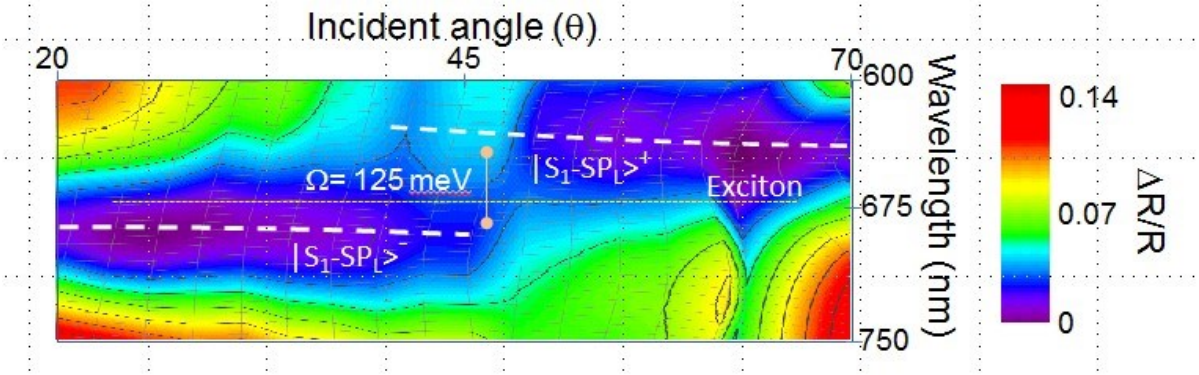

Figure 1: Contour plot of TM polarised difference reflection spectra as a function of angle

Conclusions and/or Outlook

In summary, we demonstrate here dynamic strong coupling between localised surface plasmon modes in self-standing nanorods with Frankel excitons in a porphyrin molecular J-aggregate layer though angle tuning. The enhanced exciton−plasmon coupling creating a Fano line shape in the differential reflection spectra associated with the formation of new plexciton hybrid states, leading to anti-crossing of the upper and lower cavity-polaritons with a Rabi frequency of 125 meV. The recreation of a fano like line shape was found in photoluminescence demonstrating changes in the emission spectral profile under dynamic strong coupling. This study demonstrates that J-aggregate excitons under dynamic strong coupling with plasmon modes can controllable alter the emission and absorption spectral profile through control of excitation angle.

References:

[1] Fofang, N.T., Park, T.H., Neumann, O., Mirin, N.A., Nordlander, P. and N. J. Halas. Nano Lett., 8, (2008) 3481–3487.

[2] Zheng, Y. B., Juluri, B. K., Lin Jensen, L., Ahmed, D., Lu, M., Jensen, L. and Huang, T. J. Adv. Material, 22 (2010) 3603-3607.

Boundary-enhanced lithium-fluoride luminescent thin-film detectors for ionising radiation

E. Nichelatti[a], F. Bonfigli[b], M.A. Vincenti[b], R.M. Montereali[b]*

[a] ENEA, Fusion and Nuclear Security Department, Physical Technologies for Safety and Health Division, Photonics Micro and Nano-structures Laboratory, C.R. Casaccia, Via Anguillarese 301, 00123 S. Maria di Galeria, Rome, Italy

[b] ENEA, Fusion and Nuclear Security Department, Physical Technologies for Safety and Health Division, Photonics Micro and Nano-structures Laboratory, C.R. Frascati, Via E. Fermi 45, 00044 Frascati, Rome, Italy

**e-mail: enrico.nichelatti@enea.it*

Keywords: Radiation detectors, Photoluminescence, Lithium fluoride, Colour centres, Optical confinement

Introduction

Point defects in insulators [1,2] are successfully used for radiation detectors [3]. Among them, colour centres (CCs) in lithium fluoride (LiF) – in the form of pellet, crystal or thin film – are known for their use in dosimeters [4], miniaturised optically-active devices [5] and solid-state lasers [6]. CCs are generated in LiF by different kinds of ionising radiation, including ions, extreme-UV light, γ-rays and X-rays [5,7,8].

Some kinds of aggregate CCs in LiF, particularly the F_2 and F_3^+ ones, are optically active: these latter emit in the red and green parts of the visible spectrum, respectively [2]. Moreover, they share an absorption band at ~450 nm, therefore can be excited at the same time with blue light [2]. The photoluminescence (PL) intensity emitted by F_2 and F_3^+ CCs, which have formed in LiF because of exposition to radiation, is proportional to their volumetric amount and can be conveniently related to the absorbed dose. This fact can be exploited to design and fabricate suitable detectors for several kinds of radiation, even for high-resolution X-ray imaging applications [9].

In the past recent years, attention has been especially drawn on planar luminescent LiF-film detectors [9-12], which allow for a finer tailoring of their characteristics with respect to crystals, besides offering fabrication convenience and scalability. Like LiF crystals, LiF-film detectors feature sub-micron spatial resolution [13] across a wide field of view (practically limited by the readout optics), large dynamic range (e.g. larger than PMMA), no need of development, easiness of handling, absence of sensitivity to visible and UV light (i.e. no special protection cover is needed for their conservation). Resolution values down to 80 nm were demonstrated with scanning near-field optical microscopy (SNOM) [9].

In the present work it is shown how the efficiency of such LiF-film detectors, i.e. the amount of PL that they emit after irradiation, can be enhanced by designing a planar structure where the substrate material is suitably selected and the film thickness is properly chosen [14] in order to maximise the intensity of the involved electromagnetic fields at the CC locations.

Results and Discussion

Efficiency amplifications from ~2× up to ~12× have been obtained for LiF-film detectors by using suitably designed planar configurations that introduce favourable boundary conditions [14-16]. These latter, obtained with selected semiconductor or metal-based substrates and proper LiF-film thickness values, can amplify at the same time the local densities of three kinds of electromagnetic fields: (a) the vacuum field, responsible for the rate of spontaneous emission from excited CCs; (b) the optical pump field, utilised to excite the CCs; (c) the PL field that is emitted by the CCs. A good overlapping of these electromagnetic fields, obtained by designing the device [14] by means of our ad-hoc model [17], capable of analytically evaluating PL emission from within multilayer structures of whatever solid material (metals included), together with a generally better CC-formation efficiency in polycrystalline LiF films with respect to bulks [15], results in a larger PL intensity detectable during the readout of the detector.

The theoretical dependence of readout PL intensity as a function of LiF-film thickness is shown in **Figure 1** for two kinds of elementary detectors: a LiF film on silica (SiO_2) and on silicon (Si) substrates. The detectors were assumed to have been exposed to soft X-rays so that a local distribution of CCs had been generated at the external surface of LiF. The PL emitted from this CC distribution under normally-directed optical pumping at $\lambda = 458$ nm is thought of being read in an optical system of numerical aperture equal to 0.13 and equipped with red (562-1000 nm) and green (499-529 nm) band-pass filters [15]. The plots in **Figure 1** were obtained by a 100-repetitions Montecarlo process to take into account uncertainties related to the knowledge of the material optical constants and thickness: the black lines represents the average curves, while the grey ribbons show the confidence bands of the theoretical estimations. It can be noticed from the plots how the reflective properties of Si at the emission wavelengths of F_2 and F_3^+ CCs helps in getting an efficiency which is almost double of the device with SiO_2 substrate. These theoretical values are in good agreement with experimental results [15].

Even more efficient detectors, up to the above-mentioned ~12× amplification, can be designed by choosing materials other than SiO_2 and Si for the substrate [14].

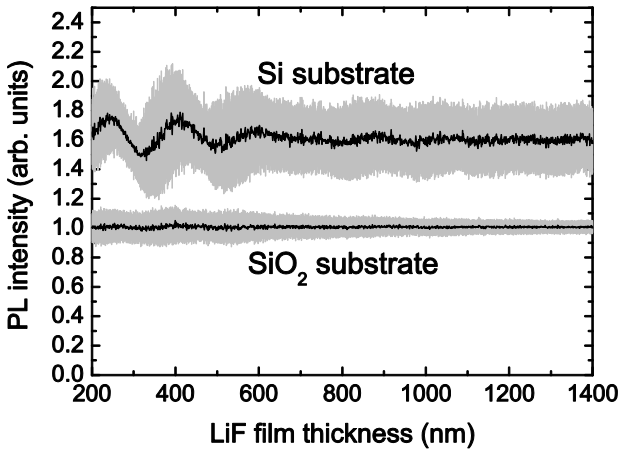

Figure 1: Theoretical Montecarlo-based simulation of the PL emitted from CCs at the surface of a LiF film on silica (SiO_2) and silicon (Si) substrate. See the text for further details.

Conclusions

Suitable design and choice of materials can sensibly improve the performances of planar luminescent LiF-film detectors for ionising radiation. As a matter of fact, boundary conditions can be created to better confine the vacuum field together with the emitted PL field and the optical pump utilised to excite the radiating CCs. So far, amplification values up to ~12× have been obtained. Work is in progress to further improve this figure still maintaining the design simple enough to allow for convenient fabrication and scalability.

References:

[1] Stoneham A M; Theory of Defects in Solids; Oxford University Press (Oxford) 1975.
[2] Fowler W B; Physics of Color Centers; Academic Press (New York and London) 1968.
[3] Shionoya S, Yen W M; Phosphor Handbook; CRC Press (Boca Raton) 1998.
[4] Lakshmanan A R, Madhusoodanan U, Natarajan A, Panigrahy B S; Photoluminescence of F-aggregate centers in thermal neutron irradiated LiF TLD-100 single crystals; phys. stat. sol. (a) 153 (1996) 265-273.
[5] Montereali R M; in Handbook of Thin Film Materials; edited by Nalwa H S, Vol. 3; Academic Press (New York) 2002; pp. 399-431.
[6] Basiev T T, Mirov S B, Osiko V V; Room-temperature color center lasers; IEEE J. Quantum Electron.; 24 (1998) 1052-1069.
[7] Nahum J, Wiegand D A; Optical Properties of Some F-Aggregate Centers in LiF; Phys. Rev.; 154 (1967) 817-830.
[8] Baldacchini G, Cremona M, d'Auria G, Montereali R M, Kalinov V; Radiative and nonradiative processes in the optical cycle of the F_3^+ center in LiF; Phys. Rev. B; 54 (1996) 17508-17514.
[9] Ustione A, Cricenti A, Bonfigli F, Flora F, Lai A, Marolo T, Montereali R M, Baldacchini G, Faenov A, Pikuz T, Reale L; Scanning near-field optical microscopy images of microradiographs stored in lithium fluoride films with an optical resolution of λ/12; Appl. Phys. Lett.; 88 (2006) 141107.
[10] Hampai D, Dabagov S B, Della Ventura G, Bellatreccia F, Magi M, Bonfigli F, Montereali R M; High-resolution X-ray imaging by polycapillary optics and lithium fluoride detectors combination; EPL; 96 (2011) 60010.
[11] Heidari Bateni S, Bonfigli F, Cecilia A, Pelliccia D, Somma F, Vincenti M A, Montereali R M; Optical characterisation of lithium fluoride detectors for broadband X-ray imaging; Nucl. Instrum. Methods A; 720 (2012) 109-112.
[12] Nichelatti E, Almaviva S, Bonfigli F, Franzini I, Montereali R M and Vincenti M A; Photoluminescence from colour centres generated in lithium fluoride thin films and crystals by extreme-ultraviolet irradiation; Nucl. Instrum. Methods B; 268 (2010) 3035-3039.
[13] Almaviva S, Bonfigli F, Franzini I, Lai A, Montereali R M, Pelliccia D, Cedola A, Lagomarsino S; Hard X-ray contact microscopy with 250 nm spatial resolution using a LiF film detector and a tabletop microsource; Appl. Phys. Lett.; 89 (2006) 54102.
[14] Montereali R M, Bonfigli F, Nichelatti E, Vincenti M A; ENEA Patent RM2013A000123.
[15] Montereali R M, Bonfigli F, Vincenti M A, Nichelatti E; Versatile lithium fluoride thin-film solid-state detectors for nanoscale radiation imaging; Il Nuovo Cimento; 36C (2013) 35-42.
[16] Montereali R M, Bonfigli F, Piccinini M, Nichelatti E, Vincenti M A; Photoluminescence of colour centres in lithium fluoride thin films: from solid-state miniaturised light sources to novel radiation imaging detectors; J. Lumin.; 170 (2016) 761-769.
[17] Nichelatti E, Montereali R M; Photoluminescence from a homogeneous volume source within an optical multilayer: analytical formulas; J. Opt. Soc. Am. A; 29 (2012) 303-312.

Laser generated nanoalloys with plasmonic and magnetic properties for SERS and nanomedicine applications

*V. Amendola**

Department of Chemical Sciences, University of Padova

**e-mail: vincenzo.amendola@unipd.it*

Keywords: nanoalloys, gold nanoparticles, silver nanoparticles, iron nanoparticles, laser synthesis, SERS

Introduction

Here we will present about the use of laser-assisted synthesis for the generation of nanoalloys and other nanostructures with plasmonic and magnetic properties useful for SERS and nanomedicine applications. In last years, laser-assisted synthesis, and in particular laser ablation synthesis in solution (LASiS), emerged as a reliable, versatile and low-cost method to obtain a variety of nanomaterials, such as metals, oxides and semiconductors.
This lecture will focus in particular on three examples of laser generated nanostructures, which are (i) Au Nanocorals, (ii) Fe-doped Au nanoparticles, and (iii) Fe-doped Ag nanotruffles.

Au Nanocorals[1]

Gold nanoparticles with efficient plasmon absorption in the visible and near infrared (NIR) regions, biocompatibility and easy surface functionalization are of interest for photothermal applications. We describe the synthesis and photothermal properties of gold "nanocorals" (Au NC) obtained by laser irradiation of Au nanospheres (Au NS) dispersed in liquid solution. Au NC are formed in two stages: by photofragmentation of Au NS, followed by spontaneous unidirectional assembly of gold nanocrystals. The whole procedure is performed without chemicals or templating compounds, hence the Au NC can be coated with thiolated molecules in one step. We show that Au NC coated with thiolated polymers are easily dispersed in an aqueous environment or in organic solvents and can be included in polymeric matrixes to yield a plasmonic nanocomposite. Au NC dispersions exhibit flat broadband plasmon absorption ranging from the visible to the NIR and unitary light-to-heat conversion. Besides, in vitro biocompatibility experiments assessed the absence of cytotoxic effects even at a dose as high as 100 μg mL^{-1}. These safe-by-designed Au NC are promising for use in various applications such as photothermal cancer therapy, light-triggered drug release, antimicrobial substrates, optical tomography, obscurant materials and optical coatings.

Fe-doped Au nanoparticles.[2]

The integration of multiple functionalities in a single object with nanometric size is crucial for the development of efficient tools for nanomedicine applications. Here we show how a synthetic approach based on laser ablation of a solid target in a liquid solution gives access to am Au-Fe alloy with the plasmonic properties of gold and the magnetic properties of iron. The structure and surface conjugation of the magneto-plasmonic nanoalloy was engineered in order to gain the functions of a multimodal contrast agent for magnetic resonance imaging, x-ray computed thomography, photoacustic imaging and surface enhanced Raman imaging.
Besides, we show that the absorption cross section of gold nanoparticles is sensibly increased when iron is included in the lattice as a substitutional dopant, i.e. in a gold-iron nanoalloy. Such increase is size and shape dependent, with the best performances observed in nanoshells where a 90-190% improvement is found in a size range that is crucial for practical applications. Our findings are unexpected according to the common believe and previous experimental observations that alloys of Au with transition metals show depressed plasmonic response.

Fe-doped Ag nanotruffles[3]

The coexistence of Fe and Ag in the same nanostructure is interesting for nanophotonics, nanomedicine, and catalysis. However, alloying of Fe and Ag is inhibited for thermodynamic reasons. Here, we describe the synthesis of Fe-doped Ag NPs via laser ablation in liquid solution, bypassing thermodynamics constraints. These NPs have an innovative structure consisting of a scaffold of face-centered cubic metal Ag alternating with disordered Ag–Fe alloy domains, all arranged in a truffle-like morphology. The Fe–Ag NPs exhibit the plasmonic properties of Ag and the magnetic response of Fe-containing phases, and the surface of the Fe–Ag NPs can be functionalized in one step with thiolated molecules. Taking advantage of the multiple properties of Fe–Ag NPs, the magnetophoretic amplification of plasmonic properties is demonstrated with proof-of-concept surface-enhanced Raman scattering and photothermal heating experiments. The synthetic approach is of general applicability and virtually permits the preparation of a large variety of multi-element NPs in one step.

References:

[1] A. Poletti et al. Laser generated gold nanocorals with broadband plasmon absorption for photothermal applications, Nanoscale, 2015,7, 13702-13714

[2]

a. S. Scaramuzza et al., Metastable alloy nanoparticles, metal-oxide nanocrescents and nanoshells generated by laser ablation in liquid solution: influence of the chemical environment on structure and composition, Phys. Chem. Chem. Phys., 2015, 17, 28076-28087.
b. V. Amendola et al., Coexistence of plasmonic and magnetic properties in Au89Fe11 nanoalloys, Nanoscale, 2013,5, 5611-5619.
c. V. Amendola et al., Strong dependence of surface plasmon resonance and surface enhanced Raman scattering on the composition of Au–Fe nanoalloys, Nanoscale, 2014,6, 1423-1433.
d. V. Amendola et al., Magneto-Plasmonic Au-Fe Alloy Nanoparticles Designed for Multimodal SERS-MRI-CT Imaging, Small, 2014, 10, 2476–2486.
e. V. Amendola et al., Superior plasmon absorption in iron-doped gold nanoparticles, Nanoscale 2015,7, 8782-8792

[3] V. Amendola et al. Laser generation of iron-doped silver nanotruffles with magnetic and plasmonic properties, Nano research 2015, 10.1007/s12274-015-0903-y.

Evidence of protein aggregates in *He-La* cells by Nano-Infrared imaging

A. Nucara [a *], *L. Baldassarre*[a], *M. Ortolani*[a], *A. Rosa*[b], *V. Giliberti*[c], *K. Kjoller*[d] *and P. Calvani*[a]

[a] Dipartimento di Fisica, Università di Roma Sapienza, P.le Aldo Moro, 2 Rome, Italy
[b] Dipartimento di Biologia e Biotecnologie Charles Darwin,Università di Roma Sapienza,P.le Aldo Moro, 2 Rome, Italy.
[c] Center for Life Nano Science@Sapienza, Istituto Italiano di Tecnologia, V.le Regina Elena 295, Rome, Italy.
[d] Anasys Instruments, Inc, 325 Chapala Street, Santa Barbara, California 93101, USA

**e-mail: alessandro.nucara@roma1.infn.it*

Keywords: imaging, protein, aggregates, cell

Introduction

Novel near-field techniques can shade light on important biological and medical issues, as drug-delivery effectiveness, protein concentration in dried cells, lipid membranes function and structure. Here, an AFM-IR experiment on fixed *He-La* cells, over-expressing proteins, is presented. The FUS (FUsed in Sarcoma) protein is sited in the cell nucleus in healthy cell, but migrates in the cytoplasm under stress condition, to form small aggregates. These latter are considered to be good candidates for a class of neuro-degenerative deseases at the cellular level [1]. In this framework, infrared nano-imaging of proteins within cell's cytoplasm can represent a powerful tool for the study of such aggregates.

By using an AFM-IR spectrometer, we performed imaging experiments in the region of the C = O absorption band of proteins (amide I) of wild type (WT) and stressed (STR) *He-La* cells, where over-expression of FUS protein was induced, achieving a lateral resolution down to 50 nm. The optical apparatus consists of a quantum-cascade laser coupled to an AFM system: the former was lasing with a repetition rate resonant with a mechanical mode of the AFM cantilever [2]. Samples were dried in air and fixed on Si substrates .

Results

Cell infrared images at the amide I absorption frequency, like that in the left panel of Figure 1, provided evidence of a large amount of proteins in the cytoplasm of both WT and STR cells. Nevertheless, in view of the intrinsic complexity of the samples, the presence of eventual anomalous distributions in the STR cells could not be directly identified in the maps.

Therefore, the images of both kinds have been accurately analyzed by using two different approaches. A classical method based on the Pair Correlation (PC) function was used to obtain the average aggregate extension and their amount within the cell's cytoplasm. This also provided an estimate of the percentage increase of aggregates formation by a comparison between WT and STR specimens. The statistical results of the PC methods have been further confirmed by digital image analysis. In particular, both methods indicated an increase of aggregate formation in STR specimens, with a lateral dimension ranging between 400 - 600 nanometers.

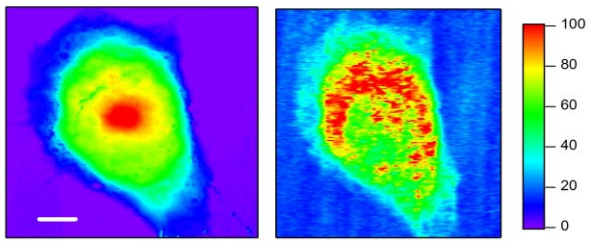

Figure 1: Left panel: AFM topograghy of a dried He-La cell. The white bar indicates 4 □m; right panel: infrared image of the same cell at the frequency of the amide I band (1650 cm^{-1}).

Conclusion

In the present experiment, we used an IR-AFM spectroscopic technique to detect the protein distribution in dried *He-La* cells, both wild and stressed, with a lateral resolution 100 times smaller than the radiation wavelength. The data analysis of the infrared maps, performed according two different methods, provided evidence of protein aggregates on the scale of 400 nm in the stressed cells [3]. Further information will be achieved in further experiments already planned on a broader spectral range. This will allow us to detect the intracellular distribution of other basic components, like nucleic acids and lipids, and their eventual modification under stress.

References:

[1] R.R. Sama el al. *J. Cell. Physiology* (2013), **228**, 2222.
[2] F. Lu M. Jin, and M. A. Belkin, Nat. Phot. 8, 307 (2014).
[3] L. Baldassarre et al. , Nanotechnology accepted for publication.

Detection, identification and structural study of proteins by Surface Enhanced Raman Spectroscopy

Maximilien Cottat[1], Cristiano D'Andrea[2], Ryohei Yasukuni[1], Natalia Malashikhina[3], Ruta Grinyte[3], Nathalie Lidgi-Guigui[1], Barbara Fazio[2], Angela Sutton[4], Olivier Oudar[4], Nathalie Charnaux[4], Valery Pavlov[3], Andrea Toma[5], Enzo Di Fabrizio[6], Nadine Varin-Blank[7], Christine Le Roy[7], Pietro G. Gucciardi[2], Marc Lamy de la Chapelle[1]

[1] Université Paris 13, Sorbonne Paris Cité, Laboratoire CSPBAT, CNRS, Bobigny, France
[2] CNR IPCF Istituto per i Processi Chimico-Fisici, Viale F., Messina, Italy
[3] Biofunctional Nanomaterials Dpt, CIC biomaGUNE, Parque tecnológico de San Sebastian, Spain
[4] Université Paris 13, Sorbonne Paris Cité, Bioingénierie Cardiovasculaire, INSERM, Bobigny, France
[5] Istituto Italiano di Tecnologia, Genova, Italy
[6] BIONEM Lab, University of Magna Graecia, Germaneto-Catanzaro, Italy
[7] Université Paris 13, Sorbonne Paris Cité, Laboratoire UMR 978, INSERM-UFR-SMBH, 74 rue Marcel Cachin, 93017 Bobigny, France

**e-mail: marc.lamydelachapelle@univ-paris13.fr*

Keywords: Provide maximum 5 keywords (or one line)

Introduction

The development of reliable, sensitive and specific biosensors is a very active research field. Among all the technique, the Surface Enhance Raman Scaterring (SERS) is one of most sensitive and has been widely used for ultrasensitive chemical analysis down to single molecule detection.[1] Its field of applications now includes chemical-biochemical analysis, nanostructure characterization and biomedical applications. SERS is based on the exploitation of the optical properties of metallic nanoparticles and on the electromagnetic field enhancement localised at the vicinity of the nanostructures and created by the excitation of the Localized Surface Plasmon (LSP).

Results and Discussion

In order to control the LSP resonance position and to optimise the SERS signal, we have used some arrays of metallic nanoparticles, made by electron-beam lithography (EBL).[2-3] The nanoparticles were in gold with different shapes: cylinders and rods. The optimization of the plasmonic nanostructures to improve their sensing properties such as their sensitivity and their easy manipulation is of first importance in order to develop a highly sensitive detection system. Several aspects can be considered in order to optimise the sensing performances: size and shape of the nanoparticles, nanoparticle coupling, molecular adhesion layer between gold nanostructures and glass…[4]

First, by controlling all these aspects, we are able to produce a highly sensitive sensor. We have determined the sensor characteristics such as its detection limit and its selectivity. We have determined that such sensor could be highly sensitive by reaching some detection limits lowest than the pico-molar. In this work, we have applied this sensor to the detection and the identification of specific proteins and we have been able to detect some specific disease biomarkers in body fluids (serum, saliva) paving the way to the potential disease diagnosis.[5]

Second, a clear connection is established between a specific structure of a protein and its function. In a given biological system, a protein exists as multiple modified forms and plays various roles, suggesting numerous conformations. In the present work, we studied the Syk protein, a kinase protein involves in the phosphorylation of others proteins and we established a link between its activation status and its conformation.

Conclusions and/or Outlook

Using SERS technique, we are able to detect and identify proteins even in complex fluids. Moreover, the spectral analysis allows a clear observation of the conformation modifications of the proteins due to their biological activity.

References:

[1] K. Kneipp, Y. Wang, H. Kneipp, L. Perelman, I. Itzkan, R. Dasari, and M. Feld, Phys. Rev. Lett. 78/9 (1997) 1667-1670

[2] J. Grand, M. Lamy de la Chapelle, J.-L. Bijeon, P.-M. Adam, A. Vial, and P. Royer, Phys. Rev. B 7, (2005) 033407, 2005.

[3] N. Guillot , H. Shen , B. Fremaux , O. Péron , E. Rinnert , T. Toury, M. Lamy de la Chapelle, Applied. Phys. Lett. 97 (2010) 023113

[4] H. Shen , N. Guillot, J. Rouxel, M. Lamy de la Chapelle, T. Toury, Optics express 20(19) (2012) 21278

[5] M. Cottat, C. D'Andrea, R. Yasukuni, N. Malashikhina, R. Grinyte, N. Lidgi-Guigui, B. Fazio, A. Sutton, O. Oudar, N. Charnaux, V. Pavlov, A. Toma, E. Di Fabrizio, P. G. Gucciardi, M. Lamy de la Chapelle, J. Phys. Chem. C 119 (2015) 15532

Tip-enhanced infrared nanospectroscopy of purple membrane proteins

Michele Ortolani[a], *Michela Badioli*[a], *Leonetta Baldassarre*[a,b], *Valeria Giliberti*[a,b], *Paolo Calvani*[a], *Alessandro Nucara*[a], *Ulrich Schade*[c], *Liljana Puskar*[c], *Peter Hegemann*[d], *Eglof Ritter*[d]

[a] Dipartimento di Fisica, Sapienza Università di Roma, Rome, Italy
[b] Istituto Italiano di Tecnologia, Centre for Life Nano Science, Rome, Italy
[c] BESSY-II, Helmoltz-Zentrum Berlin, Berlin, Germany
[d] Institut für Biologie, Humboldt Universität, Berlin, Germany

e-mail: Michele.ortolani@roma1.infn.it

Keywords: infrared spectroscopy, near-field microscopy, plasmonics, transmembrane proteins, scanning probe microscopy

Introduction

Mid-infrared (IR) spectroscopy is commonly regarded as the basic tool to identify a wide variety of molecules through their vibrational spectrum. Chemical identification at the nanoscale, which is crucial for the study of inhomogeneous materials as well as biological matter, can be achieved by combining tuneable or broadband mid-IR sources to atomic force microscopes (AFM) that provide deeply-subwavelength resolution. Scattering-type scanning near-field optical microscopy (s-SNOM), where radiation backscattered by the tip is detected in the far-field, is already an established technique for mid-IR nanospectroscopy. Recently, a novel resonant AFM-IR technique that allows a direct measurement of the absorption coefficient of few molecular layers has been introduced. Using a mid-IR pulsed laser with repetition rate matching the frequency of one of the AFM cantilever mechanical bending modes, resonant mechanical detection of the modulation of the tip-sample contact interaction is obtained [1]. Moreover, high electromagnetic field concentration is obtained through the formation of a nanogap between the gold-coated tip in contact-mode and ultraflat gold substrates where single molecular layers are dispersed [2]. Such expedients have recently allowed to enhance the sensitivity of the Photo-thermal Induced Resonance (PTIR) spectroscopy, making it possible to measure the force exerted by the anharmonic vibrations of single molecular layers on the tip, the phenomenon which is at the origin of thermal expansion at the macroscopic scale.

Results and Discussion

Here, we apply the resonant AFM-IR technique to vibrational contrast imaging of cell membranes, unraveling its potential for applications to life sciences. Our samples are flakes of purple membrane deposited on ultraflat gold. Purple membrane consists of a 4 nm thick lipid bilayer densely filled with single bacteriorhodopsin molecules (bR), a protein acting as a proton pump across the cell membrane of Halobacteria. Our experiments are performed using the NanoIR-2 system by Anasys Instruments, equipped with a Quantum Cascade Laser tuneable in the 1575-1725 cm^{-1} spectral range covering the amide-I vibrational band of proteins. In Fig. 1 we show the topography and AFM-IR maps of purple membrane flakes. Combining topography and AFM-IR maps at different IR frequencies, we can clearly identify a single membrane (SM) layer, a region with two overlapping membranes or a double-membrane (DM), and a lipid droplet (LD), as indicated by the arrows in Fig. 1b. The map in Fig. 1c taken at the amide-I peak frequency of 1660 cm^{-1} shows strong AFM-IR signal in the areas where proteins are present, and does not show any signal in the thicker lipid droplet where no protein is present. In the maps taken at IR frequency away from the amide-I vibration (1724 cm^{-1}), the membrane flakes are barely distinguishable from the gold substrate. Considering our AFM tip radius of 20 nm and the bR density in the purple membrane, we calculate that we probe the photo-expansion of about 16 bR molecules per pixel of the map. The signal-to-noise ratio is 5 in a typical map taking 15 minutes per square micron at a 50 nm resolution, therefore the resonant AFM-IR technique is sensitive to as few as ~2200 peptide bonds, corresponding to about 3 bR molecules, which is comparable to what reported in s-SNOM experiments [3].

The spectral information acquired by scanning the QCL wavelength with the tip in a specific position is consistent with transmission spectroscopy of ensembles of identical membranes in a liquid cell. A close comparison of the spectra measured by AFM-IT to those measured oin reflection mode on the same samples is engoing. We are employing FT-IR microspectroscopy with synchrotron radiation as a source, in order to reach diffraction limited spot-size of the order of the dimension of the single membrane flake [4].

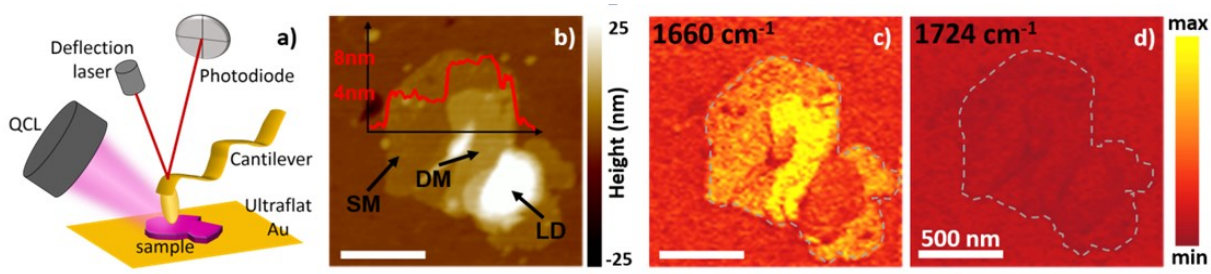

Figure 1: Fig. 1. a) Sketch of the AFM-IR setup. b) Sample topography: the arrows indicate the single membrane (SM), double membrane (DM) and lipid droplet (LD). The inset in red shows a profile across a SM-DM step. c), d) AFM-IR map taken at 1660 cm-1 and 1724 cm-1 respectively (at the amide-I peak IR frequency and away from it). The grey dashed line is the sample contour taken from the topography.

Conclusions and Outlook

The investigation of local mid-infrared absorption in nanoscale samples and materials is a promising technique for chemical identification of structures in biological samples. Photoexpansion and scattering microscopies with laser beams coupled to scanning probe tips seem to provide compatible result with similar lateral resolution and sensitivity in the case of cell membranes deposited on ultraflat gold substrates. At present, the main limitation of both types of microscopy comes from the dry atmosphere in which the membranes are immersed (instead of a physiological aqueous solution). The dry atmosphere is required, in both types of microscopy, for underdamped cantilever oscillation and for infrared beam propagation. Significant improvements to existing setups are needed to overcome this limitation.

References:

[1]. F. Lu, M. A. Belkin, "Infrared absorption nano-spectroscopy using sample photoexpansion induced by tunable quantum cascade lasers", Opt. Expr., **19**, 21 (2011).

[2]. F. Lu, M. Jin, M. A. Belkin, "Tip-enhanced infrared nanospectroscopy via molecular expansion force detection", Nat. Photonics, **8**, (2014).

[3]. S. Berweger, D. M. Nguyen, E. A. Muller, H. A. Bechtel, T.T. Perkins, M.B. Raschke, "Nano-chemical infrared imaging of membrane proteins in lipid bilayers", J.A.C.S., **135**, 49 (2013).

[4]. E. Ritter, L. Puskar, F. J. Bartl, E. F. Aziz, P. Hegemann and U. Schade, "Time-resolved infrared spectroscopic techniques as applied to channelrhodopsin" Front Mol Biosci. 2, 38 (2015) doi: 10.3389/fmolb.2015.00038

Optical Response of Single Metallic Nano-objects in a Liquid Environment Using Spatial Modulation Spectroscopy

J-M. Rye[a,b], C. Bonnet[a], F. LeRouge[b], J. Lermé[a], A. Mosset[a], M. Broyer[a], M. Pellarin[a], S. Parola[b], E. Cottancin[a]*

[a] *Institute of Light and Matter, Université Claude Bernard Lyon 1, CNRS UMR 5306, University of Lyon, Villeurbanne, France*
[b] *Laboratory of Chemistry, École Normale Supérieure de Lyon, Université Claude Bernard Lyon 1, CNRS UMR 5182, University of Lyon, Lyon, France*

**e-mail: jan-michael.rye@univ-lyon1.fr*

Keywords: nanoplasmonics, nanospectroscopy, gold nano-bipyramids, biosensing

Introduction

Metallic nano-objects may exhibit a strong optical response known as Localized Surface Plasmon Resonance (LSPR), which depends on their composition, size, shape and immediate environment. Gold nano-objects in particular have been developed in a wide variety of sizes and shapes such as spheres, cubes, rods, bipyramids and even more exotic lithographed patterns, with clear differences in their signature LSPR. Of particular interest is the potential for sensing applications that exploit the LSPR of such objects to probe the local environment. By measuring the response of individual objects, minute changes in the LSPR that would otherwise be obfuscated by ensemble measurements should be detectable.

Spatial Modulation Spectroscopy (SMS) has previously been developed by our team [1] to measure the optical response of individual nano-objects over a broad spectral range (near-UV to near-IR) in air. An intrinsic aspect of the technique is sample mapping, which enables the correlation of an individual object's optical response to its real morphology observed by electron microscopy. Our recent work has focused on the adaptation of an SMS system to a liquid environment with an eye towards biosensing applications based on gold nano-bipyramids [2]. Here we present our preliminary results with the new setup and our ongoing work.

Results and Discussion

The submersion of samples in H_2O imposes new challenges related to surface chemistry and sample preparation and so we have developed a protocol for the preparation of gold nano-bipyramid samples linked to the substrate via silanization. **Figure 1** presents the transmission spectra in H_2O of several individual gold nano-bipyramids from one such sample.

Figure 1: Transmission spectra of individual gold nano-bipyramids (~100 nm) on a silanized SiO_2 substrate in H_2O. The peak

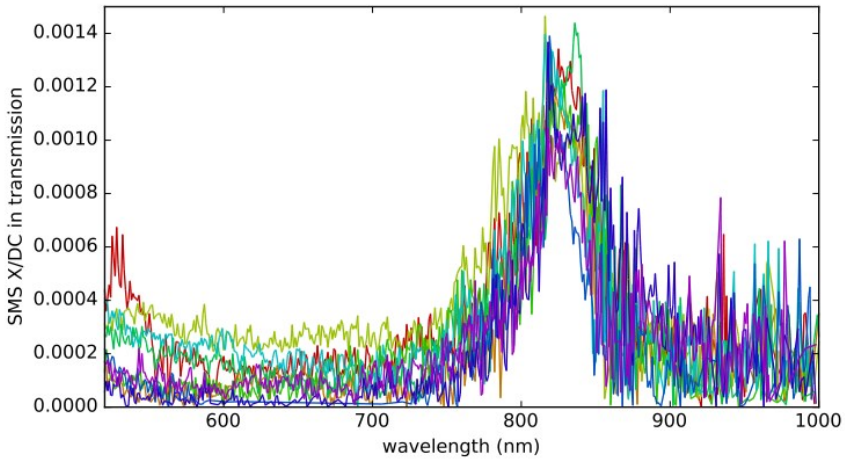

around 825 nm is due to localized surface plasmon resonance (LSPR). The limited spectral variation shows that the gold nano-bipyramids are monodisperse.

Comparisons of the spectra of the same objects in air and in H_2O have shown redshifts of the LSPR peaks as expected. When passing from H_2O back to air, the corresponding reverse shift is observed but unequal in magnitude. This is presumably due to local changes such as residue formation. This effect has not yet been fully understood and requires further study.

Conclusions and/or Outlook

Preliminary studies with the liquid SMS setup have shown that mapping and optical characterization of samples in H_2O work well with the new setup despite the constraints imposed by the use of a liquid cell. The next experiments will determine how liquids of different optical indices affect the LSPR of gold nano-bipyramids and these results will be compared to numerical simulations. The sample preparation protocol will also be developed further to functionalize the gold nano-bipyramids for preliminary sensing applications using the model streptavidin-biotin binding system. A pumping system is also planned to enable dynamic measurements of concentration gradients and thus determine the threshold of detection of a given analyte or the effect of a gradually changing optical index.

Once the model system has been shown to work we shall move on to real essays such as the detection of low concentrations of the beta-amyloid protein thought to be responsible for Alzheimer's disease.

References:

[1] Billaud P, Marhaba S, Grillet N, Cottancin E, Bonnet C, Lermé J, Vialle J-L, Broyer M, Pellarin M; Absolute optical extinction measurements of single nano-objects by spatial modulation spectroscopy using a white lamp; Review of Scientific Instruments; Volume 81 (2010) 043101

[2] Navarro J R G, Manchon D, Lerouge F, Cottancin E, Lermé J, Bonnet C, Chaput F, Mosset A, Pellarin M, Parola S; Synthesis, electron tomography and single-particle optical response of twisted gold nano-bipyramids; 23 (2012) 145707

Plasmonic hot-electron-induced charge injection into MoS_2 and WSe_2 monolayers

Zoheb Khan[a], Raul D. Rodriguez**[a,b], Andreas Horrer[c], Philipp Nagler[d], Gerd Plechinger[d], Mahfujur Rahaman[a], Manuel Martina[e], Claus J. Burkhardt[e], Christian Schüller[d], Tobias Korn[d], Monika Fleischer[c], Dietrich R.T. Zahn[a,b]*

[a] Semiconductor Physics, Technische Universität Chemnitz, 09107 Chemnitz, Germany
[b] Center for Advancing Electronics Dresden (cfaed), Technische Universität Chemnitz, 09107 Chemnitz, Germany,
[c] Institute for Applied Physics, Eberhard Karls Universität Tübingen, 72076 Tübingen, Germany
[d] Institut für Experimentelle und Angewandte Physik, Universität Regensburg, 93040 Regensburg Germany,
[e] NMI Natural and Medical Sciences Institute at the University of Tübingen, 72770 Reutlingen, Germany

**e-mail: zoheb-nazeer.khan@s2014.tu-chemnitz.de*
***e-mail: raul.rodriguez@physik.tu-chemnitz.de*

Keywords: plasmonics, hot electrons, two-dimensional, transition metal dichalcogenides, Raman spectroscopy

Introduction:

Two-dimensional transition metal dichalcogenides (TMDCs) such as MoS_2 and WSe_2 are particularly susceptible to charge injection due to their spatial confinement and semiconducting behaviour. Recently, significant efforts have been devoted to controlling the electronic properties of MoS_2 monolayers by doping, including gate-bias tuning[1], chemical doping[2], and physical adsorption[3]. Plasmon-induced hot electrons generated by photo-excitation of Au nanoparticles can also lead to n-type doping of TMDC monolayers[4]. In this contribution, we report on the localized surface plasmons excitation in Au nanoparticles beneath single layers of MoS_2 and WSe_2. The subsequent changes in vibrational, optical, and electrical properties of the TMDC monolayers were investigated via Raman spectroscopy, photoluminescence, conductive AFM and Kelvin probe force microscopy in order to evidence the effects of charge-transfer.

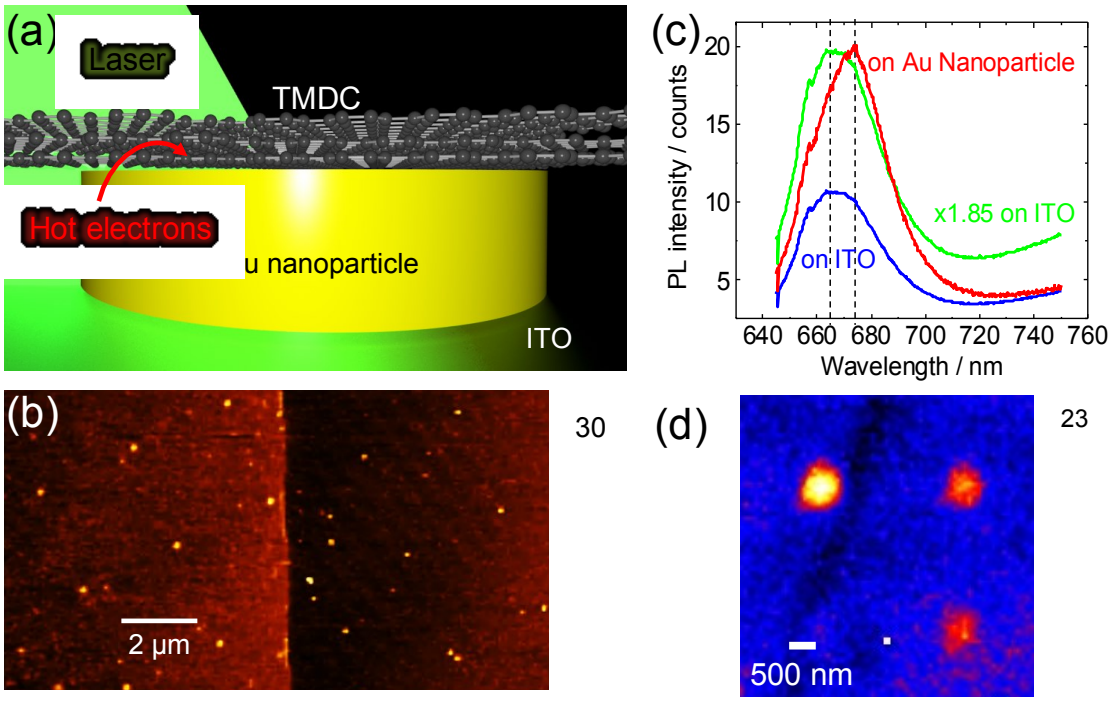

Figure 1: (a) Schematics (non-scaled) of the Au nanoparticle/2D TMDC system. (b) AFM image of the interface between a multilayer MoS_2 (left) and the single layer (right) showing array like arrangement of Au nanoparticles (bright spots) spaced by 3 µm. (c) PL spectra of the MoS_2 monolayer from regions with and without Au nanoparticles (d) PL image of the 665 nm to 675 nm band showing higher enhancement in the MoS_2 single layer around the Au nanoparticles.

Monolayers of MoS_2 and WSe_2 were obtained by mechanical exfoliation. The TMDCs were deposited on a substrate consisting of square arrays of Au nanodiscs with 3 µm period lithographically defined on ITO/glass. Figure 1a shows the schematics of the sample structure, and Figure 1b, the atomic force microscopy imaging at the multi/single-layer MoS_2 interface. The TMDC/Au nanoparticle systems were investigated with 532 nm and 638 nm laser excitations, by Raman and photoluminescence (PL) spectroscopies. Further evidence obtained from the nanoscale electrical characterization using conductive AFM and Kelvin probe force microscopy will be discussed.

Results and Discussion:
Raman and PL imaging of the sample was performed to identify the regions of monolayer MoS_2. The presence of monolayer was evidenced by atomic force microscopy and by the position and intensity of the PL band[5] and the frequency difference between out-of-plane (A_{1g}, ~ 404 cm^{-1}) and in-plane (E^1_{2g}, ~ 385 cm^{-1}) phonon modes in the Raman spectra[6]. Figure 1c shows the PL spectra from the MoS_2 monolayer with and without Au nanoparticles when excited with 638 nm laser. The red shift observed in the PL peak for the region on top of Au nanoparticle indicates the presence of negatively charged excitons (trions)[7] and therefore provides evidence of the hot electron transfer and its spatial visualization across the Au and MoS_2 monolayer interface.

Conclusions:
We have performed the spectroscopic characterization at the sub-micrometer scale of two main TMDCs deposited on Au nanoparticles. In such a system we provide unprecedented evidence of charge-transfer and doping using electrical AFM characterization at the nanoscale and Raman and photoluminescence spectroscopies at the sub-micrometer scale. The study of this arrangement of metal nanoparticles and 2D atomically-thin materials allows us to characterize, at the nanoscale, the space within which the localized effect in the monolayer occurs due to electron-doping by a single Au nanoparticle under plasmonic excitation. Our findings can be effectively driven towards realizing the size and structure of the individual components required for the development of (opto-)electronic devices such as plasmonic field effect transistors.

References:

[1] Lin, J. D.; Han, C.; Wang, F.; Wang, R.; Xiang, D.; Qin, S.; Zhang, X. A.; Wang, L.; Zhang, H.; Wee, A. T. S.; et al. Electron-Doping-Enhanced Trion Formation in Monolayer Molybdenum Disulfide Functionalized with Cesium Carbonate. ACS Nano (2014), 8, 5323–5329

[2] Mouri, S.; Miyauchi,Y.; Matsuda,K. Tunable Photoluminescence of Monolayer MoS_2 via Chemical Doping. Nano Lett. (2013), 13, 5944–5948.

[3] Tongay, S.; Zhou, J.; Ataca, C.; Liu, J.; Kang, J. S.; Matthews, T. S.; You, L.; Li, J.; Grossman, J. C.; Wu, J. Broad-range Modulation of Light Emission in Two-Dimensional Semiconductors by Molecular Physisorption Gating. Nano Lett. (2013), 13, 2831–2836.

[4] Kang, Y.; Najmaei, S.; Liu, Z.; Bao, Y.; Wang, Y.; Zhu, X.; Halas, N. J.; Nordlander, P.; Ajayan, P. M.; Lou, J.; et al. Plasmonic Hot Electron Induced Structural Phase Transition in a MoS_2 Monolayer. Adv. Mater. (2014), 26, 6467–6471.

[5] Splendiani, A.; Sun, L.; Zhang, Y.; Li, T.; Kim, J.; Chim, C. Y.; Galli, G.; Wang, F. Emerging Photoluminescence in Monolayer MoS_2. Nano Lett. (2010), 10, 1271–1275.

[6] Lee, C.; Yan, H.; Brus, L. E.; Heinz, T. F.; Hone, J.; Ryu, S. Anomalous lattice vibrations of single- and few-layer MoS_2. ACS Nano (2010), 4 (5), 2695−2700.

[7] Mak, K. F.; He, K.; Lee, C.; Lee, G. H.; Hone, J.; Heinz, T. F.; Shan, J. Tightly Bound Trions in Monolayer MoS_2. Nat. Mater. (2013), 12, 207–211.

Acknowledgments:
This work was supported by the DFG Cluster of Excellence "Center for Advancing Electronics Dresden" cfaed, with financial support from the DFG Research Unit FOR1713 SMINT.

Near-Field detection of gold nanoshells inside cells

M. D'Acunto*[a,b,c], A. Cricenti*[a], M. Luce[a]

[a] CNR-ISM, Istituto di Struttura della Materia, via Fosso del Cavaliere, 100, 00133, Rome, Italy
[b] CNR-ISTI, Istituto di Scienza e Tecnologie dell'Informazione, via Moruzzi 1, 56124, Pisa, Italy
[c] NanoICT laboratory, via Moruzzi 1, 56124, Pisa, Italy

*e-mail: mario.dacunto@ism.cnr.it
*e-mail: antonio.cricenti@ism.cnr.it

Keywords: aperture SNOM; gold nanoshells; Near-field Mie approximation; h9c2 mouse cells;

Introduction

The optical properties of metal nanoparticles play a fundamental role for their use in a wide range of applications. In hyperthermia treatment, for example, the gold nanoshells (NSs, dielectric core + gold shell) pre-embedded in a cancer cell absorb energy when exposed to appropriate wavelengths of a laser beam and heat up thus destroying the cancer cell. In this process, nevertheless, the healthy tissues (not targeted by the NSs) along the laser path are not affected; this is because most biological soft tissues have a relatively low light absorption coefficient in the near-infrared (NIR) regions, characteristic known as the tissue optical window. Over such window, NIR light transmits through the tissues with the scattering-limited attenuation and minimal heating avoiding damages to the healthy tissues. As a consequence, the identification of NSs assumed a fundamental role for the further development of such cancer treatment. The optical cross-sections and luminescent properties of gold nanoshells compare favorably with those of conventional fluorophores or quantum dots. The absorption of a single 20-nm diameter nanoshell can correspond to the absorption of 4×10^4 molecules of a common dye, like the indocyanine green, used as a photosensitizer in photodynamic therapy. But the most important characteristic of gold nanoshells is their tunability, in fact the position of the extinction peak correspondent to the plasmon resonance and the selective contributions of absorption and scattering to total extinction can be tuned changing only two parameters: the radii of the inner core and the outer shell. This tunability is particularly important if we wish to exploit the NIR tissue window from 700 to 900nm, where tissues are most transparent to light. The tunability in the NIR of barium titanate-gold NS (80nm core+ 40nm gold shell) was recently demonstrated using Mie scattering [1-2] and the possibility to identify such NSs inside mouse cells was later evidenced experimentally using an aperture SNOM [3].

In this paper, we provide numerical demonstration that the SNOM is able to locate NSs inside the cell with a particle-aperture distance of about 100nm. This result was obtained developing an analytical and numerical approach based on the calculation of the dyadic Green function in near-field approximation. The implications of our findings will remarkably affect further investigations on the interaction between NSs and biological systems.

Results and Discussion

The home-made SNOM used for such study was set operating in air in collection mode with a fixed oblique angle of illumination (θ=45°). Different illumination wavelengths ranging from visible to near infrared were used. Home-made procedure for tip manufacturing was based on chemical etching process producing tips with an aperture diameter of nearly 50nm. After the etching process, the tip are coated by a tiny metallic (evaporated aluminum) layer so as to prevent light from coupling into the fibre from anywhere other than at the aperture of the probe. In figure 1, we summarize the results experimentally obtained for the identification of gold nanoshells inside mouse cells making use of an aperture SNOM [3]. In the central image of figure 1, the overlapping of the topography of the mouse cell and the optical map collected by the SNOM shows two dark points evidenced by the arrows. Such dark points correspond to a strong reduction of the collected signal by the SNOM. This is due to the high external light absorption of the NSs plasmons interacting with the external e.m. field.

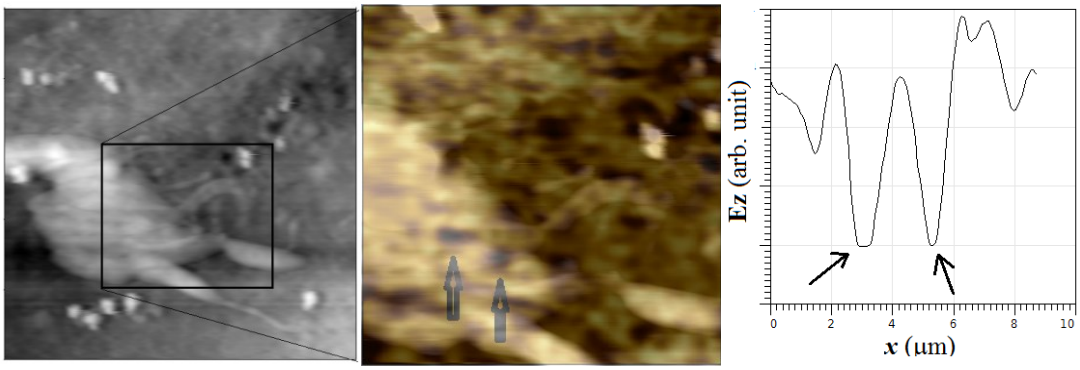

Figure 1. (Left), 20μm×20μm topography of h9c2 mouse cell recorded with a home-made aperture SNOM; (middle) an overlapping of the topography image with the correspondent optical map, the arrows denote the NS identified within the cell; (right), strong-absorption points marked by arrows in the overlapping image and denoting the dimensions of the NSs.

The penetration depth of NIR light in animal cells is very high. To have an idea of how thick the cell layer must be in order to absorb the light the extinction coefficient of the animal cell (h9c2 mouse cell in our case) is a key parameter. The penetration depth, *h*, as a function of wavelength can be estimated by the relation $h \approx 1/\mathrm{Im}\left[\sqrt{\varepsilon_{cell}(\omega)}\right]$. Being the imaginary component of the cell dielectric function negligible, the penetration depth can reach to centimeters for a wavelength falling in the NIR range. Our single cell measurements as represented in figure 1, showed a topography with a height of nearly 3μm so that all the cell is practically transparent to external NIR source light.
The measurements whose results are reported in figure 1, lead to a fundamental question: which is the height of the NS inside the cell, we will define this problem as the *z-location* question. This question is solved making use of an analytical and numerical approach based on dyadic Green function.

Conclusions and/or Outlook

Most biological soft tissues have a relatively low light absorption coefficient in the NIR regions, characteristic known as the tissue optical window. Over such window, near infrared light transmits through the tissues with the scattering-limited attenuation and minimal heating preventing the healthy tissues to be damaged. In this paper, starting from some experimental results previously obtained by our group on the identification of gold NSs inside mouse cells, we numerically demonstrate that an aperture SNOM is able to locate such nanoparticles inside cells with a depth of about 100nm. This result has been obtained developing a numerical task based on the calculation of the dyadic Green function in near-field approximation. This result is particularly significant because it gives an accurate knowledge of the depth distance for the analysis of the optical properties inside cells under the near infrared transparency window. This feature is due to a combination of two properties: the NIR transparency of biological systems and the strong absorption capability of appropriate size gold nanoshells in the near-infrared range. Our results can stimulate further developments in the field of thermal treatments of cancers or near-field plasmonics investigation of biological systems.

References:

[1] D'Acunto M, Moroni D, Salvetti O, Nanoscale Biomolecular Detection Limit for Gold Nanoparticles Based on Near-Infrared Response, Advances in Optical Technologies, (2012) 271894(1-8);
[2] Cricenti A., Luce M., Moroni D, Salvetti O, D'Acunto M, Ultrasmall clusters of gold nanoshells detected by SNOM; Optoelectronics Review 23, (2015), 39-45;
[3] D'Acunto M, Cricenti A, Luce M, Dinarelli S, Theory of near-field detection of core-gold nanoshells inside biosystems. Computer Modelling & New Technologies, 19**,** (2015), 29-37.

Near field of regular silver nanoparticles

Min. Song[a], *Patrick Andrae* [a,b], *Paul Fumagalli* [b] *and Martina Schmid* [a,b]

[a] Nanooptische Konzepte für die PV, Helmholtz-Zentrum Berlin, Hahn-Meitner-Platz 1, 14109 Berlin, Germany

[b] Institut für Experimentalphysik, Freie Universität Berlin, Arnimallee 14, 14195 Berlin, Germany

e-mail: min.song@helmholtz-berlin.de

Keywords: Scattering, near field, scanning near-field optical microscope, nanosphere lithography.

Introduction

Scanning near-field optical microscopy (SNOM) has made a remarkable contribution to studying optical properties of various surfaces on the nanometer scale [1]. Noble-metal nanoparticles have received wide attention in research and application due to their unique properties [2, 3]. In this study, the optical properties of regular silver particles on glass substrate produced by nanosphere lithography were characterized using a custom-built SNOM, which gives access to the near-field distribution of nanoparticles. In addition, Finite-Element-Method Simulations have been performed to estimate a theoretical plasmonic enhancement factor (PEF) in both periodic particle geometry without scanning probe and SNOM geometry with a scanning probe. We found that the wavelength dependent PEF differs for different particle sizes.

Results and Discussion

The hexagonally arranged silver nanoparticles were 73±10nm, 140±10nm and 200±15nm in diameter with 525±10nm nearest-neighbour distance from centre to centre. The topography of regular silver nanoparticles was obtained by scanning in shear-force mode with an aperture probe (aluminum coated, 100 nm diameter). Simultaneously, the optical images were acquired in illumination or collection mode with a 532nm continuous wave laser source as shown in Fig.1. Although the regular particles are separated, their interaction results in near-field changes in the optical images. The optical information for silver particles show a reduced transmitted near-field intensity at the particle position (dark spot) and a surrounding field enhancement (bright ring); in contrast, the reflection image shows a high intensity at the particle position (bright spot). In order to get the PEF, the transmission and reflection signals were normalized with the average background values picked from the substrate area on the same image, since there is no standard value for the SNOM results normalization. The transmission is taken into account with 90% and the reflectance of 10%, according to the transmission and reflection of the glass substrate.

$$I_{norm} = 0.9\frac{I(T)}{I_{Glass}(T)} + 0.1\frac{I(R)}{I_{Glass}(R)}$$

Normalization on the glass substrate were calculated for two independent measuring methods (collection mode, illumination mode), and the same quantitative absolute values were obtained, as shown in Fig 1. The enhancements merged to a ring in the middle of the hexagonal superstructure. Regular silver nanoparticles with different diameters and pitch sizes showed different enhanced near field.

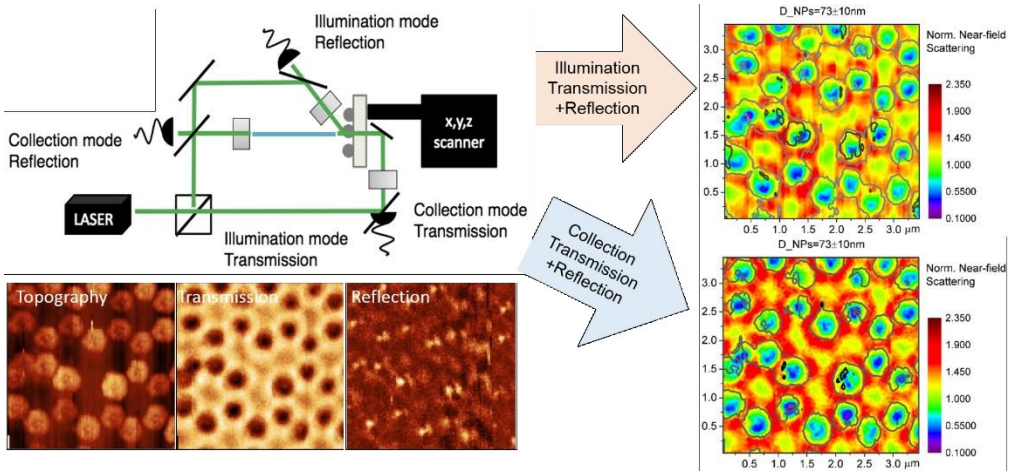

Figure 1: Left: Sketch of SNOM setup with the results got from a single measurement in illumination mode. Right: Normalization of transmission and reflection images from illumination mode and collection mode SNOM. Black contour lines represent topography. Values above 1 correspond to enhancement.

In addition, Finite-Element-Method (FEM) Simulations have been performed for different particle sizes with COMSOL software. The normalized enhancement was observed around the nanoparticle, as shown in Fig.2.

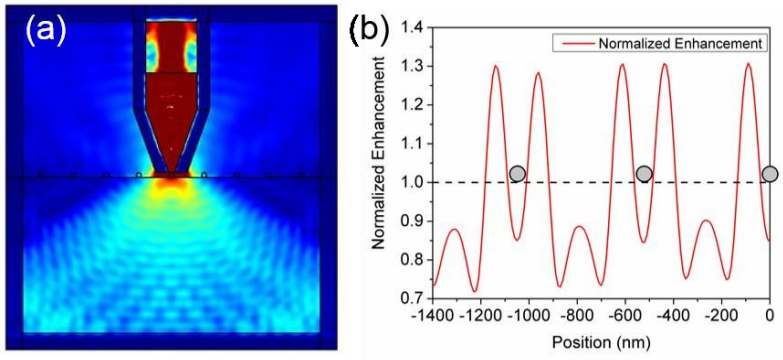

Figure 2: FEM simulation 2D model and result. Nanoparticle is 73nm in diameter and located at tip position. (a) Simulation model for illumination mode; (b) Normalized enhancement.

Conclusions and outlook

We found different regular silver nanoparticles produced different amount of plasmonic enhancement in both experiment and simulation study. Due to their near-field enhancement, silver nanoparticles are promising for the application in solar energy conversion. The light trapping and light scattering ability makes silver nanoparticles also suitable for absorption enhancement in ultra-thin solar cells, which will be our next study.

References:

[1] Hecht B, Sick B, Wild U P, Deckert V, Zenobi R, Martin O J, Pohl D W; Scanning near-field optical microscopy with aperture probes: Fundamentals and applications; J. Chem. Phys.; 112 (2000) 7761-7774.

[2] Atwater H A & Polman A; Plasmonics for improved photovoltaic devices; Nature Mater.; 9 (2010), 205-213.

[3] Noginov M A, Zhu G, Belgrave A M, Bakker R, Shalaev V M, Narimanov E E, Stout S, Herz E, Suteewong T, Wiesner U; Demonstration of a spaser-based nanolaser; Nature; 460 (2009), 1110-1112.

Triangular Silver Nanoplate Thin Film as Surface-enhanced Raman Scattering Substrate to Detect Bisphenol A

N. A. Bakar*[a], M. M. Salleh[a], A. A. Umar[a], J. Shapter[b],

[a] Institute of Microengineering and Nanoelectronics (IMEN), Universiti Kebangsaan Malaysia, 43600 Bangi, Selangor, Malaysia
[b] School of Chemical and Physical Sciences and Flinders Centre for Nanoscale Science and Technology, Flinders University, Bedford Park, Adelaide South Australia 5001, Australia

*e-mail: nab_yati@yahoo.com

Keywords: SERS substrate; self-assembly; triangular silver nanoplate film

Introduction

SERS substrate plays a main role for a sensitivity of SERS sensor to sense a specific molecule in environment pollutants application. Silver unsure in SERS has attracted an attention among researchers [1] due to a low cost of preparation (Jiang et al. 2014), a high and sharp resonance plasmon curve [2] and a strong SERS effect [3]. In this work, we studied the structure of synthesized triangular silver nanoplates and the attachment of the nanoplates on a silicon surface using 3-aminopropyltrimethoxysilane (APTMS) as a coupling agent. This triangular-shaped colloidal silver nanoplates were simply synthesized by a direct chemical reduction approach. Then the nanoplates was deposited on the silicon surface by immersing the silicon surface in the colloidal nanoplates using a self-assembly technique. Depositing the nanoplates on the surface was carried out to determine the coverage of triangular nanoplates obtained when adhesion was promoted by a coupling agent. The surface distribution of the triangular silver nanoplates was studied by varying the exposure time of the colloidal silver nanoplate to the silicon surface. Finally, bisphenol A (BPA) solution was drop-casting on the triangular silver nanoplate film formed to measure the SERS using Horiba Raman spectroscopy.

Results and Discussion

We studied the three characteristic peaks of the unique optical absorbance of triangular silver nanoplates and subsequently measured an average edge length of 26 ± 1 nm and a thickness was determined to be 7 ± 2 nm. The attachment of the nanoplates to the silicon surface and the coverage of the nanoplates increased with increasing deposition time when adhesion was promoted by a coupling agent. A monolayer and high coverage of the triangular silver nanoplate thin film was obtained after immersing in the colloidal nanoplate. This silver film formed was shown to be a good surface-enhanced Raman scattering (SERS) substrate as it gave an enormous Raman enhancement for bisphenol A (BPA). Figure 1 (A) shows the SERS spectrum of 1 mM BPA on the silver nanoplate film formed (Figure 1 (B)) after exposing the substrate to the nanoplate suspension for 2 h. The normal Raman spectrum for 1 mM BPA on the silicon surface is also provided in Figure 1 (A).

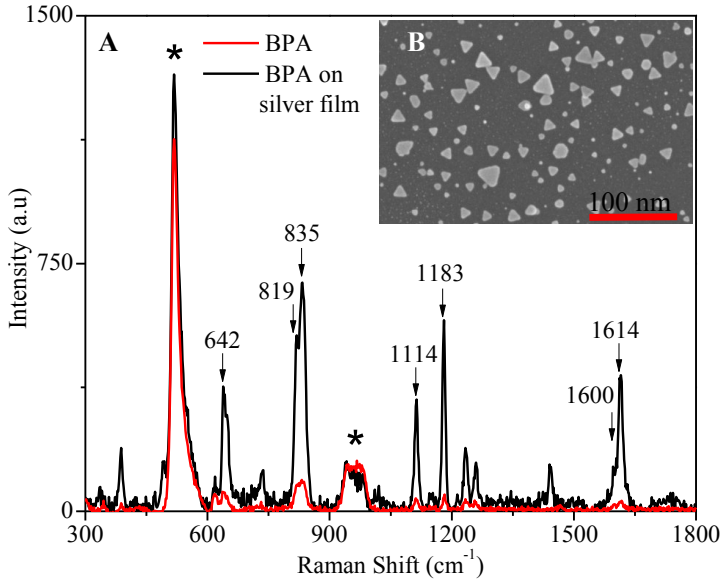

Figure 1: (A) The SERS spectrum of BPA on the triangular silver nanoplate film and Raman of BPA absorbed on a clean silicon surface. * are labels for the silicon peaks; (B) FESEM image of the triangular silver nanoplate on the silicon surface

As expected, BPA shows seven major Raman peaks at 642 cm^{-1}, 819 cm^{-1}, 835 cm^{-1}, 1114 cm^{-1}, 1183 cm^{-1}, 1600 cm^{-1}, and 1614 cm^{-1}, clearly indicating the presence of BPA on the substrate [4]. These BPA peaks were strongly enhanced when the molecule was absorbed on the silver nanoplate film, clearly demonstrating that these nanoplate films are a good SERS substrate and suitable for further investigations for incorporation in a SERS-based sensor.

Conclusions

Silver nanoplates with a triangular shape were exhibited a unique optical absorbance with two major bands and one shoulder, which are attributed to dipole resonance and quadrupole resonance due to the triangular nanoplate's shape. The assembly of the nanoplates on a silicon surface with an APTMS layer was produce a triangular silver nanoplate thin film with a high density surface. These thin films are promising for applications in SERS detectors as demonstrated by the enhanced signal obtained for bisphenol A absorbed on the silver nanoplate film.

References:

[1] Xu L, Yan W, Ma W, Kuang H, Wu X, Liu L, Zhao Y, Wang L, Xu C; Biosensors: SERS Encoded Silver Pyramids for Attomolar Detection of Multiplexed Disease Biomarkers; Advanced Materials; 27 (2015) 1799-1799

[2] Jiang Z, Wen G, Luo Y, Zhang X, Liu Q, Liang A; A New Silver Nanorod SPR Probe for Detection df Trace Benzoyl Peroxide; Scientific Reports; 4 (2014) Article no: 5323

[3] Lai W-Z, Zhao W, Yang R, Li X-G; Preparation and Optical Properties of Triangular Silver Nanoplates by A Dual-Reduction Method; Acta Physico-Chimica Sinica; 26 (2010) 1177-1183

[3] Yao W, Wang S, Wang H; Method for Detecting BPA by Surface Enhanced Raman Spectroscopy; Patent Application Publication: Alexandria, VA, USA, 2012

Resonant coupling between molecular vibrations and single goldnanorods observed by mid-infrared photoexpansion nanoimaging.

F.Appugliese[a], *T. Venanzi*[a], *M.Badioli*[a], *V. Giliberti*[a,b], *E. Calandrini*[c], *A. Toma*[c], *F. De Angelis*[c], *L. Baldassarre*[a] *and M. Ortolani*[*a]

[a] Department of Physics, Sapienza University of Rome, Italy

[b] Istituto Italiano di Tecnologia, Centre for Life Nano Science, Rome, Italy

[c] Istituto Italiano di Tecnologia, Department of Nanostructures, Genova, Italy

e-mail: michele.ortolani@roma1.infn.it

Keywords: mid-infrared antennas, nanoimaging, photoexpansion.

Introduction

Plasmonic antennas play a crucial role for chemical identification of small amounts of analyte, enabling relevant technological applications e.g. bio-sensing. In particular it is of high interest to develop mid-IR resonating antennas, since molecular vibrations occur in this frequency range (wavelengths from 5 to 15 μm).

IR spectroscopy studies demonstrated surface-enhanced detection of vibrational fingerprints using arrays of plasmonic antennas, where the antenna frequency resonates with a specific molecular vibration [1]. In this case, a Fano interference effect is observed in both absorption and scattering spectra measured in the far-field [2, 3]. However, by means of near-field techniques, which probe the optical response with a nanoscale resolution [4], a deeper insight in the near-field coupling between the molecular vibrations and the plasmonic resonance of a single antenna can be obtained.

In this work, we used mid-IR nanoimaging to visualize the local electromagnetic energy absorption by a thin polymer film in the near-field of single gold nanorods. Our near-field platform makes use of the photoexpansion effect based on the coupling of a pulsed mid-IR quantum cascade laser (QCL) in the 1575-1725 cm^{-1} range to an atomic force microscope (AFM) probe tip, working in contact-mode (NanoIR2 by Anasys Instruments).

The sample consist of gold nanorod antennas on a CaF_2 substrate, displaying different lengths in the 1-2 μm range, corresponding to resonance frequencies lying in our range as calculated by Finite-difference Time-domain simulations. After fabrication, we spin-coated a highly diluted polymer (PMMA in ethyl-lactate) and we formed a PMMA encapsulation layer by baking the sample on a hot-plate (10 nm thick above the antennas, 60 nm thick elsewhere).

We perform mid-IR nanoimaging of the encapsulated antennas at 1724 cm^{-1} (wavelength of 5.8 microns) i.e. close to the C=O stretching vibration of PMMA, and at 1660 cm^{-1}, where the PMMA absorption is negligible. The incident light polarization was always orthogonal to the incidence plane (s-polarized) and it was either parallel or perpendicular to the antenna axis. We used a dielectric tip (silicon) instead of the standard gold-coated tips for nanoimaging, so as to avoid perturbation of the antenna field distribution.

Results and Discussion

As shown in **Figure 1** strong local absorption signal is obtained at the antenna ends (hotspots). As expected, the signal at the hotspots is observed only with polarization parallel to the antenna axis.

The photoexpansion signal map is clearly related to electric field enhancement, in a way similar to what is obtained with scattering-SNOM nanoimaging [4], but it is also related to the amount of energy actually absorbed by the molecules, which here are directly probed in the near-field of the antenna. At 1660 cm-1 the electromagnetic energy absorption by PMMA is negligible, but the currents in the antenna still produce heating of the PMMA layer because of the Joule effect. Therefore, our near-field images taken at 1660cm^{-1} allow the visualization of the regions with maximum current, typically located at the centre of the nanorod.

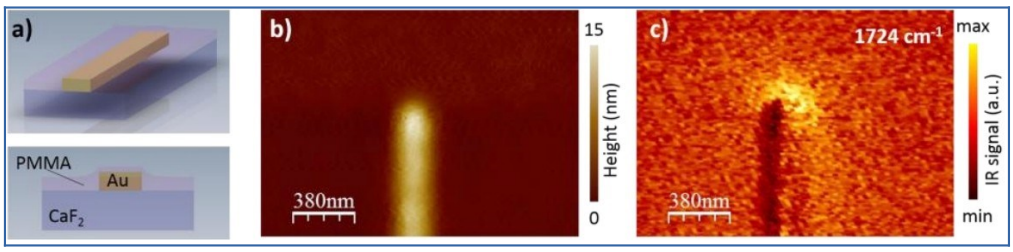

Figure 1: a) Sketch of the encapsulated gold nanorods. b) Topography of one end of a nanorod and c) corresponding IR signal at 1724 cm^{-1}.

Conclusions

Our near-field platform for mid-IR antenna characterization provides nanoscale information on the antenna fields and currents, but also allows for the direct measurement of the electromagnetic energy absorption of the target molecule by a single antenna.

The photoexpansion nanoimages can be used for the study of the resonant coupling of antennas with molecule vibrations.

References:

[1] F. Neubrech et al.; Resonant Plasmonic and Vibrational Coupling in a Tailored Nanoantenna for Infrared Detection Phys. Rev. Lett., 101, 2008.
[2] V. Giannini et al.; Fano Resonances in Nanoscale Plasmonic Systems: A Parameter-Free Modeling Approach, Nano Lett., 11 (7), 2011.
[3] T. Neumann et al.; Importance of Plasmonic Scattering for an Optimal Enhancement of Vibrational Absorption in SEIRA with Linear Metallic Antennas, J. of Phys. Chem., 2015.
[4] M. Schnell et al.;Controlling the near-field oscillations of loaded plasmonic nanoantennas, Nat. Photonics 3, 2009.

Nonlinear Microscopy of Plasmonic Oligomers using Cylindrical Vector Beams

G. Bautista[a], C. Dreser[b], M. Fleischer[b] and M. Kauranen[a]*

[a] Department of Physics, Tampere University of Technology
P.O. Box 692, FI-33101 Tampere, Finland
[b] Institute for Applied Physics, University of Tuebingen
Auf der Morgenstelle 10, 72076 Tuebingen, Germany

**e-mail: godofredo.bautista@tut.fi*

Keywords: second-harmonic generation, cylindrical vector beams, plasmonic oligomer, collective modes, metal

Introduction

Nonlinear plasmonics, which is fuelled by new advances in nanofabrication and related characterization, is expected to blossom in the coming years [1]. To date however, nonlinear plasmonic effects have been mostly studied using nanostructured surfaces and periodically-arranged individual nanoparticles or their ensembles. Metal oligomers are emerging plasmonic systems because their optical responses are dictated by the interaction of its monomer units. Such properties are intriguing because they support collective modes [2] which could be potentially attractive in tailoring light-matter interactions and background-free sensing and spectroscopy on the nanoscale.

It is known already that the collective modes supported by plasmonic oligomers can be accessed in the near- and far-field by modifying their structural symmetry and by the use of illumination schemes that depart from traditional excitation geometries and homogenous linear polarizations. More recently, it has been shown that tailored beam polarizations such as azimuthal and radial allow convenient ways to address the linear optical response of individual oligomers [3,4]. In this work, we demonstrate second-harmonic generation (SHG) microscopy (excitation wavelength of 1060 nm, pulse duration of 140 fs, repetition rate 80 MHz, numerical aperture of 0.8) of metal oligomers using radial and azimuthal polarizations [5].

Results and Discussion

Our samples consist of periodically-arranged gold oligomers that were fabricated by electron beam lithography on a glass substrate. An individual oligomer consists of eight nanobars (where each nanobar has a length of ~200 nm, width of ~100 nm, thickness of ~20 nm) that were carefully designed so that the long axis of the constituent nanobars are arranged to mimic the transverse electric field distributions of azimuthal (see Figure 1a) or radial polarizations at the beam focus. As depicted in Figure 1b, a significant SHG signal that arises from the excitation of the collective mode is detected whenever the oligomers are symmetrically excited by a polarization-matching cylindrical vector beam. This excitation sensitivity is further confirmed by the disappearance of the SHG signal upon excitation with the complementary cylindrical vector beam.

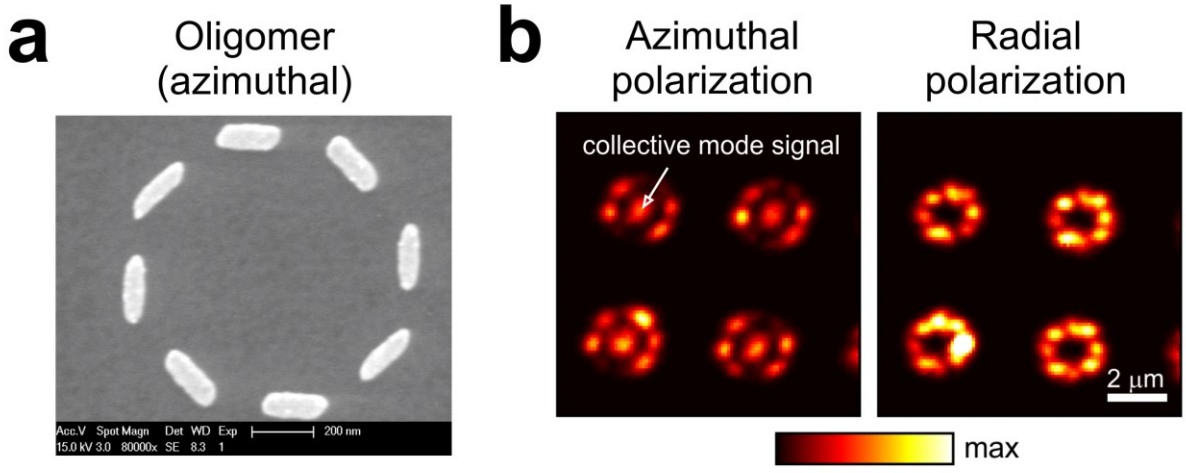

Figure 1: (a) Scanning electron micrograph of a fabricated oligomer consisting of eight nanobars that are arranged to mimic the resulting transverse electric field components of azimuthal polarization at the beam focus. (b) Corresponding SHG microscopy images of oligomers which exhibit an azimuthal symmetry using azimuthal and radial input polarizations.

Conclusions and/or Outlook

Our results show that the SHG signal from an individual plasmonic oligomer can be selectively tuned by properly matching the structural symmetry of the oligomer and the impinging polarization distribution which has not been demonstrated so far. Such capability is expected to have great potential in tailoring light-matter interactions and background-free nonlinear optical sensing and spectroscopy on the nanoscale.

References:

[1] Kauranen M and Zayats A V; Nonlinear plasmonics; Nature Photonics; 6 (2012) 737–748

[2] Hentschel M, Saliba M, Vogelgesang R, Giessen H, Alivisatos A P, and Liu N; Transition from isolated to collective modes in plasmonic oligomers; Nano Letters; 10 (2010) 2721–2726

[3] Sancho-Parramon J and Bosch S; Dark modes and Fano resonances in plasmonic clusters excited by cylindrical vector beams; ACS Nano; 6 (2012) 8415–8423

[4] Yanai A, Grajower M, Lerman G M, Hentschel M, Giessen H, and Levy U; Near- and far-field properties of plasmonic oligomers under radially and azimuthally polarized light excitation; ACS Nano 8 (2014), 4969–4974

[5] Bautista G, Huttunen M J, Makitalo J, Kontio J M, Simonen J and Kauranen M; Second-harmonic generation imaging of metal nano-objects with cylindrical vector beams; Nano Letters; 12 (2012) 3207-3212

Optical Properties of Rhodamine 6G Self-Organized in Nanostructured Hybride Films.

A. Bogoslovskaya[a], E. Bortchagovsky-[a], E. Leonenko[b], G. Telbiz[b]*

[a] V. E. Lashkaryov Institute of Semiconductor Physics of NAS of Ukraine, pr.Nauki 41, Kiev 02028, Ukraine
[b] L. V. Pisarzhevskii Institute of Physical Chemistry of NAS of Ukraine, pr.Nauki 31, Kyiv 03028, Ukraine

**e-mail: bogoslovskaya@ukr.net*

Keywords: rhodamine 6G, fluorescence, sol–gel, nanostructured hybrid films, aggregation

We investigated optical properties of rhodamine 6G in hybrid nanostructured silica films. Different approaches to the preparation of such a films allow to manage the complexation and optical properties of organic dyes impregnated into the nanoporous silica skeleton. Nanostructured SiO_2 and TiO_2 films were prepared via the template sol-gel pre-doping technique using as precursor material tetraethoxysilane or titanium isopropoxide as surfactant Pluronic 123, and dye Rhodamine 6G in different concentration. It was demonstrated that the method of deposition as well as the condensation rate of the precursor and the evaporation of the solvent reflects in the resulting complexation of the dye and its luminescent properties. The ability of the occluded Pluronic P123 mesostructures to solubilize organic molecules made these films ideal host matrices for organic dyes and molecular assemblies. Controlling the Pluronic P123 concentration we are able to control the aggregation of Rhodamine molecules and in such a way to manage optical properties of resulted films [1]. Additionally, optical properties are affected by the geometrical restriction of the aggregation and complexation of organic dyes by the structure of nanoporous silica skeleton. It was demonstrated earlier, that such films have high nonlinear properties and the potential in the use as the photonic layer in an all-optical switching device [2].

References:

[1] E. V. Leonenko, G. M. Telbiz, A. B. Bogoslovskaya, and P. A. Manoryk; Effect of aggregation of rhodamine 6g on the spectral and luminescence characteristics of hybrid mesostructured silica films; Theor. Experiment. Chem.; 50 (2015) 358-363.

[2] G. Telbiz, S. Bugaychuk, E. Leonenko, L. Derzhypolska, V. Gnatovskyy, and I. Pryadko; Ability of dynamic holography in self-assembled hybrid nanostructured silica films for all-optical switching and multiplexing; Nanoscale Res. Lett.; 10 (2015) 196-1-7.

Application of nanospectroscopy techniques in investigation of interactions Na^+,K^+- ATPase with some potential antitumor Au complexes

A.Bondžić[a], G.Janjić[b], M.Marković[a], L. Massai[c], L. Messori[c] and V.Vasić[a]*

[a] Vinča Institute of Nuclear Sciences, University of Belgrade,P.O. Box 522, Belgrade, Serbia
[b] Institute of Chemistry, Technology and Metallurgy,University of Belgrade,Njegoševa 12, Belgrade, Serbia
[c] Department of Chemistry, University of Florence, Via della Lastruccia 3, 50019 Sesto Fiorentino, Italy.
**e-mail: evasic@vinca.rs*

Keywords: Na^+/K^+ ATPase, gold complexes, DLS, fluorescence measurements

Introduction

Au (III) complexes are attracting growing attention in the field of medicinal inorganic chemistry as candidate agents for cancer treatment. Subsequent studies demonstrated profoundly different molecular mechanisms of Pt(II) and Au(III) complexes in exerting their cytotoxic effects against cancer cells. Unlike platinum drugs, it was found that proteins, rather than DNA, are the main target for the biological actions of gold complexes. Thus it was proposed that the molecular basis for the biological action of Au (III) complexes could be the modification of surface protein residues and associated loss of protein function. Na^+/K^+-ATPase is a heterodimeric transmembrane protein which regulates many cellular functions, including those associated with tumor cell growth. Recently, published studies have suggested a role for Na^+ /K^+ -ATPase in regulation of cell growth and expression of particular subunits of Na^+/K^+ -ATPase in some kinds of cancers. As a consequence, many studies were directed towards the seeking for modulators of Na^+/K^+ -ATPase which selectively target these cellular abnormalities.

Results and Discussion

Recently, we found that some stable Au(III) complexes with promising cytotoxic activities (Aubipy$(OH)_2$, Au$(OAc)_2$, AubipyC) induced the non-competitive, reversible inhibition of Na^+ /K^+ -ATPase activity, which was prevented and/or recovered in the presence of GSH and L-cysteine[1].

To further elucidate the reaction mechanism of purified protein with these promising complexes, fluorescence, DLS and zeta potential measurements combined with docking studies were performed. The interaction of Na^+/K^+-ATPase with Au(III) complexes was investigated in conditions of standard enzyme assay.

Hydrodynamic diameter of the native protein in the absence and presence of complexes obtained by DLS measurements is shown on Table 1. Measured hydrodynamic diameter indicated the increase of the average values of the particle size diameter in the case of Au$(OAc)_2$ and AubipyC. On the contrary, size diameter decreased in the case of Aubipy$(OH)_2$. Besides, the change of zeta potential indicated that the particle charge became more negative in the presence of complexes (Table 1).

Tabele 1. DLS and zeta potential values for selected system

	Partical size distribution (by number)		Zeta potential (mV)
	d (nm)	%	
Na,K /ATPase membrane fragments	95.28 2704	98 2	-30
Enzyme + AubipyC	126.3 1009	95.6 4.1	-11.5
Enzyme+Aubipy$(OH)_2$	85.76 377.8	95.4 4.6	-9.4
Enzyme+Aubipy$(OAc)_2$	147 683.8	91.7 8.3	-12.4

From these results, the conclusion can be drawn that the great number of positive complex ions is bonded on the membrane surface.

The concentration dependent fluorescence quenching of Na,K-ATPase was observed only for AubipyC and Au$(OAc)_2$. It is worthy to note that complex Aubipy$(OH)_2$ induced fluorescence quenching of tryptophan in small percent probably because it is more polar than other complexes and can not penetrate in hydrophobic environment of enzyme. The conclusion can be made that the complexes induced the quenching of tryptophan fluorescence and

that the binding sites for $Au(OAc)_2$ and AubipyC differ from the binding site for $Au(bipy)(OH)_2$. Moreover, the change of fluorescence intensity of protein was induced by conformational changes, which exerted the tryptophan in protein to the more accessible hydrophobic environment. The number of molecules of gold complexes bound to protein was calculated from the fluorescence data. Besides, these measurements confirmed the values of binding constants similar to those obtained from the inhibition experiments in our previous paper.

Combining these results with docking studies, the conclusion was made that the Au(III) complexes bind to transmembrane domain (αM1–αM6 helices), similar to cardiotonic steroids (ouabain, digoxin, and bufalin), widely used as highly specific inhibitors of the Na,K-ATPase.

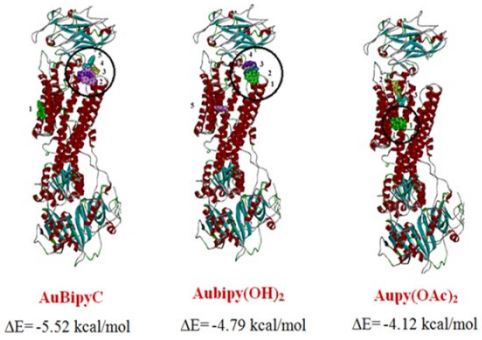

Figure 1. The ATPase in a Na^+-bounded Na,K-ATPase form (E1 conformation) in presence of Au(III) complexes.

Positively charged complexes (AubipyC and $Aubipy(OH)_2$) bind to cation-binding site, while neutral complex ($Aupy(OAc)_2$) is deeply inserted into the transmembrane domain. Binding energies for charged complexes are higher than the binding energy for neutral complex. Inhibitor binding to E1 form of enzyme probably generates a structural movement of intracellular surface area from a solvent-protected state to solvent-exposed, resulting in the removal of the N domain from the P domain.

Conclusions and/or Outlook

From these results obtained by application of different nanospectroscopy techniques, we can conclude that Au(III) complexes are strong inhibitors of Na,K-ATPase activity. By interaction with gold complexes hydrodynamic radii of membrane fragments are increased while zeta potential significantly decreases. Because of different polarity, $Aubipy(OH)_2$ quenches tryptophan fluorescence in less percent than other complexes pointing to the fact that its bonding site is far from tryptophan residues. Docking studies confirmed results obtained from fluorescence spectroscopy.

References:

[1] Petrović V, Petrović S, Joksić G, Savić J, Čolović M, Cinellu M A, Massai L, Messori M, Vasić V; Inhibition of Na^+/K^+ ATPase and cytotoxicity of a few selected gold(III) complexes; Journal of Inorganic Biochemistry, Vo 140, 2014, 228–235.

Enhanced PL-emission from an optically pumped bias driven tunneling junction

K. Braun*, X. Wang, A. M. Kern, H. Adler, H. Peisert, T. Chassé, D. Zhang, and A. J. Meixner*

Institute of Physical and Theoretical Chemistry, University of Tübingen,
Auf der Morgenstelle 18, 72076 Tübingen, Germany

*e-mail: alfred.meixner@uni-tuebingen.de
Braun.Kai@web.de

Keywords: Tip enhanced near-field optical microscopy, TERS, Plasmonics, Tunneling, Point Light Source

We demonstrate enhanced photoluminescence (PL) from an optically pumped bias driven pristine Au-substrate/Au-tip tunneling junction and a molecular junction (Au-substrate/self assembled molecular monolayer/Au-tip) with molecules chemically bound to the Au substrate. [1,2] Analyzing the emission spectra recorded as a function of bias voltage for the Au-Au junction we conclude that the enhanced intensity is induced by laser illumination and originates from the radiative decay of hot electrons closely above the Fermi level via inelastic tunneling into the plasmon modes formed by the tip-substrate gap. The optically pumped molecular junction behaves as a bias-driven superluminescent point source, operating at ambient conditions and providing almost three orders of magnitude higher electron-to-photon conversion efficiency than electroluminescence induced by inelastic tunneling without optical pumping. The enhanced emission can be modelled by rate equations taking into account hole-injection from the tip (anode) into the highest occupied orbital of the closest substrate bound molecule (lower level) and radiative recombination with an electron from above the Fermi-level (upper level), hence feeding photons back by stimulated emission resonant with the gap mode. Our study contributes to the fundamental understanding of quantum plasmonics and may lead to new applications in actively controlled photonics devices.

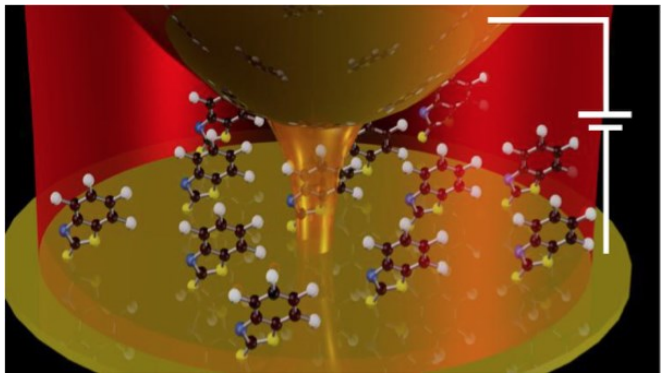

Figure 1: Sketch of the near-field region (red area) of a STM-TERS experiment, showing the tunneling junction (orange area) consisting of a sharp Au-tip and a self assembly monolayer of 2-Mercaptobenzothiazole in the center.

References:

[1] K. Braun, X. Wang, A.M. Kern, H. Adler, H. Peisert, T. Chassé, D. Zhang and A.J. Meixner, "Superluminescence from an optically pumped molecular tunneling junction by injection of plasmon induced hot electrons", Beilstein Journal of Nanotechnology 6 (1), 1100-1106 (2015).

[2] X. Wang, K. Braun, D. Zhang, H. Peisert, H. Adler, T. Chassé and A.J. Meixner, "Amplification of radiative plasmon decay by hot electron tunneling", ACS nano 9 (8), 8176-8183 (2015).

Spectroscopy of gold nanoparticles coupled to a gold film

Fang Dai[a,c], *Gaëtan Lévêque*[b], *Rana Nicolas*[c], *Pierre-Michel Adam*[c], *Monika Fleischer*[a]

[a] Institute for Applied Physics, University of Tuebingen, Auf der Morgenstelle 10, 72076 Tuebingen, Germany
[b] Institut d'Electronique de Microelectronique et de Nanotechnologie, (IEMN, CNRS-8520), Cité Scientifique, Avenue Poincaré, 59652 Villeneuve d'Ascq, France
[c] Laboratoire de Nanotechnologie et d'Instrumentation Optique, ICD CNRS UMR n°6281, Université de Technologie de Troyes, CS 42060, 10004 Troyes, France

*e-mail: fang.dai@utt.fr

Keywords: MIM structure, nanodisc, gold film, extinction, plasmon modes

Introduction

Surface plasmonics is considered as a very promising and powerful tool for biochemical sensing due to the high dependence of surface plasmons on the dielectric permittivity of the medium in close vicinity to plasmonic structures. In order to develop highly sensitive plasmonic substrates, lots of efforts have gone into the development of e.g. MIM (metal-insulator-metal) systems that give rise to higher plasmonic resonance intensity, better localization of the electromagnetic field, and easier tunability of the plasmonic resonance wavelength, attributed to coupling and hybridization of different plasmonic modes [1]. Substrates with gold nanodisc arrays coupled to a gold film across a thin insulator spacer are one of our interests. Discs on a gold film plus spacer with different disc diameters and array constants are fabricated to investigate how the distribution of the electromagnetic field is modified as a function of the geometric dimensions. Firstly, 50 nm gold film and then 4.5 nm SiO_2 spacer layer are deposited on a glass substrate by thermal and e-beam evaporation, respectively. Then nanodisc arrays are fabricated by electron beam lithography (EBL), with disc diameters of 80 nm, 110 nm, 140 nm, 170 nm, and 200 nm, and array constants of 300 nm, 450 nm, 600 nm and 1000 nm. Evaporation of 50 nm gold and lift-off follow after EBL. The dimensions of the discs are determined under the Scanning Electron Microscope (SEM), and the optical properties of the MIM system are characterized by darkfield and extinction spectroscopy with different illumination and collecting configurations. Simulations based on the Green's tensor method [2] are performed to provide an insight into the physical processes behind the experimental results.

Results and Discussion

Shown in **Figure 1** (a) is a schematic of the gold nanodiscs on gold film substrate. **Figure 1** (b-c) show scanning electron microscope images of gold nanodisc arrays of 300 nm array constants and diameters of 140 nm (b) and 200 nm (c), respectively. The nanodisc dimensions are very close to the designed layout. EBL is chosen to fabricate the nanostructures because it can provide very precise control of the sizes, shapes, patterns and locations of nanostructures, most importantly with high reproducibility.

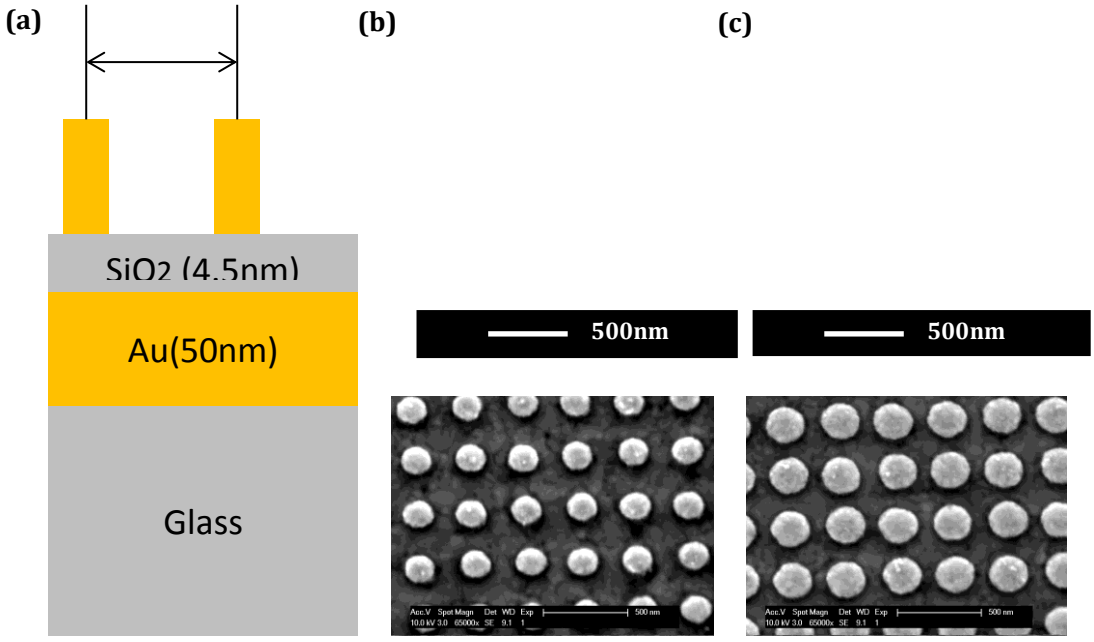

Figure 1: (a) schematic of gold nanodiscs on gold film and spacer layer substrate; scanning electron microscopy images of substrates with 300 nm array constant and disc diameters of 140 nm (b) and 200 nm (c).

Figure. 2 demonstrates sample results of the extinction measurements in both simulations and experiments. **Figure 2 (a)** displays the simulated extinction spectra of a substrate with different diameters and an array constant of 300 nm, under illumination with collimated white light under normal incidence. With the help of simulations of the near-field distribution at different wavelengths (not shown), different modes (1) to (4) can be assigned to the different resonances [3].

Figure 2 (b) shows the corresponding extinction measurement results. In this experiment, the sample is illuminated from the air side with a numerical aperture of 0.52, and the numerical aperture for collection is 0.45. By comparing the two sets of spectra, we can see that good agreement between simulations and experiments is achieved.

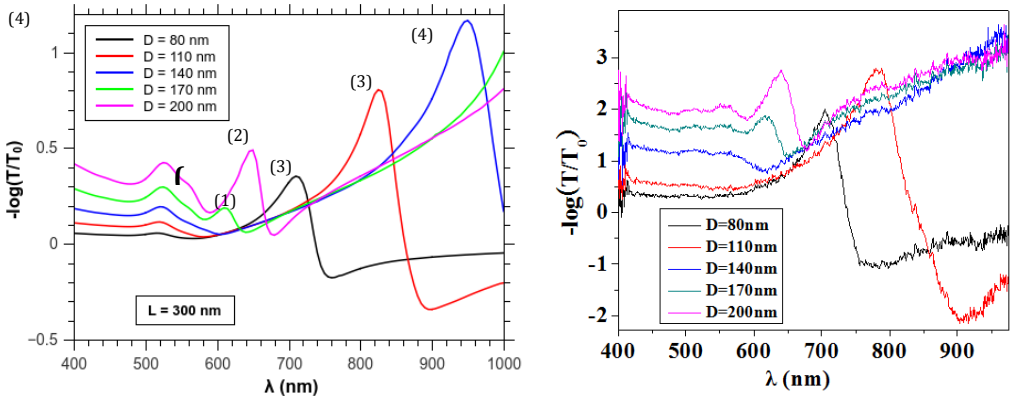

Figure 2: (a) Simulated extinction spectra for a substrate with different disc diameters and an array constant of 300 nm; (b) experimental extinction spectra for a substrate with the same dimensions as (a).

Conclusions and Outlook

The substrates with gold nanodiscs coupled to a gold film across a thin spacer layer exhibit great potential for sensing by providing a series of plasmonic modes with different physical natures that cover the whole visible wavelength regime. Other kinds of MIM systems, such as nanocones over a gold film and vertical dimers will also be fabricated and investigated. In the future, LSPR (localized surface plasmon resonance) and SERS (surface enhanced Raman spectroscopy) biochemical sensing will be conducted with these substrates.

References:

[1] Le F, Lwin N Z, Steele J M, Käll M, Halas N J, Nordlander P; Plasmons in the Metallic Nanoparticle-Film System as a Tunable Impurity Problem; Nano Lett.; 5(10) (2005) 2009–2013;

[2] Leveque G, Martin O J F, Weiner J; Transient behaviour of surface plasmon polaritons scattered at a subwavelength groove; Phys. Rev. B; 76 (2007) 155418;

[3] Nicolas R, Leveque G, Marae-Djouda J, Montay G, Madi Y, Plain J, Herro Z, Kazan M, Adam P-M, Maurer T; Plasmonic mode interferences and Fano resonances in Metal-Insulator-Metal nanostructured interface; Sci. Rep; 5 (2015) 14419

Synthesis and applications of three-dimensional carbon nanotube networks

M. Scarselli *

Università di Roma Tor Vergata, Dipartimento di Fisica, Via della Ricerca Scientifica, 00133 Roma, Italy
* email: manuela.scarselli@roma2.infn.itssisposi.it

Keywords: carbon nanotube; carbon network; hydrophobicity; pressure transducer; photocurrent

Introduction

In the last years, there has been growing interest in developing synthetic three-dimensional architectures because of the increase of active surface area gained throughout the entire three-dimensional structure. The most challenging properties of the assemblies obtained up to now, are a self-sustained arrangement, high porosity [1], structural stability, and good electrical conductivity [2]. The most recent applications are in filtration [3], separation [4], biological sensing [5], and oil-spill remediation [6] but also in mechanical actuators [7], catalytic supports [8], and super capacitors [9]. In this research field, carbon nanotubes (CNTs) are ideal building blocks for constructing three-dimensional random meshes from their overlapping. The basic idea is to link the well-known electrical and mechanical properties of the CNT one-dimensional structure, with the possibility of manipulating the arrangement and orientation of the CNTs during the synthesis process in order to obtain highly disordered interconnected 3D architectures. The first results from the research group of Gui and co-workers are very promising [2]. Similarly, we obtained three-dimensional carbon nanotube networks following a chemical vapor deposition process different from that reported in ref. 2, [10-12]. In particular, we performed a detailed study of the relationship between the observed microscopic properties of the CNT material and some potential applications that we tested.

Results and Discussion

The synthesis process followed to obtain CNT architectures, often referred to as CNT-sponges, is been described in detail elsewhere [ref]. The CNT-based products collected from the reaction chamber are light and porous and of variable dimension, as shown in **Figure 1a**. Scanning electron microscopy (SEM) analysis reveals that the material is made of randomly self-assembled, long and interconnected tubular nanostructures, with pore sizes from several nanometers to a few micrometers, **Figure 1b**. The high number of interconnections is due to the presence of topological defects induced in the carbon sp^2 lattice during the growth process. [10-12]

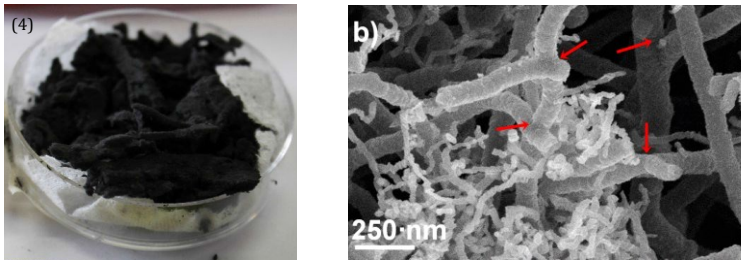

Figure 1: Photograph of a bowl containing pieces of CNT-sponges (a), SEM micrograph showing the entangled structure of the network, the red arrows point to junctions between CNTs (b).

The micro-porosity of the synthesized material is responsible of its very low density of about 15 mg/cm^3, good conductivity (electrical resistance of about 40 $\Omega \cdot cm^{-1}$) and its capability to sustain high compression loads as recently reported for our samples [10]. Furthermore, two interesting properties that originate from the high porosity and the interconnected structure are the hydrophobicity and oleophilicity. To characterize the hydrophobicity one can measure the advanced static contact angle at room temperature for water droplets of different volumes ranging from 5 to 20 μL, as shown in **Figure 2**, the presence of a composite solid–liquid–air interface explains the high value of the measured contact angle ($\Theta = 175°$), that makes this material super hydrophobic. At the same time, the CNT-sponge shows a high absorption capacity towards oils (e.g., vegetable and mineral oil), being the contact angle significantly less than 90° thus making the material lipophilic [11-12]. Interestingly, the adsorbed oil can be removed after the sponge is saturated simply through squeezing it from the sponge or through burning it. Investigation on the inner structure of the CNT network before and after oil absorption is still ongoing.

Figure 2: Photograph of water droplets of different volumes (a) on the bulk material. Photograph of the starting of the oil-adsorption process (b)

Finally, to test the capability of the system to respond to incident light and generate a photocurrent, we cut a piece of the CNT-sponge, which has a self-sustainable structure, and used it as the working electrode in a standard electrochemical cell. In this manner, it was possible to register a good photo-response of the CNT-network in the visible and near-ultraviolet range [12].

Conclusions

We demonstrate how to synthesize carbon-based three-dimensional networks following a special synthesis process. The obtained material is self-supporting and consists of curved and interconnected carbon nanotubes and to lesser extent of carbon fibers. We study the relationship between the observed microscopic properties and some potential applications. In particular, the porous nature of the network is directly responsible for the hydrophobic and the lipophilic behaviour, and the material has a strong affinity for some organic solvents and high sorption rates for oils. We also found that the system is able to generate a photocurrent in the visible and near-ultraviolet region. The preliminary results obtained enable us to predict that the reported CNT-sponges will be useful for applications in pressure-sensor applications and filtration and water treatment as well.

References:

[1] Lee J, Kim J, Hyeon T, Recent Progress in the Synthesis of Porous Carbon Materials; Adv. Mater. 18 (2006), 2073–2094;
[2] Gui X, Wei J, Wang K, Cao A, Zhu H, Jia Y, Shu Q, Wu D, Carbon nanotube sponges; Adv. Mater., 22 (2010) 617–621;
[3] Li H, Gui X, Zhang L, Wang S, Ji C, Wei J, Wang K, Zhu H, Wu D, Cao A; Carbon nanotube sponge filters for trapping nanoparticles and dye molecules from water; Chem. Commun. 46 (2010) 7966–7968;
[4] Gui X, Li H, Wang K, Wie J, Jia Y, Li Z, Fan L, Cao A, Zhu H, Wu D; Recyclable carbon nanotube sponges for oil absorption; Acta Mater. 59 (2011) 4798–4804;
[5] Qian W; Gu Z-Z; Fujishima A; Sato O; Three-Dimensionally Ordered Macroporous Polymer Materials; Langmuir 18 (2002) 4526–4529;
[6] Moura F C C, Lago R M; Catalytic growth of carbon nanotubes and nanofibers on vermiculite to produce floatable hydrophobic “nanosponges” for oil spill remediation; Appl. Catal., B 90 (2009) 436–440;
[7] Cao A, Dickrell P L, Sawyer W G, Ghasemi-Nejhad M N, Ajayan P M; Super-Compressible Foamlike Carbon Nanotube Films; Science 310 (2005) 1307–1310;
[8] García-Martínez J, Lancaster T M, Ying J Y; Synthesis and Catalytic Applications of Self-Assembled Carbon Nanofoams; Adv. Mater. 20 (2008) 288–292;
[9] You B, Jiang J, Fan S; Three-Dimensional Hierarchically Porous All-Carbon Foams for Supercapacitor; ACS Appl. Mater. Interfaces; 6 (2014)15302–15308;
[10] Camilli L, Pisani C, Passacantando M, Grossi V, Scarselli M, Castrucci P, De Crescenzi M; Pressure-dependent electrical conductivity of freestanding three dimensional carbon nanotube network; Appl. Phys. Lett. 102 (2013) 183117-3;
[11] Camilli L, Pisani C.; Gautron E; Scarselli M.; Castrucci P; D’Orazio F; Passacantando M; Moscone D, De Crescenzi M, A three-dimensional carbon nanotube network for water treatment; Nanotechnology; 25 (2014) 065701-8;
[12] Scarselli M, Castrucci P, De Nicola F, Cacciotti I, Nanni F, Gatto E, Venanzi M, De Crescenzi M, Applications of three-dimensional carbon nanotube networks; Beilstein Journal of Nanotechnology, 6 (2015) 792-798.

Optical properties of core-shell magnetite nanoparticles obtained via wet chemical synthesis

Urszula Klekotka[a]*, *Beata Kalska-Szostko*[a], *Dariusz Satuła*[b]

[a]Institute of Chemistry, University of Bialystok, Bialystok, Poland
[b]Department of Physics, University of Bialystok, Bialystok, Poland

*e-mail: u.wykowska@uwb.edu.pl

Keywords: core-shell nanoparticles, magnetite, optical properties

Introduction

Superparamagnetic ferrite nanoparticles (Fe3O4, γ-Fe2O3, α-Fe2O3 and others) possess unique chemical, electrical, thermal and magnetic properties (blocking temperature, high saturation filed, large specific area) [1]. Addition of optically active element like Ag, Au, Cu on the surface of ferrite nanoparticles, influences on the magnetic optical properties. Synthesis of the particles with layer-by-layer growth, allow to tune properties in more foreseen way. However, the fabrication of fine nanomaterials, with exact desired properties is a very difficult issue due to few reasons. Firstly, chemical procedures has main drawback that clear, homogenous and stable samples are difficult to obtain. In addition, inclusion of other metallic elements or oxides layers into nanoparticles structures, influences on their magnetic properties and layered morphology. Therefore detailed studies are needed to monitor how were obtained fine core-shell nanoparticles with desired magnetic and optical properties.

Results and discussion

In presented studies, core-shell nanoparticles were fabricated by wet chemical synthesis method in organic solvent, and argon environment. As a core, small seeds of magnetite were used. As a second shell layer pure noble metals or iron oxide was used [2]. Magnetic and optical properties of nanoparticles were examined due to: type, thickness and location of the additional layer (interlayer or surface layer). For characterization obtained nanoparticles transmission electron microscopy, X-ray diffraction, infra-red and Mössbauer spectroscopy techniques were applied. Their optical properties were observed with UV-Vis spectrometry.

In the Figure.1 A typical TEM image of magnetite nanoparticles with silver shell is presented. Size of presented nanoparticles was estimated to be 15±2 nm, similar pictures were collected for other samples. Figure 1B shows example of UV/Vis spectra of core-shell nanoparticles with Ag, Au, and Cu shells.

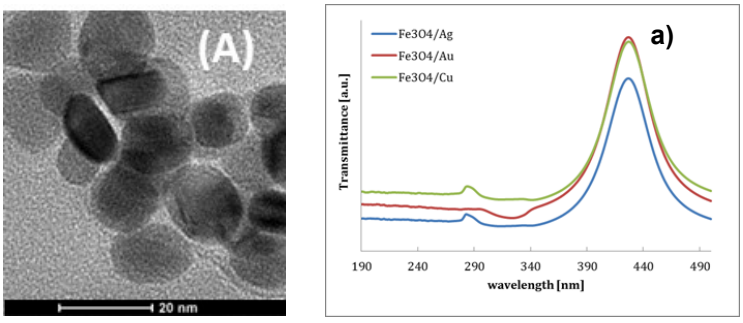

Figure 1: (A) TEM image of magnetite nanoparticles with silver outermost layer; (B) UV-Vis spectra of nanoparticles with gold, silver, or copper shell.

Conclusions and/or Outlook

By introduced layer-by-layer deposition core-shell nanoparticles with optically active layer can be obtained, what is proven by TEM and UV-Vis analysis (Figure. 1). In presented image, one type of nanoparticles is presented but the same particles morphology can be obtained for other compositions [2]. UV-Vis spectroscopy allows to monitor the influence of the optical active layer on the overall magneto-optical properties of nanoparticle system.

Mössbauer spectroscopy was done in close collaboration with Department of Physics University of Bialystok. The work was partially financed by EU founds via project with contract number POPW.01.03.00-20-034/09-00 and by NCN founds UMO-2014/13/N/ST5/00568.

References:

[1] N. Sanvicens, M. Pilar Marco; Multifunctional nanoparticles – properties and prospects for their use in human medicine; Trends in Biotechnology; 26 (8) (2008) 425-533

[2] B. Kalska-Szostko, U. Wykowska, D. Satuła; Magnetic nanoparticles of core-shell structure; Colloids and Surfaces A: Physicochemical and Engineering Aspects; 481 (2015) 527-539

DLS, AFM and DFT studies of thiacyanine dye J-aggregation on the surface of citrate capped AgNPs

B. Laban[a], *D.Vasić*[b], *M.Marković*[b], *M.Luce*[c], *V.Vodnik*[b], *A. Cricent*[c], *V.Vasić**[b]

[a] Faculty of Natural Science and Mathematics, University of Priština, Lole Ribara 29, 38220 Kosovska Mitrovica, Serbia[b] Vinča Institute of Nuclear Sciences, University of Belgrade,P.O. Box 522, Belgrade, Serbia[c]Istituto di Struttura della Materia, Consiglio Nazionale delle Ricerche, Roma, Italy

*e-mail: evasic@vinca.rs

Keywords: thiacyanine dyes, Ag nanoparticles, DLS, AFM, DFT calculations

Introduction

The anionic cyanine dye, 5,5'-dichloro-3,3'-disulfopropylthiacyanine sodium salt (TC), forms J-aggregates [1], the organized molecular assemblies composed of the great number of dye molecules in the presence of noble metal nanoparticles (NPs). The aggregation of the dye molecules is usually followed by the change of the absorption and fluorescence properties of TC-NPs assembly. Besides the NPs induced quenching of TC fluorescence, the absorption spectra are characterized by the appearance of the characteristic sharp maximum or the deap at 481 nm. The aim of this work was to apply some nanospectroscopy techniques, such as dinamic light scatering (DLS) and atomic force microscopy (AFM) for evaluation of size distributions and electrochemical properties of citrate capped AgNPs in the absence and presence of TC which formed J-aggregates on their surface. Besides, a set of simple density functional theory (DFT) calculations was performed for clarification of the possible mechanism of TC adsorption on AgNPs surface resulting in TC J-aggregation.

Results and Discussion

The particle size, zeta potential, electrophoretic mobility and conductivity are the key parameters for quantitative evaluation of particle stability in suspensions. The average NPs diameter (d_{av}) determined by DLS measurements represents the hydrodynamic diameter of the particle with hydratation shell. The obtained d_{av} values of colloid dispersion containing AgNPs and TC before and after addition of TC dye, together with zeta potential, mobility and conductivity are given in Table 1. In comparison with TEM measurements [2], d_{av} values were higher and included the added solvent and stabilizer moving with the particle. The addition of TC to the colloid dispersion additionally increased the diameter of the particles, as it included additional shell of adsorbed dye molecules at the AgNPs surface. The zeta potential measurements gave a mean values which confirmed the increasing of AgNPs – TC suspension stability. However, the conductivity of the colloid solution increased significantly, due to the replacement of capping ions (citrate and borate) with TC molecules. Besides, the electrophoretic mobility in AgNPs – TC assembly is negative, indicating that the particles acquired a net negative charge. Moreover, it became more negative with TC adsorbed on AgNPs. This negative values of electrophoretic mobility suggested that the AgNPs suspension in the presence and absence of TC should remain stable for long time, which is also in accordance with the spectrophotometric data.

Table 1 DLS measurements of average particle size diameter (d_{av}), zeta potential, mobility and conductivity of AgNPs colloid in the absence and presence of $1.6x10^{-5}$ M TC and $1x10^{-8}$ AgNPs after equilibration at 25^{o}C

	AgNPs	TC	AgNPs + TC
Concentration (M)	$2.17x10^{-9}$	$1x10^{-5}$	mixture
d_{av} (nm)	25.85±1.58	-	48.97±3.6
Zeta potential (mV)	-23.3±2.0	-	-38.3±3.1
Conductivity ($\mu S\ cm^{-1}$)	0.082±0.001	0.036±0.001	0.113±0.002
mobility	-1.82±0.15	-0.682±0.404	-3.005±0.244

Figure 1 represents AFM images of AgNPs in the absence and presence of TC. The AgNPs height (*z* direction), at a distance where the tip is repelled or attracted by the forces due to the interaction with the surface, was used to determine the diameter of bare and TC – coated nanoparticle. The histograms obtained from the AFM images indicate that the average diameters of particles were 20 nm for bare AgNPs and 50 nm for AgNPs in the presence of TC. These results are higher than those obtained by TEM, but agree very well with DLS measurements. Besides, the borate/citrate capping increased the size of bare as well as TC coated AgNPs. In the latter case, the distribution of particle size diameter is broad, with the maximum at about 50 nm. This is the result of the partial agglomeration (aggregation) of TC dye coated AgNPs, which is in accordance with TEM measurements [2].

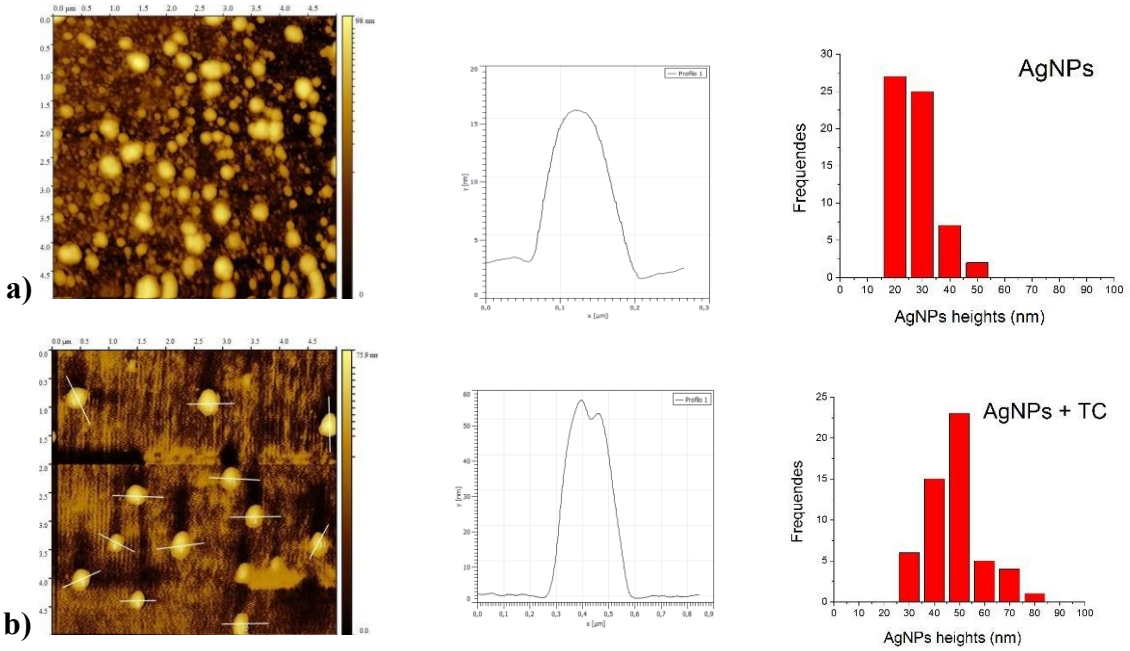

Figure 1: AFM images of bare (a), and TC coated AgNPs (b)

If comparing previously obtained absorption spectra of TC dye on AgNPs [2], most significant differences are visible in the position of exciton indicating the key role of metal boundary in the adsorption process of TC. Using the simple model which considered AgNPs surface as a single Ag atom, interacting with different parts of the dye molecule anion, obtained results suggested that TC dye is, from the thermodynamical point of view, most likely to interact with AgNPs via oxygen atom from SO_3^- groups, as also was obtained earlier in DFT study of adsorption of TC dyes on AuNPs [3] and semiconducting surfaces. In order to discuss possible mechanisms of substitution of citrate/borate anions by TC, a more precise surface model, consisting of 18-atom Ag cluster, has been established. In Table 2, energies of adsorption processes of pristine citrate and TC anions are given. Moreover, as adsorption of borate anions is in principle also possible on the AgNPs surface, two most probable types of adsorbed borate species – BO_3^{3-} and $B(OH)_4^-$, are also included.

Table 2: Adsorption energies of investigated anionic species on 18-atom Ag cluster.

species	TC dye	citrate	BO_3^{3-}	$B(OH)_4^-$
Eads / eV	-2.48	-7.94	-3.43	-1.74

All species expected on pristine AgNPs, except hydroxyborate, are bound to Ag significantly stronger than TC dye. On the other hand, it is the experimental fact that J-agregation of TC dye on AgNPs occurs only when K^+ ions are added to the system in significant excess. The attractive interaction between adsorbed citrate and K^+ ions, provides a thermodynamical driving force to drive at least one K^+ ion per adsorbed citrate out of its hydratation sphere and deposit it onto the AgNP surface. Moreover, interaction between K^+ ions and adsorbed citrate inevitably weakens citrate adsorption on the AgNPs surface, thus favoring replacement of citrate by TC dye.

Conclusions and/or Outlook

The study of particle size distribution of the bare and TC coated AgNPs using DLS and AFM methods showed that the particle size diameters agree quite well. However, the particles sizes are larger compared to the previous obtained TEM values (10 nm). This difference is the consequence of the capping layer including TC J-aggregates on the AgNPs surface. DLS calculations confirmed the TC bonding to AgNPs surface due to the interaction of oxygen from SO_3 groups with metal. Moreover, K ions in colloidal dispersion thermodinamically favored replacement of citrate by TC dye.

References:

[1]Laban B, Vodnik V, Dramićanin M, Novaković M, Bibić N, Sovilj S, Vasić V, Mechanism and kinetics of J-aggregation of thiacyanine dye in the presence of silver nanoparticles, J. Phys. Chem. C, 118 (40) (2014) 23393–23401

[2] Laban B, Vodnik V, Vasić V; Spectrophotometric observations of thiacyanine dye J-aggregation on citrate capped silver nanoparticles, Nanospectroscopy 1 (2015) 54–60

[3] S Valleau, Semion K. Saikin, Man-Hong Yung and A AspuruGuzik: Exciton transport in thin-film cyanine dye J-aggregates, J. Chem. Phys. 137, 034109 (2012)

Gap dependent plasmonic resonances of bow tie nanostructures on a flexible insulating substrate

F. Laible, K. Braun, O. Hauler, A. J. Meixner, D. P. Kern, and M. Fleischer*

University of Tuebingen
*e-mail: florian.laible@uni-tuebingen .de

Keywords: Bow tie nanostructures, Dark field spectroscopy, FEM Simulations, Transfer process

Introduction

The field-enhancement of bow tie (BT) shaped nanostructures through localized surface plasmon resonances (LSPR) is strong and highly localized. This makes this kind of structures highly interesting as, for example, surface enhanced Raman scattering (SERS) substrates [1]. The highest field-enhancement is located between the adjoining tips of the two prisms which form the BT.

The dimers are prepared on a flexible substrate, Polydimethylsiloxan (PDMS), which is elastically stretchable to up to 160% under ambient conditions [2]. Also PDMS is transparent for light in the visible range. Direct lithography processes on this substrate are challenging due to its insulating and deformable nature, while a transfer process proves to be well suited to generate nanostructures on this flexible substrate.

Results and Discussion

The top- down fabrication process of the BT nanostructures is shown in **Figure 1**. Starting with an aluminium layer on a glass substrate a resist is spin-coated onto the aluminium. The resist is then structured via electron beam lithography. A gold film is evaporated after the development of the resist. During the lift-off the unexposed resist is dissolved and the superfluous gold can be washed away. The nanostructures remain on the aluminium layer.

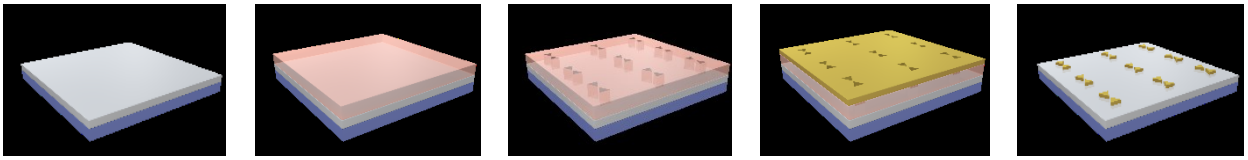

Step 1: Aluminium layer on glass substrate.

Step 2: Resist spin-coated on top.

Step 3: E-beam lithography and development.

Step 4: Evaporation of a gold film.

Step 5: Lift-off.

Figure 1: Top- down process.

The lithography pattern of one BT consists of dots with a vertical and horizontal distance, centre to centre, of 7.5 nm. To acquire a homogenous dose distribution over the exposed area a dot-by-dot proximity effect correction is applied: the exposure of each dot is represented by a double Gaussian point exposure distribution [3]. An exposure matrix contains the contribution of each dot at each location. The inverse of this matrix times the unit vector results in a vector providing a scaling factor for the dose of each dot. After the scaling the dose distribution is mostly homogenous. SEM images of two structures on aluminium (**Figure 1,** Step 5) are shown in **Figure 2**.

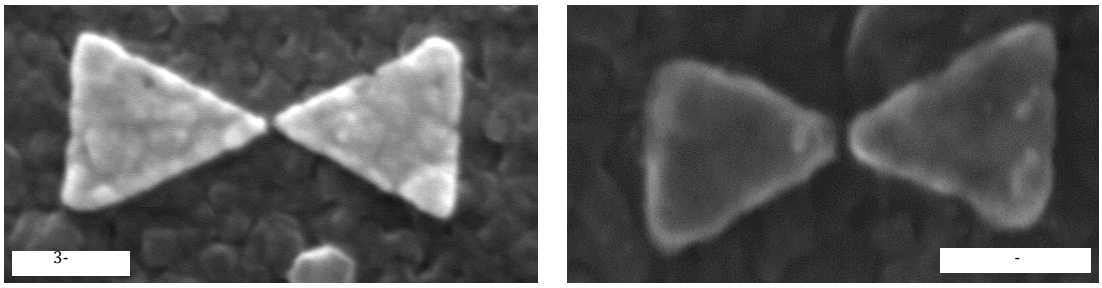

Figure 2a: BT with a vertical dimension of 290 nm and horizontal dimension of 630 nm.

Figure 2b: BT with a vertical dimension of 165 nm and horizontal dimension of 365 nm.

Figure 2: BT nanostructures on aluminium (Step 5, Figure 1) with sub- 10 nm distance between the tips.

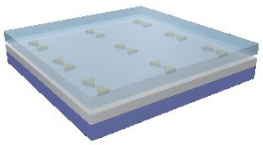

Step 6: PDMS stamp is placed on the structures.

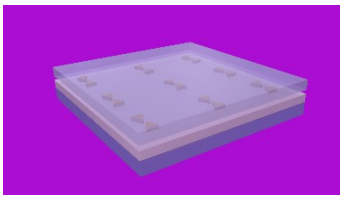

Step 7: Sandwich immersed in alkaline solution.

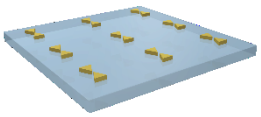

Step 8: Structures transferred to the PDMS substrate.

Figure 3: Transfer process.

Afterwards a transfer process to the flexible substrate can be performed, see **Figure 3**. A PDMS substrate is placed on top of the structures. The bulky PDMS sample sticks to the surface of the aluminium layer via adhesion. The sandwich is then placed in an alkaline solution. This solution dissolves the aluminium layer and the BT structures stick to the PDMS substrate. Note that the structures are now upside down on the flexible substrate. It is now possible to measure transmission dark field spectra of the BT structures.

Outlook

The distance between the prisms can now be modified by stretching the substrate, potentially in-situ during the measurement. Measured dark field spectra will be shown along with FEM simulations of modelled BT structures with comparable gap sizes.

References

[1] Didson S, Haggui M, Bachelot R, Plain J, Li S, and Xiong Q; Optimizing Electromagnetic Hotspots in Plasmonic Bowtie Nanoantennae; Journal of Physical Chemistry Letters; 4 (2013) 496-501.

[2] Johnston I D, McCluskey D K, Tan C K L, and Tracey M C; Mechanical characterization of bulk Sylgard 184 for microfluidics and microengineering; Journal of Micromechanics and Microengineering; 24 (2014) 035017.

[3] Chang T H P; Proximity effect in electron-beam lithography; Journal of Vacuum Science and Technology; 12 (1975) 1271-1275.

Tuning the growth for a selective nucleation of chains of Quantum Dots behaving as single photon emitters

V. Latini[*,a], *E. Tisbi*[a], *E. Placidi*[a,b], *F. Patella*[a], *F. Biccari*[c], *M. Gurioli*[c], *A. Vinattieri*[c], *F. Arciprete*[a],

[a] Università di Roma "Tor Vergata", Dipartimento di Fisica, via della Ricerca Scientifica 1, 00133 Roma, Italy

[b] Istituto di Struttura della Materia, CNR, Via del Fosso del Cavaliere 100, 00133 Roma, Italy

[c] Dipartimento di Fisica e Astronomia, LENS, Università di Firenze, Via Sansone 1, I-50019, Sesto Fiorentino (Firenze), Italy

e-mail: valerio.latini@roma2.infn.it

Keywords: Low dimensional structures, Molecular Beam Epitaxy, Semiconducting III-V materials, Microphotoluminescence, single photon emitters

Introduction

The fabrication of sophisticated Quantum Dot devices for optoelectronics, nanophotonics or quantum computing requires the capability of producing defect-free, spatially ordered and uniformly sized Quantum Dots (QDs). Combined bottom-up and top-down methods are largely used but often introduce defects, which may deeply affect QDs' optical properties [1]. Multi-stacked heteroepitaxy of self-assembled QDs provides an efficient tool for controlling both the vertical and lateral positioning of QDs and also for increasing the active material volume and tuning the optical properties due to the vertical coupling of the structures [2]. In the case of InAs/GaAs(001) QD multilayers, we have shown that it is possible to drive the nucleation to form *n*-fold InAs QD chains after the deposition of exactly *n* layers [3].

Optical spectroscopy provides useful information to assess the quality of the QDs and eventually demonstrates the quantum nature of the emitter as single photon source. In this work, both the morphology and the optical properties of the dots were deeply investigated, demonstrating that the growth conditions allowed for the dot alignment with no loss in terms of the optical quality.

Results and Discussion

Single and two-layer InAs/GaAs(001) samples were grown in a Molecular Beam Epitaxy chamber under critical conditions, leading to the selective growth of self-assembled InAs Quantum Dot chains over mounded GaAs surfaces. In the 2-layer samples the QD chains nucleated above the buried chains of the underlying layer plus an additional not-stacked chain placed at the onset of the mound, on the side facing the As flux [4] (see **Figure 1**). The new unstacked chain was referred as the *morphological* QD chain since its origin depends on the presence of elongated step bunching at the onset of the mound slopes.

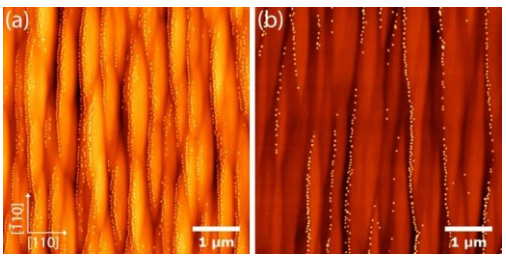

Figure 1: Representative 5 × 5 μm^2 Atomic Force Microscopy topographies of a single layer sample (a) and a two-layer sample (b). Single QD chains are apparent in (a), 2-fold chains are peculiar to (b). The chains are parallel to the [$\bar{1}$10] direction, along which the mounds appear to be stretched. The colour scale is 20 nm.

Changing the thickness of the GaAs spacer layer and the InAs deposition allowed to tune the nucleation in the second layer. Particularly, the selection of a single strain-driven stacked chain was made possible by inhibiting the nucleation of the morphological QDs at the onset of the mounds (see **Figure 2**). Finite Element Method simulations evidenced the major role of the strain field in favouring the formation of single stacked chains [5]. On the other hand, tuning properly the As/In flux ratio contributed to improving the QD ordering along the chains. In order to assess the optical quality of the InAs QDs, we measured and analyzed the photoluminescence (PL) of single QDs. First looking for the presence of multi-excitonic complexes and then checking if our dots behave as single photon emitters. In **Figure 3** we report the spectrum of a QD showing a single excitonic line;

the measurement of the second order autocorrelation function $g^2(\tau)$ of the emission line is reported in the right panel. The $g^2(\tau)$ was fitted by the function $g^2(\tau) = y_0 + A\left(e^{-|t-\tau-t_0|/\tau} + \sum_{i=1}^{N-1} e^{-|t-\tau-t_0|/\tau}\right)$, where τ is the delay between the two avalanche photodiode (APD) signals, y_0 and A are two constants, N is the number of peaks, i is an index to identify the ith peak (starting from zero), 0 is the peak at zero delay, t_0 is the time at which the first peak occurs, T is the period of the laser pulses, τ is the lifetime of the excited state and g is the value of $g^2(0)$. The result of the fit gives $g^2(0)$ a value confirming the nature of single photon emitter of the observed QD. The lifetime τ turned out to be 0.7 ± 0.2 ns. The same value was confirmed by lifetime measurements taken with a time-correlated single photon counting setup. These characteristics were found on almost all the observed QDs.

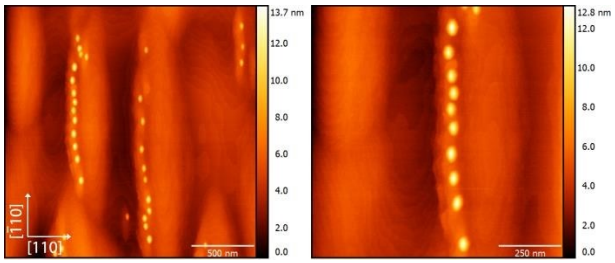

Figure 2: $2 \times 2\ \mu m^2$ (left) and $1 \times 1\ \mu m^2$ (right) Atomic Force Microscopy topographies of a 2-layer sample where the selection of single stacked chains was achieved. The single chains are around 90 nm far from the left edge of the mounds, where the naked step bunching is clearly visible.

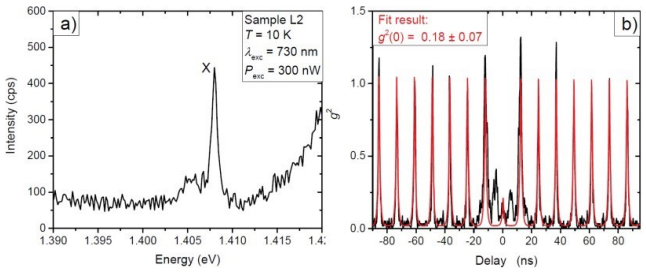

Figure 3: a) PL spectrum of a 2-layer sample showing a single exciton line indicated by the label X. b) Pulsed second autocorrelation function measured on the exciton line reported in a) (black) and its fit (red). The two small peaks, close to the t = 0 peak, are false coincidences due to the cross-talk between the APDs and they can be neglected.

Conclusions

By working at critical growth conditions for dot formation, we were able to induce the formation of InAs QD chains over rippled GaAs(001) surfaces, parallel to the [1$\bar{1}$0] direction. We grew several single and two-layer samples, where single and 2-fold chains were observed respectively. The reduction of the GaAs spacer thickness and the interruption of the InAs supply allowed to select single stacked chains in the second layer, showing how to gain control over the interplay between the strain field of the buried QDs and surface morphology. FEM simulations confirmed the major role of the strain in dominating the surface curvature effects. Micro-photoluminescence measurements confirmed the nature of single photon emitters of the observed QDs. Thus, we can conclude that the optical properties of the QDs are well supported by our growth approach, allowing a valuable spatial correlation between the QDs aligned along the chain.

References:

[1] Kiravittaya S, Rastelli A, Schmidt O G; Advanced quantum dot configurations; Reports on Progress in Physics; 72 (2009) 046502

[2] Ortner G, Bayer M, Larionov A, Timofeev V B, Forchel A, Lyanda-Geller Y B, Reinecke T L, Hawrylak P, Fafard S, Wasilewski Z; Fine structure of excitons in InAs/GaAs Coupled Quantum Dots: A Sensitive Test of Electronic Coupling; Phys. Rev. Lett. 90 (2003) 086404

[3] Placidi E, Arciprete F, Latini V, Latini S, Magri R, Scuderi M, Nicotra G, Patella F; Manipulating surface diffusion and elastic interactions to obtain quantum dot multilayer arrangements over different length scales; Applied Physics Letters, 105 (2014) 111905

[4] Arciprete F, Placidi E, Magri R, Fanfoni M, Balzarotti A, Patella F; The Unexpected Role of Arsenic in Driving the Selective Growth of InAs Quantum Dots on GaAs ACS Nano; 7 (2013) 3868

[5] Latini V, Placidi E, Arciprete F, Patella F; In-line correlation and ordering of InAs/GaAs multistacked Quantum Dots Structures; Journal of Crystal Growth; 419 (2015) 138

Preparing optical antennas on nonlinear crystals

Emre Gürdal[1], Markus Kalmutzki[2], Anke Horneber[3], Hans-Jürgen Meyer[2], Alfred J. Meixner[3], Dai Zhang[3], Dieter Kern[1] and Monika Fleischer[1]

University of Tübingen
Faculty of Science
[1]Institute for Applied Physics, [2]Institute of Inorganic Chemistry, [3]Institute of Physical and Theoretical Chemistry
Auf der Morgenstelle 10, 72076 Tübingen

e-mail: emre.guerdal@uni-tuebingen.de

Keywords: nonlinear crystal, plasmon, second harmonic generation

Introduction
In the last decade nonlinear crystals have become a common tool for frequency conversion. One second order nonlinear optical process is the so-called second harmonic generation (SHG). The interaction of two photons with a nonlinear crystal allows to create one photon with twice the energy. It is however known that the effects of SHG from nonlinear crystals are relatively weak. To enhance the process plasmonical nanoantennas are widely exploited. At the resonant wavelength of the localized surface plasmons (LSPs) a very strong near-field in the close vicinity of the antenna surface is excited, which can lead to an improvement of the nonlinear optical process [1].

Results and Discussion
We investigate the structuring of nonlinear crystals with gold nanostructures by electron beam lithography. The nonlinear crystal which we structure is a novel cyanurate Sr3(O3C3N3)2 (SCY), which exhibits a more efficient SHG than conventional crystals [2]. Since direct patterning of the crystal is challenging, transfer processes are explored. Figure 1 shows a 60 µm wide SCY crystal structured by gold nanodiscs in the shape of dimers. In this case the diameter of the discs is about 70 nm and the separation is about 50 nm. We aim to obtain discs with small gap distances and a diameter designed for optimal excitation by a pulsed femtosecond laser.

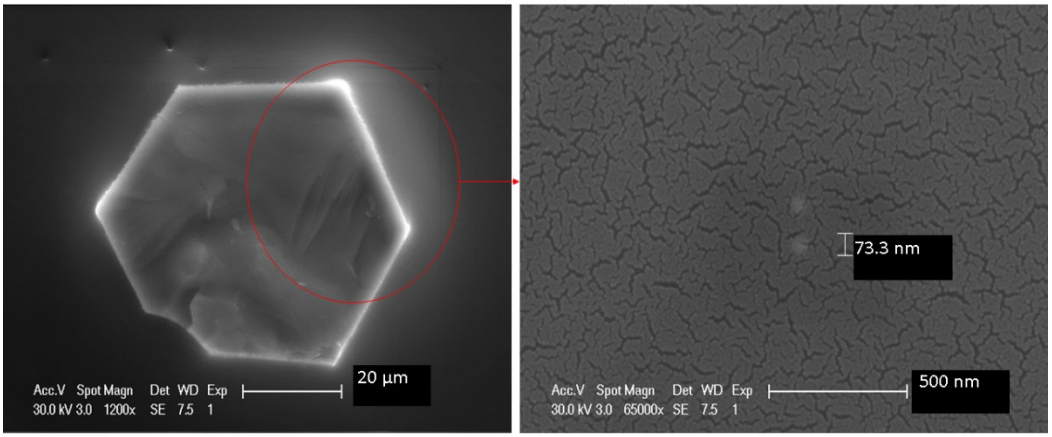

Figure 1: A structured SCY crystal with gold nanodiscs in the shape of dimers

Conclusion
Achieving structured SCY with gold nanoparticles in the shape of dimers is a challenge. An overview of the method for fabricating gold nanostructures on the surface of nonlinear crystals will be presented.

[1] Dutto, F., Heiss, M., Lovera, A., López-Sánchez, O., Fontcuberta i Morral, A., & Radenovic, A. (2013). Enhancement of second harmonic signal in nanofabricated cones. *Nano letters*, *13*(12), 6048-6054

[2] Kalmutzki, M., Ströbele, M., Wackenhut, F., Meixner, A. J., & Meyer, H. J. (2014). Synthesis and SHG Properties of Two New Cyanurates: Sr3 (O3C3N3) 2 (SCY) and Eu3 (O3C3N3) 2 (ECY). *Inorganic chemistry*, *53*(23), 12540-12545.

Polarization of SERS scattered from near-field coupled gold nanowires excited with circularly polarized light

A. Foti[1, 2], *C. D'Andrea*[1,3], *B. Fazio*[1], *E. Messina*[1], *O. M. Maragò*[1], *M. C. Giordano*[4], *C. Martella*[4], *D. Chiappe*[4,5], *A. Toma*[4,6], *F. Buatier de Mongeot*[4], *P. G. Gucciardi*[1]

[1]IPCF-CNR, Istituto per i Processi Chimico-Fisici, Messina, Italy
[2]Scuola di Dottorato di Ricerca in Fisica, University of Messina, Messina, Italy
[3]Matis IMM – CNR, Catania, Italy
[4]Dipartimento di Fisica, and CNISM, University of Genova, Genova, Italy
[5]Laboratorio MDM CNR-IMM, Brianza, Italy
[6]Istituto Italiano di Tecnologia, Genova, Italy

e-mail: gucciardi@ipcf.cnr.it

Surface Enhanced Raman Scattering (SERS) from anisotropic nanoantennas (rods, gaps, tips and so on), is strongly dependent from the polarization state of both exciting and re-radiated field. The maximum SERS enhancement is expected when the exciting beam is linearly polarized along the hot-spot direction [1-4]. For this reason circularly polarized light, whose power density is equally split along two orthogonal directions, is probably not the best choice if we want to optimize the enhancement factor of our system. Nevertheless exciting a plasmonic linear system with light polarized in this way, could be useful to better understand the coupling between the molecule and nanoantennas and the amplification processes at the basis of SERS effect. It was demonstrated that SERS radiation scattered from randomly oriented molecules adsorbed on near-field coupled gold nanowires (NWs) is always polarized along the wire-to-wire nanocavity direction, independently from the incident field polarization [1,4].
Here we tailor the experiments to the same sample exciting with circularly polarized light at 633 nm (resonant with only the nanocavity mode). As expected the unpolarized SERS intensity shows no considerable variation as the sample rotate underneath the laser beam (Fig.1a). On the contrary, looking at the polarized SERS Intensity we observe a trend clearly proportional to $\cos^2\phi$ (red line in Fig.1b), where ϕ is the angle formed the optical axis of the analyser and the nanocavity direction. The maximum of the intensity is for ϕ=0, which means that the SERS radiation is polarized along the nanocavity direction (Fig.1b) in agreement with experiments performed with linearly polarized light [1]. Finally we compare the unpolarized SERS intensity scattered from NWs using the same wavelength and power density but different excitation configurations: the first is linearly polarized and parallel to the nanocavity direction and the second is circularly polarized. We find that the latter is not exactly the half of the former, as expected at a first glance, but it is slightly more intense. Modelling the enhancement process with wavelength-dependent field enhancement tensors we get the relations ruling the polarized and unpolarized SERS intensity dependence found experimentally. We also explain the additional signal obtained for unpolarized SERS using circular excitation in terms of the beyond E^4 model.

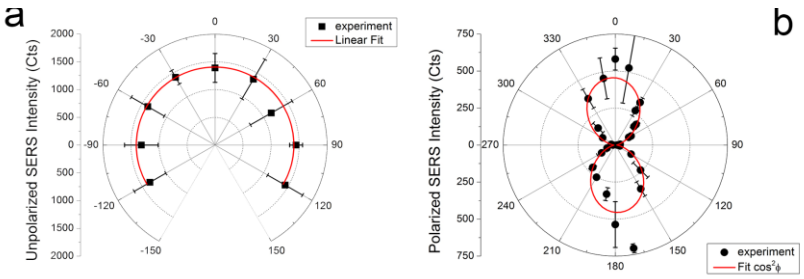

Fig. 1. Unpolarized SERS intensity trend as the sample is rotating under the circularly polarized laser excitation. (b) SERS intensity as a function of the angle ϕ between the optical axis of the analyzer and the nanocavity direction.

[1] B. Fazio et al., ACS Nano 5, 5945 (2011).
[2] C. D'Andrea et al., ACS Nano 7, 3522 (2013).
[3] C. D'Andrea et al., J. Phys. Chem. C 118, 8571 (2014).
[4] A. Foti et al., Nanospectroscopy 1, 26 (2015).

Characterization of spin-coated thin polymer films by optical spectroscopy

Alexei Meshalkin[1)], Diana Harea[1)], Oxana Iaseniuc[1)], Diana Shepel[2)], Liudmila Bets[2)]

[1)] Insitute of Applied Physics of Academy of Sciences of Moldova, Chisinau, Moldova
[2)] Institute of Chemistry of Academy of Sciences of Moldova, Chisinau, Moldova
5 Academiei str., MD-2028, Chisinau, Moldova, e-mail: dyanaharea@yahoo.com

Keywords: thin polymer films, spin-coating, optical constants, optical spectroscopy.

Introduction:
Polymer semiconductors are of wide interest for applications in electronics and optoelectronics, including light emitting diodes, thin film transistors, photovoltaic cells, and photoresists. Spin-coating is the primary process for the deposition of uniform thin and ultra thin films of polymers for these device applications. It is well known that the film thickness and refractive index play a critical role in optical applications. In this paper we report the deposition of thin polymer films of polyepoxypropylcarbazole (PEPC) by programmable spin-coating and evaluation of both the thickness and the refractive index of obtained films.

1. Motivation

A number of polymer materials have been investigated intensively for their potential applications in linear and nonlinear optical devices. Most polymer films under study were deposited by the spinning technique. Layer thicknesses between a monolayer and several micrometers are required depending on the research topic. For the optical study or application of a polymer thin film, information on thickness and optical constants refractive index and extinction coefficient is essential. Typically, the film thickness of spin coated photoresists or waveguide materials is in the range of several micrometers. However, spin-coated polymers for electronic or optoelectronic devices typically have a thickness in the sub-micron range. For example, the film thickness of conjugated polymers in light emitting diodes or photovoltaic cells is generally in the range of 50–200 nm. For such ultrathin films spin coated from dilute polymer solutions, there are just few prior studies of the spin-coating process. In this paper, we present the first experimental study of the spin coating process for the de position of thin films of carbazole-containing polymer polyepoxypropylcarbazole (PEPC). PEPC is one of the studied and widely used organic compound among carbazole containing oligomeric photoconductors [1].

2. Results and Discussion

PEPC was prepared by polymerization of monomer epoxypropylcarbazole at the presence of 1-3% potassium methylate on the anionic mechanism at temperature 80-120˚C within 2-6 hours. For the full drying they were stored in a vacuum drying chamber at 50˚C up to constant mass. Molecular weight was from 2000 to 3000.

The thin films based on synthesized polymer were prepared by spin-coating on a rigid glass substrate with the use of spin-coater SGS Spincoater G3P-8. The polymer was dissolved in toluene to form solutions of different concentrations (weight fractions of polymer). The concentration of polymer solution in toluene was varied from 2.5% upon to 12.5%. It was established that PEPC sensitized with photosensitizer CHI_3 showed high enough levels of photosensitivity to be useful in practical applications like recording media for holography [2]. Each polymer solution was spin coated onto a 5 cm glass wafer. The spin speeds were varied from 500 up to 7000 rpm, and the spin time was 20 s. The coated film was then dried at room temperature (20ºC) for 24 hours to remove the solvent completely.

The synthesized polymer was characterized by Fourier-transform infrared spectroscopy (FTIR). Ultraviolet–visible (UV–VIS) spectroscopy was used to determine the transmission profile of the PEPC films in the visible region. From the transmission spectra the thickness and refractive index were determined by method of fitting curves proposed by Swanepoel [3].

It was found that the thickness of spin-coated polymer layers was linearly depended on the solution concentration. The thickness can be varied from 170 nm up to 940 nm for the solution with concentration from 2.5% up to 12.5%. To confirm the validity of our method, we also carried out the interferometric thickness measurements and analysis with a thin film of PEPC. The difference of obtained results of two methods averaged not more than 5%. Refractive index determinations were performed in on all polymer films tested. The refractive index of the PEPC was measured on films from both pure polymer samples and with addition of CHI_3, using the Specord M40 (Carl Zeiss JENA. Every refractive index measurement taken for the pure PEPC film was 1.62, and with addition of 10% of CHI_3 lead to increase of refractive index up to 1.63. PMMA, in comparison, has a refractive index of only 1.49 [4].

Conclusions

Transparent thin films of polymer PEPC were produced using spin-coating technique from the toluene solution. It was shown the possibility of variation of PEPC film thickness by spin speed and solution concentration. The film thickness dependence on the concentration of solution is linear, but the spin speed doesn't lead to essential thickness variation. Therefore this linear dependence can be used to predict the film thickness of spin-coated

polymers if the solvent is known. The measured film thickness by transmission spectra of the PEPC polymer was found to be well correlated to the results of interferometric thickness measurement.

The refractive index of the polyepoxypropylcarbazole was 1.62, which was well above the refractive index of 1.49 for polymethylmethacrylate. It was found that the inclusion of even a small amount of a photosensitizer, such as CHI_3, was effective in producing of high refractive index material with enhanced photosensitivity properties with good optical properties compared to PMMA.

These experimental results provide a basis for understanding and optimizing the preparation of thin and ultrathin films of polymers by spin coating. Polymers with high refractive index have the potential to be used for optical applications. The optical properties of the polyepoxypropylcarbazole polymer can be used in a variety of commercial applications, including both traditional optics and non-linear optics.

References

[1] Grazulevicius J.V., Strohriegl P., Pielichowski J., Pielichowski K. Carbazole-containing polymers: synthesis, properties and applications. Prog. Polym. Sci. **28**, 2003, 1297-1353.

[2] Bivol V.V., Robu S.V., Prisacari A.M., Meshalkin A.Yu., Vlad L.A., Karaman M.I. Study of sensitometric and holographic properties of photoresist media based on carbazole-containing polymers sensitized with triiodomethane and pyran photochromic materials, High Energ. Chem+ **40**(3), 216 (2006).

[3] Swanepoel R. "Determination of the thickness and optical constants of amorphous silicon", J. Phys. E: Sci. Instrum., **16** (1983), 1214–1222.

[4] Seferis J.C. Refractive indices of polymers. In: Brandrup J, Immergut EH, Grulke EA, editors. Polymer handbook, 4th ed, vol. VI. New York: Wiley; 1999.

Label-Free Protein Detection on 3D Plasmonic Nanostructures using Surface-Enhanced Raman Scattering

Mehmet Kahraman[a] *Sebastian Wachsmann-Hogiu*[b],

[a] Department of Chemistry, Gaziantep University, Gaziantep 27310, Turkey
[b] Center for Biophotonics Science and Technology, University of California Davis, Sacramento, CA, 95817, USA.

**e-mail: mskahraman46@gmail.com*

Keywords: Label-free, Protein detection, plasmonic nanostructures, SERS

Introduction

Surface-enhanced Raman scattering (SERS) is a potential analytical technique for the detection and identification of chemicals and biological molecules and structures in the close vicinity of metallic nanostructures [1-3] with sensitivity down to single molecule [4]. Protein detection using SERS can be made using a label-free, direct approach, in which the spectra of the proteins of interest are measured, or using exogenous labels in the form of small molecules or Raman active groups that indicate the presence of those molecules of interest. Several studies have been reported regarding label-free detection of proteins and mixtures using various sample preparation methods and SERS substrates. However, improvements in sample preparation and SERS substrates are needed to obtain strong, sensitive, and reproducible SERS spectra for detection and identification of proteins. In this study, we report direct, label-free detection and identification of 6 proteins of interest via 3D plasmonic structures.

Results and Discussion

The structures are fabricated via soft lithography that yields bowl-shaped nanovoids with 1400 nm in diameter and 600 nm in depth. Figure 1 shows SEM images of the deposited latex particle on a glass slide (A) that is used as template to obtain nanovoids on the PDMS surface, Ag coated PDMS nanovoid structures (B). They carry no surface charge and provide more reproducible SERS spectra when compared with colloidal nanoparticles. This is particularly important for the detection of molecules that carry different charges and for the development of analytical assays. Visual inspection (Figure 2 A) and PCA analysis (Figure 2 B) reveal that the spectra of the 6 proteins are significantly different form each other, which demonstrate label-free, direct protein detection and characterization using this approach. Concentrations as low as 0.05 μg/mL were detected, with even lower concentrations measurements possible for higher laser power or more sensitive optical detection schemes.

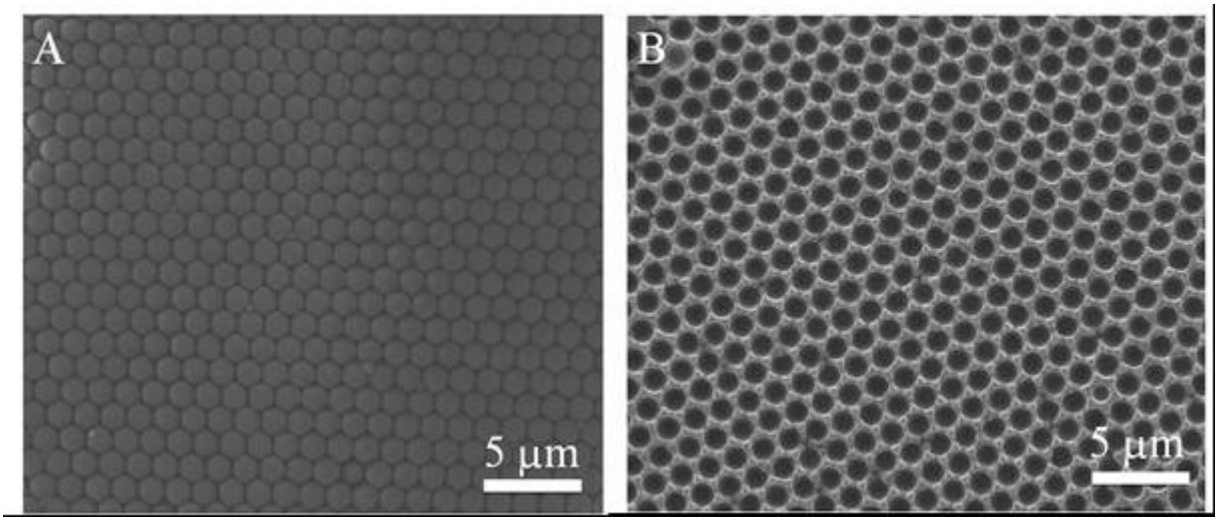

Figure 1: SEM images of deposited latex particle on a glass slide (A), Ag coated PDMS nanovoid structures (B),

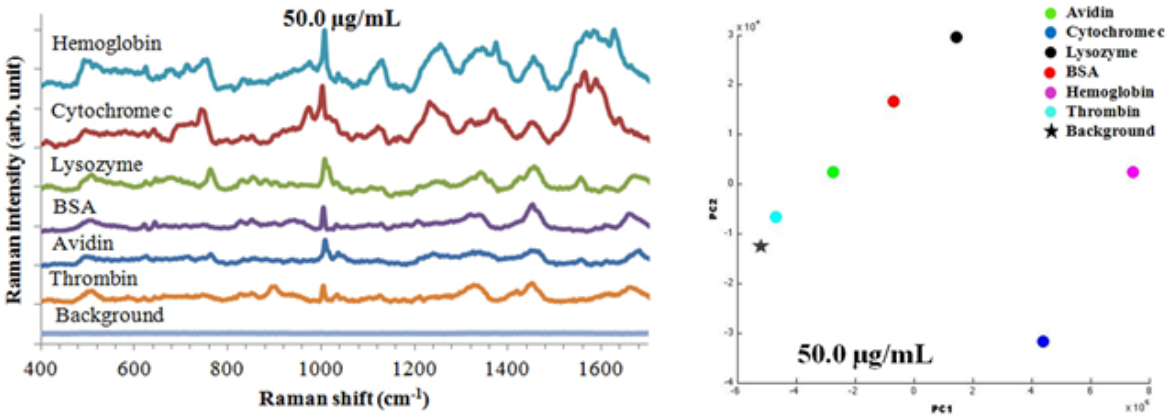

Figure 2: Comparison of SERS spectra of all proteins (50 µg/mL) used in this study (A), PCA scattering plots obtained from the SERS spectra of proteins.

Conclusions and/or Outlook

3D metallic structures were used for label-free detection and characterization of proteins. The nanovoids generated a SERS signal of the proteins of interest that is background free and independent of the protein charge.

Concentrations as low as 0.05 µg/mL could be detected for 6 different proteins. The proteins exhibited significantly different SERS spectra on these substrates, which is an important feature for future label-free direct detection approach. The approach can be also used for the quantification of proteins.

References:

[1] D. J. Jeanmaire, R. P. Van Duyne, J. Electroanal. Chem. 1977, 84, 1-20.
[2] M. Fleischmann, P. J. Hendra, A. J. McQuillan, Chem. Phys. Lett. 1974, 26, 163-166.
[3] M. G. Albrecht, J. A. Creighton, J. Am. Chem. Soc. 1977, 99, 5215–5217.
[4] S. Nie, S. R. Emory, Science 1997, 275, 1102-1106.

Fundamental parameter determination to improve spectroscopical methods

M. Kolbe[a*], P. Hönicke[a], M. Müller[a], B. Pollakowski[a], B. Beckhoff[a]

[a] Physikalisch-Technische Bundesanstalt, Abbestr. 2-12, 10587 Berlin, Germany
*e-mail: michael.kolbe@ptb.de

Keywords: spectroscopy, fundamental parameters, optical constants

Introduction

The analysis of spectroscopic methods requires in most cases the accurate knowledge of fundamental parameters (FP) and optical constants (OC) involved. One may note, that the respective uncertainties in one spectral range are influenced by those in complementary spectral ranges, as proposed by the Kramers-Kronig relation, thus one may profit by X-ray FP determinations when aiming at OC improvements. Different methods for FP determinations have been developed and validated, some of which offer the potential for OC determination extensions.

Results and Discussion

The Physikalisch-Technische Bundesanstalt operates two laboratories at synchrotron facilities in Berlin, Germany for metrological aspects. Therefore radiometrically calibrated instrumentation for photon detection is available over a broad spectral range from harder X-rays to visual and infrared radiation. This instrumentation is also used for advanced material characterization and facilitates in X-ray spectrometry the reference-free FP quantization approach.

In view of the lack of reference-materials and calibration samples, in particular at the nanoscale, reliable quantification schemes in X-ray fluorescence analysis and related methods call for higher accuracy of relevant X-ray fundamental parameters such as photoionisation cross sections[1,2], decay rates, line widths, and fluorescence yields[3], as well as Coster-Kronig and transition probabilities[4,5]. The presentation will summarize relevant results and new methodologies employed in recent X-ray fundamental parameter determinations.

Conclusions

Fundamental parameters become more and more important for quantitative analysis of spectroscopic results, where reliable reference materials are missing. The combination of complementary methods and spectral ranges allow the determination of these FP with reliable and lower uncertainties.

References:

[1] Hönicke P, Kolbe M, Müller M, Mantler M, Krämer M, Beckhoff B; Experimental Verification of the Individual Energy Dependencies of the Partial L-Shell Photoionization Cross Sections of Pd and Mo; Phys. Rev. Lett.; 113 (2014), 163001

[2] Ménesguen Y, Gerlach M, Pollakowski B, Unterumsberger R, Haschke M, Beckhoff B, Lépy MC; High accuracy experimental determination of copper and zinc mass attenuation coefficients in the 100 eV to 30 keV photon energy range; accepted by Metrologia

[3] Guerra M, Sampaio JM, Madeira TI, Parente F, Indelicato P, Marques JP, Santos JP, Hoszowska J, Dousse JCl, Loperetti L, Zeeshan F, Müller M, Unterumsberger R, Beckhoff B; Theoretical and experimental determination of L-shell decay rates, line widths, and fluorescence yields in Ge; Phys. Rev. A 92 (2015), 022507

[4] Kolbe M, Hönicke P, Müller M, Beckhoff B; L-subshell fluorescence yields and Coster-Kronig transition probabilities with a reliable uncertainty budget for selected high- and medium-Z elements; Phys. Rev. A 86 (2012), 042512

[5] Kolbe M, Hönicke P, Fundamental parameters of Zr and Ti for a reliable quantitative X-ray fluorescence analysis; X-Ray Spectrom. 44 (2015), 217–220

Fabrication of Phthalocyanine and Nanometal Based Heterogeneous Photocatalysts and Photocatalytic Applications

Aysun Korkmaz[a], *Mehmet Kahraman*[b], *Yusuf Yilmaz**[c]

[a] Department of Chemistry, Gaziantep University, Gaziantep 27310, Turkey
[b] NT Vocational School, Gaziantep University, Gaziantep 27310, Turkey

*e-mail: ysfyilmaz60@gmail.com

Keywords: Nanometal, Singlet oxygen, Phthalocyanines, Photocatalyst

Introduction

Phthalocyanines (Pcs) have been used as organic pigments for a long time. Nowadays, In addition to the traditional application of phthalocyanines, they have been used for several applications such as photodynamic therapy (PDT), photocatalytic and electrocatalyst studies. Photocatalyst based on Pcs are emerging molecules for the removal of pollutants harmful for human health and environment. The general purpose of this work is fabrication of pc based heterogeneous catalyst for the removal of organic pollutants. New thiolated Pcs were synthesized and attached to the gold or silver coated microparticles to fabricate heterogeneous catalyst. In this study tetraperiferal Pcs contain both bulky esteric groups (-$COOCH_3$) and functional -SH groups on positions was synthesized in the presence of corresponding metal salts ($MgCl_2$, $ZnCl_2$ and $GaCl_3$). Pc having the highest singlet oxygen quantum yield were selected after performing photophysical and photochemical measurement to attach to the surface of nanometal coated microparticles. The nanometal coated microparticles were used not only for improvement of the photocatalytic performance of Pcs but also to fabricate heterogeneous and recyclable photocatalysts.[1-3]

Results and Discussion

The synthesized Pcs molecules were successfully characterized by using several instrumental techniques such as UV/vis spectroscopy, NMR, and IR. The first step of the study was the determination of singlet oxygen production of the Pcs which is critical for photocatalytics and photodynamic therapy applications. For this purpose, photochemical properties of Pcs were measured and calculated to determine the highest singlet oxygen quantum yield to use for the photocatalytic studies. Recently, when Pcs are bound to the plasmonic nanoparticles surface, higher singlet oxygen quantum yield are obtained due to the heavy atom effect. The synthetized Pcs were covalently bound to the nanometal coated silica microparticles (core-shell) to fabricate novel hybrid inorganic nanomaterials to use as photocatalyst for removal of organic pollutants. The nanometal coated silica microparticles were characterized by using scanning electron microscopy (SEM). Then with a high amount of singlet oxygen production phthalocyanines esteric groups (-$COOCH_3$) amine (NH_2) connected with functional groups and bind to silica microparticle singlet oxygen were examined contributed to the production of silica Pcs. The metal coated silica microparticles was characterized using SEM-EDX to proof the presence of metal shell on the particles (Figure 1).

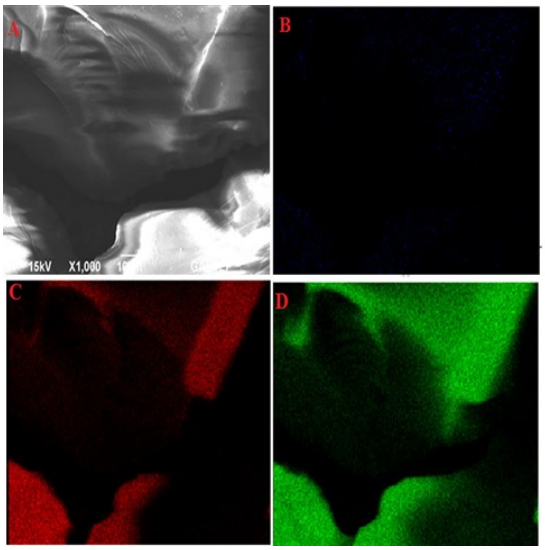

Figure 1: EDX mapping of silver coated silica microparticles, A) SEM image, B) Ag, C) O, and D) Si

The EDX mapping demonstrates that, the microparticles were successfully coated with silver layer. Figure 2 shows the photography of color changes from bare silver coated silica (a) to silver coated silica modified with Pcs(b).

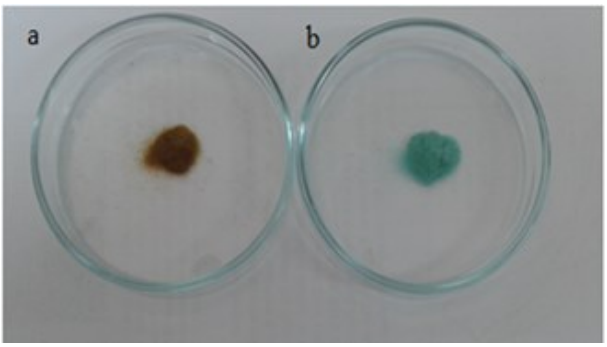

Figure 2: Photography of bare silver coated silica (a) and silver coated silica modified with Pc (b).

The color of silica coated microparticles modified Pcs were turned from brown to green due to the presence of Pcs on the microparticles which is evidence of the attachment of Pcs.

Conclusions and/or Outlook

The results demonstrate that new thiolated Pcs were successfully synthesized and attached to the nanometal coated silica micropartices. The fabricated nano-Pc hybrid nanomaterials will be used for the color removal from wastewater.

References:

[1] Ogunbayo, T. B., Nyokong, T. 2011. "Photocatalytic transformation of chlorophenols under homogeneous and heterogeneous conditions using palladium octadodecylthio phthalocyanine", Journal of Molecular Catalysis A: Chemical, 350, 49– 55.

[2] Modisha, P., Nyokong, T., Antunes, E. 2013. "Photodegradation of Orange-G using zinc octacarboxy phthalocyanine supported on Fe3O4 nanoparticles", Journal of Molecular Catalysis A: Chemical, 380, 131– 138.

[3] Sharma, R. K., Gulati, S., Pandey, A. 2013. "Polyfluorinated–zinc(II)phthalocyanine complex immobilized on silica: A novel, highly selective and recyclable inorganic–organic hybrid catalyst for the synthesis of biologically important 1,5-benzodiazepines", Inorganica Chimica Acta, 397, 21–31.

Spectroscopy characterization of polycarbonate variety Lexan 121R in composite thin films with cerium oxide nanoparticles

C. Larosa*[a], R. Praminick[b], S. Jegina[c] , Z. Zelca[c], S. Kukle[c] N. Bragazzi[d]

[a]Department of Surgical Science and Integrate Diagnostic University of Genoa, Italy and INBB
[b]Department of Polymer Science and Technology, Calcutta University, 92 Acharya Prafulla Chandra Road, Kolkata 700 009, India.
[c]Riga technical university, faculty of material science and applied chemistry institute of design Technologies, Kipsalas Str.6LV-1048,Riga, Latvia
[d]School of Public Health, Department of Health Sciences (DISSAL), University of Genoa, Italy

*e-mail: Claudio.Larosa@unige.it

Keywords: Polycarbonate, seed crystallization, cerium oxide nanoparticles, amorphous

Introduction

Polycarbonate (PC) is considered as an amorphous, robust, thermoplastic polymer with remarkable optical properties due to repetition of linear polyester of carbonic acid and dihydric phenol monomer in a free chain configuration, which confer rigidity to the structure.[1] The daily infringement of common solar light spectra within this thin polymer assembly, with transparency in the visible solar spectrum (value up to 70%), can be observed for window or roofs and many other applications. However, PC remains a soft material vulnerable to the effects of damage versus solar radiation and the introduction of nanoparticles may represent a valid solution to increase the shield to the u.v range and to retard effect of fragmentation and colour changes. Among metal nanoparticles, few lanthanide particles have properties to stabilize and screener this soft material from photo-initiated degradation.[2] Cerium oxide nanoparticles offer this quality and employ to reduce the effect of damage with an appropriate shield in the UV range and is currently used also as component for screen filter in catalyst or to smooth scratches from glass surface.[3] In more detail, the property to shield polycarbonate from UV radiation of solar spectra derive from electronic configuration of cerium with 4f level, which permit the transition to the 5d configuration of one active electron, which is generally a vacuum UV transition.[4] After this transition the depression in energy is substantial and was found to depend on the strength of the static field generated by the ionic near neighbours. If these interactions are strong enough, the 5d transitions may be shifted into the visible. During the particles nucleation an assembly of atoms was observed. A standard atoms number assembly in nano particles scale with a medium size of 28 ± 5 nm of diameter was dispersed in polycarbonate to obtain a final solution and by solution casting was deposit in a petri disk; evaporate and at the end, composite thin films with standard thickness of 1-2μ was emerging. The slower removal of chlorinates solvents in controlled humidity room from composite solution is a crucial step during the configuration of the amorphous state condition of transparent not crystalline thin film, which ensures transparency without opacity or translucent effects or remarkable changes from amorphous to crystal domain. In thin films, degradation was induced by an *u.v* lamp to simulate and accelerate photo- degradation to the air interface. Samples were characterized by spectroscopy absorption and infrared FTIR spectroscopy to evaluate the effect of damage by carbonate group shift in frequency and chains fragmentation. Atomic force microscopy was also used to characterize thin samples film with a so far not know unexpected data: cerium oxide nanoparticle induce a changing of state from amorphous to crystalline. Amorphous state is a predominant and common natural condition in polycarbonate were polycarbonate chains are present in a not limit space configuration, without restrict conditions of chain packages domine. Several ordinate crystalline domine is observed by optical microscopy characterization[5] as white spherulites shape but in a measure of 3 % of contents on the complete PC. This domine state of PC can be altered by prolonger heating of PC for a time of one week at low temperature. The introduction of cerium oxide nanoparticles in PC could irreversible altered the final configuration of polycarbonate chain by cluster network formation of long range between particles. A good degree of dispersion of particles in PC was achieved by using sonochemical method performed for 5 min. at medium frequency and limit power.

Result and discusses

Spectroscopy FTIR measurement on PC in Figure 1 is reported. In a) we report reference of PC and in b) the common absorption spectra of cerium oxide nanoparticles in the range of 300-600nm as an optical filter device shown. Is our interest to found the change of rigidity of the chain and atomic force microscopy was used to characterize thin film of PC/cerium oxide nanoparticles composite where at current time and at the best of our knowledge only in part this date was predict in literature and represent an unexpected data. In Figure 2 are reported four series of images acquired using AFM in tapping mode, using a silicon tip, where in the first image is shown the topography of polycarbonate films and in the second frame are reported naked cerium oxide nanoparticles with (cubic shape in a lattice) not well define but with estimate dimension of ~30 nm, which confirm the native dimension supply from dispenser and in the three image was reported dry film of PC where are shown cerium oxide

nanoparticles, while in image four are clear in evidence the effect of crystallization induced by the presence of cerium oxide nanoparticles. The effect of crystallization is well known in literature, starting from the first pioneer study on the films induced but solvent but also gold nanoparticles[6], acetone[7] or other complex ionic molecule such are surfactants.[8] May be the presence of particles in polycarbonate can induce a major and restrict packaging in the polycarbonate chain or can drive spherulites growing.

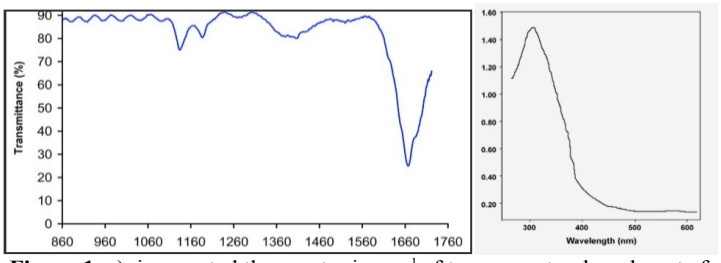

Figure 1. a), is reported the spectra in cm^{-1} of transparent polycarbonate from pellets while in b) absorption spectra of cerium oxide nanoparticles in chloroform.

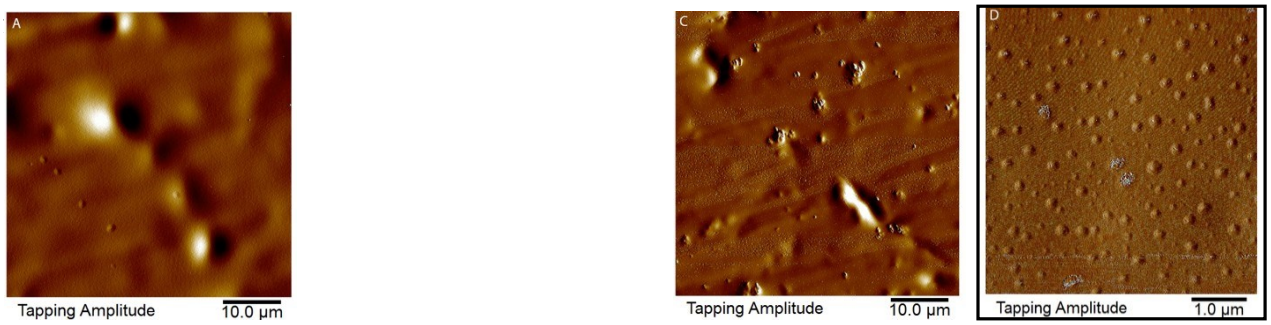

Figure 2. a), b), c), d) a) Polycarbonate thin film from a PC/chloroform solution 3% (W/V), b) cerium nanoparticles 1% in chloroform, c) composite films cerium oxide nanoparticles/polycarbonate in a ratio of 2 % (W/W). d) PC film consequence and induction of crystallization domine by using naked cerium oxide nanoparticles.

Acknowledgement

This work was performed in the Institute of Design Technologies of Riga in the Technical University under the supervisor of Prof. Silvija Kukle. We are deeply grateful for the financial support to perform a short temp scientific mission STSM in the COST action MP 1206 of electrospinning program. The authors are grateful to Dr. Erich Kny, chairman of the action, also for this possibility to discovery and to performed experiment in another country.

Conclusions

The crystallization is a transition state matter from amorphous to crystalline in a thermoplastic polymer where the native properties are amorphous with 1-2% of crystalline domine. An ordinate packaging state with ordinate domine could be induced by vapour solvent at low pressure or by using nanoparticles as seed naked particles of crystallization without a capping agent is here reported and discusses. The effects on the crystallization on PC have a random behaviour and appear uniformly distributed in the film. They appear as spherulites zone inside thin film of polycarbonate, and not derive doesn't a consequence to the slower or accelerate chlorinate solvent evaporation by using a humidity room controller. Cerium oxide nanoparticles certain play a role in the crystallization of thin polycarbonate film derived from a solution of three compounds.

References:

[1] Larosa C, Stura E, Eggenhöffner R, Nicolini C; Optimization of optical properties of polycarbonate film with thiol gold- nanoparticles; Materials; 2 (2009) 1193-1204;

[2] Siegmann A, Geil P H; crystallization of polycarbonate from the glassy state. Part 1 thin Films cast from Solution; J. Macromol. sci. phys.; 42; (1990) 239-272;

[3] Gu H, Soucek. M D; Preparation and Characterization of Mono disperse Cerium Oxide Nanoparticles in Hydrocarbon Solvents. Chem. Mater.; 19 (5); (2007) 1103–1110;

[4] Liu X, Zhou K, Wang L, Wang B, Li Y; Oxygen Vacancy Clusters Promoting Reducibility and Activity of Ceria Nanorods; J. Am. Chem. Soc., 131 (9); (2009) 3140–3141;

[5] Krzysztof K. K. Koziol , Dolgner k, Tsuboi N , Kruse J, Zaporojtchenko V, Deki S, Faupel F; Dispersion of Gold in Polycarbonate by Vapour-Induced Crystallization; Macromolecules; 37 (6); (2004) 2182–2185;

[6] Von Falkai Bv, Rellensman W. Kristallisation von polycarbonaten II. Dilatometrische untersuchungen an poly-4,4 - dihydroxidiphenyl- 2,2-propan-carbonat. Makromol Chem; 88(1); (1965) 38–53;

[7] Mercier J P, Groeninckx G, Lesne M. Some aspects of vapour-induced crystallization of polycarbonate of bisphenol A: polymer Simposia; 16, (4) (1967) 2059–2067;
[8] Suldarajan P R, Singh S, Moniruzzaman M; Surfactant-Induced Crystallization of polycarbonate, macromolecules; 37 (2004) 10208-10211;

Cantilever with pyramidal gold tips for tip-enhanced Raman spectroscopy

M. Martina[ab*], *C.J. Burkhardt*[a], *M.Fleischer*[b]

[a] NMI Natural and Medical Sciences Institute at the University of Tübingen, 72770 Reutlingen, Germany
[b] Eberhard Karls University Tübingen, Institute for Applied Physics, 72076 Tübingen, Germany

**e-mail: manuel.martina@nmi.de*

Keywords: AFM cantilever, tip-enhanced Raman spectroscopy, template stripping, carbon

Introduction

Raman spectroscopy allows us to investigate the chemical composition, the mechanical properties such as stress and strain, the crystallinity and the doping of a broad variety of materials. Yet, the cross-section of Raman scattering is in the range of 10^{-29} cm² to 10^{-30} cm² for non-resonant molecules and thus low compared to Rayleigh scattering and fluorescence. This causes difficulties when investigating not bulk but ultra-thin layers or surfaces of materials. Furthermore, the lateral resolution is typically limited by the excitation laser spot size, and only some hundred nanometres resolution can be achieved.

A promising approach to overcome these limitations is tip-enhanced Raman spectroscopy (TERS). Here, the sample surface is approached by a metallic tip using a scanning probe microscopy feedback mechanism. By focusing the excitation laser on the probe, a localised surface plasmon at the tip or surface plasmon polaritons guided to the tip form a 'hotspot'; a strong and localised electrical field. Using these techniques, Raman enhancement of several orders of magnitude and resolution defined by the tip size can be achieved.

For the fabrication of such tips several methods have been proposed over the last years. Probes for scanning tunnelling microscopy (STM) or shear force microscopy are mainly fabricated by the electrochemical wet etching of gold or silver wires. TERS Probes for atomic force microscopy feedback (contact mode, tapping mode) are fabricated by coating commercially available cantilever tips with metal, either by sputter deposition or evaporation.

We present a metal moulding process for the fabrication of TERS cantilevers, which has already been used successfully to fabricate wire based TERS STM probes.

Materials and Methods

A <100> silicon wafer is coated with a 600 nm thick silicon oxide mask layer, and openings of $(20\ \mu m)^2$ are structured using optical lithography and dry etching, as depicted in **Figure 1**. Pyramidal pits are produced by anisotropic wet etching in potassium hydroxide, and oxidization is performed in an oven under oxygen atmosphere. A 200 nm thick gold / chromium layer and afterwards a 3 µm thick layer of silicon nitride are deposited. Using optical lithography and dry etching, cantilevers are structured. Finally, a 500 µm thick SU-8 chip layer is spin coated and structured by lithography, and cantilevers are released using 1% HF.

Results and Discussion

Following the described process, cantilevers for tip-enhanced Raman spectroscopy were fabricated in batches. Tip radii, metal surface topography and defects were investigated using scanning electron microscopy (SEM). We found that our cantilever tips exhibit the same properties as TERS STM probes fabricated by us in the past using a similar approach and a comparable performance is expected.

Deploying the fabricated cantilevers, TERS was performed in a coupled AFM/Raman setup using 633 nm excitation on samples with a gold surface functionalized in 10^{-6} M MGITC solution, a Raman resonant dye molecule. Additionally, TERS measurements have been performed on isotopically labelled graphene and ultra-thin carbon layers.

Conclusions and/or Outlook

We present a batch process for the reproducible fabrication of cantilevers with tips suitable for tip-enhanced Raman spectroscopy. These cantilevers have been characterized by SEM and have been used in a combined AFM/Raman setup for TERS.

In the future, we want to fabricate cantilevers with pyramidal tips out of silver and aluminium to allow for TERS with 532 nm excitation. Also, we want to further investigate ultra-thin carbon, parylene and polyimide layers and promote TERS as a valuable tool for surface science.

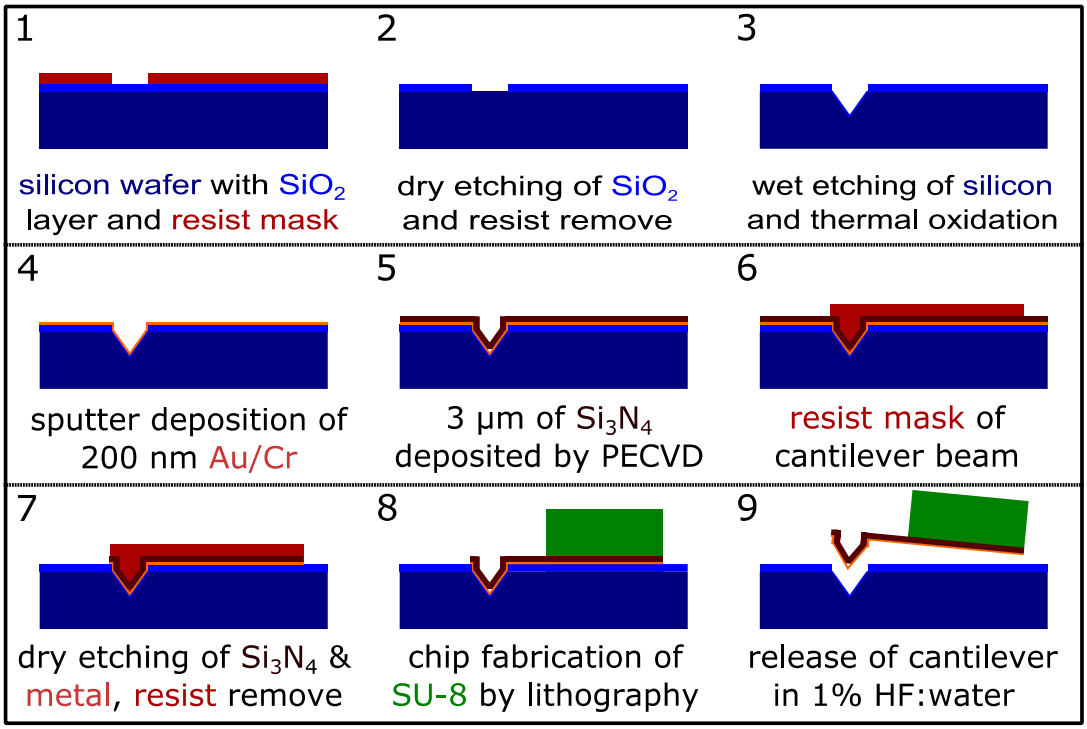

Figure 1: Process scheme for the fabrication of TERS cantilevers with a metal moulding process

Ellipsometric investigation of the interaction and splitting of surface and localized plasmons.

T. Mishakova[a]*, *E. Bortchagovsky*[b]

[a] Institute of High Technology, Taras Shevchenko National University of Kiev, Volodymirska str.64, Kiev 01601, Ukraine

[b] Institute of Semiconductor Physics of the National Academy of Sciences of Ukraine, pr.Nauki 41, Kiev 03028, Ukraine

e-mail: mishakov@e-mail.ua

Keywords: surface plasmon, localized plasmon, Rabi splitting, ellipsometry

Introduction

It is well known that two interacting resonances hybridize and split producing energy gap between two hybridized modes instead of two independent resonances. Different parameters of interacting systems play role in the determination of such a splitting. The most popular system for the investigation of such an interaction is a molecular layer on the surface of a metal supporting surface plasmon [1]. Regulating the distance between the layer with molecular exciton and the surface allows to control the strength of the exciton-plasmon interaction. However bleaching and no possibility to regulate parameters for chosen molecules restrict the flexibility of such investigations. The exchange of the layer of molecules by nanoparticles possessing localized plasmon makes such a system more convenient for investigations. Possibilities to manage parameters of localized plasmon by size, shape and the concentration of nanoparticles opens new perspectives for such a task.

Spectroscopic investigations of such a system were already reported [2]. In the present work we used ellipsometry to check plasmonic interactions. Ellipsometry is a method, which allows to register plasmon resonance position and to monitor not only amplitude but phase information too. The latter is important for the reconstruction of the whole picture of the interaction and splitting as well as allows to obtain information about near-field local interactions from parameters of far field.

Results and Discussion

Obtained results clearly demonstrate splitting of resonances and different effectiveness of the energy transfer at different angles of incidence. One example is shown in Figure 1.

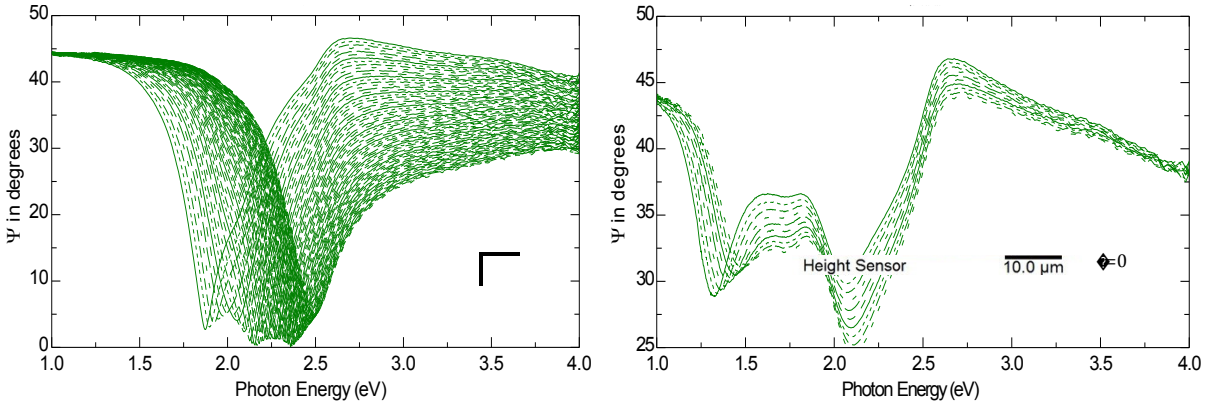

Figure 1: Spectral behaviour of ellipsometric angle Ψ for the system with deposited nanoparticles measured at internal reflection with the excitation of surface plasmon at different angles of incidence.

It is well seen the existence of few optimal conditions for the total transfer of the energy of p-polaeized radiation to the system of interacting surface and localized plasmons. More over, exceeding of the ellipsometric angle over 45^0 indicates decreasing of the intensity of s-polarizad radiation after reflection, what may be attributed to the excitation of localized plasmon laterally along the surface.

Panel "b" of **Figure 1** shows only few curves of the angle Y, which clearly demonstrates the existence of few resonances. So the behaviour visible in the panel "a" is produced by not the "standard" curve with one minimum but the curves with complex shape.

Another parameter influencing the registered behaviour is the interparticle interaction. Example for divverent surface coverage of particles with the diameter of 50 nm is shown in **Figure 2**.

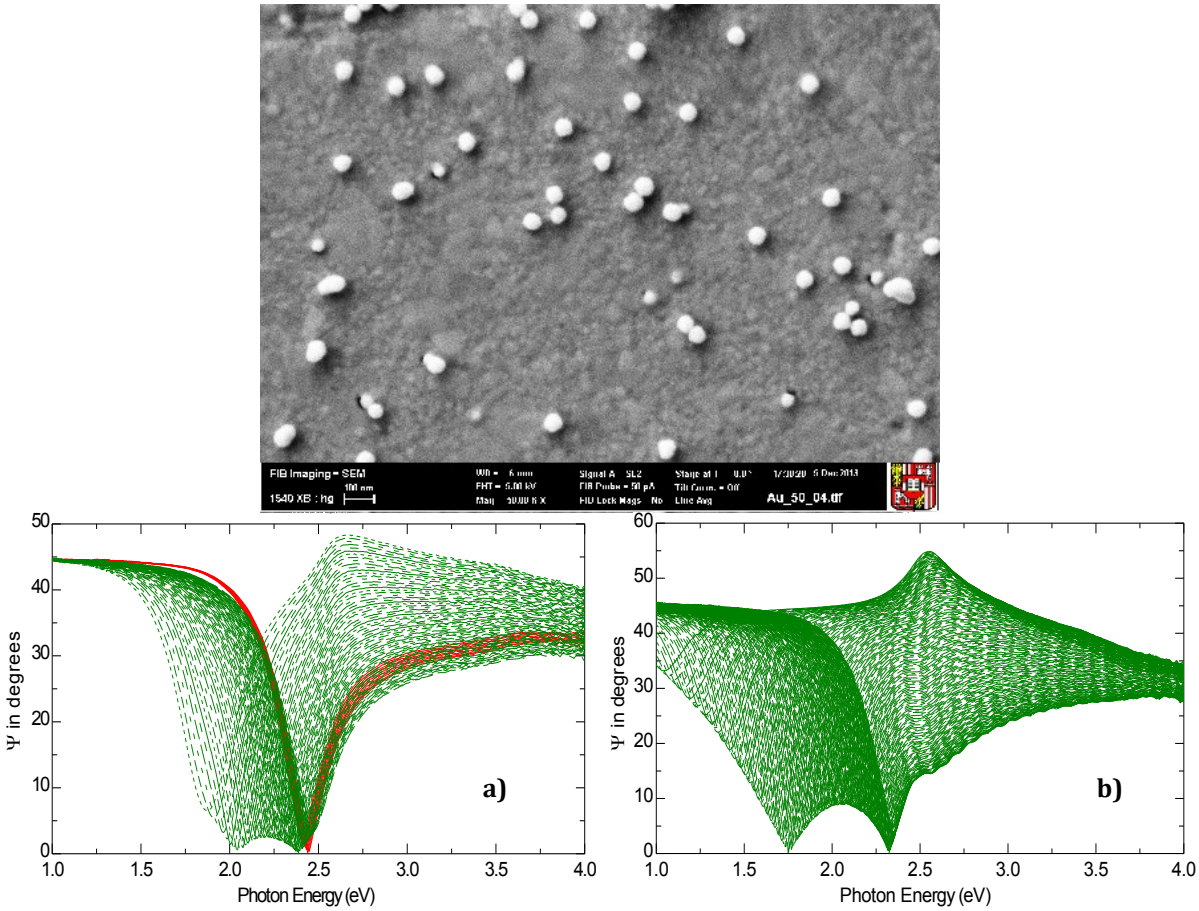

Figure 2: Spectral behaviour of ellipsometric angle Ψ for the system with deposited nanoparticles of the diameter 50 nm shown in upper panel measured at internal reflection with the excitation of surface plasmon at different angles of incidence for different surface coverages. Red – dependences for clean gold surface.

Electron microscopic picture of the surface with deposited spherical nanoparticles of the diameter of 50 nm is demonstrated together with the behaviour of ellipsometric angle for two different surface coverages. On the panel "a" the behaviour for the clean gold surface is shown by red.

Conclusions and/or Outlook

Ellipsometry is the relevant method for the registration of surface plasmon [3] and interparticle interactions [4]. It is demonstrated that it has high potential in the investigation of the splitting of different plasmonic resonances. Providing additional phase information, which is not shown here, its method supplies more rich information about the object of investigations. It should reveal additional details of the plasmonic interactions. We also hope the simultaneous registration of amplitude and phase characteristics of resonances would allow to reveal the spectral shift between near-field and far-field resonances.

References:

[1] P. Törmä and W.L. Barnes, "Strong coupling between surface plasmon polaritons and emitters", Rep. Prog. Phys. **78** (2015) 013901-1-34.

[2] A. Rueda, M. Stemmler, R. Bauer, Yu. Fogel, K. Müllen, and M. Kreiter, "Localized plasmons seen by propagating surface plasmons: unique determination of their dielectric response", J Phys Chem C **112** (2008) 14801-14811.

[3] E. G. Bortchagovsky, "Possibilities of ellipsometry with the surface plasmon excitation in the investigation of thin films in comparison with separated ellipsometry and surface plasmon spectroscopy", SPIE Proc. **3094** (1997) pp.239-249.

[4] E. G. Bortchagovsky, T. O. Mishakova, and K. Hingerl, "Ellipsometry of monolayers of metallic nanoparticles taking into account depolarization", Thin Solid Films **571** (2014) pp.625-630.

Influence of silver nanoparticle clusters on photoluminescence of single- and few-layer MoS_2

U. Ralević*[a], G. Isić*[a], M. Musić[a], U. Bogdanović[b], V. Vodnik[b], R. Gajić[a]

[a]Center for Solid State Physics and New Materials, Institute of Physics, University of Belgrade 11080 Belgrade, Serbia
[b]Vinča Institute of Nuclear Sciences, University of Belgrade

P.O. Box 522 Belgrade, Serbia

*e-mail: uros@ipb.ac.rs, isicg@ipb.ac.rs

Keywords: silver nanoparticles, molybdenum disulfide, Raman spectroscopy

Introduction

Monolayers of semiconducting transition metal dichalcogenides (TMDs), such as molybdenum disulfide, exhibit encouraging light-emitting and nonlinear optical properties at visible frequencies. This means that TMDs have a high potential for use in future ultracompact active and nonlinear optical devices [1], provided an efficient light coupling mechanism is arranged. A possible approach to enhance the light-matter interaction in TMDs is the use of noble metal nanostructures [2] which can confine light to extremely small volumes via the excitation of localized surface plasmons. Here, we use Raman and photoluminescence (PL) spectroscopy to investigate the influence of the spherical citrate capped nanoparticle (NP) clusters, on light emitted from single- and few-layer MoS_2 excited by a 532 nm laser.

Results and Discussion

Figure 1(a) shows the PL map of the pristine MoS_2 sample where the color quantifies the average PL intensity over the 550 nm - 700 nm spectral window. The pristine MoS_2 flake consists of parts having a different number of layers, as seen from the optical microscopy image in the **Figure** 1(a) inset. The number of layers can also be inferred from the intensity of the PL spectra: thinner flakes have larger PL, see **Figure** 1(b), and also from the relative position of the two characteristic Raman modes, see **Figure** 1(c), with respect to each other: thinner flakes have the two modes closer to each other than thicker ones. We find that the bright red area in **Figure** 1(a) represents single-layer MoS_2, while the dark red and blue areas represent the bi- and tri- layer MoS_2, respectively. The PL exhibits two peaks, corresponding to the A and B excitons of MoS_2.

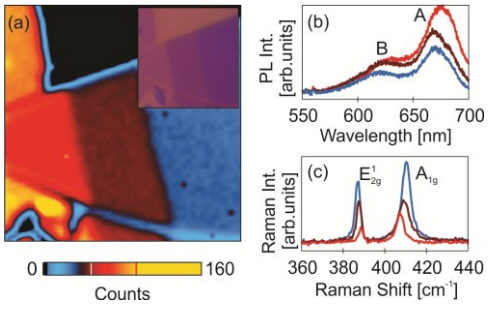

Figure 1: (a) Raman maps of the pristine MoS_2. Optical microscope image of the MoS_2 is shown in the inset. (b) PL spectra of the pristine MoS_2. (b) Raman spectra of the pristine MoS_2. The excitation wavelength is 532 nm.

Figure 2(a) displays a PL/Raman map of MoS_2 covered by citrate capped silver NP clusters. This map is obtained under same conditions as the one in **Figure** 1(a). Bright areas in **Figure** 2(a), i.e. the hot spots, represent the regions of enhanced PL/Raman signal. The hot spots are formed within the clusters consisting of a large number of NPs with diameters in the 10-50 nm range. **Figure** 2(b) shows PL/Raman spectra acquired at the hot spots in **Figure** 2(a) located on the single-, bi- and three- layer MoS_2. The sharp spectral features in regions I and II originate from the citrate ion vibrational modes boosted by means of surface-enhanced Raman scattering (SERS). The MoS_2 B peak falls in region II but is being masked by citrate ion Raman signatures. Meanwhile, the MoS_2 A peak is easily distinguished in region III (650-700 nm), except in case of high intensity hot spots when it becomes masked by the wide PL background of the NPs. At first glance, the PL/Raman spectra looks as if the SERS signals of citrate ions on the surface on NPs are added to the PL of MoS_2. A comparison of the spectra collected at different points on and in the vicinity of the hot spots, see **Figure** 2(c), however, reveals that, apart from the signal mixing, the MoS_2 A peak is enhanced by

factors of 1-1.5. The spectral position of the A peak does not change regardless of how thin MoS2 is, under these conditions.

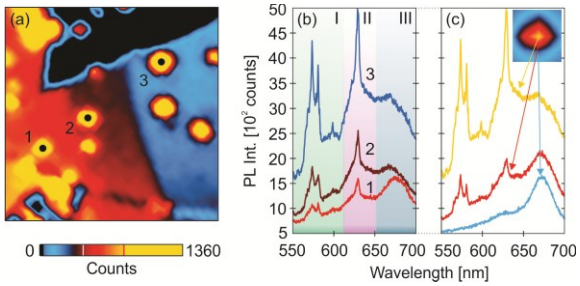

Figure 2: (a) PL/Raman maps of the MoS_2 after deposition of the citrate capped silver NPs. (b) PL/Raman spectra acquired within three different hot spots marked by 1, 2 and 3 in panel (a). (c) PL/Raman spectra acquired at different positions within one of the hot spots which is shown in the inset. The excitation wavelength is 532 nm.

In order to explain the origin of the enhancement, we show the linear enhancement factor (colormaps), $|\mathbf{E}|/|\mathbf{E}_0|$, and the corresponding electric field (red arrows), **E**, of an isolated and two closely spaced silver NPs on a dielectric substrate upon illumination by a plane wave, $\mathbf{E}_0\exp(-i\omega t)$, in **Figure** 3. The diameter of NPs is 10 nm, and the excitation wavelength is 532 nm. The angle of incidence is 45° and the wave is linearly polarized along the NP 'dimer' in **Figure** 3(b).

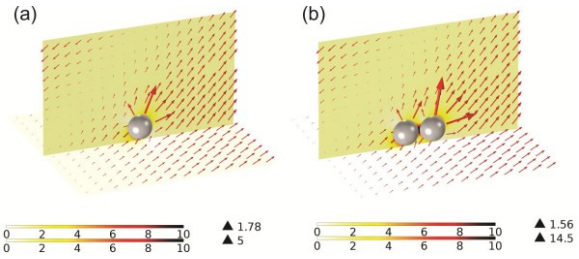

Figure 3: Linear enhancement factor for (a) a single silver NP and (b) a silver NP dimer on a dielectric substrate upon illumination by a plane wave having a wavelength of 532 nm.

As it can be seen, even an off-resonance excitation of the NPs leads to formation of the hot spots in between closely spaced NPs. Large NP clusters are expected to have even higher enhancement factors, with hot spots formed also in between closely spaced NPs. In fact, the enhanced citrate ion Raman signal, which we see in our experiments, most probably comes from the citrate ions located between the Ag NPs. Furthermore, the enhancement factors are large in the vicinity of the NPs surface, exactly where the electric field is larger, as it can be noted by observing **Figures** 3(a) and 3(b). While the values of the enhancement factor play an important role, in case of MoS_2 one needs to consider the electric field distribution as well. Optically thin 2D materials, such as MoS_2, are responsive only to the optical fields having the electric field parallel to their plane. The electric field at the surface of the NPs has a large component normal to the surface of the NPs and a small component lying in the plane of the substrate, as it can be seen in **Figures** 3(a) and 3(b). Therefore, we conjecture that the small in-plane electric field component is responsible for the enhancement of the PL A peak which we observe in our experiments.

Conclusions and/or Outlook

The PL/Raman spectra of NP clusters on MoS2 exhibits spectral features corresponding to the surface-enhanced Raman modes of the citrate ions and to photoluminescence of a pristine MoS2 layer. Comparable intensities of the Raman and PL signatures in these spectra, and the spectral stability of the exitonic A peak in the presence of NP clusters indicate mixing between the two signals. However, analysis of the Raman spectra acquired on and in the vicinity of the individual hot spots shows the enhancement of the MoS2 PL A peak by factors of 1-1.5, suggesting that the electric fields of NP clusters interact with the underlying MoS2. Employing finite element based rigorous simulations on a simplified-model system we have demonstrated that, indeed, the NP cluster in- plane electric field component plays crucial role in the enhancement of the MoS2 PL spectra. The weak enhancement is, thus, due to weak in-plane electric field which is also unable to change the spectral position of the A peak.

References:

[1] Xia F., Wang H., Xiao D., Dubey M., Ramasubramaniam A.; Two-dimensional material nanophotonics; Nature Photonics; 8 (2014) 899-907

[2] Eda G., Maier A.S.; Two-Dimensional Crystals: Managing Light for Optoelectronics; ACS Nano; 7 (2013) 5660–

Fabrication of mercaptoethanol-capped CdS nanoparticles: synthesis optimization and bio-imaging applications

*G.Yu. Rudko**[1], V.I. Fediv[2], I.S. Davydenko[2], E.G.Gule[1], O.I.Olar[2], A.O. Kovalchuk[1]*

[1]V. Lashkaryov Institute of Semiconductor Physics of National Academy of Sciences of Ukraine, 45, Pr. Nauky, Kiev, 03028, Ukraine
[2]Department of Biophysics and Medical Informatics, Bukovinian State Medical University, 42 Kobylyanska st., 58000, Chernivtsi, Ukraine.

e-mail: g.yu.rudko@gmail.com

Keywords: Nanoparticles,bio-imaging, mercaptoethanol,CdS, luminescence.

Introduction

Rapid development of nanoparticles (NP) fabrication techniques opens vast possibilities of their applications in various fields. Among these fields the bio-imaging domain is recently in the focus of technologists' interest because NPs have several important advantages as compared to the organic dyes that are traditionally used for the visualization of biological tissues in fluorescence microscopy (broad band of absorption, tunable color of the emitted light, long-term photo-stability, and improved contrast). The progress in designing new nano-tools for of biomedical diagnostics sets the task of well-grounded theoretical substantiation for the parameters and procedures of NPs fabrication [1].

The present report deals with the detailed analysis of fabrication conditions and synthesis procedures targeting to produce capped NPs for visualization of biological tissues. The recommendations obtained as a result of this analysis are successfully applied for fabrication of visible light-emitting NPs; their suitability for bio-imaging is proved by visualization and identification of morphological features of the chorial villi and extravillous structures of placenta.

Results and Discussion

NPs for biological applications have to meet the demands of low toxicity and bio-compatibility. The frequently used light-emitting A^2B^6 NPs (CdS, CdSe) contain cadmium ions which tend to bind to thiol groups of certain bio-molecules; thus, they can cause significant damage [2]. To avoid harmful action of cadmium on the biological objects we fabricated the capped NPs. For capping we choose 2-mercaptoethanol [$HS-(CH_2)_n-OH$]. The molecules of this chemical compound contain thiol (–SH) groups at the molecule terminus. It is this sulfur group, which adheres to Cd ions in NPs and prevents binding of Cd ions to bio-molecules in a tissue studied. Another important aspect of capping with mercaptoethanol is the enhancement of the colloid stability.

To optimize NPs fabrication conditions we theoretically analyzed the chemical reactions probabilities under the conditions of variable concentrations of precursors and pH value of the growth solution. We started with calculating the content of the ionic species being the products of dissociation and hydrolysis reactions of precursors in the growth solution. The content of the following ions was analyzed: the products of Na_2S dissociation – ions Na^+, S^{2-} and the products of their subsequent hydrolysis in water – ions H_2S, HS^-, S^{2-}; the products of $CdCl_2$ dissociation – ions Cd^{2+}, Cl^-, and, respectively, the products of hydrolysis – $Cd(OH)^+$, $Cd(OH)_2^0$, $Cd(OH)_3^-$. To calculate the mole fractions of the hydrolysis products in the growth solution depending on the medium pH, we have analyzed the material balance equations for cadmium and sulphur. Based on these considerations we deduced the conditions that provide the most favorable multi-component ensemble of chemical species in the solution: the rationalized composition of the growth medium ensures the dominating of the reaction of CdS NPs formation and suppresses all other possible reactions that could yield undesirable compounds.

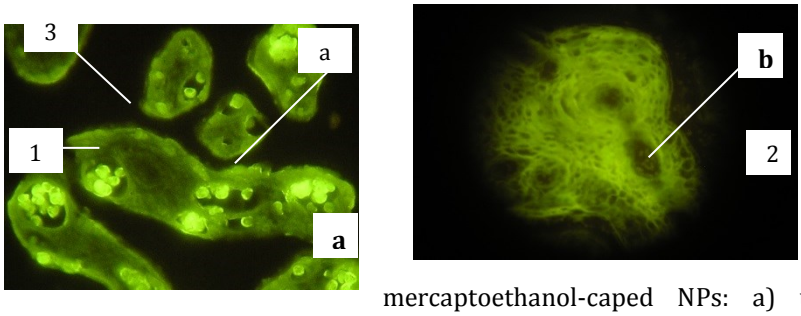

Fig.5. Microscopic images (a,b) of histological sections of placenta tissue dyed using mercaptoethanol-caped NPs: a) unaltered human

placental terminal villi; b) human intermediate stem villus with artery and vena and rough collagen. The identified cellular forms are: 1 – trophoblast, 2 – endotheliocyte, 3 – erythrocytes.

We synthesized the mercaptoethanol-capped CdS NPs by colloidal synthesis route using the optimized values of the precursors concentrations and pH. The NPs thus fabricated show bright visible emission under UV excitation. They were used for dyeing of the fixed histological sections of human placenta. Fig.1 shows the fluorescence microscope image of histological sections of placenta tissue.

Conclusions

The theoretical analysis of the content of the mole fractions of various ionic species being the products of dissociation and hydrolysis reactions with precursors in the growth solution was done. Based on the analysis of chemical reaction probabilities and material balance equations for cadmium and sulphur ions we found out the ranges of optimal parameter values for successful fabrication of NPs suitable for bio-imaging. Application of NPs for dyeing the histological samples of placenta demonstrated possibility to analyze characteristic cellular forms of placenta, such as erythrocytes, syncytiotrophoblasts and endotheliocytes

References:

[1] Drbohlavova J, Adam V, Kizek R, Hubalek Y: Quantum Dots — Characterization, Preparation and Usage in Biological Systems. Int J Mol Sci 2009, 10:656-673.
[2] Walling M, Novak J, Shepard J: Quantum dots for live cell and in vivo imaging. Int J Mol Sci 2009, 10:441-491.

Ultra–fast carriers relaxation in bulk silicon following photo–excitation with a short and polarized laser pulse

Davide Sangalli[1, 2] *and Andrea Marini*[1, 2]

[1] Istituto di Struttura della Materia of the National Research Council,
Via Salaria Km 29.3, I-00016 Montelibretti, Italy

[2] European Theoretical Spectroscopy Facilities (ETSF)

The development of ultra–short laser pulses has opened the opportunity to in- vestigate the dynamics of electrons on the *fs* time–scale (1 *fs* = 10^{-15}*seconds*). After the photo–excitation with such lasers pulses, electrons are in a regime which is highly out–of–equilibrium. Here we present a novel numerical ap- proach, based on the merging of the out–of–equilibrium Green's function method with the *ab–initio* Density–Functional–Theory, to describe this regime in semi–conductors. Silicon is used as reference material to show the physical process involved. The simulations are also compared with recent two photon photo–emission measurements. We show that different processes take place:

(i) scattering between degenerate states, that is activated by the symmetry breaking induced by the external field, (ii) $L \rightarrow X$ inter–valley scattering, and, finally, (iii) the relaxation towards the termal equilibrium.

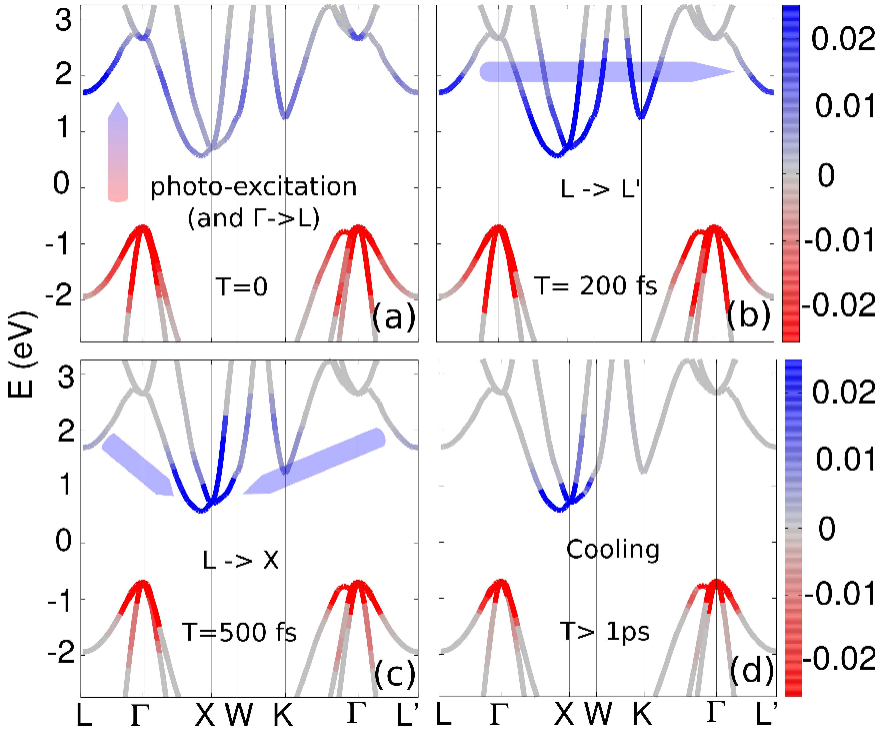

Time-snapshots of the carriers occupations of the entire band structure taken at times t = 0, 200, 500 fs and t > 1 ps. In each snapshot the arrows schematically represent the dominant channel that drives the dynamics. The initial excitation is followed by an ultra-fast $L_1 \rightarrow L'$ transition. Then the slower $L_1 \rightarrow X_1$ channel will fill the surroundings of CBM that, locally, will be populated with an high temperature Fermi distribution. Finally, on a longer time-scale, this distribution will be cooled down and the energy transferred to the lattice. Image from Europhys. Lett. 110, 47004 (2015).

Pencil Drawn Mono- And Few Layer Graphene/Graphite Layered Structures On Any Substrate

G. Shmavonyan, A. Mailian

Department of Microelectronics and Biomedical Devices, National Polytechnic University of Armenia, 105 Teryan street, Yerevan, 0009, Armenia

A non-conventional rubbing method of obtaining mono- and few layer graphene/graphite structures on any substrate is suggested. The samples were prepared by repeatedly rubbing a parent graphite rod along the same path upon the surface of different insulating (paper, ceramic, glass, plastic) and semiconducting substrates. The graphene/graphite layered structure and properties of the obtained rubbed-off material are investigated by optical microscopy, atomic force microscopy, scanning and transmission electron microscopy, as well as Raman spectroscopy. The observed phenomenon is universal, does not depend on the material of the substrate and could find a widespread application.

The interest toward the physical properties of graphite thin films increased in recent past following the discovery of fascinating properties in graphite single layers - graphene. Few-layer graphene is a unique material with its own potential for device applications.[1] Therefore, more and more attention is turned to few-layer graphene [2,3]. The expected next step should be attaining selective conductivity, providing, at the same time, high electronic qualities by modifying electronic band structure of few-layer graphene.

A rubbing method of obtaining self-organized few-layer graphene sheets on graphite structures is suggested. Layered structures are obtained by a method of rubbing a bulk graphite rod onto an insulating substrate. As the whole structure obtained on printing paper by this method exhibits physical properties of a highly layered semiconducting material, the topmost layer contains self-organized few-layer graphene sheets due to repeated manipulation of combined compressing-transferring-cleaving of flakes. It is found that the structure, as well as the topmost layer exhibits peculiar physical properties: a) the top layer is ordered stacked and crystallographically oriented perpendicular to the surface of the structure, b) the carrier mobility is anisotropic through the thickness of the structure with the highest value at the top of the structure.

The discovered regularities and observations testify to mono- and few layer graphene/graphite structure promising to obtain a critical importance in achieving selective conductivity and high carrier mobility in the graphite/graphene system. The method allows easily obtaining graphene with pencil directly on paper, as well as graphene-based electronic components and circuits on paper and other substrates, which could enable flexible and cheap electronics.

References

1. Bunch J.S., Yaish Y., Brink M., Bolotin K., McEuen P.L. *Nano Letters* **5**, 287, (2005).
2. Shmavonyan G., Mailian A., Mailian R. The 10th International Conference on Nanosciences & Nanotechnologies (NN13), Abstract book, p. 280, July 9-12, 2013, Thessaloniki, Greece.
3. Mailian A., Mailian R., Shmavonyan G. The 10th International Conference on Nanosciences & Nanotechnologies (NN13), Abstract book, p. 53, July 9-12, 2013, Thessaloniki, Greece.

Confocal spectroscopy of GaN/InGaN core-shell multiple quantum wells on self-organized GaN rods

G. Tamulaitis*[a], D. Dobrovolskas[a], A. Vaitkevičius[a], H. Svidras[a], B. Foltynski[b], C. Giesen[b], M. Heuken[b]

[a] Semiconductor Physics Department and Institute of Applied Research, Vilnius University, Sauletekio 9-III, 10222 Vilnius, Lithuania
[b] AIXTRON SE, Kaiserstr. 98, 52134 Herzogenrath, Germany

*e-mail: gintautas.tamulaitis@ff.vu.lt

Keywords: InGaN, self-organized nanorods, multiple quantum wells, confocal luminescence spectroscopy

Introduction

The last two decades of development made the InGaN-based light emitting devices widely available for various optical applications including general lightning. However, the growth of high-quality InGaN structures is still hampered by a large density of defects that originate inside the structures mainly because of the absence of suitable substrates for homoepitaxy. As a result, the efficiency of the InGaN-based light emitting diodes (LEDs) is far from its physical limits. Therefore, a qualitatively different approach is needed to overcome the current technological limitations of InGaN-based LEDs.

Recently, III-nitride nano- and microrods have attracted attention as the potential hosts for the active layers in the next LED generation, because their three-dimensional structure has many potential advantages as compared to the conventional two-dimensional (2D) counterparts. The unique growth mechanism of vertically aligned GaN rods results in the formation of nearly dislocation-free single semiconductor crystals due to a small contact area of the rods with the substrate. Thus, the released lattice strain provides the appropriate conditions for growing the rods on the substrates which the lattice constant, which is considerably different from that of InGaN. Although the InGaN structures in the commercially available LEDs are currently being grown on the lattice-mismatched sapphire substrate, a more cost-effective silicon substrate is preferred for the mass production. Furthermore, due to a large surface to volume ratio of the nanorod structure, the light emitting area is effectively increased as compared to the conventional 2D structures. Most promisingly, InGaN/GaN multiple quantum wells (MQWs) can be grown on non-polar (*m*-plane) sidewall facets of the GaN rods. All these advantages are expected to improve the emission wavelength stability and the efficiency of InGaN LEDs.

Results and Discussion

In this work, the spatial distribution of the photoluminescence (PL) in self-organized GaN microrods and GaN microrods with GaN/InGaN core-shell MQW structures was analyzed. The rods under this study were grown in a catalyst-free mode by using the MOCVD technique on Si(111) substrate covered by a AlN buffer layer and a SiN masking layer. Three InGaN/GaN quantum wells were deposited on the GaN microrod sidewall facets. The nominal thicknesses of the well and barrier were 2 and 4 nm, respectively. We employed the confocal spectroscopy to study the PL in the isolated rod structures and obtained the longitudinal and transverse cross-section images of PL parameters. A CW laser diode emitting at 405 nm was used as an excitation source.

The PL spectra of the GaN microrods with GaN/InGaN core-shell MQWs consist of two peaks. The long-wavelength peak at 570 nm originates from the GaN microrod core. This defect-related PL band is common in bulk GaN samples. The short-wavelength peak was the most intense at the sidewalls of the rod and was attributed to the emission of MQWs [see **Figure 1(b)**]. The spatially averaged wavelength of the MQW emission peak is 455, 492 and 534 nm for samples grown at the TMIn molar flow of 2.6, 5.2 and 10.4 μmol/min, respectively [**Figure 1(a)**]. The PL band peak positions did not change as the excitation power density was increased by an order of magnitude. This shows that the quantum confined Stark effect is absent in these samples and confirms the expectation that the MQW structures are fabricated on non-polar GaN facets. It was also found that the PL intensity is distributed inhomogeneously. Bright spots that show intense MQW-related PL band were resolved on the sidewalls of the rods. The density of the bright spots is larger at the top than near the bottom of the rod. The bright spots might be attributed to the InGaN quantum dots (QDs) formed on GaN microrod walls. The formation of the QDs is most probably induced by antisurfactant effect of SiN layer which is deposited during fabrication to promote the vertical rod growth. The QDs are sparse at the bottom of the rod, where SiN layer is the densest, but InGaN layer coalesces at the top and uniform QWs are formed. Moreover, the defect-related PL band is more pronounced at the bottom of the rod, while the MQW-related PL band dominates at the upper part of the rod. The results suggest that MQWs are formed inhomogeneously along the GaN rod.

Polarization-resolved measurements showed that the PL emission from GaN/InGaN core-shell MQW is polarized perpendicular to the c-axis, as it is expected for nonpolar InGaN structures. The highest emission polarization ratio ρ=0.54 is found to be at the top of the rod but decreases to ρ=0.14 at the bottom.

The confocal microscopy showed that GaN microrod structures are hexagonally shaped. The rods are up to 70 µm long and their diameter varies from ~2 µm at the bottom to ~4 µm at the top of the rod [**Figure 1(c)**]. Although, the rods are found to be predominantly vertically aligned on the substrate, randomly orientated rods were also frequently observed. PL intensity mapping images showed that the substrate is covered with hexagon-shaped areas which emit intense PL band peaked at 570 nm. The areas were attributed to GaN nucleation seeds that did not initiate vertical rod growth. It is argued that microrods are favourable to nanowires for LED applications due to a simpler device processing, like easier contact fabrication. However, more experiments are needed to optimize the diameter and position control during the growth.

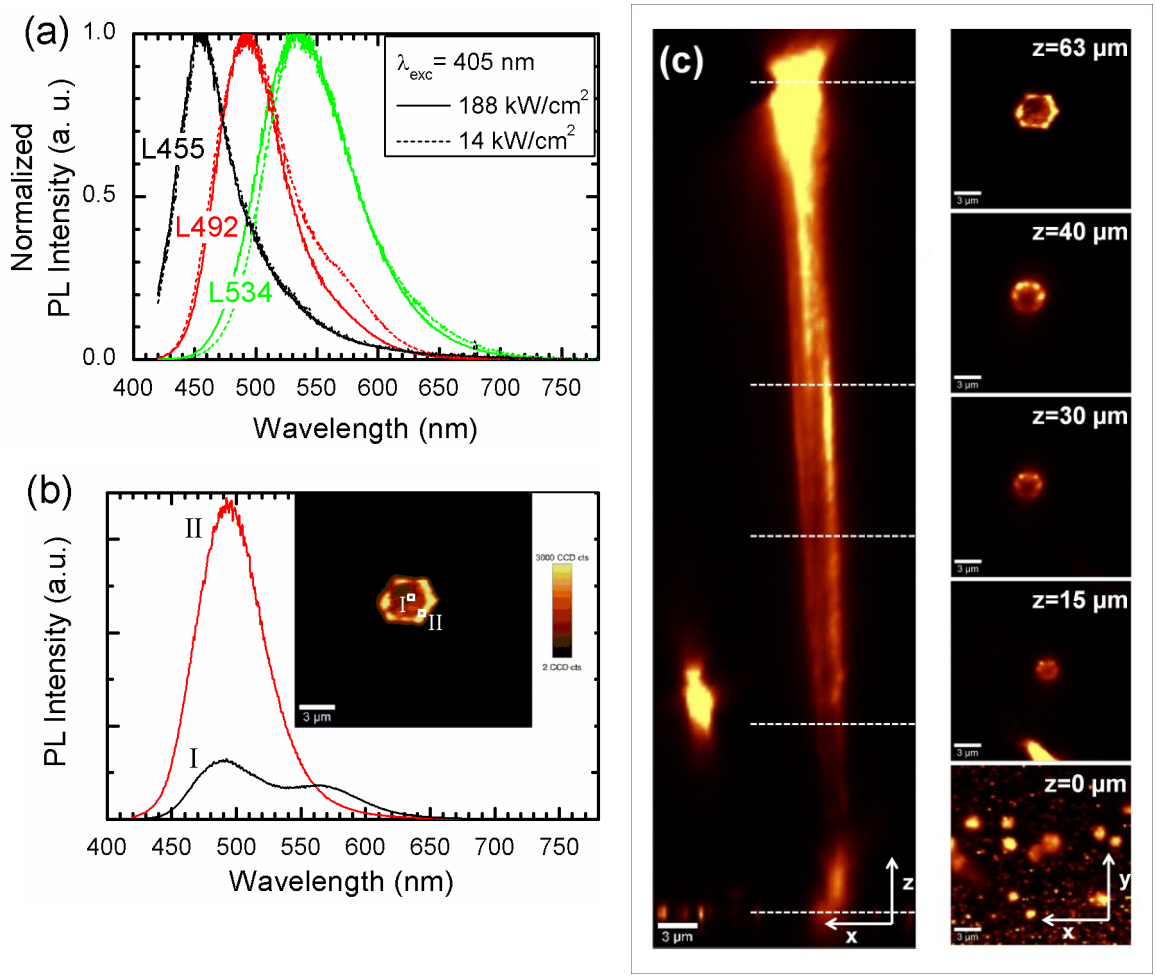

Figure 1: Photoluminescence spectra of GaN microrods series with GaN/InGaN core-shell MQWs obtained at low (dashed lines) and high (solid lines) PL excitation power densities in samples grown at TMIn molar flow of 2.6, 5.2 and 10.4 µmol/min indicated as L455, L492, and L534, respectively (a); the spatial distribution of the emission intensity at the top of the L492 microrod (the inset of b) and PL spectra in the spots labelled as I and II; the longitudinal (left column of c) and transverse (right column of c) cross-section images of PL intensity of the L492 microrod.

Conclusions

In conclusion, the spatial PL distribution in self-organized GaN microrods with GaN/InGaN core-shell MQW structures, which has been studied using confocal spectroscopy, shows that GaN microrod structures of good optical quality can be grown on low-cost silicon substrates by MOCVD technique. There is no quantum confined Stark effect in the quantum wells deposited on the side walls, and the light emitted from the QWs is strongly polarized. However, the QWs are inhomogeneous along the microrod axis. Quantum dots are formed on the bottom part of the side walls.

Germanium bowtie antennas for vibrational mid-infrared near-field spectroscopy.

T. Venanzi[a], *F. Appugliese*[a], *E. Calandrini*[c], *V. Giliberti*[a,b], *M. Badioli*[a], *A. Toma*[c], *F. De Angelis*[c], *L. Baldassarre*[a], G. Scappucci[d,e] and M. Ortolani[a]

[a] 1 Department of Physics, Sapienza University of Rome, Italy

[b] Istituto Italiano di Tecnologia, Centre for Life Nano Science, Rome, Italy

[c] Istituto Italiano di Tecnologia, Department of Nanostructures, Genova, Italy

[d] School of Physics, University of New South Wales, Sydney, NSW 2052, Australia

[e] QuTech, Delft University of Technology, Lorentzweg 1, 2628 CJ Delft, The Netherlands

**e-mail: michele.ortolani@roma1.infn.it*

Keywords: mid-infrared antennas, germanium plasmonics, heavily doped germanium, near-field imaging.

Introduction

The unique vibrational fingerprints of molecules lie in the mid-infrared (mid-IR) frequency range (wavelengths from 5 to 15 microns), hence vibrational mid-infrared spectroscopy is an important tool for the identification and characterization of different chemical species. However, the spectral identification of nanometer-size molecules is hampered by the weak interaction of such systems with infrared light. Therefore mid-infrared spectroscopy has taken advantage of plasmonics in order to improve the sensitivity of the technique and decrease the lowest detectable amount of analyte [1].

In this regard, the investigation of different mid-infrared plasmonic materials has attracted wide interest with the aim of developing novel mid-infrared plasmonic platforms for spectroscopy and sensing [2, 3].

In this work, we present preliminary Fourier transform IR (FTIR) spectroscopy and fabrication results on mid-infrared bowtie antennas fabricated out of heavily n-type doped germanium, grown by molecular beam epitaxy of germanium layers intercalated with exposure to phosphine gas to grow single layers of donors [4]. Heavily doped germanium (free carrier density around 10^{19}-10^{20} cm^{-3}), due to the small value of its effective mass $m^*=0{,}12\ m_e$, displays plasma frequencies in the mid-infrared, which can be selected by carefully tuning the doping values [5]. Therefore, tight field confinement in this spectral range is expected for resonantly excited germanium antennas. In addition, germanium-based devices hold promises for CMOS-compatible integrated plasmonic mid-infrared sensors.

The aim of our work is the near-field characterization of the field enhancement in the gap of the germanium bowtie antennas to assess the capabilities of such structures for spectroscopic studies of small amounts of molecules. The experimental setup (NanoIR2 by Anasys Instruments) consists of a pulsed quantum cascade laser (QCL) in the 1575-1725 cm^{-1} range (around 6 mm) coupled to an atomic force microscope (AFM) working in contact mode. This platform for near-field spectroscopy and imaging exploits photoexpansion to reveal the absorption of a substance under the tip. Therefore the electric field enhancement is visualized by monitoring the local energy absorbed by a thin polymer film in the gap of the bowtie antennas.

Results and Discussion

Since higher values of field confinement occur just below the plasma edge, we performed FTIR quasi-normal incidence reflection measurements to characterize the plasma frequencies of germanium samples with different doping levels. In this way, we selected the most suitable sample for the fabrication of bowtie antennas in the frequency range of our QCL.

Hence, bowtie antennas were fabricated from the chosen germanium sample by focused ion beam (FIB) milling, as shown in **Figure 1**. Improvements in the fabrication process are underway in order to obtain sharper edges and to remove the residual amorphous germanium due to the redeposition of the milled material.

Encapsulation of the antennas with PMMA enables the mapping of electric near-field distribution via the local absorption of the polymer. To this end it is possible to excite the C=O stretching vibration peaked at 1732 cm^{-1} whose tail lies in our spectral range. We are testing different thicknesses of the PMMA encapsulation layer to optimize of the photoexpansion signal while reducing topographic artefacts.

To perform the near-field characterization we have modified the optical path of our commercial system in order to rotate the incident light polarization in the plane of the antennas. In addition, we mounted silicon tips to be able to measure without altering the near-field distribution.

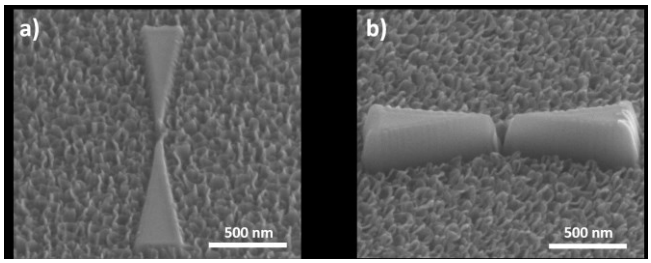

Figure 1: Scanning electron microscope images of germanium antennas fabricated by FIB milling: a) top view b) side view.

Conclusions and/or Outlook

We have fabricated heavily doped germanium antennas encapsulated in a polymer layer and modified the optical path of our near-field setup in order to perform a spatial characterization of the electromagnetic energy absorption in the gap of the antennas. Such characterization will set the ground to engineer germanium antennas for mid-infrared vibrational sensing.

References:

[1] F. Neubrech et al., Resonant plasmonic vibrational coupling in a tailored nanoantenna for infrared detection, Phys. Rev. Lett., 101, 2008.
[2] L. Baldassarre et al., Mid-Infrared plasmon-enhanced spectroscopy with germanium antennas on silicon substrates, Nano Lett., 15 (11), 2015.
[3] D. Rodrigo et al., Mid-Infrared plasmonic biosensing with graphene, Science, 349, 2015.
[4] G. Scappucci et al., New avenues to an old material: controlled nanoscale doping of germanium, Nanoscale, 5, 2013.
[5] E. Calandrini et al., Determination of the free carrier concentration in atomic-layer doped germanium thin films by

Gold–polyaniline hybrid nanocomposite for electrocatalytic application

*V. Vodnik** [a], *U. Bogdanović*[a], *I. Pašti*[b], *G. Ćirić–Marjanović*[b], *M. Mitrić*[a], *S.P. Ahrenkiel*[c]

[a]Vinča Institute of Nuclear Sciences, University of Belgrade, P. O. Box 522, 11001 Belgrade, Serbia
[b]Faculty of Physical Chemistry, University of Belgrade, Studentski Trg 12–16, 11158 Belgrade, Serbia
[c]South Dakota School of Mines and Technology, 501 E. Saint Joseph St., Rapid City, SD 57701, USA

**e-mail: vodves@vinca.rs*

Keywords: polyaniline, Au nanoparticles, nanocomposite, conductivity, electrocatalyst

Introduction

In the quest for superior performance, nanostructured conducting polymer polyaniline (PANI) has been combined with multi–functional metal nanoparticles to obtain new nanocomposite materials. These nanostructures are important since they combine the properties of low–dimensional organic conductor with high surface area materials. Here, we present gold–polyaniline (Au–PANI) nanocomposite prepared by a simple interfacial polymerization method, based on the oxidizing properties of $HAuCl_4$, which initiates the polymerization process of aniline at the interface of water/toluene biphasic system. The formation of Au nanoparticles (AuNPs) or Au–PANI nanocomposite can be controlled to a certain degree by varying the ratio of initial Au^+ and aniline concentrations. Under optimal condition ($HAuCl_4$/aniline ratio is 1:2), green dispersion of Au–PANI nanocomposite is produced in aqueous phase, whose morphology, structure and physico-chemical properties are investigated in details. As the electrocatalytic properties of materials towards the electrochemical oxygen reduction reaction (ORR) is extremely important, due to the role of ORR in contemporary energy conversion technologies, we turn our attention to the electrocatalytic ORR process on the electrode modified with Au–PANI nanocomposite, with the aim of developing highly active Pt–free ORR catalyst with appreciable catalytic performance.

Results and Discussion

The chemical oxidative polymerization was performed at the interface between an organic layer (toluene) that contains dissolved aniline and an aqueous layer containing the Au^{3+} as oxidant (Figure 1). As the reaction proceeds, PANI forms across the interface where all the components needed for polymerization come together. After synthetic procedure, it was found that nanocomposite contains high amount of Au (28.85 wt.%). The microstructural analysis of Au–PANI nanocomposite powder obtained after isolation procedure reveals that PANI macromolecules were organized into three–dimensional granular nanostructures with Au nanorods as dominate structure distributed in it (Figure 1). It is important to note that Au–PANI nanocomposite powder, isolated from the as–synthesized aqueous dispersion, can later be easily re-dispersed in water. This property is highly appreciated in terms of material's storage (where powder form is more desirable than dispersion due to lower volume and absence of leakage), processing (usage of obtained aqueous dispersion to prepare conductive coatings for various applications) and environment protection (usage of water as eco–friendly solvent).

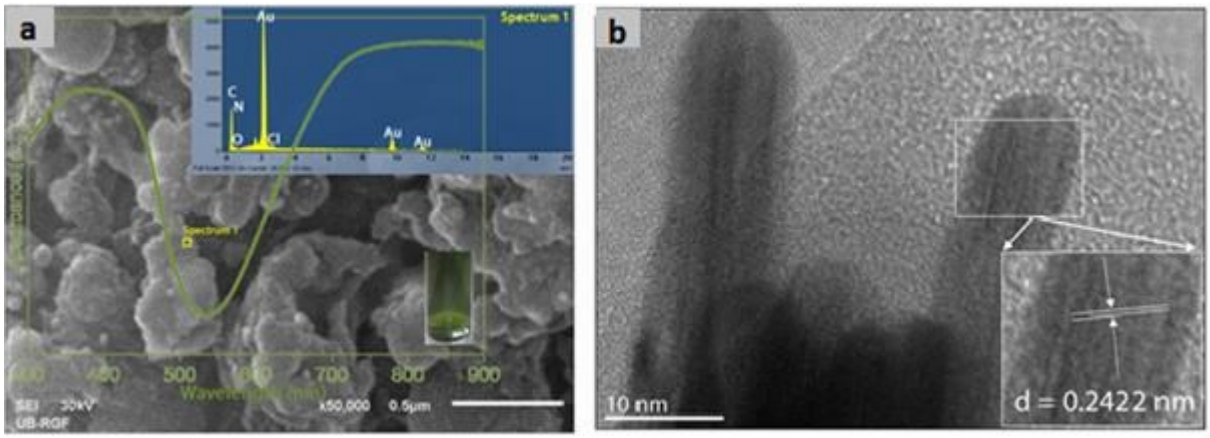

Figure 1: a) SEM image of Au-PANI nanocomposite with EDX and absorption spectra; b) TEM image of nanocomposite

The formation of conducting emeraldine salt form of PANI in nanocomposite was confirmed by UV–Vis, FTIR and Raman spectroscopy. Moreover, Raman spectroscopy identified two types of spectral profiles having different relative intensity of the bands that belong to emeraldine salt and phenazine–type segments thus indicating fine inherent structural inhomogeneity at the macromolecular level that in Au–PANI nanocomposite.

The interaction of phenazine–type segments with AuNPs surfaces induced a local surface enhanced Raman scattering effect. Besides, the electrical conductivity of nanocomposite (1.19 S cm^{-1}) was found to be four–fold higher than that of the polymer PANI itself (0.29 S cm^{-1})[1], due to more conducting Au nanorods dispersed in less conducting PANI matrix, which enables formation of long ("infinite") conducting pathways and consequently drastically increase the conductivity.

Catalytic activity of Au–PANI towards the electrochemical oxygen reduction reaction (ORR) was investigated in O_2–saturated 0.1 M KOH solution using RDE voltammetry. Compared to other Au–based ORR catalysts reported so far [2], Au–PANI nanocomposite presented here, provided fast charge transfer kinetics (high ORR onset potential) and high selectivity for O_2 reduction to water (OH^-). This is possibly due to enhanced Au surface oxophilicity in the presence of PANI, which is indicative of enhanced chemisorption properties.

Conclusions and/or Outlook

The presented Au-PANI nanocomposite with granular morphology and Au nanorods distributed in it, shows relatively high conductivity and excellent electrocatalytic performance towards the electrochemical O2 reduction, with high ORR onset potential and good selectivity. This makes it a promising candidate for a new class of Pt–free ORR catalyst with appreciable catalytic performance.

References:

[1] Bogdanović U, Vodnik V, Ahrenkiel S P, Stoiljković M, Ćirić–Marjanović G, Nedeljković J M; Interfacial Synthesis and Characterization of Gold/Polyaniline Nanocomposites; Synthetic Metals; 195 (2014) 122–131;

[2] Song J, Yuan J, Li F, Han D, Song J, Niu L; Tunable Activity in Electrochemical Reduction of Oxygen by Gold–Polyaniline Porous Nanocomposites; Journal of Solid State Electrochemistry; 14 (2010) 1915–1922;

Optical Properties of Silver-Titanium Dioxide Nanocomposites

P. Nyga[a]*, S. Chmiel[a], M. Szczurek[a], M. Liszewska[a], M. Stefaniak[a], J. Firak[a], M. Michalska-Domanska[a], J. Mierczyk[a], M. Norek[b]

[a] Institute of Optoelectronics, Military University of Technology, Warsaw, Poland
[b] Department of Advanced Materials and Technologies, Military University of Technology, Warsaw, Poland

e-mail: piotr.nyga@wat.edu.pl

Keywords: silver nanoparticles, plasmon, titanium dioxide, TiO_2, nanocomposite

Nanoscale metal-dielectric and metal-semiconductor structures and composites have huge potential in many science and engineering fields. Various combinations of such nanostructures are considered for applications in sunlight harvesting processes like photovoltaics, photoelectrochemical water splitting, heat generation, but also for substrates for surface enhanced Raman and infrared spectroscopies and many more.
Usually fabrication methods of nanostructures are relatively expensive considering cost per surface area, for example electron beam lithography. Fabrication of metal island films or semicontinuous metal films using electron beam physical vapour deposition (EB-PVD) technique is one of the inexpensive methods of production of plasmonic metal nanostructures on surface or embedded in dielectric or semiconductor host. When thin silver or gold layer is deposited using EB-PVD, randomly arranged metal nanostructures form semicontinuous film. Size and shape of nanostructures and thus also optical properties of the film can be controlled by choosing specific deposition process conditions. [1,2]
Here we present the details of optical and electrical properties of titanium dioxide (TiO_2) films and silver nanoparticles-titanium dioxide (Ag-TiO_2) layered nanocomposites fabricated using EB PVD technique. We varied several parameters of the fabricated structures and EB PVD process including silver and TiO_2 layer thickness, number of layers, deposition temperature, oxygen dosage during deposition of TiO_2 and post fabrication annealing.
Films were deposited on glass substrates using PVD system with base pressure of 1E-6 mbar. Mass thickness was monitored with quartz crystal microbalance. Most of the films were deposited at 200ºC. During TiO_2 deposition oxygen was introduced to vacuum chamber and base pressure of 2E-4 mbar was maintained. This procedure resulted in titania films without absorption in visible and near-infrared. When TiO_2 was deposited without addition of oxygen films with absorption in visible and near-infrared were obtained. TiO_2-Ag composites were fabricated through sequential deposition of titania and silver. Some films were heated in muffle furnace at different temperatures. Characterization of nanostructure of silver films deposited on top of TiO_2 layer was performed using SEM microscopy. The titania crystalline forms composition was tested using Raman spectroscopy. Optical properties of fabricated composites were characterized using spectrometer equipped with integrating sphere.
Utilizing the semicontinuous nature of silver films we achieved structures with broadband absorption. The level and spectral width of absorption can be tuned by design. Through number of silver layers and their thickness the absorption level of composite can be adjusted from about 10% to above 90% in the visible and/or near-infrared range.

The research was financed by the Polish National Centre for Research and Development grant no LIDER/23/22/L-3/11/NCBR/2012.

References:

[1] Nyga P, Drachev V P, Thoreson M D, V M Shalaev; Mid-IR plasmonics and photomodification with Ag films; Applied Physics B; 93 (2008) 59-68;
[2] Thoreson M D, Fang J, Kildishev A V, Prokopeva L J, Nyga P, Chettiar U K, Shalaev V M, Drachev V P; Fabrication and Realistic Modeling of 3D Metal-Dielectric Composites; Journal of Nanophotonics; 5 (2011) 051513-051513-17;

Conditioning of Metal Nanowires by Laser Processing

J. Butikova[a], *B. Polyakov*[a], *S. Vlassov*[a, b], *L. Dorogin*[c], *K. Šmits*[a], *M. Antsov*[b], *S. Oras*[b], *R. Zabels*[a], *R. Lõhmus*[b]

[a] Institute of Solid State Physics, University of Latvia, Ķengaraga 8, Rīga LV-1063, Latvia
[b] Institute of Physics, University of Tartu, Ravila 14c, 50412, Tartu, Estonia
[c] Peter Grünberg Institute / Institute for Advanced Simulation, Forschungszentrum Jülich, Wilhelm-Johnen-Straße, 52428, Jülich, Germany

**e-mail: but@latnet.lv*

Keywords: metal nanowires, laser processing, nanodumbbells, nanotribology, nanomanipulations

Introduction

Manipulation of nanoscale objects provides essential data for development of future nanoscale devices. Nanoparticles are the most thoroughly studied objects for nanomanipulation. Tribological behaviour of nanostructures featuring higher aspect ratio, e.g., nanowires, has been studied to a significantly less extent. Due to much larger contact area and adhesion/friction in comparison to nanoparticles, the manipulation of elongated objects may be problematic. For example, the displacement of Ag nanowires on a smooth silicon substrate is almost impossible without severe damaging and breaking of nanowires [1]. At the same time, mobile or movable elongated nanostructures are of high interest as possible components of nanoelectromechanical systems (NEMS). Advantages of nanoparticles and nanowires from the tribological aspect can be combined in a nanodumbell-like structure produced by pulsed laser processing of metal nanowires. Electric field induced by laser light is concentrated at the ends of a metal nanowire causing them to melt and round. Resulting structure resembles dumbbell with two bulbs connected by nanowires. Specific geometry of metal nanodumbbells makes them promising candidates for knuckle-joints and other movable component in NEMS applications.

Results and Discussion

Formation of nanodumbbells is a complex dynamic process. It involves extreme temperature gradients, and includes rapid heating and melting of the ends of nanowires, contraction of liquid droplets into spheroidal bulbs and followed by rapid solidification.

After the absorption of laser pulse energy, a nanowire starts to melt; liquid droplets grow in volume and move towards the centre of a nanowire [2]. Surface tension tends to minimize the surface area of a droplet, and makes it spherical. The temperature of the parts of a nanowire close to the liquid bulbs approaches the melting point, causing a local decrease of Young's modulus, and resulting in the detachment of the parts from the substrate pulled by the growing droplet. Adhesion at the central part of a nanowire that rests on the substrate is reduced significantly due to inverse dependence of surface free energy on temperature. However, the temperature in the central part of a nanowire is below the melting point, since the nanowire preserves its original crystalline structure. When the nanodumbbell is cooled down, the middle part becomes a crystallisation nucleus, and defines the epitaxial crystallisation of the melted part of the wire towards the end bulbs. After solidification, there is an elastic stress tending to restore the straight profile of the bent part connecting two bulbs. If the part of the nanowire adhered to the substrate is short enough, and adhesion force is less than restoring elastic forces. The middle part of the nanowire can get detached from the substrate, and the nanodumbbell will rest on the end bulbs only. Remarkably, that in spite of rapid cooling, the end bulbs are crystalline [3].

Investigation of the internal structure of Au and Ag nanodumbbells in TEM (**Figure** 1) shows a clear dependence between bulb size and internal structure. Diameter of the nanowire connecting the end bulbs is equal to the initial diameter of a nanowire, while diameter of the end bulb depends on the length of melted part of a nanowire. Small bulb preserved original crystalline structure of the nanowire, whereas for the bigger bulbs, twinned structure different from the original one was observed. A grain boundary can be seen in the interface between the melted end and the body of the nanowire (**Figure** 1 a-c). Medium-sized bulbs partially preserved the original structure of the nanowire (**Figure** 1 d). Such association between the structure and size of the bulb may be related to the fact that temperature gradient between the bulb and the nanowire is smaller in the case of small bulbs, and melted part is able to follow the original crystalline structure of the nanowire. In a bigger bulb, more competing crystallization nuclei forming an independent grain are possible [4].

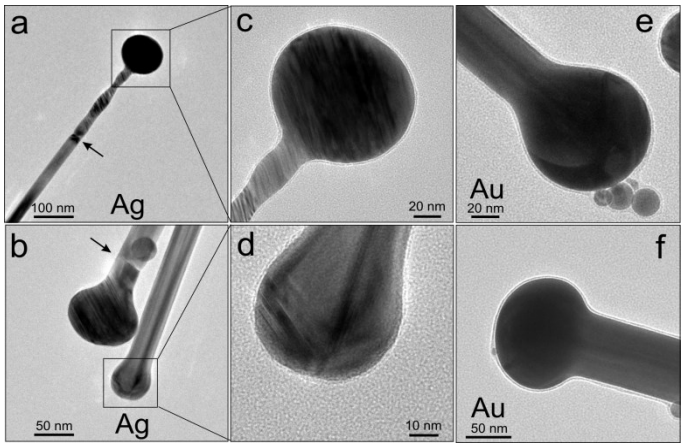

Figure 1: TEM images of Ag (a, b, c, d) and Au (e, f) NDs end bulbs. Arrows indicate grain boundary

During the typical in situ SEM manipulation experiment, the nanodumbbell overcomes the static friction force and rolls over. Then, it rotates around one of its ends at almost zero force. During manipulation experiments, nanodumbbells exhibited several regimes of motion: sliding, rolling, and rotational motion. Sliding, or translation, was observed rarely. Rolling of a nanodumbbell onto the other side was observed more frequently. The most common scenario was rotation of a nanodumbbell around one of its end bulb.

Conclusions and/or Outlook

Ag, Au and Cu nanodumbbells were produced by laser-induced melting of corresponding nanowires. The final configuration of a nanodumbbell is a result of the complex interaction the intrinsic effects and adhesion, while a nanowire is detached from the substrate. Shape and morphology of nanodumbbell structures were studied by SEM and TEM methods. Dependence of the crystalline structure on the size of the end bulb was demonstrated. After the laser processing, both the end bulbs and the connecting nanowire of a metal nanodumbbell preserve their crystallinity, which is crucial for many possible applications of the nanodumbbells The geometry of nanodumbbells makes them promising candidates for applications in MEMS/NEMS and attractive objects for nanotribological studies enabling to study different regimes of motions: sliding, rolling, and rotation.

References:

[1] Vlassov S, Polyakov B, Dorogin L, Antsov M, Mets M, Umalas M, Saar R, Lõhmus R, Kink I; Elasticity and yield strength of pentagonal silver nanowires: in situ bending tests; Materials Chemistry and Physics; 143 (2014) 1026–1031

[2] Polyakov B, Vlassov S, Dorogin L, Novoselska N, Butikova J, Antsov M, Oras S, Lohmus R, Kink I; Some aspects of formation and tribological properties of silver nanodumbbells; Nanoscale Research Letters; 9(1) (2014) 186

[3] Liu L, Peng P, Hu A, Zou G, Duley W, Zhou Y; Highly localized heat generation by femtosecond laser induced plasmon excitation in Ag nanowires; Applied Physics Letters; 102 (2013), 073107

[4] Polyakov B, Vlassov S, Dorogin L, Butikova J, Smits K, Antsov M, Oras S, Zabels R, Lohmus R; Metal nanodumbbells for nanomanipulations and tribological experiments; Physica Scripta; 90(9) (2015) 094007

Coupling single quantum dots to plasmonic nanocones

A. Bräuer[1*], *R. Jäger*[2], *K. Scherzinger*[2], *J. Fulmes*[1], *S. Jäger*[2], *S. zur Oven-Krockhaus*[2], *D. A. Gollmer*[1], *A. J. Meixner*[2], *D. P. Kern*[1], *M. Fleischer*[1]

[1] Institute for Applied Physics, University of Tübingen
Auf der Morgenstelle 10, 72076 Tübingen, Germany
[2] Institute of Physical and Theoretical Chemistry, University of Tübingen
Auf der Morgenstelle 18, 72076 Tübingen, Germany

e-mail: annika.braeuer@uni-tuebingen.de

Keywords: quantum dots, plasmonic nanocones, field-enhancement, photoluminescence, blinking

Introduction

Plasmonic nanostructures are very well suited for assisting with the detection and characterization of single or few quantum dots (QDs) due to their well-tuneable plasmon resonance wavelengths depending on size, material and geometry. As QDs have unique optical properties of their own, such as broad absorption and narrow emission bands as well as bright and stable photoluminescence, hybrid systems consisting of both components are of major interest for various applications. Excitation along the symmetry axis of the cone leads to a highly enhanced near-field at the tip [1-3]. By bringing a QD into close vicinity of the tip of a nanocone, its emission characteristics can be altered, as the radiative and non-radiative decay rates are influenced by the increased density of local optical states [4].

Gold nanocones were fabricated on a glass substrate with a thin indium tin oxide (ITO) layer with a geometry adjusted such that the out-of-plane resonance matches the emission of core-shell CdSe/ZnS QDs at 650 nm.

Hybrid structures consisting of both, gold nanocones and QDs, were then produced with a self-aligned technique [5] which allows to place QDs with a lateral accuracy of about 10 nm on a variety of structures at the same time. Therefore a wide range of hybrid systems was prepared and investigated optically [6].

Results and Discussion

Core-shell CdSe/ZnS QDs were chemically bound to the tips of gold nanocones following a process given in [5] and shown in **Figure 1**. The amount of successfully linked QDs was imaged by raster scanning the sample through the focus of a radially polarized laser beam at 488 nm and estimated to be around 70%.

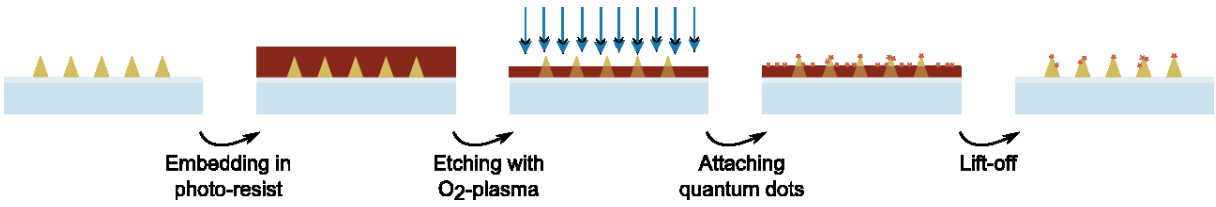

Figure 1: Fabrication scheme of hybrid systems. Nanocones are embedded in resist, the tips are then bared by O_2-etching. The QDs are attached with thiol-chemistry followed by a lift-off process to remove the residual resist.

The photoluminescence signal was recorded for bare cones, QDs on glass and QDs on cones. We observed a higher signal for the QDs bound to the tips of the cones as well as less dramatic intensity fluctuations compared to the QDs on glass. To verify the presence of only one QD at the tip, time traces of the emission intermittency of the spectrally integrated signal of a QD on glass and of a QD bound to the tip of a cone were recorded and are exemplarily shown in **Figure 2**. Similar results were obtained for measurements on other hybrid structures. For the measurement on the hybrid system (**Figure 2**, left) the time trace shows clear jumps in intensity between a maximum and a minimum level as well as on-off fluctuations. The observed two-level blinking strongly indicates that there is only one QD attached to the tip.

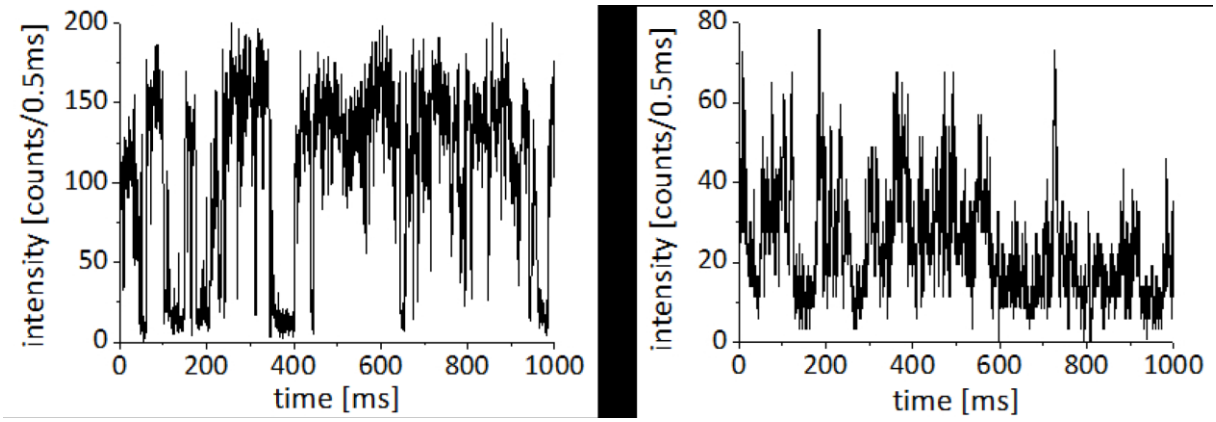

Figure 2: Intensity trajectories of a single QD bound to the tip of a cone (left) and of an isolated QD on a glass cover slide exposed to air (right). Note the difference in intensity scales.

The trace looks different for an isolated QD on a glass cover slide (**Figure 2**, right). No jumps between two clearly distinguishable levels can be seen. Also the dark states seem to prevail.

Further investigations on the fluorescence and life times of the hybrid system will be discussed in another presentation.

Conclusions

We fabricated and investigated a novel hybrid system composed of gold nanocones with few or single QDs attached to the tips of the cones and observed fundamental changes in the emission behaviour of the quantum emitters compared to bare ones on glass slides. These hybrid systems may lead to an improved understanding of the interaction between quantum emitters and plasmonic nanostructures as well as of the physical mechanisms involved in the emission of a photon from such a system.

Further investigations need to be done, experimentally and theoretically, concerning fluorescent lifetimes and fluorescence intermittency, e.g. in relation to the position of the plasmon resonance.

References:

[1] Fleischer M, Stanciu C, Stade F et al.; Three-dimensional optical antennas: Nanocones in an apertureless scanning near-field microscope; Applied Physics Letters; 93 (2008) 111-114

[2] Horrer A, Schäfer C, Broch K et al.; Parallel fabrication of plasmonic nanocone sensing arrays; Small; 9 (2013) 3987-3992

[3] Schäfer C, Gollmer DA, Horrer A et al.; A single particle plasmon resonance study of 3D conical nanoantennas; Nanoscale; 5 (2013) 7861-7866

[4] Kern AM, Zhang D, Brecht M et al.; Enhanced single-molecule spectroscopy in highly confined optical fields: from λ/2-Fabry-Pérot resonators to plasmonic nano-antennas; Chemical Society Reviews; 43 (2014) 1263-1286

[5] Fulmes J, Jäger R, Bräuer A et al.; Self-aligned placement and detection of quantum dots on the tips of individual conical plasmonic nanostructures; Nanoscale; 7 (2015) 14691-14696

[6] Meixner AJ, Jäger R, Jäger S et al.; Coupling single quantum dots to plasmonic nanocones: optical properties; Faraday Discussions; (2015) doi:10.1039/c5fd00074b

Asymmetric nanocones for efficient transversal far field coupling into longitudinal plasmonic oscillations

C. Dreser[a], *D. P. Kern*[a], *M. Fleischer*[a]

[a] Institute for Applied Physics, University of Tübingen, Germany

**e-mail: christoph.dreser@uni-tuebingen.de*

Keywords: plasmonics, nanoantennas, field enhancement

Introduction

One aim of the research on plasmonic nanostructures is the enhancement and confinement of the electric field of an incoming electromagnetic wave. These optical antennas have broad applications, for example in surface-enhanced Raman spectroscopy (SERS) [1], single-molecule detection [2] or scanning near-field optical microscopy (SNOM) [3].

Nanocones are well-suited for such applications as they can easily be fabricated from various metals [4-5] and have a very sharp tip with a radius lower than 10 nm. Several applications of metallic nanocones are shown in [6-7].

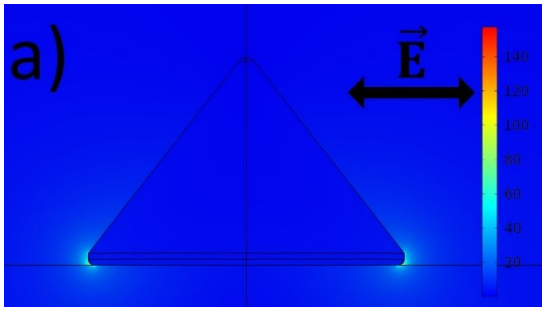

The major problem for an efficient plasmon excitation along the vertical axis and consequential high electric field enhancement at the tip of the cone is that the electric field vector of the exciting external electromagnetic wave should be parallel to the vertical axis. This is only the case for certain laser modes or the illumination of the cones from the side. Simulations have shown that the electric field at the tip is not enhanced if the incoming wave is TE polarized **(Figure 1 a)**. Therefore the excitation of many cone tips at once under perpendicular incidence is not possible. But for many potential applications it is beneficial that the electric field of the light be enhanced at the tips of many cones simultaneously.

0.02

0.01

Results and Discussion

As a solution for this problem we introduce a deflection of the tip. Simulations **(Figure 1 b)** have shown that the tip of an oblique cone is excited even by an electromagnetic wave which is TE polarized. The asymmetric geometry supports the transformation of a transversal (parallel to the substrate) electric far field to a longitudinal (parallel to the axis) plasmonic excitation.

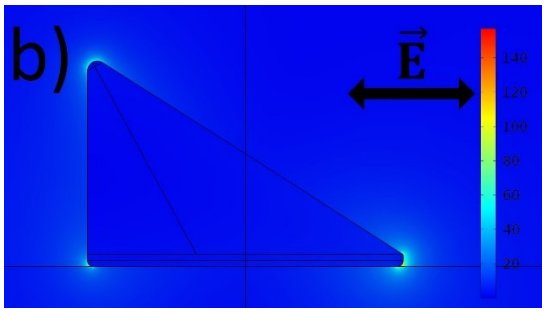

Starting from simulations and already existing fabrication processes [4,8] two processes for the fabrication of oblique nanocones were developed. The first one is based on transferring aluminium oxide masks via argon ion etching under an angle into a gold layer. The second process is based on inclined electron beam lithography and subsequent inclined evaporation of gold.

1

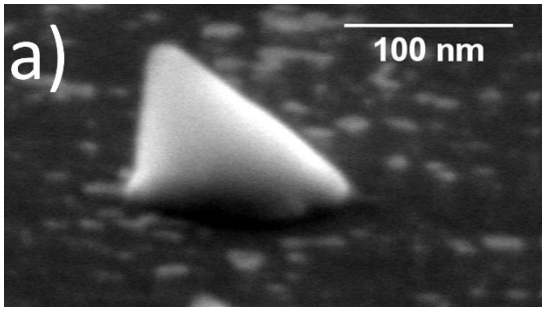

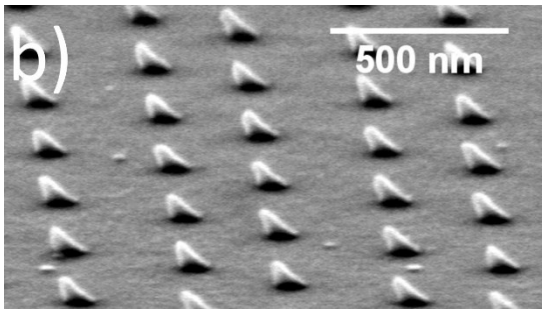

Figure 3 a): Simulation of the electric field distribution near a symmetric nanocone when excited with an electric field vector parallel to the cone base.

Electron micrographs of oblique cones are shown in **Figure 2**. The geometric properties of the nanocones can be influenced in different ways. The etching or evaporation angles, respectively, have a major influence on the displacement of the tip. Furthermore the sizes of the etch masks or rather the holes in the resist determine the size of the cone base. Examples of the fabrication will be shown together with dark-field and extinction spectra as well as corresponding simulations of the plasmonic modes.

Conclusions and Outlook

Inclined electron beam lithography was successfully established and oblique nanocones with various geometries were fabricated. In future the fabrication processes will be further optimized to gain better control over the geometric properties. The properties of the oblique cones will be investigated by linear and non-linear optics. Furthermore their application for SERS and single molecule detection is intended.

References:

[1] Jeanmarie D L et al.; Surface Raman spectroelectrochemistry, part 1: heterocyclic, aromatic, and aliphatic amines adsorbed on the anodized silver electrode. J. Electroanal. Chem.; 84 (1977) 1–20
[2] Kern A M et al.; Enhanced single-molecule spectroscopy in highly confined optical fields: from λ/2-Fabry–Pérot resonators to plasmonic nano-antennas; Chem. Soc. Rev.; 43 (2014) 1263-1286
[3] Fleischer M; Near-field scanning optical microscopy nanoprobes; Nanotechnol. Rev.; 1 (2012) 313
[4] Reichenbach P et al.; Nonlinear optical point light sources through field enhancement at metallic nanocones; Opt. Express; 22 (2014) 15484
[5] Kontio J M et al.; Nanoimprint fabrication of gold nanocones with ∼10 nm tips for enhanced optical interactions; Optics Letters; 34 (2009) 1979-1981
[6] Horrer A et al.; Parallel Fabrication of Plasmonic Nanocone Sensing Arrays; Small; 9 (2013) 3987
[7] Schäfer C et al.; Capturing molecules with plasmonic nanotips in microfluidic channels by dielectrophoresis; Lab Chip; 15 (2015) 1066
[8] Fulmes J et al.; Self-aligned placement and detection of quantum dots on the tips of individual conical plasmonic nanostructures; Nanoscale; 7 (2015) 14691

Single Wall Carbon Nanotubes induce molecular and ultrastructural changes in endothelial cells. The potential impact on the atherosclerotic process

I. Sammarco[a*], *G. Fasciglione*[b], *G. Lesci*[c], *V. Scacco*[d], *M. Luce*[d], *D. Di Pierro*[b], *L. Ferrucci*[e], *A. Pietroiusti*[a], *M. Coletta*[b], *A. Magrini*[a], *A. Cricenti*[d*]

[a] Department of Biomedicine and Prevention, University of Rome Tor Vergata, Rome, Italy
[b] Department of Clinical Sciences and Translational Medicine, University of Rome Tor Vergata, Italy
[c] WAPH Technology Corp. 1920 N COMMERCE PARKWAY, Weston, FL 33326, US
[d] Institute for the Structure of Matter, Italian National Research Council, Rome, Italy
[e] Department of Biology, University of Rome Tor Vergata, Rome, Italy

*e-mail: sammarco@uniroma2.it
*e-mail: antonio.cricenti@ism.cnr.it

Keywords: Single Wall Carbon Nanotubes, Endothelial Cells, Atherosclerosis, Metalloproteinases, Roughness

Introduction

Single Wall Carbon Nanotubes (swCNTs) may have the potential to contribute to the development and progression of cardiovascular disease, atherosclerosis included, as shown by Li et al. [1] in Apo E-/- mice. Atherosclerosis is an inflammatory disease, in which, since the earlier stages, a feature of the pathophysiology is the "endothelial dysfunction"(2). In this work we wanted to check if swCNTs could accelerate the atherosclerosis process. At this end, we treated the Ea.hy926 human endothelial cell line with pristine CNTs, and studied different end-points to understand if the cells acquired an inflammatory phenotype. We also imagined the cells with atomic force microscope (AFM) to detect possible ultrastructural alterations.

Results and discussion

Single-wall carbon nanotubes were purchased from Nanocyl , Belgium. The characterization of swCNTs was performed using spectroscopic (FTIR, Raman, UV-Visible), diffraction (XRD), microscopic (TEM, SEM), thermal gravimetric (TGA / DSC) and chromatographic techniques (GC-MS/MS). Furthermore, we performed the BET, the size distribution, and the Zeta potential. We bought the Ea.hy926 endothelial cell line from American Type Culture Collection (ATCC), a cell line that maintains the characteristics of the primary endothelial cells (3). In the WST-1 cytotoxicity assay, the nanotubes are toxic for the cells, but only after 48-72 h, and only at 50-200 μg/ml. Probably the cells, in the latter experimental points, begin to recover vitality (Data not shown). To check the oxidative stress, we performed the Oxygen Radical Antioxidant Capacity (ORAC) (4) and malondialdehyde (MDA) (5) tests. In our hands, as the concentration of CNTs increased, in ORAC test there was an average reduction of about 30% of the anti-oxidant capacity of the cells, while there was a significant rise of MDA (Data not shown). Overall, these results indicate that cells undergo a significant increase in oxidative stress. We made an extensive investigation of various classes of metalloproteinases (MMPs) and Tissue inhibitors of metalloproteinases (work in progress) (6). The MMPs play a key role in regulating the degradation of the extracellular matrix. In many studies the clearest evidence is for a positive relationship between MMP-9 expression and plaque instability. Instead TIMPs inhibit the enzymatic activity of MMPs. A tight balance between MMP proteolysis and TIMP expression is necessary for tissue homeostasis. In atherosclerosis, TIMPs are upregulated, especially at the base of plaques, and in part counteract the destructive potential of MMPs. In fig.1 we show the western blot (WB) for MMP-9, and in fig.2 for TIMP-1. As you can see, MMP-9 increases with time and the concentration, while TIMP-1 has the opposite trend. This could mean that CNTs provoke an imbalance between MMPs and their inhibitor, and could help plaque rupture and /or accelerated atherosclerosis.

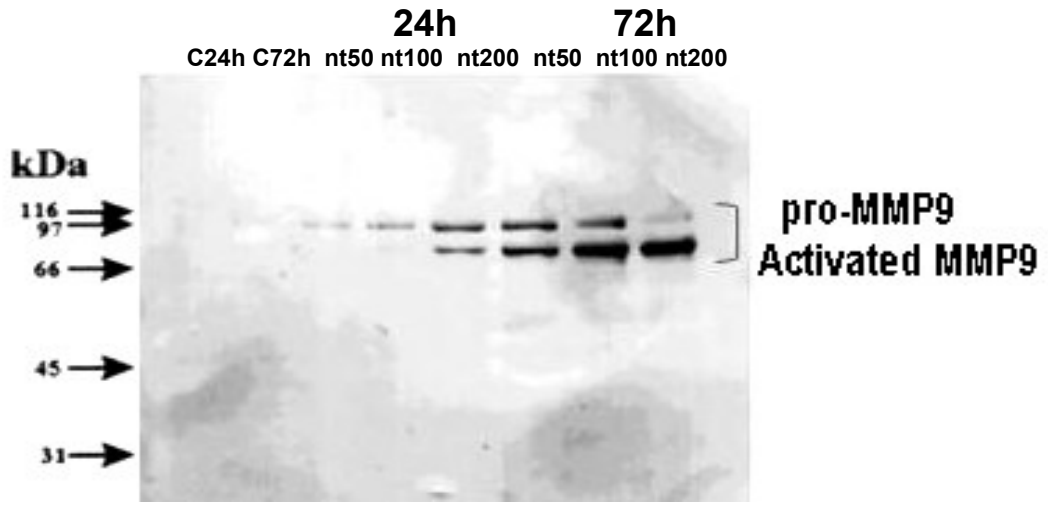

Fig.1

Fig.2

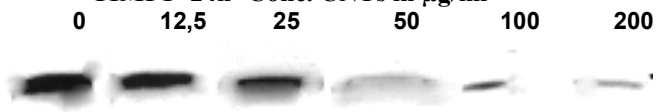

To verify ultrastructural changes in cell surface, we used atomic force microscope. Because the AFM can generate images of the plasma membrane structure in great detail, the instrument can be used to estimate the surface roughness. This parameter is a tool for investigating the membrane–cytoskeleton integrity. A large decrease in the surface roughness value is indicative of alterations produced by destabilization of the filament cytoskeleton network. This is our case: fig.3 is a typical image of Ea.hy926 cell line , and in fig.4 and 5 you can see that both in the central and peripheral regions, the roughness of treated cells decreased in a statistically significant way. We are working to see how this roughness variation may influence the process of atherosclerosis.

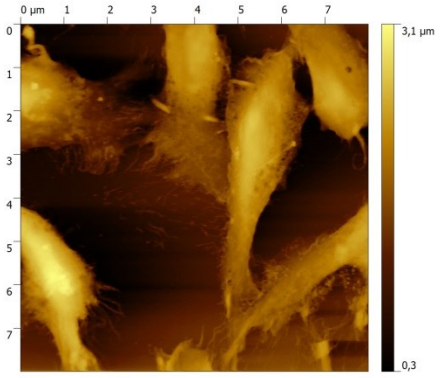

Fig.3

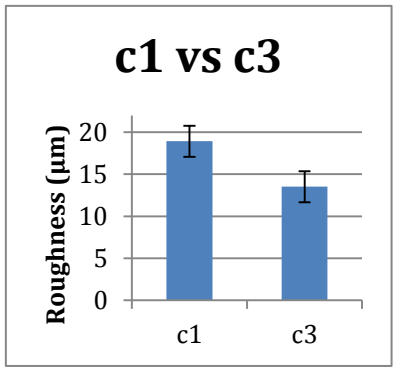

Fig.4

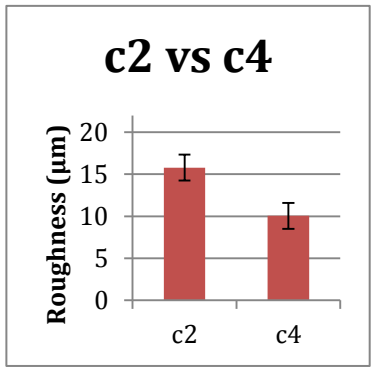

Fig.5

C1 and C2 are, respectively, central and peripheral regions of untreated cells.
C3 and C4 are, respectively, central and peripheral regions of treated cells.
C1 vs C3: P = 0.00008166 C2 vs C4: P < 0.00005

References

[1] Li Z, Hulderman T, Salmen R, Chapman R, Leonard SS, Young SH, Shvedova A, Luster MI, Simeonova PP. Cardiovascular effects of pulmonary exposure to single-wall carbon nanotubes. Environ Health Perspect. 2007 Mar;115(3):377-82.

[2] Gimbrone MA Jr, García-Cardeña G. Endothelial Cell Dysfunction and the Pathobiology of Atherosclerosis. Circ Res. 2016 Feb 19;118(4):620-36.

[3] Edgell CS, et al. Endothelium specific Weibel-Palade bodies in a continuous cell line EA.hy926. In Vitro Cell Dev. Biol. 26: 1167-1172, Dec1990.

[4] Amorati R, Valgimigli L, Advantages and limitations of common testing methods for antioxidants. Free Radic Res. 2015 May;49(5):633-49.
[5] Czerska M, Mikołajewska K, Zieliński M, Gromadzińska J, Wąsowicz W, Today's oxidative stress markers. Med Pr. 2015;66(3):393-405.
[6] Amin M, Pushpakumar S, Muradashvili N, Kundu S, Tyagi SC, Sen U. Regulation and involvement of matrix metalloproteinases in vascular diseases. Front Biosci (Landmark Ed). 2016 Jan 1;21:89-118.

Participants to the 3rd Annual Conference of the Cost Action Mp1302 Nanospectroscopy

ISBN 978 88 8080 207 5